STRUCTURE AND PROPERTIES OF CRYSTALLINE POLYMERS CRYSTALLIZED OR PROCESSED UNDER MOLECULAR ORIENTATION

SUONG-HYU HYON

INSTITUTE FOR CHEMICAL RESEARCH
KYOTO UNIVERSITY
KYOTO, JAPAN

1978

STRUCTURE AND PROPERTIES OF CRYSTALLINE POLYMERS CRYSTALLIZED OR PROCESSED UNDER MOLECULAR ORIENTATION

SUONG-HYU HYON

INSTITUTE FOR CHEMICAL RESEARCH
KYOTO UNIVERSITY
KYOTO, JAPAN

1978

CONTENTS

GENERAL INTRODUCTION

The macroscopic properties, such as the thermodynamic, spectroscopic and macroscopic physical properties, for crystalline polymers, of course, depend on the supermolecular structure as well as the phase structure of samples. However, since crystalline polymers are composed of very anisotropic long-chain molecules, the supermolecular structure and the phase structure are greatly varied by molecular orientation during their production. For example, the characteristic fiber structure of crystalline polymers will have been brought about by a macroscopic stretching involving molecular orientation. Thus, the mechanism of the formation of the supermolecular structure through processes involving molecular orientation such as fiber- or film-forming processes as well as the macroscopic properties of the resultant products have extensively been studied in connection with the molecular orientation (1-12).

However, since the molecular orientation cannot be simply related to the macroscopic deformation, critical consideration of experimental results in terms of molecular orientation has not been possible in those studies. On the other hand, if polymers have crosslinked units in the molecular structure, the macroscopic deformation produces more definitely molecular orientation so that the molecular orientation can be controlled to some extents. For example, lightly crosslinked polymers have rubbery elasticity in the molten state and the deformation of molecular chains may be described in terms of the macroscopic

deformation(13-17). Hence, if the polymers are cooled to a lower temperature after deformed in the molten state, the crystallization can be achieved under a controlled molecular orientation. It was found by the author and others(18-22) that this mode of crystallization for a lightly crosslinked linear polyethylene produces a unique crystalline structure associated with excellent anisotropic properties such as a high melting temperature and transparency. The utilization of molecular crosslinking not only enabled us to consider the structural change accompanying the macroscopic deformation in terms of molecular orientation but also gave us polymer products with very high degree of molecular orientation. This thesis reviews a series of work concerning the supermolecular structure and the macroscopic properties of some crosslinked and uncrosslinked polymers processed under molecular orientation.

Throughout the work, in addition to the supermolecular structure of samples, special attention has been focussed on the phase structure, or the structure regarding an order of molecules, using a recent broad-line NMR technique developed by Bergmann and Nawotki(23-26), and the author and others(27-32).

This thesis contains the following twelve chapters.

Chapters 1,2,3 and 4 are mainly devoted to the structure and properties of polyethylene prepared under uniaxial stretching. To elucidate the mechanism of crystallization under molecular orientation, systematic experiments have been made on the crystallization of lightly crosslinked polyethylene films stretched to various extents in the molten state. In Chapter 1, the structure and properties of lightly crosslinked

polyethylene gel crystallized from the melt under uniaxial stretching are studied in comparison with those of a fibrous polyethylene prepared by usual stretching at temperatures below the melting point. Furthermore, in this chapter a new concept of the mechanism for crystallization under stretching is proposed.

In Chapter 2, the phase structure and molecular mobility of lightly crosslinked polyethylene gel crystallized from the melt under uniaxial stretching are investigated by a recently developed technique of broad-line NMR spectroscopy. The NMR spectrum taken in a wide range of temperature is analyzed by decomposing into three parts according to a technique developed by Bergmann and Nawotki, and the author and others; the broad, medium and narrow components. The method of this three component analysis is also described.

It is concluded that if a lightly crosslinked linear polyethylene with an adequate crosslink density is stretched in the melt and cooled with holding the stretched length, a very unique phase structure associated with high melting temperatures appears, in which highly oriented crystalline material coexists with less oriented, relaxed amorphous molecular chains. This conclusion suggests a possibility to produce polyethylene fibers with excellent mechanical properties sa well as heat-resistance. In Chapter 3, the preparation of boiling-water resistant fibers from linear polyethylene is described.

In Chapter 4, the broad-line NMR spectrum of polyethylene fibers with different draw ratios is analyzed in terms of molecular mobility in connection with the multi-phase structure of samples. The results

are served to elucidate the detailed structure of fibers.

Chapters 5,6,7 and 8 are mainly devoted to the structure and properties of lightly crosslinked polyethylene crystallized or processed under uniaxial compression. As is well known, when a crystalline polymer is subjected to mechanical deformation by processes such as drawing or rolling, the molecular chains in both the crystalline and amorphous phases tend to align parallel to the direction of deformation. In Chapter 5, the preferential planar orientation of crystal planes in lightly crosslinked polyethylene films crystallized from the melt under uniaxial compression is discussed by wide-angle X-ray diffraction techniques. High density polyethylene prepared under normal conditions is usually opaque, but recently a number of papers have appeared describing procedures for preparing transparent polyethylene of high crystallinity. These procedures involve rather critical conditions such as a very high pressure or high rate of shear. However, highly transparent films with high crystallinity could be made under usual conditions by utilizing irradiation crosslinking. Chapter 6 deals with this procedure for preparing transparent films and described the structure and properties in detail. The origin of transparency is also discussed.

Several studies have recently been reported on the molecular motion of drawn polyethylene using broad-line NMR. However, there has been no report on sample crystallized from the melt under molecular orientation. Chapter 7 deals with a more detailed analysis of phase structure and molecular mobility in a lightly crosslinked polyethylene prepared under various conditions involving molecular orientation by a three component

analysis of broad-line NMR spectrum.

It is found in the preceding chapters that if a lightly crosslinked polyethylene is uniaxially compressed in the melt, a very transparent film with a high melting temperature can be produced. This suggests a possibility of the production of transparent film by a conventional rolling process in a commercial scale. In Chapter 8, the preparation of transparent film by continuous rolling is described.

As reviewed in the forgoing chapters, when crystallized from the deformed molten state, lightly crosslinked polyethylene films exhibit a very unique phase structure. The products obtained from this mode of crystallization are not only very useful in the practical application of the polymer because of the macroscopic properties, but also the mechanism of the formation of such a phase structure will be of foremost importance in elucidating the general mechanism of the crystallization under high molecular orientation irrespective of the presence of crosslinkings. Similar mode of crystallization will be conducted also for other crystalline polymers, provided those have adequate crosslinked units in the molecular structure.

Chapters 9,10,11 and 12 are mainly devoted to the structure and properties of other crystalline polymers, such as isotactic polypropylene, polyvinylidene fluoride, and polyvinyl alcohol, crystallized from the amorphous state under molecular orientation.

In Chapter 9, the orientation of crystal planes in lightly crosslinked isotactic polypropylene crystallized from the melt under uniaxial compression is discussed by means of wide angle X-ray diffraction.

In Chapter 10, the structure and properties of crosslinked isotactic polypropylene crystallized from the melt under uniaxial compression are examined by means of small angle X-ray, DSC, and Vibron.

In Chapter 11, the structure and properties of lightly crosslinked polyvinylidene fluoride crystallized from the melt under uniaxial stretch and compression are discussed.

In Chapter 12, the structure and properties of polyvinyl alcohol stretched at the amorphous state and annealed are described.

References

1. P.J.Flory, J.Chem.Phys., 15, 397 (1947).
2. A.N.Gent, Trans.Faraday Soc.,50, 521 (1954).
3. W.R.Krigbaum and R.J.Roe, J.Polym.Sci., A-2, 4391 (1964).
4. E.M.Andrews, Proc.Roy.Soc.(London), A277, 562 (1964).
5. J.F.M.Oth and P.J.Flory, J.Am.Chem.Soc., 80, 1297 (1958).
6. J.F.M.Oth and P.J.Flory, Kolloid-Z., 162, 124 (1959).
7. P.J.Flory, Science, 124, 53 (1956).
8. L.Mandelkern, D.E.Roberts, A.F.Diorio, and A.S.Posner, J.Am.Chem. Soc., 81, 4148 (1959).
9. A.N.Gent, J.Polym.Sci., A-3, 3787 (1965).
10. H.G.Kim and L.Mandelkern, J.Polym.Sci., A2, 6, 181 (1968).
11. A.Ziabicki, in Man-Made Fiber, H.F.Mark, M.Atlas, and E.Cernia, Eds., Interscience, New York, 1967, p.13
12. K.Katayama, T.Amano, and K.Nakamura, Kolloid-Z.u.-Z.Polym., 226, 125 (1968).
13. J.T.Judge and R.S.Stein, J.Appl.Phys., 32, 2357 (1961).
14. R.Kitamaru and L.Mandelkern, J.Polym.Sci., B2, 1019 (1964).
15. R.Kitamaru, H.-D.Chu, and W.Tsuji, J.Polym.Sci., B-5, 257 (1967).
16. H.-D.Chu, R.Kitamaru and W.Tsuji, J.Appl.Polym.Sci., 10, 1377 (1966).
17. R.Kitamaru and H.-D.Chu, Bull.Inst.Chem.Res., Kyoto Univ., 46, 97 (1968).
18. R.Kitamaru, H.-D.Chu, and S.-H.Hyon, Macromolecules, 16, 337 (1973).
19. S.-H.Hyon, H.Taniuchi, and R.Kitamaru, Bull.Inst.Chem.Res., Kyoto Univ., 51, 91 (1973).
20. R.Kitamaru and S.-H.Hyon, Makromolekulare Chem., 175, 255 (1974)

21. R.Kitamaru, C.Tsuchiya, and S.-H.Hyon, Bull.Inst.Chem.Res., Kyoto Univ., 52, 436 (1974).

22. S.-H.Hyon, R.Kitamaru, H.Taniuchi, N.Tamura, and N.Hayakawa, Kobunshi Ronbunshu, 32, 240 (1975).

23. K.Bergmann and K.Nawotki, Kolloid-Z.u.Z.Polym., 219, 132 (1967).

24. K.Bergmann, Ber.Bunsenges Phys.Chem., 74, 912 (1970).

25. K.Bergmann and K.Nawotki, Kolloid-Z.u.Z.Polym., 250, 1094 (1972).

26. K.Bergmann, Kolloid-Z.u.Z.Polym., 251, 962 (1973).

27. R.Kitamaru, F.Horii, and S.-H.Hyon, J.Polym.Sci.Polym.Phys.Ed., 15, 821 (1977).

28. R.Kitamaru, F.Horii, and S.-H.Hyon, ACS Polym.Prepr., 17(2) 549 (1976).

29. R.Kitamaru and F.Horii, Adv.Polym.Sci., Springer-Verlag, Heidelberg, in press.

30. F.Horii and R.Kitamaru, J.Polym.Sci.Polym.Lett.Ed., in press.

31. S.-H.Hyon,F.Horii, and R.Kitamaru, Bull.Inst.Chem.Res., Kyoto Univ., 55, 248 (1977).

32. R.Kitamaru and S.-H.Hyon, J.Polym.Sci.Macromol.Rev., 14, (1978) in press.

Chapter 1.

STRUCTURE AND PROPERTIES OF LIGHTLY CROSSLINKED POLYETHYLENE, CRYSTALLIZED FROM THE MELT UNDER UNIAXIALLY STRETCHING

1.1. Introduction

Linear polyethylene can be usually stretched uniaxially to high extents at high temperatures below the melting point and produces the so-called fiber structure in which molecular chains are predominantly oriented parallel to the stretching direction. Contrary, at temperatures above the melting point even if it is stretched, such fiber structure can hardly be expected because of the rapid relaxation of stretched molecular chains. However, if the polymer has an adequate intermolecular crosslinks, even when stretched in the molten state at temperatures well above the melting point, the molecular chains are stretched definitely according to the macroscopic deformation(1) and upon cooling the crystallization will be brought about by the stretched molecular chains with a very rapid rate and a structure with a high degree of molecular chain orientation is produced. At temperatures below the melting point, there necessarily exist some amounts of crystalline material as crystallites due to the very high crystallizability of the polymer. Hence, upon stretching in such a state below the melting point, molecular chains in the amorphous region will be first stretched and the orientation or realignment of crystallites will follow.

On the other hand, when a crosslinked sample is stretched in the molten state, since molecular chains are stretched according to the macroscopic deformation, upon cooling to lower temperatures, trans-

formation to the crystalline state will be first taken place from the stretched molecular chains. It is found that this mode of crystallization produces a very unique phase structure associated with many characteristic properties that are sometimes advantageous for the practical uses(1-6). This chapter deals with the structure and properties for samples produced in this mode of crystallization in comparison with those for samples produced by stretching at temperatures below the melting point.

1.2. Experimental Part

Samples

A molecular weight fraction of linear polyethylene with a viscosity-average molecular weight of 3.8×10^5 was obtained by a liquid-liquid separation technique from an unfractionated polyethylene sample, Sholex 5551-H (a high density polyethylene, manufactured by Japan Olefin Chemical, Ltd. with a listed viscosity-average molecular weight of 2.1×10^5). Films of this sample about 0.5-1.0 mm thick were irradiated to a dosage of 8.5 Mrad in vacuum with ^{60}Co at room temperature. The irradiated samples thus obtained were next extracted with boiling xylene with 0.1 % 2,6-di-t-butyl-p-cresol added as an anti-oxidizing agent in order to remove the soluble fraction and dried in vacuum at about 50°C at least for 2 weeks. The soluble fraction w_s was evaluated to be 0.16. The density of intermolecular crosslinks (molar fraction of units crosslinked) of the gel samples thus obtained was approximately evaluated to be 2.4×10^{-4}, using

a relation $\rho_g = (R/R_c)(M_o/M_\eta)(1+w_s)$ according to the theory of gel formation for linear polymers(7, 8). Here, R and R_c are the dosage irradiated and critical dosage for the incipient gelation, respectively. M_o and M_η are fundamental molecular weight of methylene group (14.0) and viscosity-average molecular weight of the sample before the irradiation.

The samples were melted under a hydrostatic pressure in order to remove the voids produced by the extraction with xylene and after cooled to room temperature those were uniaxially stretched in two kinds of procedures as described below. (a) A piece of sample was uniaxially stretched to different extents at a rate of 500 %/sec after melted perfectly in a silicone oil bath at 160°C and cooled to room temperature while holding the stretched length (Procedure a). (b) A piece of sample was uniaxially stretched to different extents at a rate of 500 %/min at 100°C and after kept for 5 min it was cooled to room temperature (Procedure b).

In the procedures a and b, the stretching was achieved in the molten state and in the partially crystalline state, respectively. The stretched samples will be designated by the temperature when stretched and the draw ratio α_z which is defined to be the ratio of the length of stretched specimen to the original length.

Estimation of Molecular Orientation

The molecular orientation of stretched samples has been estimated separately for the crystalline and amorphous phases by using wide angle

X-ray and birefringence techniques.

The degree of orientation for molecular chain vectors can be described by the orientation factor(9)

$$f=(3\langle\cos^2\varphi\rangle-1)/2 \tag{1}$$

Here ϕ is an angle of a molecular chain vector to the stretching direction. The orientation factor f_c for c-axis in crystallites was obtained from an X-ray diffraction scan for the (002)-crystal plane, using a relation

$$f_c=\int_0^{\pi/2} I_{hkl}(\varphi)\cdot\frac{3\cos^2\varphi-1}{2}\cdot\sin\varphi d\varphi\Big/\int_0^{\pi/2} I_{hkl}(\varphi)\sin\varphi\, d\varphi \tag{2}$$

Here I_{hkl} (ϕ) is the diffraction intensity from the (002) crystal plane when sample is fixed in a position such that the stretching direction (fiber axis) makes the angle of ϕ to the inner bisector of X-ray incident and the (002)-diffractive beams.

The quantity for the amorphous molecular chain vectors f_a was evaluated from a birefringence measurement with the f_c and the degree of crystallinity from density measurement, using the relation(10)

$$\Delta n=X_c f_c\Delta_c^\circ+(1-X_c)f_a\Delta_a^\circ \tag{3}$$

Here, the intrinsic configurational birefringence is neglected. Δn designates the birefringence measured, X_c the volume fraction of the crystalline material. Δ_c° and Δ_a° are the theoretical quantities(11) for

perfectly oriented crystalline and amorphous molecular chains, respectively; $\Delta_c^\circ = 0.0572$, $\Delta_a^\circ = 0.0428$ were adopted (11).

Small Angle X-ray Scattering (SAXS)

The SAXS patterns were abtained at room temperature with a point collimation Rigaku Denki small angle X-ray camera. Ni-filtered Cu-K_α radiation was used. The working conditions were carried out under vacuum with 50kV, 80mA, and 0.3 mm primary beam diameter and a specimen to film distance of 300 mm. A small angle camera with a Kratky collimation (Cu-K_α, Scintillation counter) was used to obtain quantitative characteristics of small angle scattering. The long period, $d = \lambda/2\mathrm{Sin}\theta$ (where λ is the Cu-K_α wavelength and 2θ the scattering angle of the primary beam) was found from the position of the maximum in the scattering curve after subtraction of the diffuse scattering.

Fusion and Enthalpy Change in Fusion

The fusion curve was obtained by a differential scanning calorimetry with use of the Perkin Elmer DSC 1-B by a heating rate of 10 °C/min. The amount of the sample used was about 2-3 mg and the correction of temperature was made with use of pure Indium. The melting point was defined to be a temperature where the fusion finally terminated. The enthalpy change in the fusion was estimated by planimetry of the fusion curve with a reference datum for purified benzoic acid.

1.3. Orientation of Molecular Chains in the Crystalline and Amorphous Phases

Figure 1 shows the wide angular X-ray diffraction patterns taken with a flat camera using a nickel filtered Cu-K_α beam for samples uniaxially stretched to different degrees in the melt and cooled (Procedure a). It is seen that for the 1.5-fold drawn sample the diffraction from the (020) crystal plane of the orthorhombic crystal form for this polymer locates on the equator whereas the (200) and (110)-diffractions locate in azimuthal angles close to the meridian and intermediate directions as arcs separated into two, respectively. This implies that upon stretching to such a small extent a crystalline structure appears, in which the b-axis orients perpendicular to the stretching direction while the a-axis orients rather parallel to the direction. This result is phenomenally in accord with the morphological change for a crosslinked polyethylene, when it was stretched 2-fold and cooled after melting, reported by Judge and Stain(5) and discussed as "a-axis orientation" . However, we note here that upon stretching to such a low degree the b-axis orients perpendicular to the stretching direction while the a-axis does not orient parallel to the direction but in an intermediate angle.

Upon further stretching beyond 2 times the (200), (110)-diffractions as well as (020)-diffraction tend to gather on the equator and all diffractions from the (hk0)-crystal planes such as (110), (200), (210), (020) and etc. become to be sharp points when drawn to higher degrees. The result evidently indicates that, when the crosslinked sample is uniaxially stretched and cooled, a very high degree of

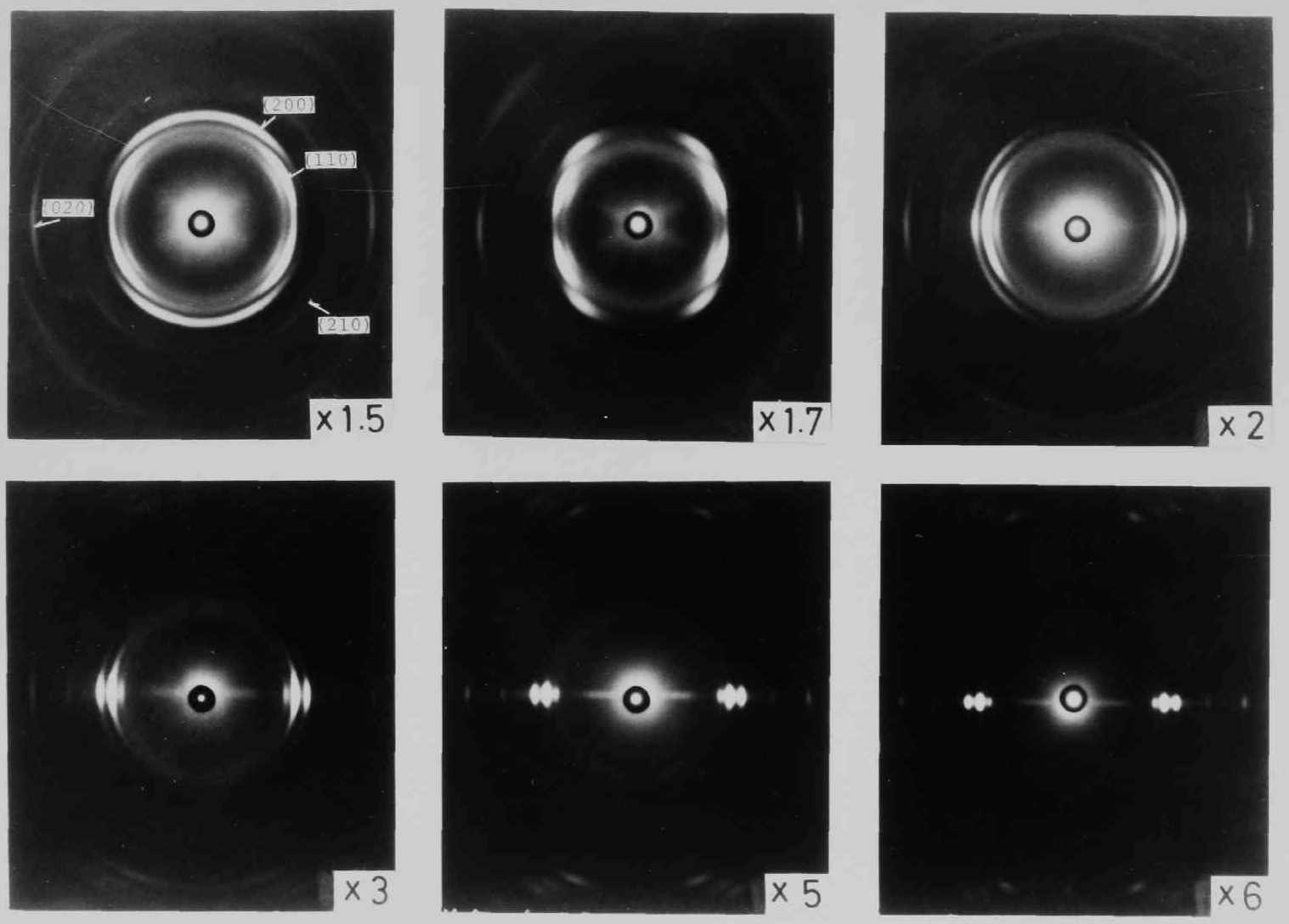

Fig.1. Wide angle X-ray diffraction patterns for the gel sample drawn to different degrees in the molten state at 160°C. The draw ratio is indicated in each pattern. X-ray beam was introduced perpendicular to the drawing direction (vertical in the figure)

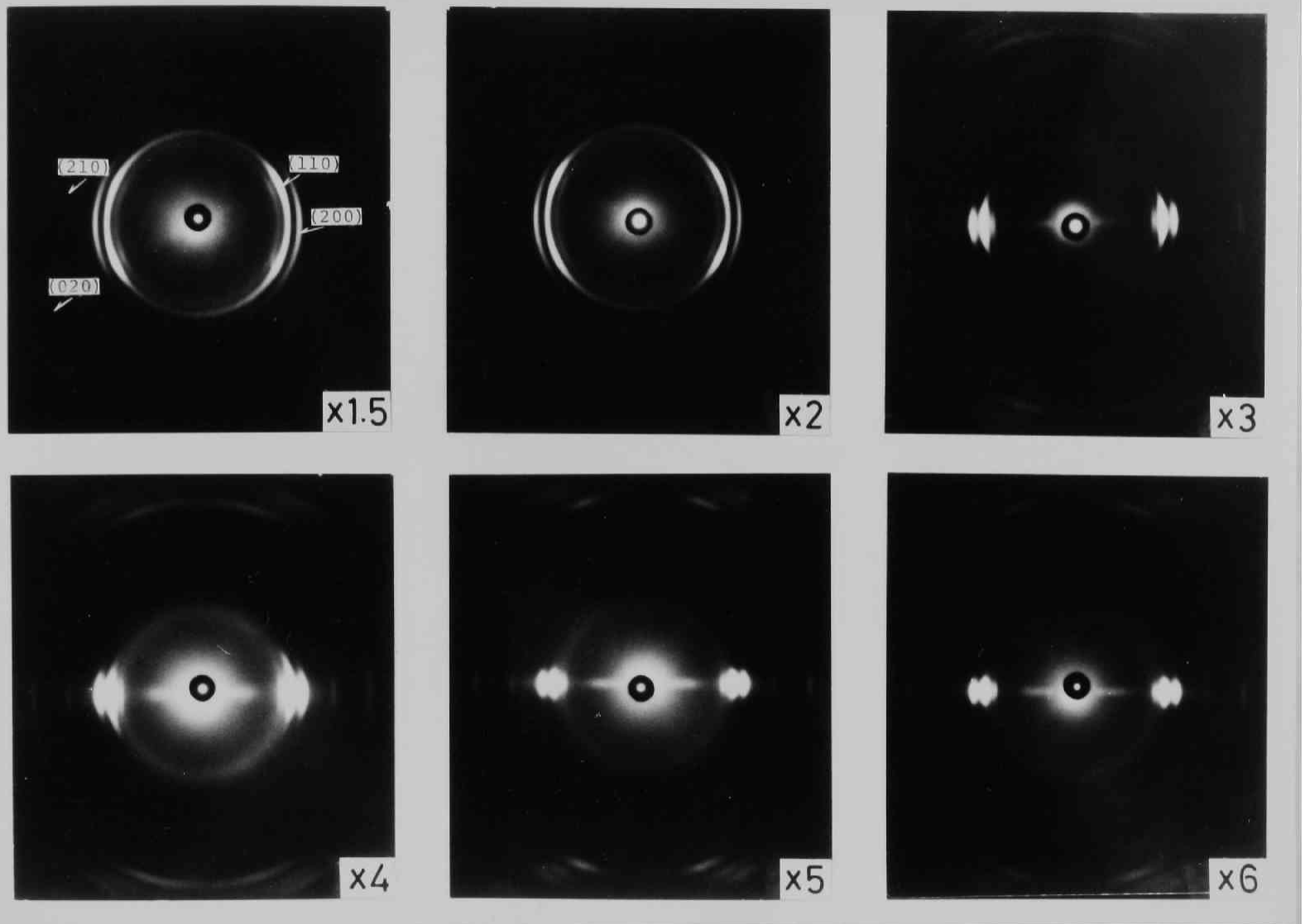

Fig.2. Wide angle X-ray diffraction patterns for the gel sample drawn to different degrees in the partially crystalline state at 100°C. The draw ratio is indicated in each pattern. X-ray beam was introduced perpendicular to the drawing direction (vertical in the figure).

orientation of the c-axis in the crystallites appears in compliance with the macroscopic stretching.

On the other hand, the X-ray patterns are shown in Figure 2 for samples drawn at 100°C. The orientation of the c-axis appears in the beginning of the stretching and increases highly with stretching but to lesser degrees in comparison with that for samples made by stretching in the melt. The diffractions from (hk0) planes in Figure 2 (x6) are located on the equator but they are not so sharp as those in the Figure 1 (x6).

In Table 1, the orientation of the c-axis to the stretching direction is filed as the orientation factor f_c for the two series of samples as a function of draw ratio.

Table 1. Characterization of the Crosslinked Gel Sample, Uniaxially Stretched in the Molten State at 160°C and the Partially Crystalline State at 100°C.

Sample	Draw ratio	$\nu(1-\lambda)_d$	Δn	f_c	f_a
Drawn at 160°C	3	0.582	3.43×10^{-2}	0.973	0.110
	4	0.625	3.73x	0.987	0.126
	5	0.630	3.92x	0.993	0.216
	6	0.636	4.07x	0.996	0.266
Drawn at 100°C	3	0.596	3.87×10^{-2}	0.969	0.327
	4	0.614	4.23x	0.974	0.490
	5	0.636	4.51x	0.985	0.603
	6	0.648	4.76x	0.987	0.731

f_c;Orientation factor of molecular chain vector in the crystalline phase
f_a;Orientation factor of molecular chain vector in the amorphous phase
Δn;Total birefringence

It is seen that, when drawn in the molten state, extremely high degree of orientation of the c-axis is attained, such as f_c is 0.996 for 6-fold drawing. On the other hand, when drawn at 100°C the f_c could not exceed 0.987 even if highly stretched.

In Table 1, are also filed the birefringence Δn as well as the degree of crystallinity $(1-\lambda)_d$ obtained from density measurements. The last colomn shows the values of f_a (evaluated from this quantities) for two series of samples as a function of draw ratio. For the samples stretched in the melt, the value of f_a stays in very low values such as less than 0.266 even if highly stretched while the f_c increases rapidly and reaches a values close to unity as the draw ratio increases. On the contrary, for the samples stretched at 100°C the f_a increases to a very high level with increasing draw ratio but the f_c is smaller than that for the former series of samples. These results evidently show that when the crosslinked sample is stretched to a high degree in the melt and cooled to lower temperatures a very unique structure is produced; the crystallites, of which c-axis is highly oriented to the stretching direction, coexist with amorphous molecular chains not oriented appreciably to the direction. Contrary, the samples stretched at 100°C have a structure, in which the crystallites, oriented highly but to lesser extents than for the former series of samples, coexist with highly oriented amorphous molecular chains.

We note here that such a unique structure in which very highly oriented crystallites coexist with unoriented amorphous molecular chains was obtained only by the special mode of crystallization for the sample

with a proper amount of crosslinks.

1.4. Size of Crystallites

Figures 3 and 4 show the small angular X-ray diffraction patterns for the two series of samples, stretched at 160°C in the melt and at 100°C in the partially crystallized state, respectively. For samples stretched in the melt the two-point pattern is always recognized throughout the draw ratios, from 1.5-fold to 6-fold. The diffraction points approach the center of the pattern with increasing draw ratio, showing an increase of the crystallites size. Such a two-point pattern has been reported for uncrosslinked samples crystallized under high shear rate through processes such as the melt-spinning of the polymer(12-16). But we note here that the distinct two-point pattern for the crosslinked sample crystallized from the stretched molten state holds to the highest degree of stretching, showing very ordered crystalline structure for this sample. Contrary, the two-point diffraction for the melt-spun sample diffuses in the direction perpendicular to the spinning direction with increasing shear rate, showing disordering of the crystalline structure.(13,16)

On the other hand, when stretched at 100°C the patterns obtained are quite different as can be seen in Figure 4. A six-point diffraction pattern appears at a draw ratio of 1.5 and upon further stretching a discrete lamella-like diffraction appears, lengthening parpendicular to the stretching direction and becoming to be a little inclined lamella-like four-point diffraction at the higher degrees

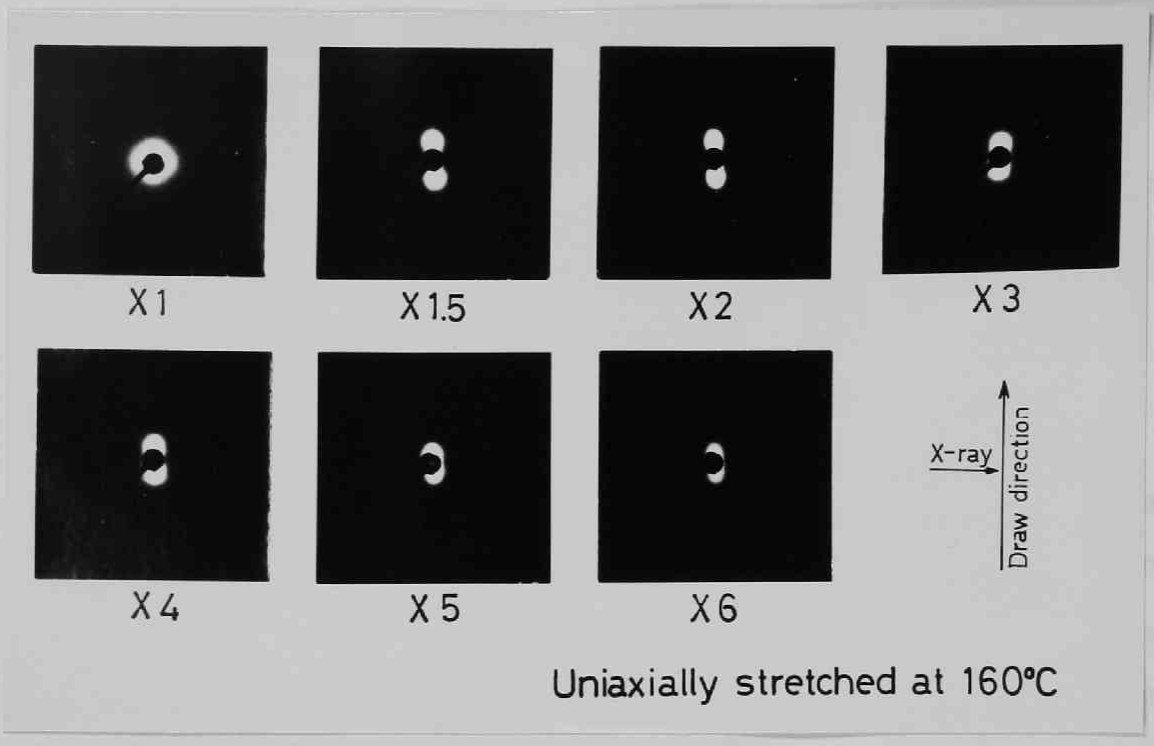

Fig.3. Small angle X-ray diffraction patterns for the gel sample drawn to different degrees in the molten state at 160°C. The draw ratio is indicated in each pattern.

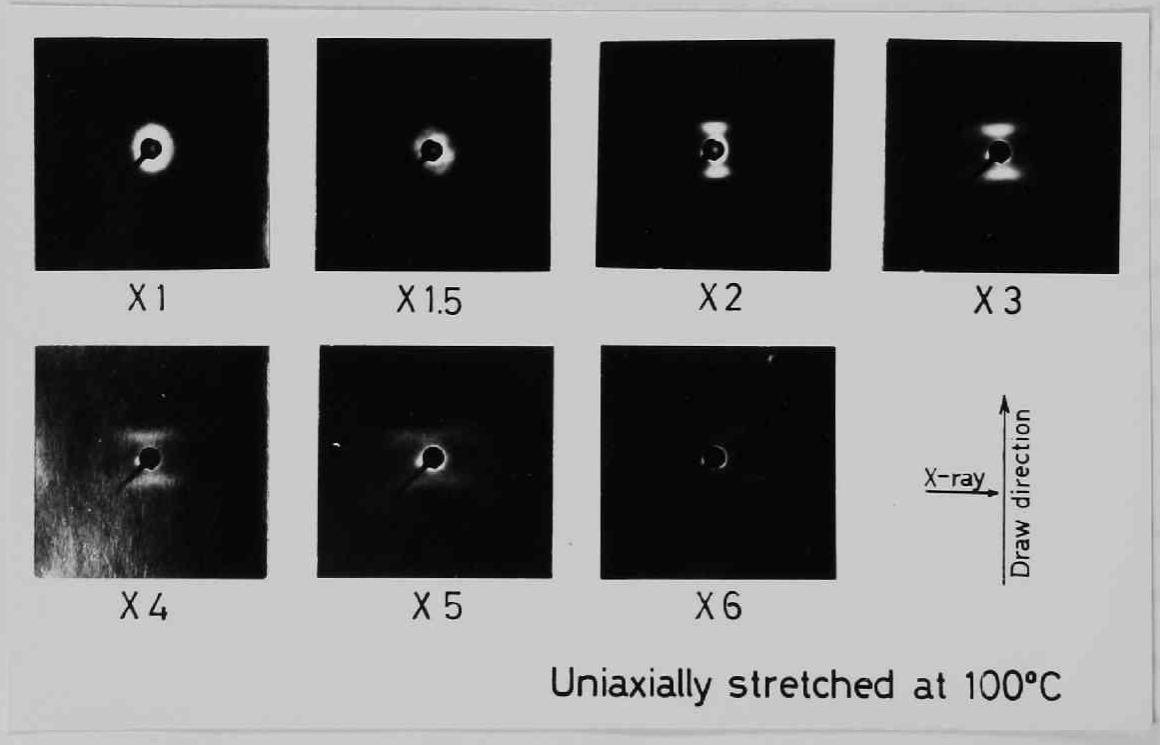

Fig.4. Small angle X-ray diffraction patterns for the gel sample drawn to different degrees in the partially crystalline state at 100°C. The draw ratio is indicated in each pattern.

of stretching. The result implies that upon stretching in the unmelted state the disordering of the structure becomes enhanced while the stretching in the melt such disordering does not take place.

In Figure 5 the diffraction intensity measured with a Kratky camera is plotted against 2θ angle for the two series of samples, stretched 2,4, and 6-fold, in the two modes respectively. There is observed a very enhanced difference in behavior between the two series of samples. For samples stretched in the melt the 2θ angle at the maximum intensity decreases while the maximum intensity increases with increasing draw ratio. On the contrary, for samples stretched at 100°C the 2θ angle at the maximum intensity increases while the maximum intensity decreases with increasing draw ratio. In Figures 6 and 7, the d-spacing evaluated from the 2θ angle at the maximum and the maximum intensity are plotted against draw ratio for the two series of samples. When the crosslinked sample is stretched in the partially crystallized state, the long spacing as well as the maximum intensity are decreased as the draw ratio increases.

It is reported by Peterlin and others(17-19) that when uncrosslinked sample is stretched at high temperatures in the partially crystallized state the diffraction intensity decreases with increasing draw ratio while the long spacing does not depend on the draw ratio but depends on the stretching temperature. They attributed the decrease of the diffraction intensity with stretching to a decrease of the density difference between the crystalline and amorphous phases.
It was considered that the decrease of the density difference would

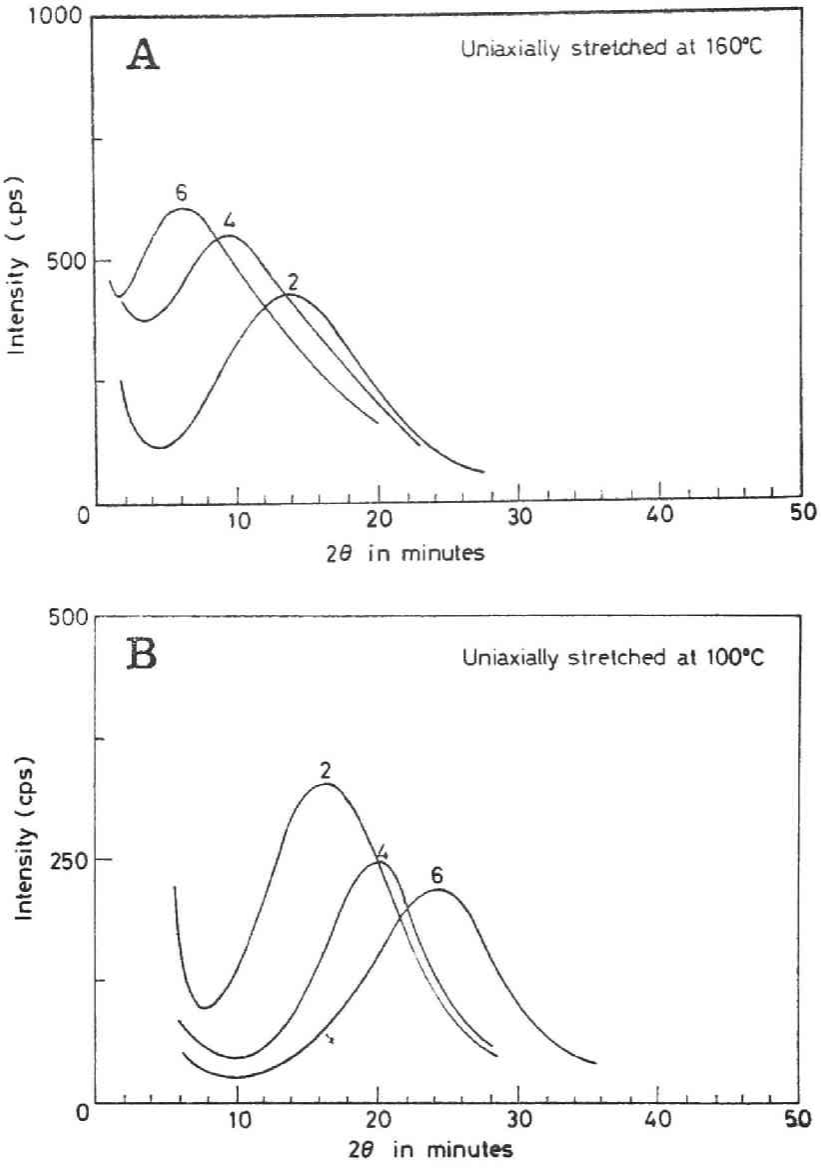

Fig.5. Angular dependence of small angle X-ray scattering of the gel sample, stretched in the molten state at 160°C (A), and in the partially crystalline state at 100°C (B). The draw ratio is indicated in each curve.

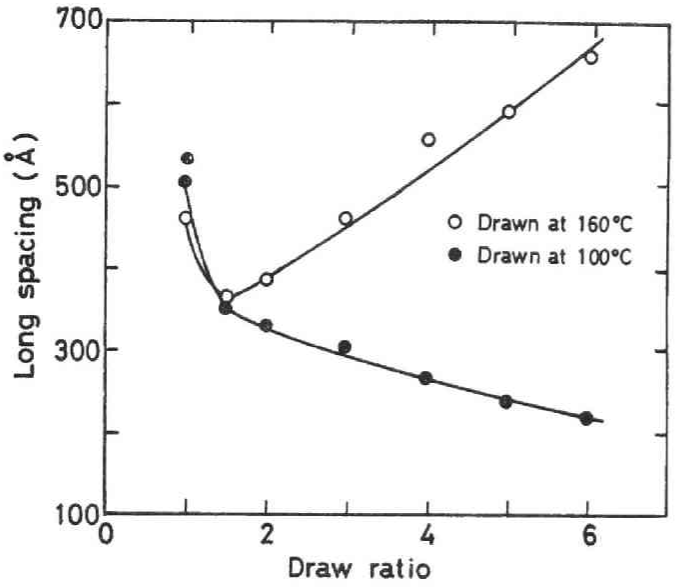

Fig.6. The long period calculated from data in Figure 5 against the draw ratio for the gel sample drawn in the molten and crystalline states.

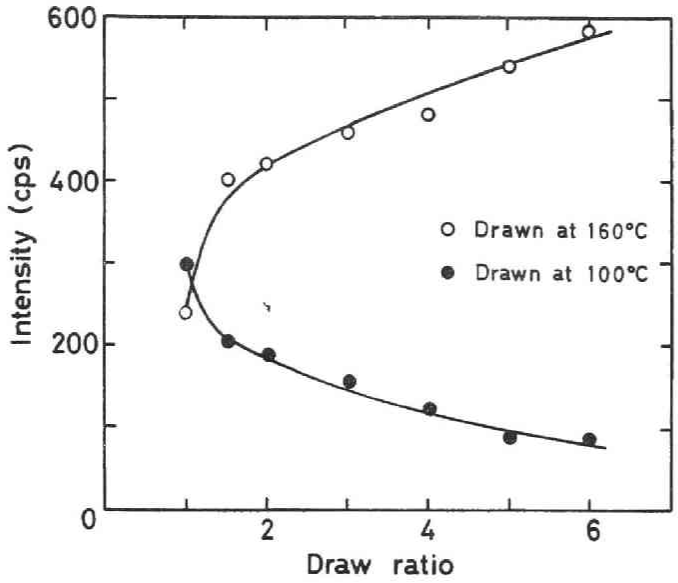

Fig.7. The small angle scattering intensity taken from Figure 5 against draw ratio for the gel sample drawn in the molten and crystalline states.

be brought about by the decrease of density in the crystalline phase due to a production of defects as well as the increase in the amorphous phase due to the stretched state of molecular chains(with the macroscopic stretching). The reason for the decrease of the diffraction intensity recognized here for the crosslinked sample stretched in the partially crystallized state will be similar to that discussed by them for uncrosslinked sample. On the other hand, the decrease of the long spacing for the crosslinked sample with stretching at 100°C will probably be attributable to the fact that the crosslinking units cause a more severe restriction on the reorganization of molecular chains accompanying stretching.

On the other hand, a very characteristic feature is recognized in changes of the long spacing and the maximum intensity for the crosslinked sample when stretched in the melt, the both increase with increasing draw ratio. The increase of the diffraction intensity implies a very unique structural feature of those samples. As mentioned in the foregoing section, those samples have a structure that the crystallites, oriented highly to the stretching direction, coexist with rather unoriented amorpnous molecular chains (see Table 1; $f_c \simeq 1.00$, $f_a \leq 0.266$). Therefore, the density of the amorphous phase is considered to be unaltered in a low level even if stretched highly. The crystallites are not only highly ordered but the density of those (unit-Cell density) is evaluated as high as 1.001 by an X-ray diffraction measurement. Accordingly the difference in the density between the crystalline and amorphous phases is considered not to decrease but increase upon

stretching in the melt. This will result in the enhanced increase of the diffraction intensity together with the highly ordering of the crystallites.

The enhanced increase of the long spacing with increasing draw ratio will be significant in relation to the mechanism for the formation of the structure. For the crystallization, if we assume the formation of a cylindrically shaped nucleus that contains ρ molecular chains in cross section and ζ repeating units of long chain-molecule along the length of the cylindrically shaped nucleus, the critical size of the nucleus for growing is given by relations(20),

$$\rho^* = 4\pi\sigma_u^2 \; / \; \Delta f_u^2 \qquad (4)$$

$$\zeta^* = 4\,\sigma_e \; / \; \Delta f_u \qquad (5)$$

Here Δf_u is the free energy of fusion per repeating unit of molecule, σ_u and σ_e are the lateral interfacial free energy per repeating unit and the interfacial free energy per molecular chain at the cylinder end, respectively. At a crystallization temperature T close to the melting temperature T_m, the equations reduce to,

$$\rho^* \simeq \frac{4\pi\sigma_u^2 T_m^2}{\Delta h_u^2 \Delta T^2} \qquad (6)$$

$$\zeta^* \simeq \frac{4\,\sigma_e T_m}{\Delta h_u \Delta T} \qquad (7)$$

Here Δh_u designates the enthalpy change in fusion per repeating unit of chain-molecule and ΔT the degree of undercooling; $\Delta T = T_m - T$. Since the melting temperature increases with increasing molecular orientation (3), the actual degree of undercooling ΔT must be appreciably increased as the degree of macroscopic uniaxial stretching increases. Therefore eqs.(6) and (7) suggest that the critical size of the nucleus for growing must become smaller upon stretching. Accordingly, if the size ζ of nucleus along molecular chain holds to be relatively ungrown even after exceeding the critical dimension, the long spacing must be shorten upon stretching, if the long spacing is considered to comparable to the ζ. Such shortening of the long spacing was in fact reported by Kobayashi and others (21,22) when uncrosslinked polymer was crystallized from the melt under high rates of shear. Contrary to this, when the crosslinked sample is crystallized under stretching the long spacing is greatly increased. This fact must indicate a difference in the mode of growing of the nucleus after exceeding the critical dimensions. When the crosslinked sample is stretched in the melt, the majority of molecular chains in the structure are stretched in compliance with the macroscopic deformation as discussed. It will be intuitively understood that the growing of a crystallite in the direction parallel by such stretched molecular chains must be achieved rapidly or almost instantly so far as such stretched molecular chains are available. The enhanced increase of the long spacing recognized here will be explained by this mechanism. On the other hand, the shortening of the long spacing for uncrosslinked

samples crystallized under high rates of shear will be caused by the fact that molecular chains in the melt are rather insensible to rate of shear and the stretched molecular chains available during the crystallization are limited and rapidly dissipated and the growing of a crystallite parallel to the molecular chain becomes to be inhibited.

1.5. Fusion and Melting Temperature

Figure 8 shows the DSC fusion curves for the two series of samples. For the samples drawn in the partially crystallized state the fusion curve is not altered although somewhat elevating of the melting temperature could be recognized with increasing draw ratio. For the samples drawn in the melt abnormally high melting temperatures are recognized with increasing draw ratio.

In Table 2, listed are the melting temperature and the enthalpy of fusion for the drawn samples estimated from the fusion curves. The melting temperature and heat of fusion increase in accordance with the increase of draw ratio. But the quantities for the sample crystallized from the melt under stretching are appreciably greater than those for the sample stretched in the partially crystalline state.

If the stretched conformation of molecular chains is held after fusion, the melting point is to be heightened due to the decrease of the entropy change in fusion. The present DSC scanning was carried out without holding the macroscopic length of samples. The observed high melting points suggest that the macroscopic shrinkage has not

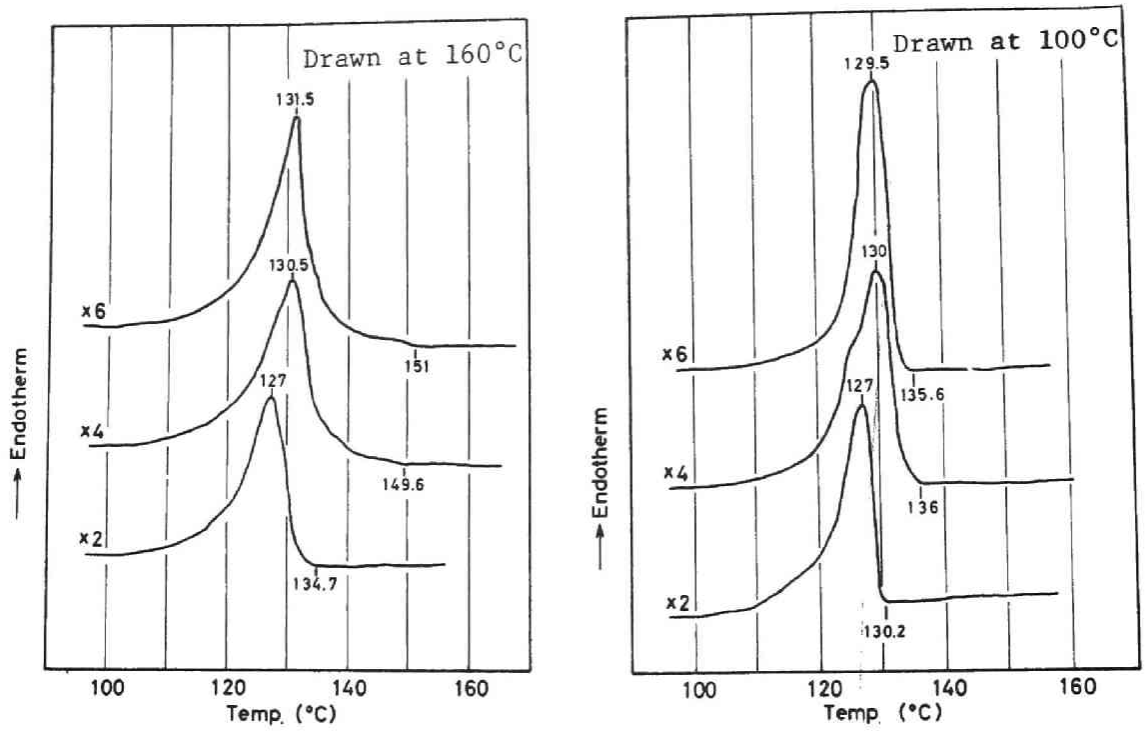

Fig.8. DSC thermograms for the gel sample drawn to different degrees at 160°C and 100°C. The draw ratio is indicated in each thermogram.

Table 2 Melting Point and Heat of Fusion for Uniaxially Stretched Gel PE Sample.

Sample	Draw ratio	Melting Point (°C) Tmax	Tend	Heat of Fusion ΔH(cal/g)
Crystallized from the melt(isotropic) for 4 weeks at 130°C		129.5	133.2	37.8
Drawn at 100°C	2	126.9	130.2	35.1
	3	129.9	136.0	36.4
	4	130.0	136.5	36.8
	5	131.5	136.2	37.2
	6	129.5	135.6	37.5
Drawn at 160°C	2	127.0	134.7	34.2
	3	130.5	147.5	38.4
	4	130.5	149.6	39.2
	5	131.5	150.0	40.3
	6	131.5	151.0	42.5

completed within the time scale of the scanning due to the relaxed state of molecular chains in the noncrystalline region of the melt-drawn samples. In fact it was reported by the author and others(27) that the original length for a crosslinked sample drawn in the melt was recovered only by swelling with a proper solvent but not only with heating. In any case, the high melting temperatures observed the very stable crystalline form of these samples, comprised of very ordered crystalline region with unoriented, relaxed amorphous molecular chains.

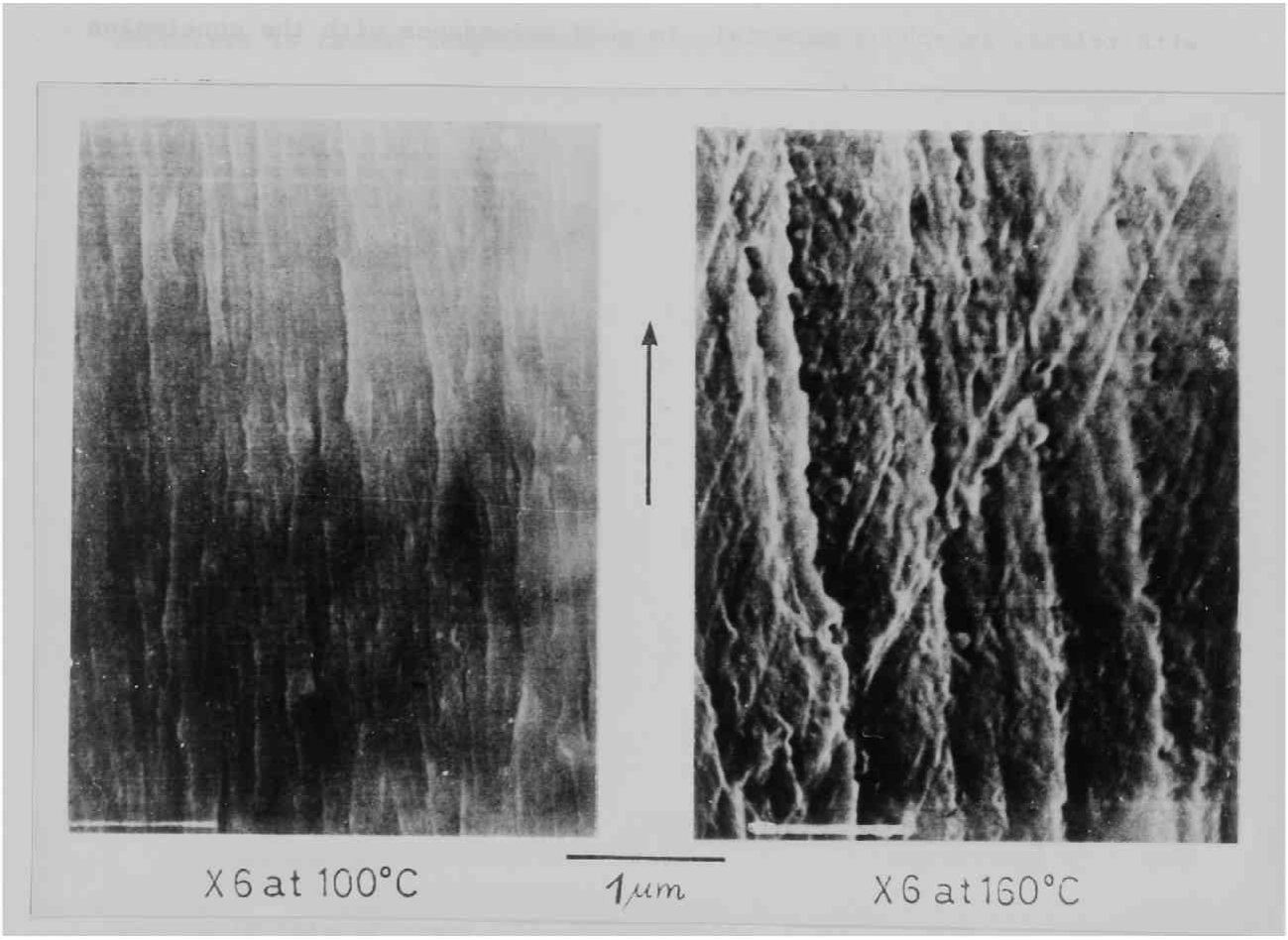

Fig.9. Scanning electron microscope photographs for the 6-fold stretched gel at 100 and 160°C. The draw direction is vertical.

1.6. Scanning Electron Microscope

In Figure 9 is shown the surface of samples drawn to 6 times under various condition observed by a scanning electron microscope. The surface shown in Figure 9(A) is composed of fibrils. However, the picture shown in Figure 9(B) is quite different. Micrograph of samples drawn in the melt shows a similar type of lamella arrangement nearly perpendicular to the draw direction as recognized for a fuming nitric acid-treated sample (23,24), which is the indicative of longitudinal fibril boundaries. This picture will show the very ordered crystallites structure with relaxed amorphous material, in good accordance with the conclusion discussed in the foregoing sections.

1.7. Mechanism for Crystallization under Stretching

It is revealed in the foregoing sections that if a lightly cross-linked polyethylene is uniaxially stretched in the melt a particular mode of crystallization appears. When it is highly stretched, the transformation to the crystalline form occurs with an extremely rapid rate and a special crystalline structure appears in which the crystallites orient to a very high degree with the c-axis parallel to the stretching direction but the molecular chains in the amorphous phase are rather unoriented and associated with a larger molecular mobility. The very rapid rate of crystallization will be well understood by an entropy decrease with stretching that results in the increase of the undercooling for the crystallization. Since the crystallization is thought to be conducted from stretched molecular chains in the system, the molecular chains remained in the amorphous phase will be rather unoriented and in a relaxed state. Thus, the very special phase structure produced

under high degrees of stretching will be well understood.

However, if the crosslinked sample is crystallized from the melt under a low degree of stretching, a unique orientation of the crystallites is observed as previously described. The b-axis of the orthorhombic crystal form of the polymer orients perpendicular to the stretching direction while the a- and c-axes orient rather parallel to the direction. This b-axis perpendicular orientation is phenomenally in accord with phenomena observed by Judge and Stein (5) and by Spruiell and White (26). The mechanism of the appearance of such a special structure is rather complicated but it is thought to be of very important in considering the general feature of the crystallization under stretching irrespective of the presence of crosslinks. We consider this problem briefly.

The mechanism of the crystallization under stretching has been argued by many investigator(5, 22, 25). For example, Keller and Hill(25) argued this kind of phenomenon as a result of the formation of the so-called row structure. In the mechanism argued by them, ribbon-like crystallites were assumed to grow spirally perpendicular to a needle-like nucleus originated along the stretching direction. For the formation and the growth of such ribbon-like crystallites, regularly folding back of molecular chains was assumed to occur repeatedly as a matter of course. However, such a repeated folding back of molecular chains in the course of crystallization could not be amenable, if we consider the very rapid rate of crystallization and the phase structure of the product.

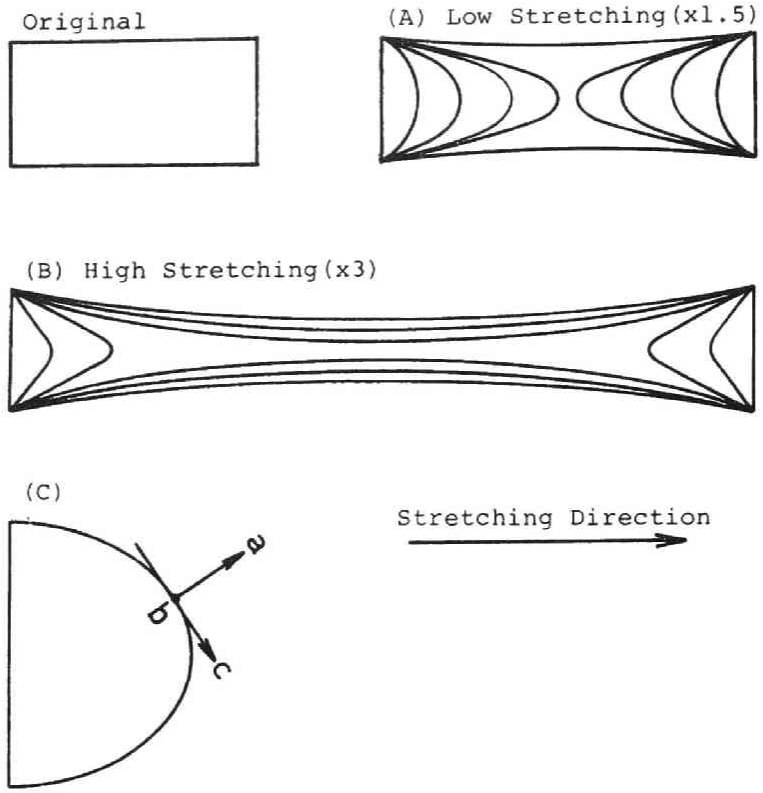

Fig.10. Schematic diagram for the shear lines or shear planes in the structure of a film sample stretched to different degrees.

When a piece of lightly crosslinked sample is stretched, the shear lines or shear planes produced in the structure can be schematically expressed in Figure 10. Under a high degree of stretching, the shear lines are thought to be mostly parallel to the stretching direction as shown in the figure (B). But under a low degree of stretching, the shear lines will be comprised of parabolas or ellipsoids as shown in the figure (A).

On the other hand, it will be exclusively evidenced from the experimental results in Chapter 6 that, when the crosslinked polymer film is crystallized from the uniaxially compressed melt, the nuclei

for the crystallization are produced with the a-axis perpendicular to the shear plane; namely perpendicular to the film plane (see the discussions of the mechanism for the formation of the (200) planar orientation, Chapter 6). Therefore, it is very likely that when the sample is uniaxially stretched the nuclei for the crystallization are produced with a-axis perpendicular and c-axis parallel to the shear lines and those grow in holding the direction of the crystal axes as shown in the figure (C). In this orientation of the crystal axes, the b-axis is always perpendicular to the stretching direction irrespective of the degree of stretching and a- and c-axes orient in intermediate angles, the c-axis comes to orient parallel to the stretching direction at a high degree of stretching. Since the flow lines are thought to make an intermediate angle to the stretching direction in the average under a low degree of stretching, the formation of the special orientation of the crystal axes; the b-axis perpendicular, and a- and c-axes parallel to the stretching direction (see the figure C), will be easily understood without assuming the improbable regularly folding back of molecular chains in the course of crystallization. The inevitability for the crystallization with the a-axis perpendicular to the shear plane could not be theoretically confirmed at the present time, but it is believed that such a crystallization habit always appears in the crystallization or re-crystallization under conditions involving molecular orientations.

1.8. Conclusion

If a crosslinked polyethylene of adequate crosslink density is uniaxially stretched in the molten state, the molecular chains in the structure are elastically stretched according to the macroscopic deformation. Upon cooling to a lower temperature from such a stretched state, a fiber structure with very unique phase structure is produced, in which highly oriented crystallites coexist with unoriented and relaxed amorphous molecular chains. The formation of such a unique phase structure is considered to be caused by the fact that, upon cooling from the stretched state, the transformation to the crystalline form occurs with a extremely rapid rate from stretched molecular chains, producing the very high degree of orientation of crystallites parallel to the stretching direction and remaining unoriented molecular chains in the amorphous region.

The products obtained from this mode of crystallization are not only associated with many properties advantageous of the practical use such as high melting temperature and high dimensional stabilities but also the mechanism of the formation of such a unique structure is very interesting to elucidate the general feature of the crystallization of the polymer under stretching. In this mode of crystallization, a rather peculiar orientation of the crystal axes of the orthorhombic crystal form of the polymer is observed in a low degree of stretching, the b-axis orients in the direction perpendicular to the stretching direction while the a-axis rather parallel or intermediate angles to the stretching direction. The mechanism for the formation of such crystal planes has been discussed by many investigators from different

points of view but assuming repeatedly folding back of molecular chains. However, it is argued in this Chapter that the formation of such a peculiar orientation of the crystal axes should not be considered by any mechanism involving improbable repeated folding back of molecular chains. It is pointed out that the formation of such orientation of the crystal axes, including the formation of the high degree of orientation of the c-axis in the high degree of stretching, is plausibly understood without assuming such folding back of molecular chain, by the crystallization habit of this polymer that the nucleation and growth of the crystallization occur in such a manner that the a-axis orients perpendicular to the flow line or the shear plane and the c-axis orients as possibly as parallel to the stretching direction.

References

1. R.Kitamaru and H.-D.Chu, Bull.Inst.Chem.Res., Kyoto Univ., 46, 97 (1968).
2. R.Kitamaru, H.-D.Chu, and W.Tsuji, J.Polym.Sci., B-5, 257 (1967).
3. H.-D.Chu, R.Kitamaru, and W.Tsuji, J.Appl.Polym.Sci., 10, 1377 (1966).
4. R.Kitamaru, C.Tsuchiya, and S.-H.Hyon, Bull.Inst.Chem.Res., Kyoto Univ., 52, 436 (1974).
5. J.T.Judge and R.S.Stein, J.Appl.Phys., 32, 2357 (1961).
6. W.R.Krigbaum and R.-J.Roe, J.Chem.Phys., 41, 737 (1964).
7. W.H.Stockmayer, J.Chem.Phys., 12, 125 (1944).
8. P.J.Flory, J.Am.Chem.Soc., 69, 30 (1947).
9. J.J.Hermans, P.H.Hermans, D.Vermeas and A.Weidinger, Rec.Chim.Trav., 65, 427 (1946).
10. R.S.Stein and F.H.Noriss, J.Polym.Sci., 21, 381 (1956).
11. R.S.Stein, J.Polym.Sci., 31, 327 (1957).
12. W.O.Statton, J.Polymer Sci., 28, 423 (1958).
13. K.Katayama, T.Amano, and K.Nakamura, Kolloid Z.-Z.Polym., 226, 125 (1968).
14. V.I.Gerasimov and D.Ya.Tsuvankin, Vysocomol.Soyed., A-12, 2599 (1970).
15. M.J.Hill and A.Keller, J.Macromol.Sci.Phys., B5, 591 (1971).
16. T.Hashimoto, N.Yasuda, S.Suehiro, S.Nomura, and H.Kawai, Polymer Preprints, ACS, 11, 118, No.2 (1976).
17. R.Corneliussen and A.Peterlin, Makromol.Chem., 105, 193 (1967).
18. A.Peterlin and R.Corneliussen, J.Polym.Sci., A-2, 6, 1273 (1968).
19. A.Peterlin and G.Meinel, Makromol.Chem., 142, 227 (1971).

20. L.Mandelkern, "Crystallization of Polymers", McGraw-Hill Book Comp., 1964, New York.

21. K.Kobayashi and T. Nagasawa, J.Macromol.Sci.Phys., B4, 331 (1970).

22. T.Kawai, M.Iguchi, and H.Tonami, Koll.-Z.u.Z.-Polym., 221, 28 (1967).

23. A.Peterlin and K.Sakaoku, Kolloid-Z., 212, 51 (1966).

24. R.J.Samuels, J.Polym.Sci., A-2, 6, 1101 (1968).

25. A.Keller and M.J.Machin, J.Macromol.Sci.(Phys.), B1(1), 49, (1967).

26. J.E.Spruiell and J.White, Polym.Eng.Sci., 15, 660 (1975).

27. R.Kitamaru, H.-D.Chu, and S.-H.Hyon, Macromolecules, 6, 337 (1973).

Chapter 2.

PHASE STRUCTURE AND MOLECULAR MOBILITY OF LIGHTLY CROSSLINKED POLYETHYLENE, CRYSTALLIZED FROM THE MELT UNDER UNIAXIALLY STRETCHING BY BROAD-LINE NMR SPECTROSCOPY

2.1. Introduction

Broad-line NMR measurements are useful in studying the detailed structure of solid polymers since fluctuations in the molecular mobility are directly reflected in changes in the NMR spectrum. In early studies (1) of the broad-line proton magnetic resonance of polyethylene, the spectrum was analyzed in terms of contributions from two groups of protons, i.e. one belonging to the crystalline region and the other to the amorphous region, based on the so-called two phase crystalline model of polymers. However, since the mass fraction of the crystalline region estimated by this method was appreciably larger than the crystallinity obtained from other methods such as density measurements or X-ray diffraction analysis, further detailed studies in relation to the phase structure of the polymer have rather been limited. Recently, following Bergmann and Nawotki(2-5) a number of investigators(6-9) more critically analyzed the spectrum by considering also a contribution from protons in the intermediate region between the crystalline and amorphous regions.

It has been concluded in Chapter 1 that if the crosslinked sample is crystallized from the melt under uniaxial stretching a unique morphological structure is produced. The crystallites (with large

dimensions) oriented highly parallel to the stretching direction coexist with a large amount of rather unoriented amorphous molecular chains. In order to study the molecular mobility or relaxation phenomena in relation with such morphologically unique phase structure of the sample, we have inquired the broad-line proton NMR spectrum in a wide range of temperature. Comparison was also made between samples stretched in the two modes (described in Chapter 1).

2.2. Spectrometry and Analysis

The first derivative NMR absorption spectrum was obtained over a wide range of temperature from -100 to +40°C for two series of drawn samples with a JNM-PW-60 NMR Spectrometer (JEOL Ltd.), fixing samples in a position, the fiber axis being parallel to the magnetic field. The magnetic field swept slowly was modulated at 35 Hz and amplitude of 0.4 G under a constant sub-field with a frequency of 60 MHz.

The spectrum observed was analyzed by a technique(10-13) based on the method developed by Bergmann and Nawotki(2-5) and the author and others(10,12), decomposing into three parts; broad, medium and narrow components. The first derivative of a broad-line spectrum can be described in the three terms as a function of strength of the main magnetic field in the measurement.

$$y(H) = w_b y_b(H, \beta_b) + w_m y_m(H, \beta_m) + w_n y_n(H, \beta_n) \tag{1}$$

with

$$w_b + w_m + w_n = 1$$

Here, H can be conveniently expressed by the deviation in gauss unit of the field from the center of the resonance ($H = H' - H_0$) ; y_b, y_m, and y_n are the elementary spectra of the broad, the medium, and the narrow components, respectively. Those are considered to be contributed from protons belonging to the crystalline region, and hindered rotating and micro-Brownian mobile methylene groups in the amorphous region, respectively. β_b, β_m , and β_n determine the line-width and breadth of the respective elementary spectra; w_b, w_m, and w_n designate the respective mass fractions. Each elementary spectrum is normalized as

$$\int_{-\infty}^{\infty} \int_{-\infty}^{H} y_i(H, \beta_i) dH = 2, \qquad i = b, m, \text{and } n. \tag{2}$$

The parameters in eq.(1) are to be determined so as to minimize the sum Φ of the squares of the difference between the observed and calculated spectra over the full range of H:

$$\Phi = \sum_j \{ y_{obs}(H_j) - A\, y(H_j) \}^2. \tag{3}$$

Here A is a parameter which adjusts the amplitude of the spectrometry. The success for this three-component analysis relies on adequate choice for the elementary spectra. Hence, we review briefly the elementary spectra used for this series of work.

Broad Component The elementary spectra for the broad components were obtained by changing the line-width of the spectrum at -160°C for each sample but keeping the shape unchanged. When the spectrum $y_s(H)$ at -160°C for the sample has the line-width of ΔH_s, an elementary spectrum $y_b(H)$ with a line-width ΔH_b can be constructed as

$$y_b(H) = \chi y_s(\gamma H), \qquad \gamma = \Delta H_s/\Delta H_b \tag{4}$$

Here χ designates the nomalization factor.

Medium Component The elementary spectra for the medium component were derived by Bergmann and Nawotki(2, 3) on the basis of a spectrum calculated by Gutowsky and Pake(14) for paired protons such as in 1,2-dichloroethane with hindered rotation around the C-C bond.

$$y_m(H, \beta_m) = \frac{1}{4(6\pi)^{1/2}\alpha\beta_m^3}\int_{-\alpha}^{2\alpha}\frac{(2H+h)\exp\left\{-\frac{(2H+h)^2}{8\beta_m^2}\right\}+(2H-h)\exp\left\{-\frac{(2H-h)^2}{8\beta_m^2}\right\}}{(1+h/\alpha)^{1/2}}dh \tag{5}$$

with $\alpha = (3/2)\mu r^{-3} = 4.0 \pm 0.1$ G.

Here r is the distance between the paired protons, μ is the magnetic moment of the proton. However, the molecular mobility in the amorphous region in the polymer where the rotation around C-C bonds is hindered is not so simple as expected by eq.(5). The equation cannot adequately

reproduce the medium component of the spectrum. It is reported by Bergmann and Nawotki(4) that for actual spectra for polymers a following expression reproduces more adequately the medium component.

$$y_m(H, \beta_{mg}, \beta_{ml}) = N \frac{\partial}{\partial H} \exp\left(-\frac{H^2}{2\beta_{mg}^2}\right) \cdot \frac{\beta_{ml}^2}{\beta_{ml}^2 + H^2} \tag{6}$$

Here N designates the normalization factor. Clearly this equation in integrated form is the product of Gaussian and Lorentzian distribution functions; β_{mg} and β_{ml} define the line-widths of the two components, respectively. Here, the former represents eq.(5) to a sufficient approximation for $\beta_m \geq 2$ G and the latter was introduced to express the coupled rotational and/or the translational motion of proton pairs in the polymer, discussed by Pechhold(15).

Narrow Component The absorption spectrum for polyethylene cannot be described by a single-Lorentzian even in the molten state.[13,16] However, the deviation from one Lorenzian is not enhanced for well-fractionated samples in the melt[13] and, furthermore, becomes negligible as the temperature decreases(16). Accordingly, the differential form of a Lorentzian distribution can be used for the elementary spectrum of the narrow component

$$y_n(H, \beta_n) = 4\pi^{-1} \beta_n^{-3} H/(1 + \beta_n^{-2} H^2)^2 \tag{7}$$

or in the integrated form

$$y_n(H, \beta_n) = 2(\pi\beta_n)^{-1}/(1 + \beta_n^{-2} H^2) \tag{8}$$

Here, β_n is related to the line-width ΔH_n by $\beta_n = (\sqrt{3}/2)\,\Delta H_n$ and

$$\int_{-\infty}^{\infty} Y_n(H, \beta_n)\, dH = 2$$

However, since the line-width of the narrow component is generally rather small for most samples studied, the line shape is distorted by the amplitude of the modulation H_m. It is well known that if the condition $H_m \leq \Delta H/5$ is fulfilled, distortions due to the H_m are negligible. Since this condition is generally not fulfilled for the narrow component, the distortion due to the H_m must be taken account. Taking into account this effect, we obtain following expression for a Lorentzian line as a function of H, β_n, and H_m.

$$\begin{aligned} y_n(H, \beta_n, H_m) &= a_1(H)/H_m \\ &= \frac{2}{\pi^2 \beta_n H_m} \int_{-\pi}^{\pi} \frac{\cos\phi\, d\phi}{1 + \beta_n^{-2}(H + H_m \cos\phi)^2} \end{aligned} \tag{9}$$

The finite integral appearing in the right hand of the equation has been solved by many investigators(3,12,17-21). Substituting $\tan(\phi/2)=x$, we obtain

$$y_n(H, \beta_n, H_m) = \frac{2}{\pi^2 \beta_n H_m} \int_{-\infty}^{\infty} \frac{(1-\chi^2)\, d\chi}{\xi \chi^4 + 2\eta \chi^2 + \zeta} \tag{10}$$

with

$$\xi = \beta_n^{-2} (H - H_m)^2 + 1$$
$$\eta = \beta_n^{-2} (H^2 - H_m^2) + 1$$
$$\zeta = \beta_n^{-2} (H + H_m)^2 + 1$$

Then the finite integration is easily obtained with use of the complex integration as

$$y_n (H, \beta_n, H_m) = \frac{2^{3/2}}{\pi \beta_n H_m} \cdot \frac{\zeta^{1/2} - \xi^{1/2}}{(\xi\zeta)^{1/2} \{(\xi\zeta)^{1/2} + \eta\}^{1/2}} \tag{11}$$

Here $y_n(H, \beta_n, H_m)$ is normalized as

$$\lim_{H_{m1} \to 0} \int_{-\infty}^{\infty} \int_{-\infty}^{H} y_n (H, \beta_n, H_m)\, dH = 2$$

Least Squares Estimation For the three-component analysis employed in this series of work, eq.(1) should be rewritten as

$$y(H) = w_b\, y_b (H, \Delta H_b) + w_m\, y_m (H, \beta_{mg}, \beta_{ml}) + w_n\, y_n (H, \beta_n, H_m) \tag{12}$$

Here $y_b(H, \Delta H_b)$, $y_m(H, \beta_{mg}, \beta_{ml})$, and $y_n(H, \beta_n, H_m)$ are given by eqs.(4), (6), and (11), respectively. The parameters ΔH_n, β_{mg}, β_{ml}, β_n, two of w_b, w_m, w_n, and A in eqs.(12) and (3) are to be determined so as to minimize the sum of squares of the difference between the observed and calculated spectra over the full range of field in which the resonance appears. This least squares calculation was carried out according to the so-called simplex method* which was proposed by Spendley et al.(23)

---

* Instead of the simplex method, any algorithm(22) for least squares estimation of nonlinear parameters may be used.

---

and developed by Nelder and Mead(24). Since the peak of the broad component was clearly recognized and the line-width could be determined for most spectra examined, the parameter ΔH_b was equalized to the line-width or fixed to be a value slightly larger than it by 0.1-0.3 G and the remaining six parameters were allowed to float until the best fit was obtained according to the algorithm. Thus the optimum set of the parameters in eq.(12) was determined for each observed spectrum and the mass fractions w_b, w_m, w_n as well as the line-widths or the second moments of the three components were discussed in connection with the phase structure of samples.

The three-component analysis described here is able to use universally for many crystalline polymers such as polyoxymethylene(5), polyethylene oxide(5), polyvinylidene chloride(5), nylon-6(5, 25), polypropylene(5), and etc., if a proper elementary spectrum is used for the broad component depending on the polymer sort. The spectrum for a

polymer at a very low temperature, where any local motion of chains is generally hindered, does not depend appreciably on the crystallinity but coincides with that of the completely crystalline material to a sufficient approximation. Therefore, as the elementary spectrum for the broad component a spectrum observed at a very low temperature for the respective polymer or its highly crystalline sample if available can be universally used.

2.3. Results and Discussion

Figure 1 shows the spectrum taken at room temperature for the two samples drawn 6 times by the two modes together with the three components analyzed in the procedure mentioned above. Here, the samples were fixed, the fiber axis of those was parallel to the direction of the magnetic field.

It is known that the spectrum for oriented samples depends on the alignment of sample to the direction of the field in the measurement. This will be because some molecular mobilities in a special direction to the field do not produce appreciable effects on the spectrum. In the alignment of the stretched samples parallel to the field direction, the broad component was observed as broad as the highest (largest ΔH_b), and the separation from other compoents associated non-crystalline regions was most distinct. Hence, we are only concern with spectra taken in such alignment in this paper for convenience.

Table 1 summarizes the results of the three-component analysis for drawn samples, together with the degree of crystallinity $(1-\lambda)_d$ obtained

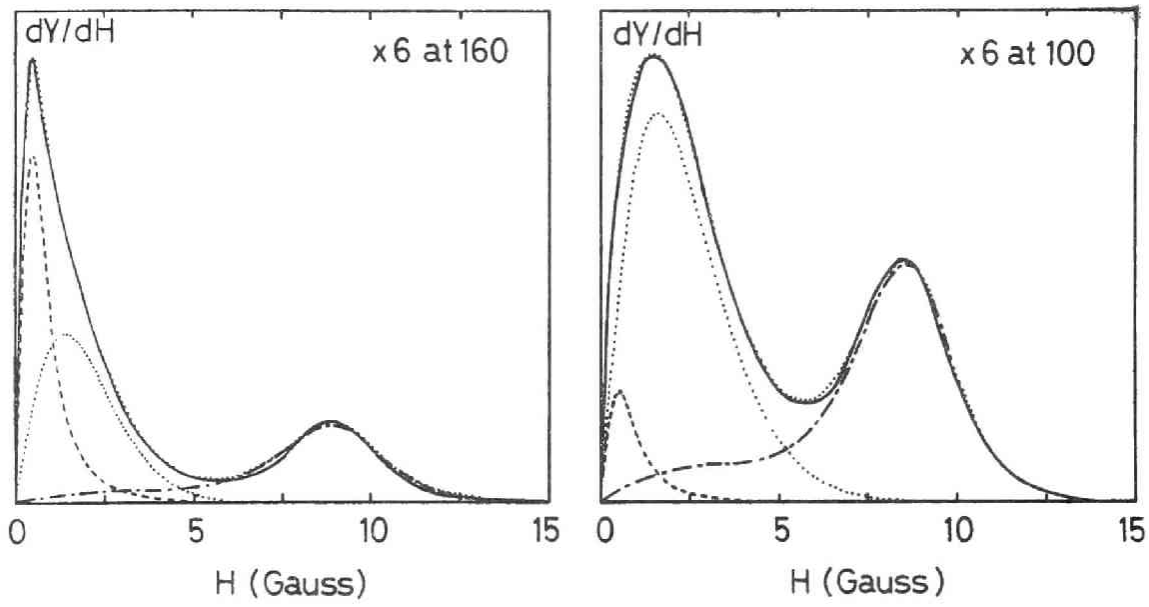

Fig. 1. Three-component analysis at room temperature for 6-fold stretched gel at 160 and 100°C. Dashed, dotted, and broken lines indicate narrow, medium, and broad components, resp. Thick dotted and the solid lines indicate the composite curve for the three components and the experimental spectrum, respectively.

from density measurements. Here, w_b, w_m, w_n, and ΔH_n, ΔH_m, ΔH_n, designate the mass fraction and the line-widths of the broad, medium and narrow component, respectively. $\langle \Delta H_2^2 \rangle_m$ is the second moment of the medium component.

As can be seen, the sample stretched in the melt comprises abundant narrow component with a very narrow line-width and less amount of medium component. Contrary to this, for the sample stretched at 100°C the medium component is not only abundant but also its line-width is very wide. These results suggest that the former sample has a very mobile

Table 1. Results of Three Component Analysis for the 6-fold Stretched Gel at 160°C and 100°C.

Sample	$(1-\lambda)_d$	Mass Fraction			Line Width (gauss)				Second Moment (gauss^2)	
		w_b	w_m	w_n	ΔH_b	ΔH_m	ΔH_n	$\Delta H'_n$	$\langle \Delta H_2^2 \rangle_b$	$\langle \Delta H_2^2 \rangle_m$
stretched at 160°C	0.636	0.673	0.213	0.114	17.8	2.8	0.8	0.9	27.5	3.2
stretched at 100°C	0.648	0.689	0.294	0.017	17.0	3.2	0.9	1.0	24.8	4.3

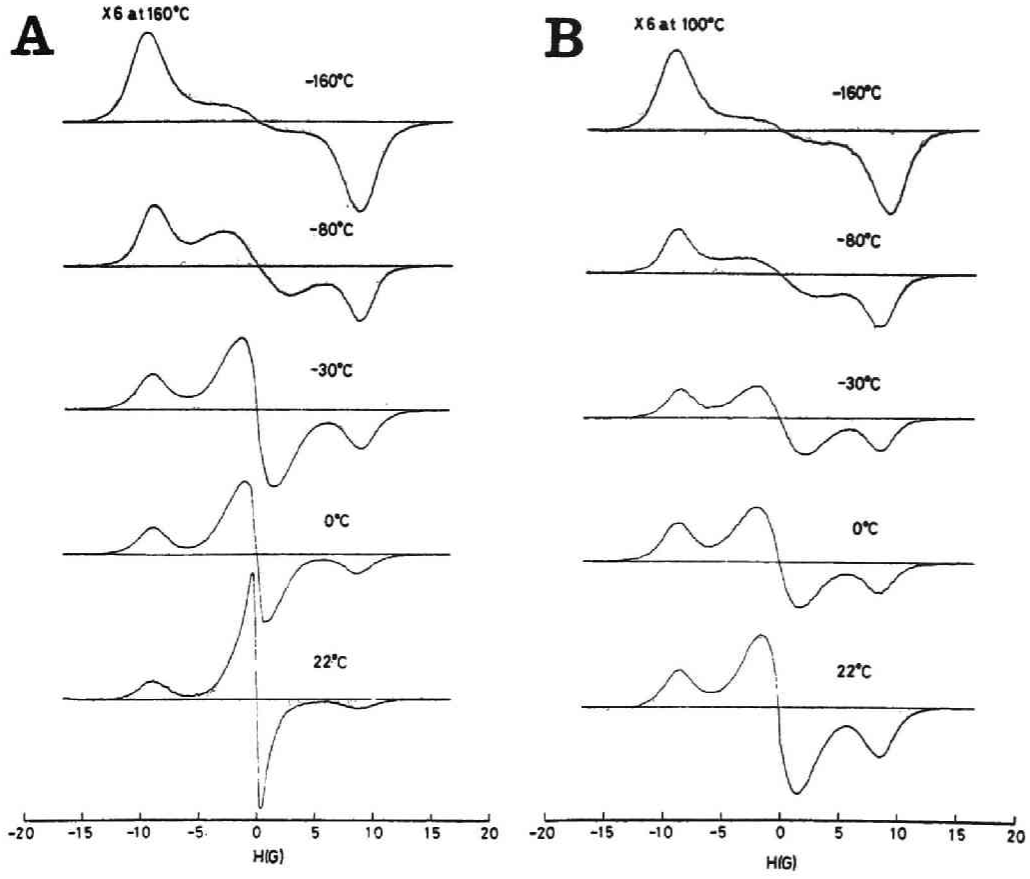

Fig.2. NMR spectra at various temperatures for gel sample stretched at 160°C (A) and at 100°C (B).

amorphous content whereas the latter has a rather great amount of immobile amorphous content, since the smaller line-width is associated with larger molecular mobility.

Figure 2 shows the changes of the NMR derivative absorption spectra with temperature for two drawn samples. The spectra for the two samples are similar with each other at lower temperatures, but enhanced difference between the spectra for the two samples is clearly seen with increasing temperature. The results of the three-component analysis conducted for the two samples

over a wide range of temperature are shown in Figure 3. Here, the mass fractions, the line-width or second moment are plotted against temperature. For the both samples, at a temperature below -100°C the medium component w_m appears and increases with the decrease of the broad component w_b as temperature increases. This suggests that a local molecular motion, which corresponds to the so-called γ-relaxation recognized in dynamic mechanical or dielectric measurements, originates in the noncrystalline region and spreads over the whole noncrystalline region.

At about -50°C the narrow component appears with decreasing w_m for the sample stretched in the melt. This suggests that a molecular motion with larger mobility such as a micro-Brownian motion of molecular chains, corresponding to the so-called β-relaxation, originates and spreads the noncrystalline region. On the other hand, for the sample stretched at 100°C, the narrow component does not appear until 0°C and even if the temperature further rises it does not increase appreciably. This suggests that the noncrystalline material of this sample has a rather restricted conformation of molecular chains and such larger mobility as the micro-Brownian motion could not appear appreciably but to only a limited extent.

The difference in the phase structure between the two samples is evidently recognized also in the second moments and the line-widths of the medium and narrow components, respectively. Smaller values for both of $\langle \Delta H_2^2 \rangle_m$ and ΔH_n are associated with the sample stretched in the melt over a wide range of temperature. This evidently shows larger molecular mobility in the noncrystalline regions for this sample.

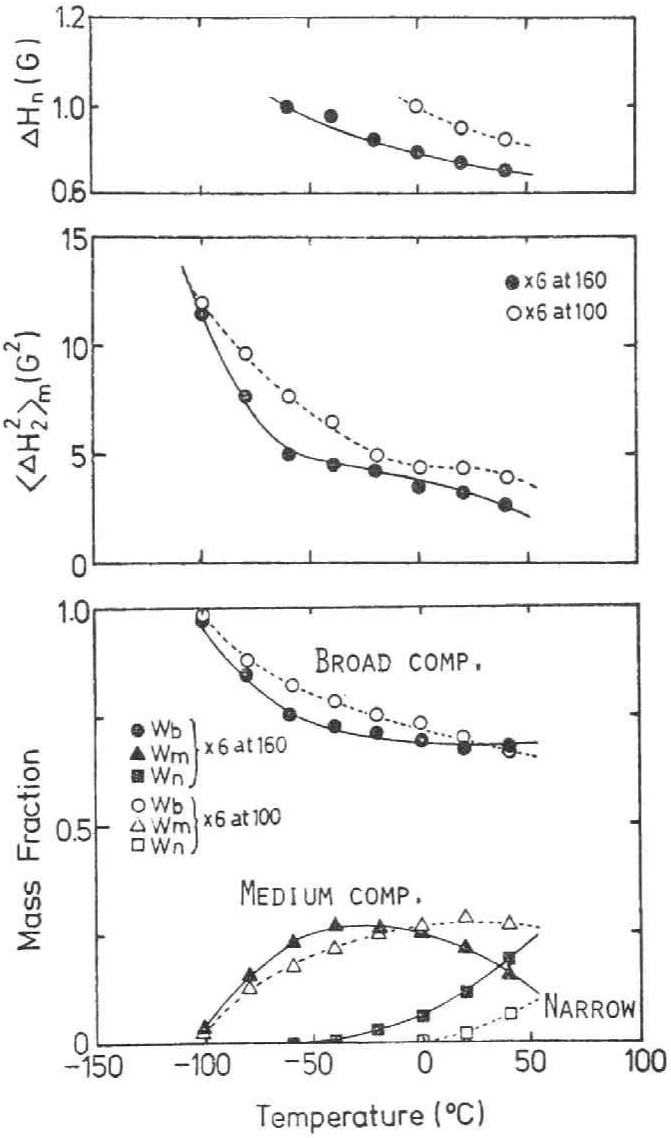

Fig.3. Mass fractions, line-widths or second moment of three components as a function of temperature for 6-fold stretched gel at 160°C and 100°C.

It was already concluded by X-ray and birefringency studies that the molecular chains in the noncrystalline regions for this sample are rather unoriented although the crystallites are highly oriented with c-axis parallel to the stretching direction. The NMR analysis cited here evidently adds an important information to this conclusion that the molecular chains in the noncrystalline regions are not only unoriented but also they are in a versatile conformation of molecular chains with larger mobility.

Reference

1. C.W.Wilson and G.E.Pake, J.Polym.Sci., 10, 503 (1953)
2. K.Bergmann and K.Nawatki, Kolloid-Z.u.Z.Polym., 219, 132 (1967)
3. K.Bergmann, Ber.Bunsenges Phys.Chem., 74, 912 (1970)
4. K.Bergmann and K.Nawotki, Kolloid-Z.u.Z.Polym., 250, 1094 (1972)
5. K.Bergmann, Kolloid-Z.u.Z.Polym., 251,962 (1973)
6. E.W.Fischer, H.Goddar, and W.Piesczek, J.Polym.Sci., C32, 149 (1971)
7. H.G.Zachmann, Kolloid-Z.u.Z.Polym., 251, 951 (1973)
8. O.Phaovibul, J.Loboda-Cackobic, and R.Hosemann, Makromol.Chem., 175, 2991 (1974)
9. J.B.Smith, A.J.Mnuel and I.M.Ward, Polymer, 16, 57 (1975)
10. R.Kitamaru, F.Horii and S.-H.Hyon, J.Polym.Sci.Polym.Phys.Ed., 15, (1977)
11. R.Kitamaru, F.Horii and S.-H.Hyon, ACS.Plym.Preper., 17, 549 (1976)
12. R.Kitamaru and F.Horii, "NMR Aproach to the Phase Structure of Linear Polyethylene", Adv.Polym.Sci., Springer-Verlag, Heidelberg, in press.
13. F.Horii, R.Kitamaru, and T.Suzuki, J.Polym.Sci.Polym.Lett.Ed., 15, 65 (1977)
14. H.S.Gutowsky and G.E.Pake, J.Chem.Phys., 18, 162 (1950)
15. W.Pechhold, Kolloed-Z.Z.Polym., 228, 1 (1968)
16. W.L.F.Golz and H.G.Zachmann, Kolloid-Z.Z.Polym., 247, 814 (1971)
17. U.Eichhoff and H.G.Zachmann, Ber.Bunsenges Phys.Chem., 74, 919 (1970)
18. H.Wahlquist, J.Chem.Phys., 35, 1708 (1961)
19. G.W.Smith, J.Appl.Phys., 35, 1217 (1964)
20. R.Arndt, J.Appl.Phys., 36, 2522 (1965)
21. H.A.Buckmaster and J.C.Dering, J.Appl.Phys., 39, 4486 (1968)

22. For example, J.Kowalik and M.R.Osborne; Methods for Unconstrained Optimization Problemes, American Elsevier Publ., New York, 1968

23. W.Spendley, G.R.Hext, and F.R.Himsworth, Technometrics, 4, 441 (1962)

24. J.A.Belder and R.Mead, Computer J., 7, 308 (1965)

25. K.Ogawa, F.Horii, S.-H.Hyon, R.Kitamaru, T.Yasuda, and T.Okuno, Polym.Prepr., Japan, 26, 8 (1977)

Chapter 3

THE PREPARATION OF A NEW TYPE OF SYNTHETIC FIBER FROM LINEAR POLYETHYLENE BY IRRADIATION CROSSLINKING

3.1. Introduction

Synthetic fibers with excellent mechanical properties such as high tenacity and low elongation at the break can be produced from linear polyethylene with a proper average molecular weight through a conventional melt spinning and following drawings. In comparison with other synthetic fibers those are excellent in various properties such as electro resistance and chemical stability. Hence, those are widely used at present when such properties are required. However, since the melting temperature or softening point of those fibers are not high enough and usually shrink to high extents if boiled in water or heated in air at relatively low temperatures such as 110°C, their uses as usual clothing fibers are rather limited.

The polyethylene fibers, as those are first spun from the melt through a screw extruder, are very dull such that those tenacity is as low as 1 gram per denier and elongation at the break exceeds several hundred percents even if those are spun with a very high rate of stretch. To improve these fiber properties those are usually drawn to high extents at high temperatures below the melting point of the polymer after melt spinning. This heat-drawing process sufficiently increases the tenacity and decreases the elongation at the break. However, it never elevates the melting point and no improvement in those poor

heat-resistant property is obtained but the temperature at which the fibers begin to shrink by heating becomes lower owing to the improved molecular orientation parallel to the drawing direction of the process. In the circumstances fibers that simultaneously have excellent mechanical and heat-resisting properties have not been made from polyethylene to date. However, in a recent paper(1) it is found that if a lightly crosslinked polyethylene of adequate crosslink density is crystallized from the melt under conditions involving high degree of molecular orientation, a transparent product with very high melting temperature is obtained. Furthermore the origin of the transparency and the high melting temperature for the sample is investigated in relation to the crystalline structure(2). These works may suggest a possibility to prepare fibers with excellent mechanical properties as well as high melting temperature from linear polyethylene by irradiation crosslinking. This chapter deals with a novel method to prepare such fibers.

3.2. Experimental

Samples

A commercial whole polymer Marlex 50 from Philips Petroleum Co. was used as starting material. It had a viscosity average molecular weight of 136×10^3.

Spinning

The polymer was extruded out through an orifice of 2.0 mm diameter

at a temperature of 220°C by a spinning apparatus equipped with a screw of 15 mm diameter and wound up on a cylindrical bobbin at room temperature with stretch rates of 1.0 or 5.0. Here, the stretch rate is defined to be a ratio of the winding speed to the speed by which the molten polymer is extruded out from the orifice. Hence a stretch rate of 1.0 means that the melt-spinning was done without stretch. The smaller and larger stretch rates gave us filaments with diameters of 1.5 mm and 0.67 mm, respectively.

Irradiation

The filaments wound on a cylindrical bobbin were next irradiated with an electron beam from 2 MEV Van de Graaff in air to dosages of 10, 20, and 30 mega-rads, respectively. The dose rate was 0.24 mega-rad per second and the samples bobbin was rotated during the irradiation. The gel fraction W_g of the irradiated samples (mass fraction of the non-soluble part in the total mass) was evaluated by extracting with boiling xylene and drying. The results are listed in Table 1.

As well-known, the presence of air greatly reduces the crosslinking effect of irradiation but relatively large values of W_g are imparted to the samples depending on the stretch rates, though the W_g are of course much smaller than that when the irradiation was conducted in vacuo(1). It is supposed that because very high rate of irradiation was employed the diffusion of air in the solid samples during the irradiation was much limited and the effect thereof on the crosslinking was minimized.

Table 1. The Gel Fraction of the Filaments and the Dosage Irradiated.

Sample	Dosages irradiated in mega-rads		
Filament spun with a stretch rate of	10	20	30
1 (non-stretch)	0.127	0.430	---
5	0.314	0.533	0.612

Drawing

The irradiated and non-irradiated filaments were next drawn in air or water at various temperatures. Here, the irradiated samples were used without extracting those soluble fractions. The non-irradiated samples could be drawn only at temperatures below the melting point of the polymer but the irradiated samples could be drawn to high extents even at much higher temperatures, since those had rubbery elasticity in the molten state because of the presence of inter-molecular crosslinkages introduced by the irradiation. Under the circumstances the non-irradiated samples were drawn at temperatures of 25 and 100°C, and the cross-linked samples were drawn to different extents at temperatures of 25, 100, and 180°C. The drawing at 25 and 180°C was conduced in air but that at 100°C was done in boiling water. The various fiber properties of the drawn samples were measured and the results are summarized in Tables 2 and 3.

Measurements of Fiber Properties

The density was measured by a conventional density gradient column of toluene and carbon tetrachloride at 30°C.

The strength and elongation at the break and Young's modulus were measured by a tensile tester, Tensilon MT-III from Toyo Baldwin Co. with a stretching rate of 200 %/min at 25°C.

The heat resistance was estimated with the length shrinkage of samples when boiled in water or heated in air. The fibers tested were boiled in water for one hour under a load of 10 mg/denier and the shrinkage was measured. The results are shown in the last columns in Tables 2 and 3. The length change of the samples under a load of 10 mg/denier was observed during heating in air with a rate of 1°C/min. The shrinkage based on the original length before the heating was plotted against temperature in Figure 1.

3.3. Results and Discussion

Some fiber properties of the drawn filaments that were made from the melt-spinning without stretch and irradiation according to the aforementioned procedures are shown in Table 2. The filament spun without stretch is very dull as shown by its very low strength and extremely large elongation at the break (see data for Sample 1 in the table). The effects of the irradiation to 10 or 20 Mega rads on the tensile properties are rather negligible if minor decrease in the elongation was recognized (Samples 4 and 8). However, enhanced

Table 2. The Properties of the Filaments Spun Without Stretch and Drawn after Irradiation.

Sample		Drawing		Density	Tensile Properties			
No.	Description	Temp. °C	Ratio*	g/cm^3	Strength at Break g/denier	Elongation at Break %	Young's Modulus kg/mm^2	Shrinkage in Boiling water, %
1	non-irradiated Wg = 0	-	(non-drawn)	0.9463	0.23	590	---	---
2		25	8.5	0.9480	----	---	---	13.3
3		100	8.5	------	3.21	30	314	8.3
4	Irradiated 10 Mrad Wg =0.127	-	(non-drawn)	0.9463	0.22	560	34	---
5		25	7.0	0.9480	----	---	---	16.5
6		100	9.5	0.9495	3.4	15.8	333	8.5
7		180	14.3	0.9466	2.8	15.8	431	2.1
8	Irradiated 20 Mrad Wg =0.435	-	(non-drawn)	------	0.22	340	---	---
9		25	5.0	------	----	---	---	14.5
10		100	7.8	------	2.8	23.4	258	8.9
11		180	10.0	------	3.2	21.1	323	2.3

* Ratio of the length of drawn filaments to the original length before the draw.

improvement in the fiber properties is obtained by the drawing for both non-irradiated and irradiated samples irrespective of the irradiation and the temperature at which the drawing was conducted. Thus fibers that have a high strength as large as more than 3 g/denier and a small elongation as low as 30% were obtained. However, the filaments made from non-irradiated sample shrink more than 8 percents even if drawn at a high temperature of 100°C in boiling water. Contrary, the filaments from the irradiated samples drawn at a temperature of 180°C not only have excellent fiber properties but also they shrink only to 2 or little larger percents in boiling water. Note the data for Samples 7 and 11. These exhibit enough high strength and low elongation at the break together with high moduli.

In Table 3, the fiber properties made by the melt-spinning with a stretch rate of 5 and following irradiation and drawing are listed. In this case also, it is shown that if the irradiated samples are drawn in the molten state to high extents, the tensile mechanical properties not only are improved but also the resistance to boiling water is improved. Although the shrinkage percents in boiling water for those filaments made from the spinning with the higher stretch rate are little larger than those for samples made from the spinning without stretch (shown in Table 2), the heat-resistance of those is still excellent. For example, the shrinkage percent of Samples No. 14, 17, and 18 in air is plotted against in Figure 1. Sample 18 that was obtained from the crosslinked sample by drawing in the molten state does not shrink appreciably until 110 or 120°C, while the fibers drawn at the lower

Table 3. The Properties of the Filaments Spun with a Stretch Rate of 5 and Drawn after Irradiation.

Sample		Drawing		Density	Tensile Properties			
No.	Description	Temp. °C	Ratio*	g/cm^3	Strength at Break g/denier	Elongation at Break %	Young's Modulus kg/mm^2	Shrinkage in Boiling water, %
12	non-irradiated Wg = 0	-	(non-drawn)	0.9326	0.54	813	52.6	2.2
13		25	6	0.9352	----	---	---	14.0
14		100	5.5	0.9428	----	---	---	4.8
15		100	12	0.9483	4.68	18.4	361.9	8.3
16	Irradiated 10 Mrad Wg =0.314	-	(non-drawn)	0.9332	0.52	713.4	57.7	---
17		100	5.5	0.9405	----	---	---	4.8
18		180	5.5	0.9420	1.99	56.4	256.7	2.1
19		180	9.0	0.9495	2.67	12.4	344.7	4.2
20	Irradiated 20 Mrad Wg =0.533	-	(non-drawn)	0.9336	0.45	620	56.2	---
21		100	5.5	------	2.03	94	178.4	3.7
22		180	7.5	0.9463	3.11	10.5	359.0	6.7
23	Irradiated 30 Mrad Wg =0.612	-	(non-drawn)	0.9340	0.44	560	55.7	---
24		100	5.5	------	2.00	66.4	184.4	8.3
25		180	5.0	0.9420	2.52	41.2	203.4	5.3

* Ratio of the length of drawn filaments to the original length before the draw.

temperatures below the melting point begin to shrink at much lower temperatures.

Thus a novel method to prepare a new type of fiber that has excellent mechanical and thermal properties from linear polyethylene is principally established. As mentioned already the practical use for polyethylene fibers is much limited by those poor heat-resistant properties despite those excellent mechanical, chemical, and electric properties. Moreover, olefinic synthetic fibers including isotactic

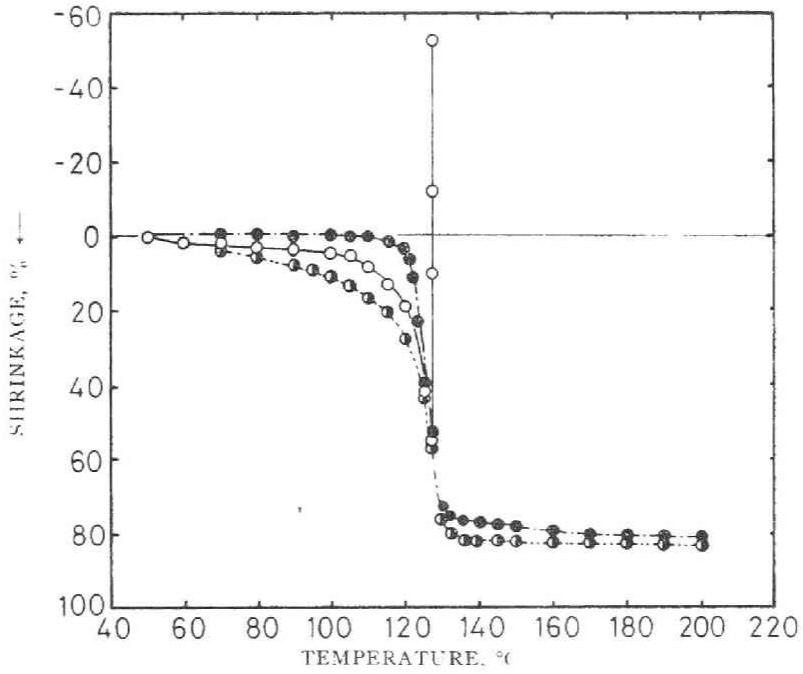

Fig. 1. Shrinkage percents *vs.* temperature for 5.5-fold drawn filaments at different temperatures. Open, half closed, and closed circles show data for uncrosslinked filament drawn at 100°C, 10Mrad-irradiated filaments drawn at 100°C and at 180°C, respectively(Samples 14, 17, and 18 in Table 3, respectively).

polypropylene fibers are sometimes disliked by those waxy feel in the use for clothing fibers. It was noted that the waxy feel of the polyethylene filaments was almost removed by the irradiation crosslinking and following drawing in the molten state. Therefore, the procedure reported here to improve the heat-resistant properties and remove waxy feel of polyethylene fibers will become to be of very interest according to the progress in petroleum and radiation industries.

However, to realize this procedure in the industrial scale many problems still remain to be resolved. For example, as discussed elsewhere(1) crosslinked units must be introduced into polyethylene fibers by irradiation at least more than one unit per one polymer molecule to guarantee the rubbery elasticity of the polymer in the molten state, that enable us to draw in that state. Hence, if a lower molecular weight sample is used, the larger amount of crosslinked units (the larger crosslink density) is needed. However, since crosslinked units act as non-crystallizable units during the crystallization, those should be as fewer as possible in so far as the rubbery elasticity in the melt is guaranteed. Thus it is clear that the molecular weight sample to be used should be as large as possible.

As a matter of fact, when a lower molecular weight of sample was used, any improvement in the heat-resistant properties of the resultant products was not recognized. However, if the molecular weight becomes to be large the melt-spinning will become to be very difficult. Even the polymer with a molecular weight of 136×10^3 that was used in this work was very difficult to spin so that enough thin filament could not

be obtained by the present spinning technique. If higher stretch rate is employed for the spin, of course thinner filaments could be obtained, but it will result in an increase of molecular orientation before the irradiation crosslinking. As the result, the character of the process during which the crystallization is achieved under high degree of molecular orientation will be lost. Thus the spinning technique for a polymer with very high molecular weight and hence with very high viscosity in the melt without occurrence of appreciable molecular orientation will be one of problems to be resolved to realize the process reported in this chapter for the practical application.

References

1. R.Kitamaru, H.-D.Chu, and S.-H.Hyon, Macromolecules, 6, 337 (1973).

2. R.Kitamaru and S.-H.Hyon, Makromolekulare Chemie, 175, 255 (1974).

Chapter 4.

PHASE STRUCTURE AND MOLECULAR MOBILITY OF POLYETHYLENE FIBERS BY BROAD-LINE NMR SPECTROSCOPY

4.1. Introduction

Crystalline polymers are generally transformed into the so-called fiber structure by uniaxial stretching at temperatures between the glass and melting temperatures of the polymers. In such fiber structures X-ray diffraction and optical birefringence analyses reveal that molecular chains in both of the crystalline and amorphous regions are preferentially oriented parallel to the stretching direction. However, the detailed phase structure of those remains obscured, although it is of very importance in relation to the tensile and dyeing properties in the practical use.

We have shown that a refined broad-line NMR analysis renders important information of the phase structure in terms of molecular mobility for linear polyethylene samples (1-5). It was found that the phase structure of polyethylene depends greatly on the molecular weight as well as the crystallization modes, including crystallization from the pure melt and from dilute solution(1-4). For drawn polyethylene fibers, Fischer et al.(6) have studied the effects of annealing and stress on the phase structure by analyzing the broad-line NMR spectrum. In this chapter the NMR spectra of polyethylene fibers drawn to different degrees is analyzed in a very wide range of temperature(7). The results

are served to elucidate the effects of drawing on the phase structure and temperature dependence thereof.

4.2. Experimental Part

Samples

A commercial whole polymer Sholex 6009M from Japan Olefin Chem. Ltd. was used as starting material. It had a viscosity-average molecular weight of 8.0×10^4. The polymer was extruded out through an orifice 2.0-mm diameter at 220°C by a spinning apparatus equipped with a screw of 15-mm diameter and wound up on a cylindrical bobbin at room temperature with a draft ratio of about 17. The filaments obtained were then drawn to different degrees with a continuous drawing machine in polyethylene glycol bath at 100°C. The samples are characterized by draw ratio, defined to be ratio of the drawn length to the original.

Estimation of Molecular Orientation

The molecular orientation of stretched samples was inquired separately for the crystalline and amorphous phases by using an wide angle X-ray and birefringence techniques. For samples with higher draw ratios, the orientation factor for c-axis of the orthorhombic crystal form was evaluated with use of the diffraction from (002) crystal plane was used. While, for samples with draw ratios lower than 2 times, since the (002) diffraction could not be detected with sufficient precision, the orientation factors for a- and b-axes of the crystal lattice were first evaluated with diffractions from (200) and (020) crystal planes, respectively, and then the quantity for the molecular chain axis was obtained

using the relation that the summation of all quantities for the a-, b-, and c-axes of the crystal lattice is zero. The detailed procedure for the estimation is described in Chapter 1.

Spectrometry and Analysis

The first derivative NMR obsorption spectrum was obtained over a wide range of temperature -80∿+40°C for drawn polyethylene fibers randomly packed into a glass tube 18-mm diameter with a JNM-PW-60 NMR Spectrometer (JEOL Ltd.). The magnetic field slowly swept was modulated at 35 Hz and amplitude of 0.4 G under a constant sub-field with a frequency of 60 MHz.

The spectrum observed was analyzed by a technique(1-5) based on the method of Bergmann and Nawotki(8-11), decomposing into three parts; broad, medium and narrow components. The detailed technique for the analysis is given in Chapter 2.

4.3. Spectrum Analysis at Room Temperature

Figure 1 shows the spectra for samples with draw ratios of 1, 2, 4, 6, 8, and 10 with the three-component analysis. It is shown that all spectra are well analyzed by the three components, although they differ in shape to a great extent depending on the draw ratio. In the spectra of the samples with higher draw ratios, three clear peaks can be explicitly recognized as reported for the stretched samples(12, 13).

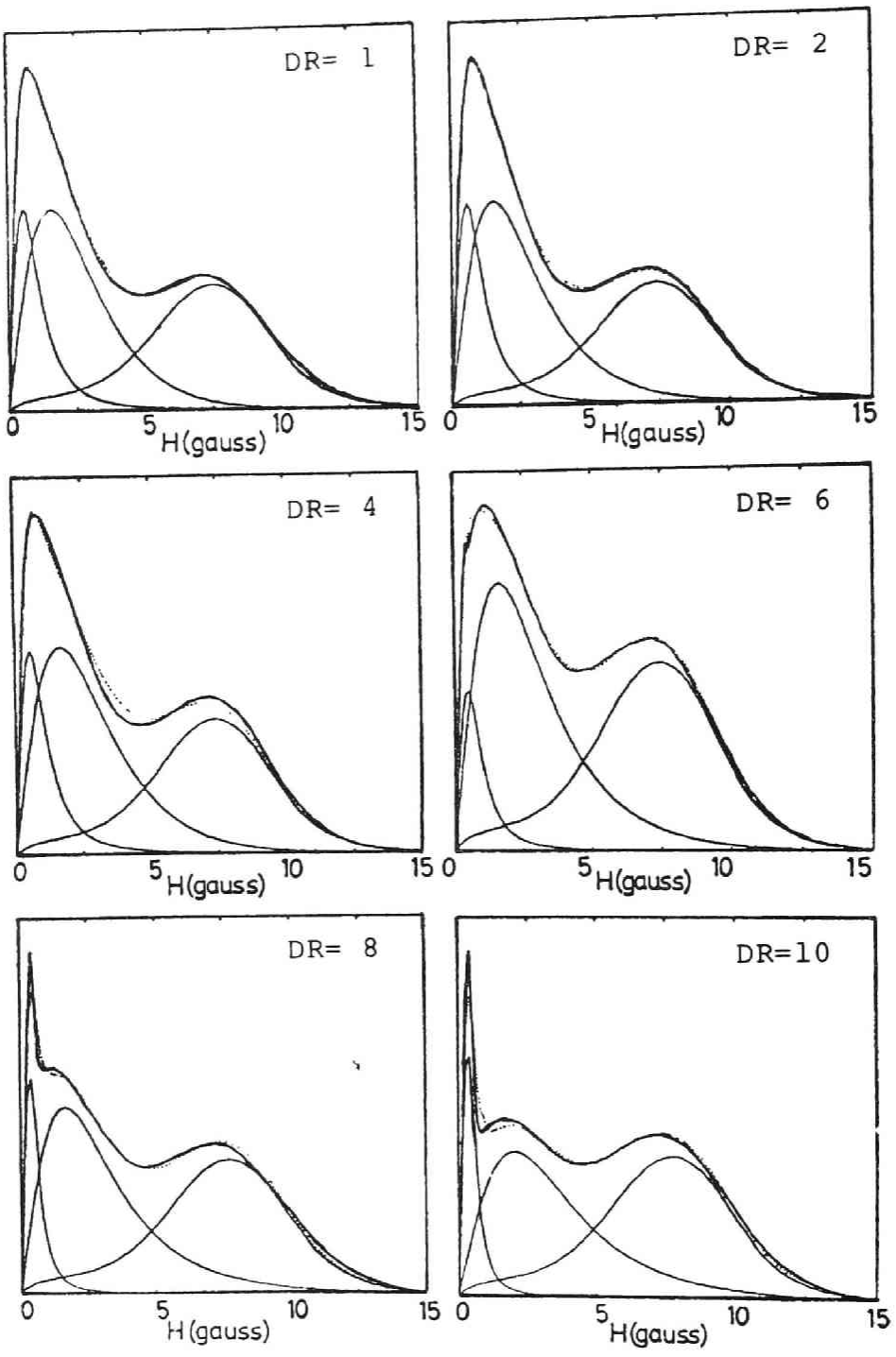

Fig. 1. Three-component analysis at room temperature for polyethylene fibers drawn to different degrees. The draw ratio(DR) is indicated in each figure. The thick solid and dotted lines indicate the experimentally observed spectra and the composite spectra the three components, respectively. Thin solid lines indicate the narrow, medium, and broad components, respectively, from the left side.

Table 1 summarizes the results of the three-component analysis, together with the densities of the samples measured at 30°C and orientation factors of the molecular chain vector in crystalline and amorphous phases. Here, w_b, w_m, w_n, and ΔH_b, ΔH_m, ΔH_n, designate the mass fractions and the line-widths of the broad, medium and narrow components, respectively. $\langle \Delta H_2^2 \rangle_m$ is the second moment of the medium component. It is shown that both of f_c and f_a increase with increasing draw ratio. This suggests that a typical fiber structure is produced by the drawing procedure. The molecular chains not only in the crystalline region but also in the noncrystalline region are preferentially oriented parallel to the stretching direction with increasing draw ratio.

It is to be noted here that the mass fraction of the broad component is not altered appreciably by drawing so that $w_b \simeq 0.689 \pm 0.009$ independent of draw ratio. On the other hand, the density increases from

Table 1. Three-Component Analysis for Drawn Polyethylene Filaments

Draw Ratio	Density at 30°C (g/cm^3)	Orientation Factor		Mass Fraction			Line Width and Sec.Mom. in G and G^2, resp.			
		f_c	f_a	w_b	w_m	w_n	ΔH_b	ΔH_m	$\langle \Delta H_2^2 \rangle_m$	ΔH_n
1	0.9502	0.383	0.293	0.685	0.257	0.058	15.0	3.19	5.9	1.00
2	0.9512	0.615	0.494	0.679	0.263	0.058	14.8	3.06	6.3	0.98
4	0.9532	0.739	0.733	0.680	0.268	0.052	14.8	3.25	6.9	0.98
6	0.9546	0.855	0.835	0.691	0.288	0.021	14.9	3.28	8.4	0.80
6*	0.9581	0.863	0.797	0.711	0.266	0.023	14.9	3.28	6.4	0.80
8	0.9602	0.924	0.884	0.698	0.287	0.015	15.2	3.36	9.5	0.45
10	0.9662	0.972	0.898	0.698	0.289	0.013	15.2	4.06	11.3	0.40

* annealed at 100°C for 1 hr under fixed state.

0.9502 to 0.9662 with increasing draw ratio. If a constant density is assumed for the amorphous material, this result must imply the increase of the degree of crystallinity with stretching. However, the density of the amorphous material may be changed appreciably with stretching. For example, it was reported by Peterlin and others(14) by X-ray scattering analysis that the density of the amorphous content was increased when stretched to high extents. If the unit-cell density is assumed to be 1.00 and the density of the amorphous region is assumed to change from 0.85 to 0.89 with drawing referring to their result, the degree of crystallinity is estimated to be unchanged within the experimental error such as 0.698 ± 0.04. This value is in good accord with the w_b obtained by the NMR analysis. If different velues are assumed for the density of the amorphous region, the result may be changed appreciably. However, at the present time we may conclude that the degree of crystallinity is not changed appreciably by drawing and the w_b well corresponds to the crystalline fraction in a similar manner for undeformed samples(1-4).

On the other hand, the analysis results concerned with the noncrystalline components are greatly altered with drawing. A significant increase in $\langle \Delta H_2^2 \rangle_m$ is recognized with increasing draw ratio. This is considered as a result of the fact that the molecular chains in the noncrystalline region are oriented as shown by the increase of f_a and the versatility of the conformation is confined upon stretching.

Furthermore, a significant decrease in both of the w_n and ΔH_n is recognized with increasing draw ratio. It shows that some amorphous

molecular chains with liquidlike mobility are stretched with macroscopic drawing and come to contribute to the medium component with losing the liquidlike mobility. Some narrow component remains even after drawing to the highest draw ratio. This will be contributed from protons that belong to methyl end-groups or methylene groups adjacent to them. Since these protons are thought to be insensible to the macroscopic stretching and to be mobile, the decrease of ΔH_n with increasing draw ratio will be well understood.

In conclusion, the spectrum analysis at room temperature shows several important changes in the phase structure upon stretching at 100°C. Before stretching the sample filament has a phase structure approximately similar to the bulk-crystals previously discussed(1-3), although some preferential orientation of molecular chains parallel to the filament direction exists as suggested by the f_c and f_a larger than zero. It comprises the lamellalike crystallites and amorphous interfacial and interzonal materials. Such a phase structure is drastically changed with macroscopic stretching at the high temperature and the so-called fiber structure is produced.

In the fiber structure, molecular chains in the crystalline region are not only highly oriented parallel to the fiber axis but also a majority of molecular chains in the noncrystalline region are highly oriented so that the conformational versatility as well as the mobility of molecular chains are much limited. But even in highly drawn fibers a significant amount of amorphous material with a liquidlike mobility still exists if minor.

4.4. Temperature Dependence of the Phase Structure

I have discussed the phase structure of the fiber samples as a function of the draw ratio in terms of molecular mobility by analyzing the spectrum at room temperature. I next consider the phase structure as a function of temperature by the three-component analysis of the spectrum in a wide range of temperature.

Figure 2 demonstrates the three-component analysis of spectra for the polyethylene fibers. Despite of the large difference in the overall line shape, the composite curve of the three components analyzed is in good accord with the spectrum observed in the wide range of temperature.

In Figure 3 the mass fractions and the line widths or the second moment of the three components for samples with draw ratios of 1, 6, and 10 are plotted against temperature. It is evident that the temperature dependence of the three components can be essentially understood in terms of the β- and γ-relaxation phenomena recognized in mechanical and dielectric measurements as discussed for the bulk- and solution-crystallized samples(3,4). However, the detailed temperature dependence varies greatly with the draw ratio.

The medium component appears at a temperature higher than -100°C and increases with rising temperature, gradually as the draw ratio increases. The mass fraction of the broad component decreases and reaches an asymptotic level as the temperature rises, but this decreasing of the broad component is retarded as the draw ratio increases. This suggests that the γ-relaxation temperature, in which a local motion of molecular chains is produced in the non-crystalline region, tends to shift to a higher temperature with increasing draw ratio.

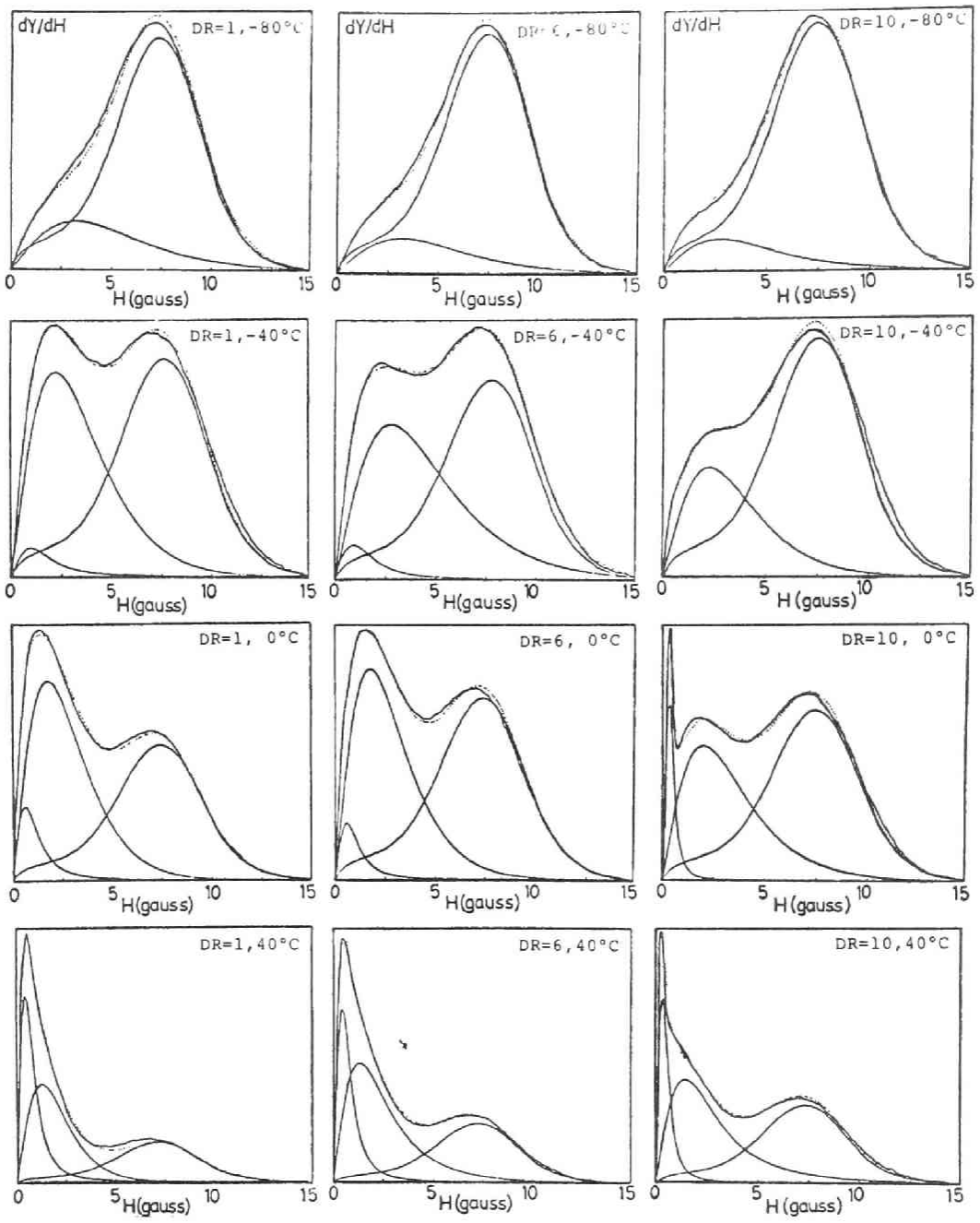

Fig. 2. Three-component analysis for drawn polyethylene fibers in a wide range of temperature. See the legend in Fig.1 about the distinction of lines. For the spectra of the all samples at -80°C and the 10-fold drawn sample at -40°C, only the medium and broad components are plotted since no narrow component was detected.

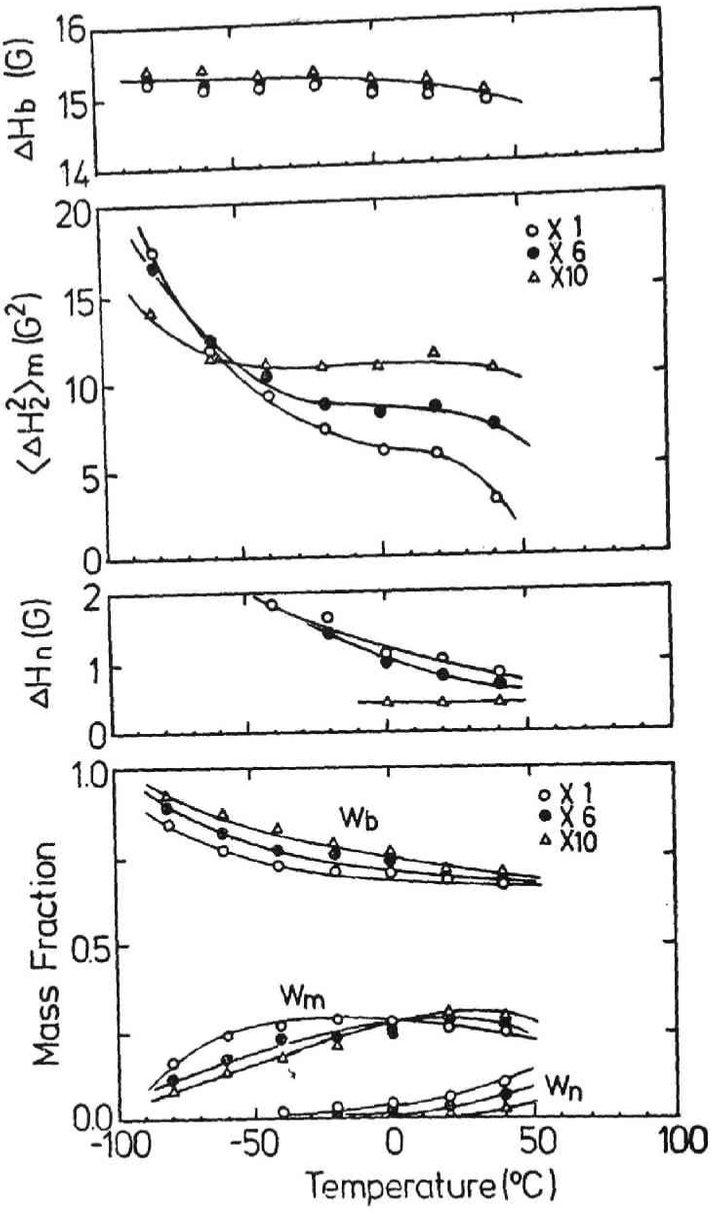

Fig. 3. Mass fractions, line-widths or second moment of three components as a function of temperature for drawn polyethylene fibers. o, •, and Δ indicate the results for the undrawn filament, and the filaments drawn 6 and 10 times, respectively.

As a result, the temperature region in which the w_b actually corresponds to the crystalline fraction is shifted to a higher temperature region such as above room temperature for the highly drawn samples, whereas the w_b well represents the crystalline mass fraction in a temperature range of -40 to +50°C for the bulk-crystallized samples(2,3). The similar effect of drawing is also evidently recognized in the behavior of the narrow component, implying that the β-relaxation process associated with the micro-Brownian motion of molecular chains in the noncrystalline region is shifted to a higher temperature with increasing draw ratio.

Such elevation of γ- and β-relaxation temperatures with increasing draw ratio will be due to the limited mobility of molecular chains in the noncrystalline region. As pointed out in the foregoing section the amorphous molecular chains align preferentially parallel to the drawing direction. Therefore, the conformational versatility and mobility of such molecular chains are considered to be much restricted.

Such highly restricted molecular mobility is also suggested by a very characteristic change of the $\langle \Delta H_2^2 \rangle_m$ with rising temperature. The $\langle \Delta H_2^2 \rangle_m$ of 10-fold drawn sample decreases in accord with the increase of the w_m as the temperature increases but it holds a very high level larger than 10 G^2 in a temperature range of about -50°C to +40°C and again decreases above 40°C. This characteristic S-type behavior and the high values of $\langle \Delta H_2^2 \rangle_m$ are approximately equivalent with those for the bulk-crystal with a low molecular

weights (3). In the low molecular weight bulk-crystallized sample, the molecular chains that contribute to the medium component must be composed of short molecular chains that are excluded from the basal plane of lamella crystallites. Such molecular chains must be in a rather extended chain conformation and comprise a parallel intermolecular alignment perpendicular to the basal plane of a crystallite (3). The large values and characteristic temperature dependence of $\langle \Delta H_2^2 \rangle_m$ recognized for the both kinds of samples may be associated with the highly extended molecular chain conformation in the amorphous region.

For the 10-fold drawn sample the ΔH_n remains in a very low level such as about 0.4 G over a temperature range examined. As discussed already, the narrow component for such a highly drawn sample will be mainly contributed by protons belonging to methyl end-groups or adjacent methylene groups insensible to the macroscopic drawing. Such components will be rather mobile even at lower temperature. Thus, the very small value of ΔH_n for the highly drawn sample will be well understood.

4.5. Effect of Swelling Agent

If partially crystalline polymers are immersed in a proper swelling agent, the phase structure of the polymers could be more distinctly examined because the swelling heightens the molecular mobility preferentially in the amorphous region. Such an attempt for stretched

polyethylene was carried out by Peterlin and Olf(15) by NMR spectroscopy. They compared the NMR spectra of drawn and undrawn samples immersed in non-protonated solvents such as tetrachloroethylene(C_2 Cl_4). It was reported that an enhanced narrowing of the narrow component took place for the undrawn sample but no effect was recognized for the drawn sample while the broad component was held unaltered for both samples. It is thought that the swelling could not appreciably heighten the molecular mobility in the amorphous region in the drawn sample, because amorphous molecular chains are in a greatly stretched conformation for such a drawn sample.

We have analyzed the spectra for the samples with different draw ratios immersed in CCl_4 at room temperature for 2 weeks(7). Figure 4 shows the spectra for 6- and 10-fold drawn fibers immersed in CCl_4. Enhanced changes are recognized by the immersion in the narrower components of the spectra, while no appreciable change is recognized in the broad component.

In Figure 5 the mass fractions of the three components and the second moment of the medium component are plotted against draw ratio. The parameters in relation to the broad component are not altered by the immersion but those in relation to the medium and narrow components are enhancedly changed by the immersion, depending on the degrees of drawing. For the samples with smaller draw ratios the medium component decreases and the narrow component increases with immersing in CCl_4, with concomitant decrease of $\langle H_2^2 \rangle_m$. These results evidently show that upon immersing in CCl_4 the molecular chains in the interfacial region become

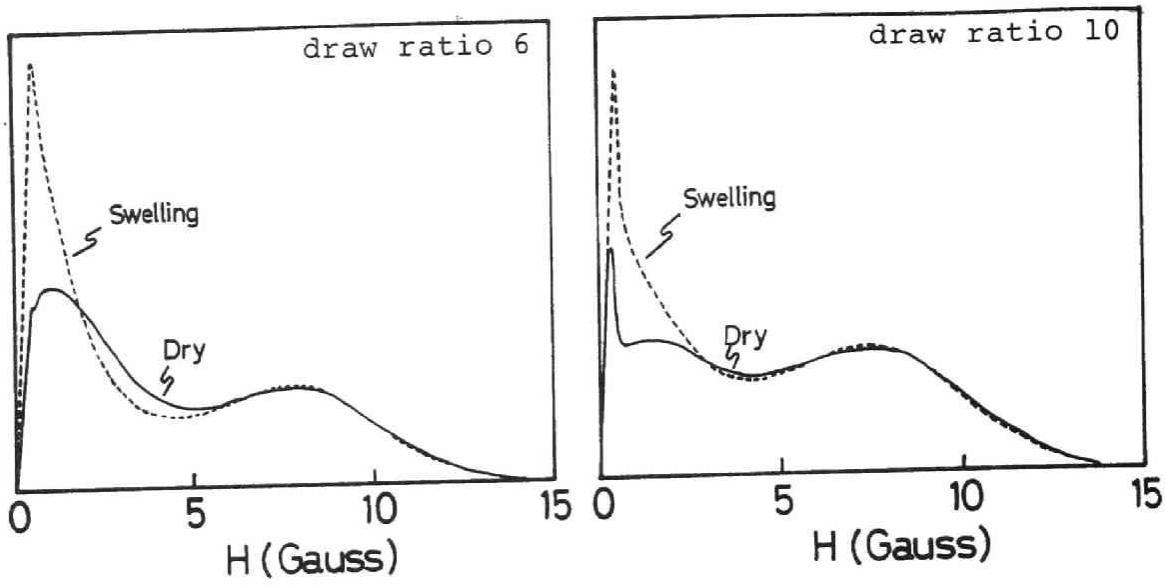

Fig. 4. The NMR spectra for 6 and 10-fold drawn filaments in the dry and swollen states in CCl_4. The solid and dotted lines indicate the results in the dry and swollen states, respectively.

to be mobile so as to exhibit a liquidlike mobility and contribute to the narrow component. The mobility of molecular chains that still contribute to the medium component is also heightened by the immersion. Since the molecular conformation in the interfacial region is rather versatile for such samples with smaller draw ratios, CCl_4 molecules will penetrate rather deeply in the region if the amount is minor. On the other hand, the effects of CCl_4 become to be negligible with the increase of draw ratio in good accord with the result of Peterlin and Olf (15). In such samples, because of the restricted molecular conformation of the amorphous material, CCl_4 molecules will not penetrate in the amorphous

region so as to give appreciable effects on the spectra.

Thus, the spectroscopy of samples immersed in CCl_4 further support the conclusion obtained in the foregoing sections that the molecular chains in the amorphous region of the drawn samples are in a restricted conformation due to the high degree of molecular orientation.

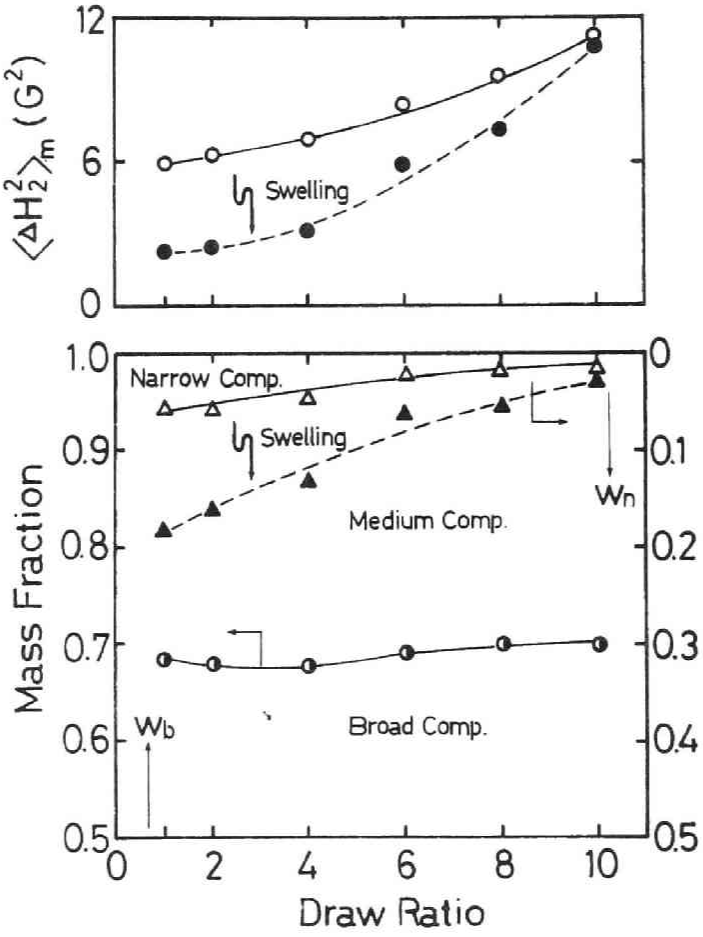

Fig. 5. Second moment of the medium component and mass fractions of the three components as a function of the draw ratio. The open and closed symbols indicate the data in the dry and swollen states, respectively. The half-closed circles indicate the data for the broad component, unaltered by the swelling.

4.6. Conclusion

The NMR spectrum analysis shows that the phase structure of the drawn fibers is quite different from that of undeformed samples. The undrawn filament obtained by a melt-spinning has an approximately similar phase structure to the bulk-crystals with corresponding molecular weight. However, the structure is drastically changed with drawing. The highly drawn filaments comprise the crystalline material as well as a noncrystalline component more than 25% in a similar manner as undeformed bulk-crystals. Nevertheless, the molecular mobility and conformation of molecular chains in the noncrystalline component are quite different. The majority of molecular chains are almost fully extended parallel to the fiber axis and associated with a very limited molecular mobility over a wide range of temperature. The swelling agents such as CCl_4 hardly heighten the mobility of such highly extended molecular chains in the noncrystalline region. However, a noncrystalline material with liquidlike mobility evidently exists if the amount is minor even in the 10-fold drawn sample.

References

1. R.Kitamaru, F.Horii and S.-H.Hyon, J.polym.Sci.Polym.Phys.Ed., 15, 821 (1977)
2. R.Kitamaru, F.Horii and S.-H.Hyon, ACS, Polym.Prepr., 17, 549 (1976)
3. R.Kitamaru and F.Horii, "NMR Aproach to the Phase Structure of Linear Polyethylene", Adv.Polym.Sci., Springer-Verlag, Heidelberg, in press.
4. F.Horii and R.Kitamaru, J.Polym.Sci. Polym.Phys.Ed., in press.
5. R.Kitamaru and S.-H.Hyon, Macromolecular Review, 14, in press (1978)
6. E.W.Fischer, H.Goddar, and W.Piesczek, J.Polym.Sci., C32, 149 (1971)
7. S.-H.Hyon, F.Horii, and R.Kitamaru, Bull.Inst.Chem.Res.,Kyoto Univ., 55, 248 (1977)
8. K.Bergmann and K.Nawotki, Kolloid-Z.Z.Polym., 219, 132 (1967)
9. K.Bergmann, Ber.Bunseges.Phys.Chem., 74, 912 (1970)
10. K.Bergmann, Kolloid-Z.Z.Polymer, 251, 962 (1973)
11. K.Bergmann and K.Nawotki, Kolloid-Z.Z.Polym., 250, 1094 (1972)
12. D.Hyndman and G.G.Origlio, J.Polym.Sci., 39, 556 (1959)
13. J.Loboda-Cackovic, R.Hosemann and W.Wilke, Kolloid-Z.Z.Polym., 235, 1253 (1969)
14. W.Glenz, N.Morosoff and A.Peterlin, J.Polym.Sci.Polym.Lett.Ed., 9, 211 (1971)
15. A.Peterlin and H.G.Olf, J.Polym.Sci., A-2, 4, 587 (1966)

Chapter 5.

ORIENTATION OF CRYSTAL PLANES IN LIGHTLY CROSSLINKED POLYETHYLENE CRYSTALLIZED UNDER UNIAXIAL COMPRESSION

5.1. Introduction

If a crosslinked system is uniaxially deformed in the melt, molecular chains in the structure are to be deformed in compliance with the macroscopic deformation according to the following relation (1), in so far as the affine deformation is assumed,

$$< R^2 >_\alpha \; / \; < R^2 >_0 \; = \; (2\alpha_z^{-1} + \alpha_z^2) \; / \; 3 \qquad (1)$$

Here $<R^2>_\alpha$ and $<R^2>_0$ designate the mean square of the end-to-end distance of the molecular chains in the deformed and isotropic states, respectively. α_z is the degree of macroscopic deformation of the sample in Z-direction. It coincides with "draw ratio" defined in Chapter 1 for uniaxial stretching and with "compression ratio" defined later for uniaxial compression. If a uniaxial compression is carried out for a film sample so as to reduce the thickness to 1/3, 1/7, or 1/10, for example; namely α_z = 1/3, 1/7, or 1/10, the molecular chains must be significantly extended according to the compression as suggested by the values of $<R^2>_\alpha \; / \; <R^2>_0$ = 2.04, 4.67, or 6.67, respectively. Hence, if a lightly crosslinked sample of adequate

crosslink density is uniaxially compressed in the melt, the crystallization will be conducted under high molecular orientation upon cooling and a unique phase structure is expected to produce in a similar manner as uniaxial stretching. This chapter deals with the crystallographical morphology for samples crystallized in such a manner.

5.2. Experimental Part

Preparation of samples

A commercial high density polyethylene from Hoechst with a viscosity average molecular weight of 2.5×10^6 was used in this study. A lightly crosslinked sample was made by irradiation of this material with γ-ray from ^{60}Co. Films about 1.5 mm thick of the polymer was irradiated to a dose of 2.7 megarads in vacuum at room temperature.

~~irradiated to a dose of 2.7 megarads in vacuum at room temperature.~~ The gel fraction (mass fraction of the nonsoluble part to the total mass) of this irradiated sample was 0.9 and the densities of crosslinked units and the free end groups were evaluated approximately to be 1.4×10^{-4} and 1.1×10^{-5}, respectively. The crosslinked sample was next compressed to different extents between two metal plates at 160-180°C and crystallized by cooling to room temperature over a period of 15 minutes. In this procedure, the film thicknesses were reduced in accord with the increase of the degree of compression. The degree of

compression was expressed by the ratio between the film thicknesses before and after compression. The orientation of the crystal planes in these samples was studied by three X-ray diffraction techniques described later.

Estimation of Planar Orientation by Wide Angle X-ray Diffraction

The crystalline structure of samples was inquired with three different X-ray techniques.

"Method 1" ; The radiograph was taken with a flat camera with Ni-filtered Cu-K_α radiation. The X-ray beam was introduced to samples, either parallel or perpendicular to the sample films.

"Method 2" ; Since the samples were uniaxially compressed perpendicular to the film plane, the crystallites in the structure are assumed to be randomly oriented about the normal to the film plane. In such a case, the spatial distribution of each crystal plane in a sample could be defined solely as a function of angle between two normals to the film and to a crystal plane. The geometry for this is shown in Figure 1. Here, vector P^*_{hkl} represents a crystal plane (hkl) in the reciprocal crystal lattice and the sample is fixed in the coordinate system (x, Y, z), the z-axis of which coincides with the normal N_f. Thus, the distribution function Φ_{hkl} for each P^*_{hkl} in the sample can be expressed as a function of ϕ. In order to evaluate this distribution function $\Phi(\phi)$ for different crystal planes such as the (110), (200), and (011) crystal planes, a detailed X-ray scan was made for the samples with different compression ratios. The diffraction intensity

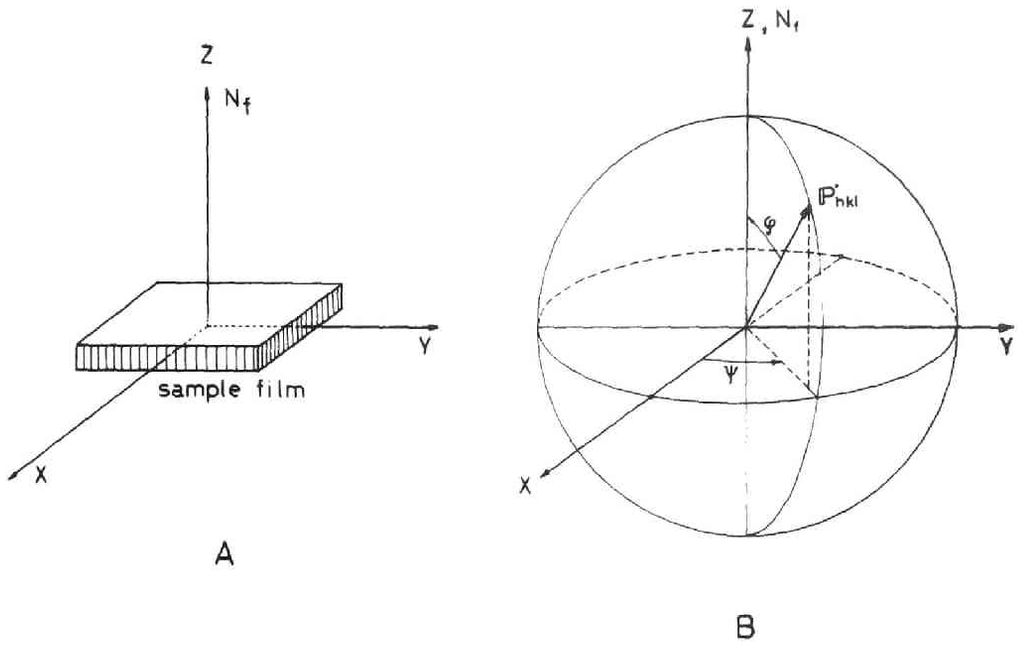

Fig.1. Geometry of spatial distribution for a crystal plane P* in samples.

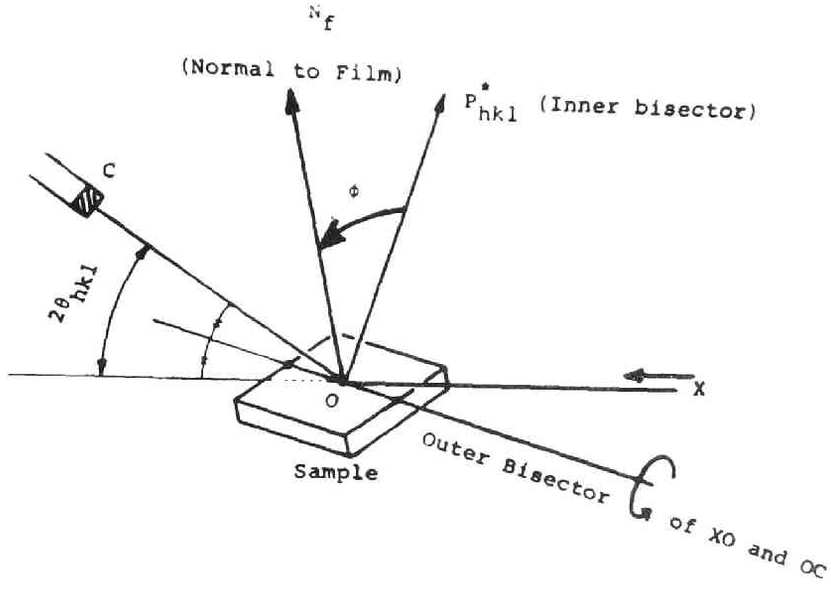

Fig.2. Geometry for an X-ray scan.

of the (110), (200), and (011) crystal planes was recorded by a proportional counter. As shown in Figure 2, the counter and the normal to the samples film (N_f) were first set at 2θ (Here, θ designates the Bragg's angle for each crystal plane), and in a position of the inner bisector of the incident and diffractive beams, respectively. Secondly, the normal to the sample film was rotated about the outer bisector, and at every 5° of the rotating angle ϕ the diffractive intensity $I(\phi)$ was recorded as a function of ϕ. Here at the every rotating angle ϕ the recording was also carried out with rotating the counter in a wide range that covers the 2θ angle in order to subtract the base line. The $I(\phi)$ obtained here for each crystal plane is considered to represent the distribution function $\Phi(\phi)$. The effect of ϕ on the mass of sample which actually contributed to the diffraction was not considered in this series of work, since it was thought to be minor in this mode of scan except ϕ=90° where the X-ray beam illuminated the film edge of sample.

"Method 3" ; Another X-ray scan was made in a similar manner as a routine scan for crystals of monomeric substances to identify those macroscopic surfaces. The diffraction was recorded with the proportional counter rotated around an axis perpendicular to both of the incident beam and the normal to the sample film N_f while the sample was also rotated around the same axis. The counter and the N_f were first set at angles of zero and 90° against the incident beam respectively and rotated so that the rate of the rotation for the former was twice that for the later.

The intensity thus recorded at angles of 2θ, where θ corresponds to each Bragg's angle for crystal planes, is diffractions from the crystal planes parallel to the film surface of samples. In this scan, therefore, one can know what kind of crystal planes in the samples is parallel to the film surface.

5.3. Results and Discussion

Studies with the Method 1 X-ray diffraction photographs were taken for samples with the compression ratios of 1, 3, 4, 5, 6, 8, and 10 with a flat camera. When the X-ray beam was introduced to samples perpendicular to the film surface of samples, the X-ray pattern obtained was composed of uniform circular rings for all samples. This indicates a random distribution of crystalline phases or crystal planes in the samples around the normal to the sample film (uniaxial random distribution around the normal N_f), independent of the degree of compression. On the other hand, when the photograph was taken with an X-ray beam parallel to the film surface, very enhanced change in the pattern was observed depending on the degree of compression. The X-ray patterns shown in Figure 3 manifest the change in the diffraction intensity in each circular diffraction for crystal planes (110), (200), (210), and (020).

Before considering these patterns, we must note the spatial geometry for the X-ray diffraction by the flat camera technique. Since an X-ray beam is introduced to samples from a direction parallel

Fig.3. X-ray patterns for the crosslinked sample. The compression ratio are indicated each pattern. To detect the (210)- and (020)-diffraction, the inner part of the sensitive film including the (110)- and (200)-diffractions were somewhat covered.

to the film surface and a sensitive film perpendicular to the incident beam is exposed to the diffractive beam, its geometry can be shown by Figure 4. To consider the spatial distribution of crystal planes in samples, we assume here that vector P^*_{hkl} which represents the crystal plane (hkl) in the reciprocal lattice coordinate is statistically distributed in space. Then, a diffraction circle on the X-ray film defined by the Bragg's angle for a crystal plane considered is caused by the vectors P^*_{hkl} that makes an angle of $\pi/2 - \theta$ to the X-ray incident beam. In addition, the diffraction at the point D defined by an angle of Ω on the circle is caused by the vectors P^*_{hkl} that further makes an angle of ϕ to the normal to the sample film. Here, ϕ, Ω and the

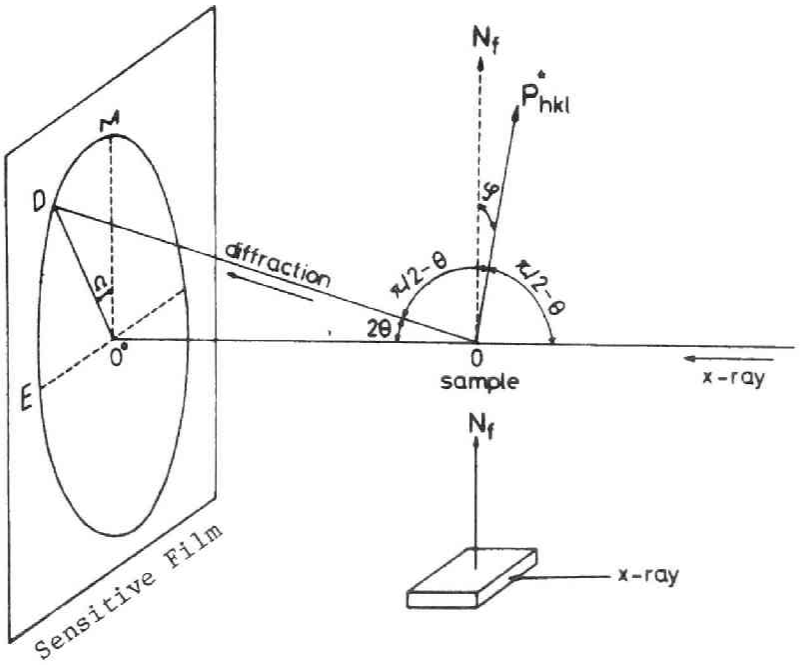

Fig.4. Geometry for a flat camera X-ray technique.

Bragg's angle θ are correlated each other with an equation,

$$\cos\phi = \cos\theta \cdot \cos\Omega \qquad (2)$$

Thus, the diffraction patterns obtained by the flat camera can be considered in terms of the spatial distribution of the crystal planes in samples. Since a dual orientation of the crystal planes (200) and (110) parallel to the film surface appears at the higher compression ratios(2), we first consider a hypothetic diffraction pattern when either crystal plane P^*_{200} or P^*_{110} is oriented preferentially parallel to N_f. Then the points diffracted on the flat camera from each crystal plane can be easily calculated with use of the eq.(2) for both orientations.

If either P^*_{200} or P^*_{110} is located parallel to N_f in a crystallite, then the angles of P^*_{110}, P^*_{200}, P^*_{210}, and P^*_{020} to N_f; namely the angle ϕ in the eq.(2) for each crystal plane in either case, can be easily evaluated by referring to the reciprocal lattice of the orthorhombic crystal form of polyethylene. Using the angle ϕ obtained in this manner with proper numerical values for θ and the lattice parameters, the points diffracted on the flat camera in both cases of the orientations were determined by the eq.(2). The results are listed in Table 1 as values of Ω. Now consider the significance of the X-ray patterns shown in Figure 3. At a compression ratio of 3, the intensity of the (110)-diffraction decreases in both meridional and equatorial directions,

Table 1. The Diffractive Points from Various Crystal Planes on the Flat Camera for (110) and (200) Parallel Orientation to N_f.

(hkl)	Ω , degree	
	P_{200}^* // N_f (200)-orientation	P_{110}^* // N_f (110)-orientation
110	55.6	67.0, (0)*
200	(0)*	55.4
210	34.0	12.4, 86.8
020	90.0	28.9

Values were calculated with the orthorhombic crystal form, a =7.410, b =4.945, c =2.548 A°, and λ =1.5418 A°. * The imperfect parallel orientation of either P_{200}^* or P_{110}^* where P_{200}^* or P_{110}^* makes angle of each Bragg's angle with N_f (ϕ = 0) should result in diffractions on meridian (Ω = 0) of each diffractive circular ring. The diffractions on the meridian are brought about by vectors that make an angle of θ with N_f. Furthermore, it is to be noted that, if the c-axes are located parallel to the film surface and some crystallites are distributed randomly around the c-axes, the diffraction peak should more or less appear on the meridian for all (hk0)-crystal planes.

showing diffuse four points maxima at intermediate angles. The (200)-diffraction converges into the meridional directions, losing its intensity at the equatorial and intermediate angles. Table 1 suggests that the (200)-orientation gives an enhanced intensity at the Ω-angles of 55.6 and zero for the (110)- and (200)-diffractions, respectively. Hence, correspond to Ω angles appeared for each diffraction, the (200)-orientation should be thought to have already appeared by the compression ratio of 3. On the other hand, since no enhanced intensity is observed at the Ω-angle of zero for the (110)-diffraction, it is thought that the (110)-orientation has not appeared as yet by this compression ratio.

As the compression ratio increases beyond 3, significant change in the X-ray patterns is recognized. The four points maxima observed for the (110)-diffraction at the compression ratio of 3 become obscure again by gradual increase in the diffraction intensity at the meridional angles. Beyond the compression ratio of 6, the (110)-diffractions converge to six points at the intermediate and meridional angles, this six points pattern becoming to be very explicit by the highest compression ratios of 8 and 10.

For the (200)-diffraction, it is observed that the intensity at the intermediate angles lost at the compression ratio of 3 recovers and converges to four maxima as the compression ratio increases from 4 to 5, emphasizing its intensity on the meridian beyond the compression ratio of 6 to 10. At the highest compression ratios six maxima are explicit, two of those being on the meridian.

The above-mentioned change in the X-ray patterns by further increase of the compression ratio beyond 3 will be explained by gradual occurrence of the (110)-orientation in addition to the (200)-orientation that has appeared in ahead at the compression ratio of 3. The diffuse four points maxima for the (110)-diffraction at the compression ratio of 3 by the (200)-orientation would become obscure as the compression ratio increased to 4 and 5 with gradual increase of the intensity at Ω = 0 and 67.0 due to the gradual appearance of the (110)-orientation. The distinct six points maxima for the (110)-diffraction observed at the compression ratios larger than 6 will be caused by rather perfect orientations of both crystal planes, (200) and (110).

The two maxima on the meridian will be originated by an imperfect (110)-orientation, and the four maxima will be composed of superposed maxima, each of which is at Ω=55.6 and 67.0 by the (200)- and (110)-orientations respectively.

Also the (110)-orientation will be responsible for the four points maxima of the (200)-diffraction at the intermediate angles around Ω= 55.4° that is originated at a compression ratio of 4 or 5 and established distinctly at compression ratios beyond 6.

The diffractions from the crystal planes (210) and (020) were not seen clearly in the patterns printed in the text, but examining of those original patterns gave some information of the crystal planes orientation. The (210)-diffraction lost its intensity in both meridional and equatorial directions at a compression ratio of 3, but after indicating a spurious uniform circular distribution at the intermediate compression ratios the diffractions tended to converge into rather lower angles of Ω and the equatorial angles. The (020)-diffraction indicated an enhanced intensity on the equator at a compression ratio of 3, and at the highest compression ratio it also exhibited enhanced intensity at lower angles of Ω around 28.9°. The above-mentionaed observations for the (210)- and (020)-diffractions can be also understood by progressive appearance of the (200)- and (110)-orientation of the crystal planes.

Thus all informations of the diffraction patterns for the (110), (200), (210) and (020) crystal planes lead a conclusion that during the crystallization under the two-dimensional compression the (200)-

orientation first appears at a relatively low compression ratio and the (110)-orientation follows at the higher compression ratios.

Studies with the Method 2 The plots of the quantity $I(\phi)\cdot\sin\phi$ vs. ϕ for the diffractions of crystal planes (110), (200), and (011) obtained by "X-ray Scan 2" for samples with different compression ratios are shown in Figure 5. These plots should reveal the spatial orientation of the crystal planes appearing in the samples with different compression ratios.

For convenience of consideration, the quantity $\Phi(\phi)\cdot\sin\phi$ for the (110), (200), and (011) diffractions is plotted vs. ϕ for several hypothetical distributions in Figure 6. Here, the distribution function $\Phi(\phi)$ is assumed to be a function only of ϕ(uniaxial random orientation around the normal to the film surface). The curves 1 in Figure 6 indicate an isotropic random distibution of crystallites. Curves 2, 3, and 4 indicate the distributions when all c-axes are located parallel to the film surface and crystallites are rotated statistically around the c-axes with an equal probability (Curves 2), or with a pronounced probability (Curves 3 and 4) at the positions where the P^*_{200} and P^*_{210} point to the direction of $\phi = 0$, respectively. Here, a Gaussian distribution around the c-axes is assumed for the latter two cases. Curves 3 and 4 in Figure 6(a) and 6(b) are expressed by a Gaussian distribution,

$$\Phi(\phi)\cdot\sin\phi = n(2\pi)^{-1/2}\sigma^{-1}\exp(-(\Delta\phi)^2\cdot 2^{-1}\cdot\sigma^{-2}) \qquad (3)$$

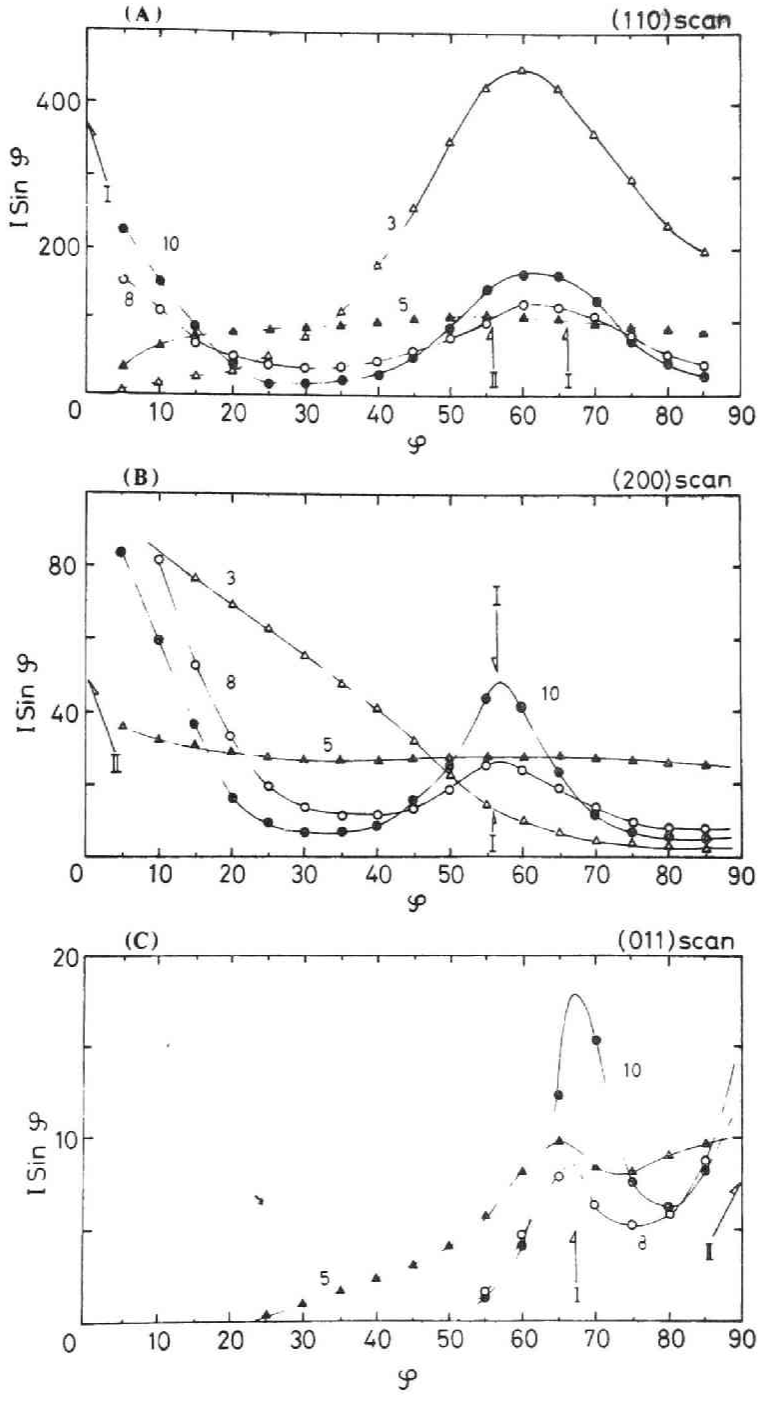

Fig. 5. $I(\phi)\cdot\sin\phi$ *vs.* ϕ of the crystal planes (110); Fig.(A), (200); Fig.(B), and (011); Fig.(C) for lightly cross-linked sample. Data for samples with compression ratios of 3;(Δ), 5;(▲), 8;(o), and 10;(●), respectively. Arrows I indicate the peak position for the (110) crystal plane orientation and arrows II indicate that for the (200) crystal plane orientation.

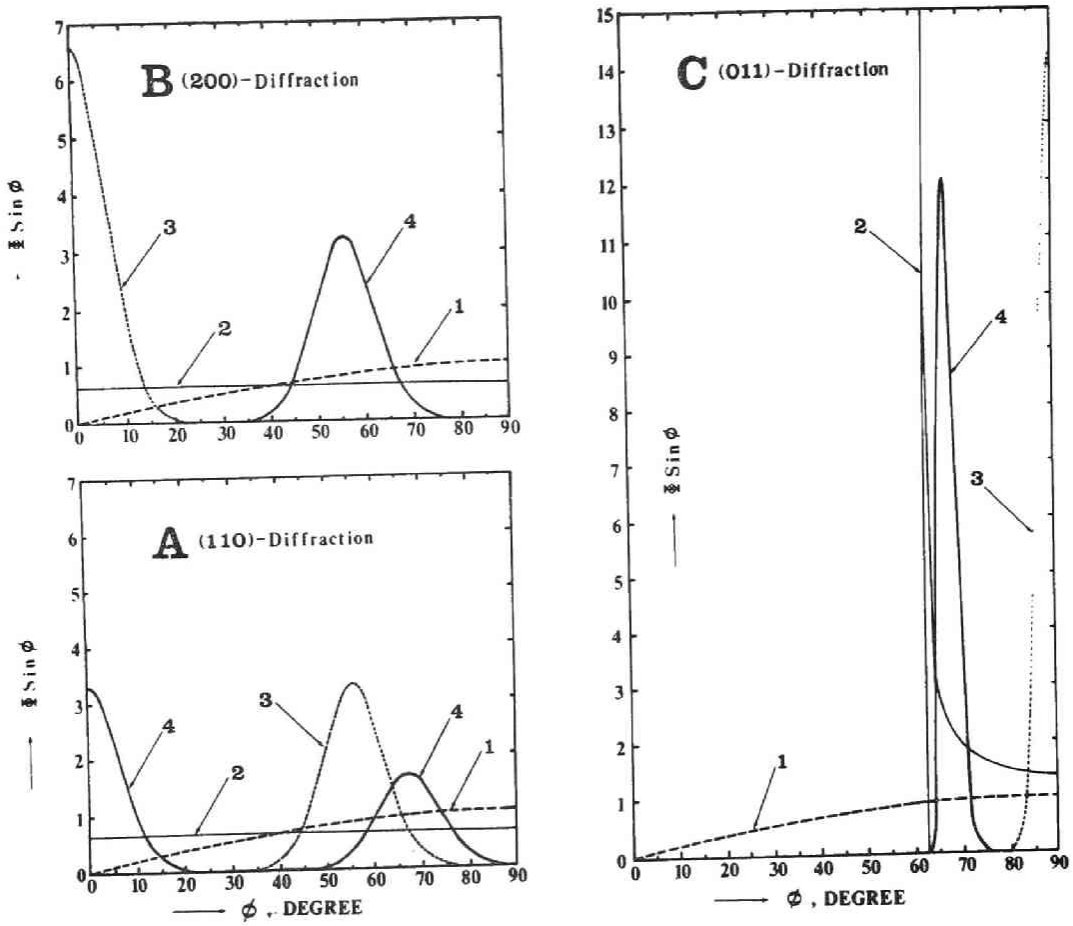

Fig.6. $\Phi(\phi)\cdot\sin\phi$ vs. ϕ for the diffractions (110) (Fig.(A)), (200) (Fig.(B)), and (011) (Fig.(C)) for hypothetical distributions of crystallites. Curves 1: isotropical random distribution of crystallites; curves 2,3, and 4: all c-axes are located parallel to the film surface, and the crystallites are statistically rotated around the c-axes with equal probability (Curve 2), or with a pronounced probability at positions where the P^{*}_{200} and P^{*}_{110} point to the direction of $\phi = 0$ (Curves 3 and 4, resp.). See text for details. (Different line symbols for curves are for better distinction)

with $\sigma = 0.12$ and $n = 1$, 2, or 1/2. Here $\Delta\phi$ is the angular difference in radian units from each angle at peaks. All curves including curves 1 and 2 are normalized so that

$$\int_0^{\pi/2} \Phi(\phi) \cdot \sin\phi \, d\phi = 1 \qquad (4)$$

For the two samples with the highest degrees of compression 8 and 10, it can be shown from very minor intensities for the (011) diffraction at angles less than 60° (Figure 5-C) that the c-axes are mostly located parallel to the sample film*. Hence for these two samples, the spatial orientation of the crystallites can be compared with the data in Figure 5 referring to the hypothetical curves 3 and 4 in Figure 6 or the arrows in Figure 5 where only peak positions are indicated. As a result, the dual crystalline structure in which the (200) and (110) crystal planes are oriented preferentially parallel to the film surface is concluded in good accord with the conclusion reached in the last section(2,6,7).

However, for the samples with the lower degrees of compression, the parallel orientation of the c-axis to the film surface is not so enhanced. E.g. as shown in Figure 5-C, appreciable (011) diffraction intensity is recognized for the sample with a compression ratio of 5 at angles of $\phi < 60°$. Hence, in this sample the c-axis parallel

---

* Since P^*_{011} makes an angle of 27.2° to the c-axis (62.8° to the b-axis), no intensity at angles less than 62.8° for the (011) diffraction indicates that the c-axes are parallel to the film surface(2).

orientation is rather incomplete. For the sample with the smallest compression ratio of 3, the (011) diffractions could not be plotted against the angle ϕ with a reasonable experimental precision. Hence, the data are not shown in the figure but the c-axis orientation is thought to be very incomplete. Therefore, consideration of the orientation of crystallites for this sample will be somewhat complicated.

For the sample with the smallest compression ratio of 3, the data for the (110) and (200) diffractions are shown in Figure 5-a and 5-b. The (110) diffraction appears in a range between 5° and 90° with a peak at an angle of about 60°, but no intensity is recognized in the vicinity of 0°. Referring to Figure 6-a, it must be concluded that an orientation corresponding to curve 3 is present in this sample whereas an orientation, corresponding to curve 4 is absent. Hence, the (200) parallel orientation is thought to have already appeared by the smallest compression ratio of 3 in the absence of the (110) orientation, although the c-axis orientation is incomplete. The peak position of about 60° is little higher than that suggested by curve 3 in Figure 6-a but this will be caused by contributions of crystallites oriented in a manner corresponding to curves 1 and 2 in the figure. The appearance of the (200) parallel orientation for the sample is also confirmed by the data of the (200) diffraction (shown in Figure 5(B)) as well as the (020) diffraction, which is not shown in the figures because the data were quite similar to Figure 5-a if the angular axis was converted so that $\phi_{020}=90-\phi_{200}$.

Contrary to this, the data of the (110) and (200) diffractions (Figure 5-a and 5-b) for the sample with the compression ratio of 5

seem to correspond to curve 2 in Figure 6 which might indicate the non-existence of both of the (200) and (110) orientations. However, since the firm existence of both orientations is known for the samples with the higher compression ratios and in fact the data of the (011), the diffractions shown in Figure 5-C are thought to correspond to a composite curve of curves 1, 2, 3, and 4 in Figure 6-c, it must be concluded that both parallel orientations of the (200) and (110) crystal planes are presented in this sample. The resemblance of the (200) and (110) diffractions for this sample to curve 2 in Figure 6 is only spurious and thought to be caused by an additional diffuse (110) orientation to the (200) orientation that already has appeared at a lower compression ratio. Thus a very important conclusion must be reached here namely that between the parallel orientations of the (200) and (110) crystal planes the (200) orientation first appears for the relatively smaller compression ratios and the (110) orientation follows for the higher compression ratios, the distributions of both orientations becoming sharp as the compression ratio further increases.

Studies with the Method 3 In order to confirm the progressive appearance of the (200) and (110) parallel orientations with the increase of the compression ratio and to study the relative mass fraction between the two orientations an X-ray study was made by the Method 3. The data for the samples with compression ratios of 1, 3, 5, 8, and 10 are shown in Figure 7. In this mode of scan, the diffraction intensity recorded at angles of 2θ where θ corresponds to each Bragg angle for

the crystal planes is due to crystal planes parallel to the film surface of the samples. Accordingly, the relative mass fraction between the parallel orientations of the planes can be determined from the data in Figure 7. When crystallites in samples are randomly distributed in space, it is known by the data for the sample with a compression ratio of 1 (not compressed, isotropic sample) and by an early work of Bunn(3)

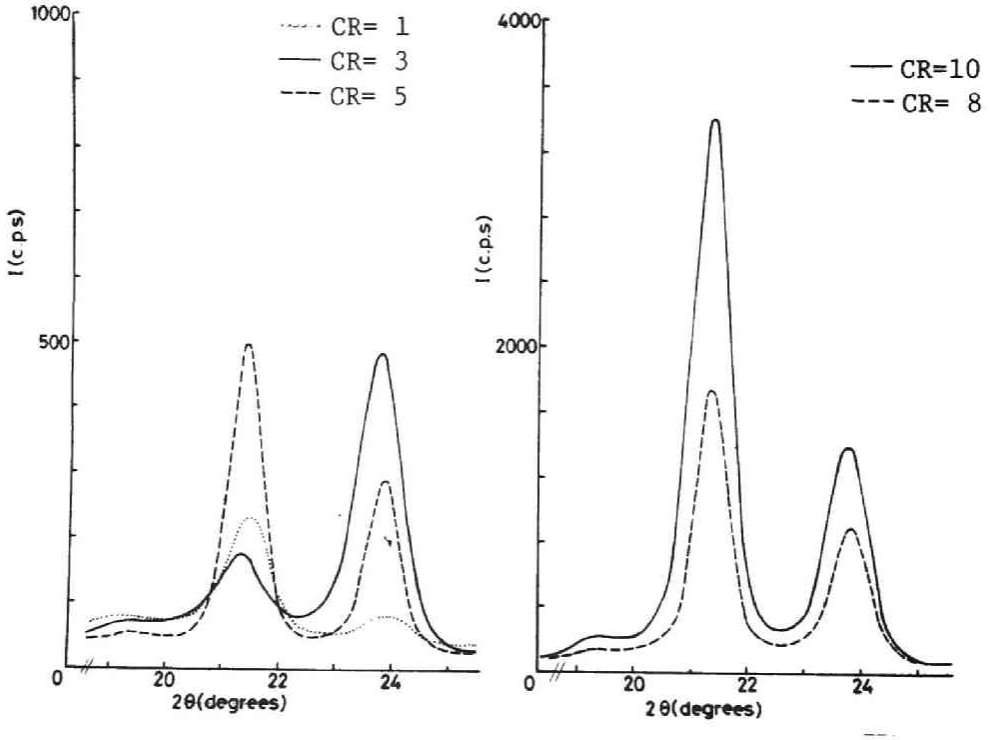

Fig. 7. X-ray diffraction profiles for the lightly crosslinked sample. Compression ratios are indicated as numbers in each profile. (Different line symbols for curves are for better distinction)

Table 2. The Intensity Ratio between the (110)- and (200)- Diffractions and the Relative Existence Ratio between the (200)- and (110)- Orientations for Samples with Different Compression Ratios.

Compression ratio of samples	Intensity ratio I_{110} / I_{200}	Relative existence ratio between the (200)- and (110)- orientations $M_{200/100}$
1	4.56	----
3	0.295	7.73
5	1.78	1.30
8	2.26	1.00
10	2.53	0.90

that the intensity ratio of the (110) diffraction to the (200) diffraction at each 2θ angle is in an order of 4 to 5. However, the intensity ratio is significantly altered with the increase of the compression ratio. This quantity was determined from the data in Figure 7 by use of proper base-lines for each curve and listed in the second column in Table 2.

If we designate I_{110} and I_{200} as intensities of the (110) and (200) diffractions at each 2θ, the relative mass fraction $M_{200/110}$ of (200) and (110) orientations may be evaluated by

$$M_{200/110} = (I_{200} / I^0_{200}) / (2 I_{110} / I^0_{110}) \qquad (5)$$

Since the equation can be re-written as

$$M_{200/110} = (I^0_{110} / 2 I^0_{200}) (I_{110} / I_{200}) \qquad (6)$$

and the quantities in the last brackets in Eq.(6) are given in Table 2, the relative mass fraction can be evaluated for the samples with different compression ratios and it is shown in the last column of Table 2. Here, I^0_{110} and I^0_{200} are the intensities for the randomly oriented sample without compression.

The ratio I^0_{110} / I^0_{200} is given to be 4.56 on the first line of the second column in Table 2. The value of 7.73 for the relative mass fraction for a compression ratio of 3 which is much higher than unity should be nothing but exhibit a firm appearance of the (200) orientation at this compression ratio in the absence of the (110) orientation. The relative mass fraction decreases rather abruptly to 1.30 at a compression ratio of 5 and gradually decreases to 1.00 and 0.90 as the compression ratio increases to 8 and 10. This means that the (110) orientation appears at a compression ratio of 5 to an extent which corresponds to the (200) orientation in mass, and subsequently both orientations progressively become enhanced and completed with changing

slightly the relative mass ratio between them. Thus, a very characteristic X-ray pattern should be obtained for a sample with a high compression ratio of 10 by a flat camera technique when an X-ray beam is introduced parallel to the film surface of the sample(2).

5.4. Conclusion

It is confirmed by three X-ray techniques that if a lightly crosslinked film is two-dimensionally compressed between two metal plates in the molten state and crystallized by cooling to room temperature, the orientation of the crystal planes (200) and (110) parallel to the film surface of the sample appears in the structure. Between these two orientations, the (200)-orientation first appears at a relatively low degree of compression such as 3 and the other follows at higher degrees of compression such as larger than 5, both becoming explicit and sharp progressively according to the increases of the degreee of compression.

After appearing of both orientations, those are approximately comparable in mass so that the relative mass ratio between the (200)- and/ (110)-orientations gradually decreases from 1.30 to 0.90 as the compression ratio increases from 5 to 10.

This type of (110) or (200) orientation has been occasionally recognized for polyethylene samples when a sample film is biaxially stretched(4) or uniaxially stretched(5) with holding the width at higher temperatures irrespective of the presence of crosslinks in the

structure. Such orientation of crystallites is thought to appear universally when the polymer is crystallized or processed under conditions involving high degrees of planar shear. However, it is not necessary that both the (110) and (200) orientations occur simultaneously. For example, it was reported by us that, when uncrosslinked polyethylene film was rapidly compressed at 130°C from the melt or rolled at temperatures above 80°C only the (200) orientation appeared but when rolled at lower temperatures both of the (200) and (110) orientations appered(1,6,7).

These experimental results with the advancing appearance of the (200) orientation mentioned above should lead a conclusion that between the two orientations the (200) orientation is of more importance than the (110) orientation in considering the mechnism of crystallization under conditions involving a high degree of planar shear.

References

1. R.Kitamaru and S.-H.Hyon, Macromolecular Review, 14, (1978) in press
2. R.Kitamaru, H.-D.Chu, and S.-H.Hyon, Macromolecules, 6, 337 (1973).
3. C.W.Bunn, Trans.Faraday Soc., 35, 482 (1938).
4. G.C.Adams, J.Polym.Sci., A-2, 9, 1235 (1971)
5. I.Sakurada, K.Kaji, K.Nakamae, and S.Wadano, Bull.Inst.Chem.Res., Kyoto Unv., 44, 168 (1966).
6. R.Kitamaru and S.-H.Hyon, Makromol.Chem., 175, 255 (1974).
7. S.-H.Hyon, H.Taniuchi, and R.Kitamaru, Bull.Inst.Chem.Res., Kyoto Unv., 51, 91 (1973).

Chapter 6.

STRUCTURE AND PROPERTIES OF LIGHTLY CROSSLINKED POLYETHYLENE CRYSTALLIZED FROM THE MELT UNDER UNIAXIAL COMPRESSION

6.1. Introduction

A number of papers have appeared recently(1-11) describing procedures for preparing transparent polyethylene of high crystallinity. Southern and Porter(1) obtained a transparent polyethylene strand by crystallization of the flowing melt of the polymer in a capillary rheometer under very high pressure and shear (the capillary-flowing procedure). Wang, Kwei, and Chen(4) developed a procedure for preparing transparent film by dropping molten polyethylene between two rotating polished rollers that were kept at room temperature and were kept in contact with each other with high pressure (the quenched-roll procedure). It was also reported that a transparent filament could be obtained by plastic flow of the polymer either in a capillary(6) or in tapered dies(7) under very high pressure. The properties of the various transparent products, of course, were different but the products exhibited some common characteristics, such as high moduli or high melting temperatures together with high transparency. This suggests similar crystalline structures that resulted from similar modes of crystallization.

During "capillary-flowing," or "quenched-rolling," or "plastic-flowing" procedures, transparent products are obtained by either

crystallization or recrystallization under conditions of high molecular orientation. To attain such structures, rather severe conditions such as very high pressure and shear are thought to be necessary. However, if high molecular orientation during the crystallization is sufficient to obtain transparent products, any other procedures of crystallization that involve high degrees of molecular orientation would result in a similar product in the absence of high pressure and shear.

A lightly crosslinked polyethylene of adequate crosslink density can be elastically deformed in the molten state until molecular chains are almost fully extended(12). If the lightly crosslinked polyethylene is crystallized from such a deformed state by cooling to room temperature, the crystallization of orientated molecular chains will be achieved in the absence of high pressure and shear. This chapter concerns this crystallization method for preparing transparent films and describes the film properties in detail.

6.2. Experimental Part

Crosslinking and Uniaxial Compression

For the purpose of the crystallization with uniaxial compression to produce a unique phase structure, the crosslink density (the mass fraction of the crosslinked units in the entire mass) should be adequate. It must be minimum so far as to guarantee the elastic deformation of samples in the molten state, because the crosslinked units act as noncrystallizable units as pointed out also in Chapter 1. For this

purpose, samples of higher molecular weights are preferable to use, since such samples produce necessary gel contents with minimum dosage of irradiation(13, 14, 15).

Table 1 summarizes three starting materials and their irradiation procedures mainly used in this series of work. The one is a molecular weight fraction with a very high molecular weight and the others are non-fractionated commercial whole polymers with different molecular weights. The molded films of those about 1.5 mm thick were irradiated with high energy ionizing radiations or electron beams in vacuum.

As can be seen, the densities of crosslinked units and free end groups are different but all samples displayed rubbery elasticity in the molten state such that they could be stretched uniaxially more than tenfold. They were compressed to different extents between two polished metal plates at 160-180°C and cooled to room temperature over a period of 15 min according to the procedure described previously in Chapter 5. Sample 1 was used after extracting its soluble fraction, but Samples 2 and 3 were used without removing those soluble fractions. In this procedure, the film thicknesses were reduced and the compressed samples were characterized by the compression ratio $1/\alpha_z$ defined to be the ratio between the film thicknesses before and after compressions.

Wide-angle X-ray Diffraction

"X-ray Scan 1" : In this scan, the diffraction was recorded with the proportional counter rotated around an axis perpendicular to both of the incident beam and the normal to the film surface of the samples

Table 1. Starting Materials and Irradiation Procedures.

Starting material	Sample 1; Molecular weight fraction of Hostalen ($\bar{M}_\eta = 3.4 \times 10^6$)[a]	Sample 2; Commercial whole polymer, Hostalen ($\bar{M}_\eta = 2.5 \times 10^6$)[a]	Sample 3; Commercial whole polymer, Marlex 50 ($\bar{M}_\eta = 0.136 \times 10^6$)[a]
Radiation beam	X-Ray from Van de Graaff	Electron from Van de Graaff	γ-Ray, ^{60}Co
Dosage in Mrad ($=10^4$ j/kg)	0.25	2.7	22.5
Irradiation in *vacuo* at	150°C	room temperature	room temperature
Gel fraction after irradiation, Wg	0.97	0.90	0.77
Crosslink density[b] of the irradiated products, ρ_t, in fraction of units crosslinked in the entire system	1.7×10^{-5}	1.4×10^{-4}	1.2×10^{-3}
Concentration of free end groups of the irradiated products, ρ_e, in mass fraction of free end groups in the entire system	8.2×10^{-6}	1.1×10^{-5}	2.1×10^{-4}

a; *Cf.* reference (18).

b; The crosslink density was calculated according to the relations, $\rho_t = 0.66 \times 10^{-4}R$ and $\rho_t = 0.53 \times 10^{-4}R$ based on informations of irradiation crosslinking on linear polyethylene(15). Here, R is the dosage irradiated in Mrad ($= 10^4$J/kg) units.

while the samples were also rotated around the same axis. The counter and the normal to the film surface first set at angles of zero and 90° respectively, to the incident beam rotated so that the rate of rotation for the former was twice that for the latter.

The diffraction profile obtained by this scan was employed to study the relative mass ratio between the (200) and (110) crystal plane orientations, because the diffraction in this scan was brought about only from crystal planes parallel to the film surface. Also this scan was used to evaluated the unit-cell dimensions and the crystallite size in directions perpendicular to the (200) and (110) crystal planes of the samples. For the crystallite size determination Cu-K_α-radiation, generated by 40 kV and 20 mA was used. The scan was conducted with a time constant of two seconds, slits of 0.1 mm and 1/6° for the incident and diffractive beams respectively, a rate of scan of 1/8° per min, and a chart speed of 10 mm/min.

Small-angle X-ray Scattering

Small angular X-ray pattern: This was obtained with a point collimation camera with use of a Ni-filtered Cu-K_α beam. The samples were exposed to X-rays from different directions under conditions of 100 mA and 50 kV by an anode rotating type of X-ray generator, Rotaflex From Rigaku-Denki Co.

"X-ray Scan 2": This scan in low angular range was conducted by an apparatus equipped with three slits as usual for the incident beam and one slit for the diffractive beam. The diffraction intensity was

recorded with a scintillation counter rotating with a rate of 4' per min at a distance of 30 cm from the samples on a rotating recording chart. The angle at maximum intensity was determined from the diffraction profile thus obtained by correcting for an effect of scattering by air and converted to linear dimension, d-spacing according to Bragg's law.

"X-ray Scan 3": This scan was made by a "high dissolution X-ray low-angular U-slit camera" developed by Kratky et al.(16, 17). The detailed conditions were as follows. The X-ray beam used was Ni-filtered Cu-K_α, the thickness of the filter was 10 μm. It was generated by use of an X-ray generating bulb, designed by Kratky et al.(16, 17). The scan was made at 23.5 ± 0.5°C by automatically recording the time when the diffraction intensity reached a fixed dose of $1 \cdot 10^4$ counts at every angle of 0.8' by a scintillation counter equipped with a pulse height analyser. The distance between the counter and the samples was 215 mm, the entrance and counter slits were 30 μm and 60 μm respectively. The counter slit length was 11.0 mm and, the length limit was 18 mm. The diffraction intensity at each angle was determined within an experimental error of ± 0.5%.

6.3. Melting Temperature and Transparency

The samples made by this mode of crystallization under uniaxial compression exhibit very high melting temperatures in a similar manner to the samples made by uniaxially stretching, further with excellent transparency. Table 2 summarizes the melting temperature and trans-

Table 2. Melting Temperature, Density, and Transparency of Films Made from the Crosslinked Polyethylene Listed in Table 1 with Different Compression Ratios.

	Compression Ratio (α_z^{-1})	Density (at 30°C)	Melting Temp.(°C)	Transparency[c]
Sample 1	10	0.942	155.0	+++
Sample 2	1[a]	0.935	137.6	
	1[b]	0.932	136.8	
	6	0.9370	151.5	++
	8	0.9378	153.2	+++
	10	0.9380	155.0	+++
Sample 3	1[a]	0.950	137.5	
	1[b]	0.935	130.7	
	3	0.937	129.8	
	4	0.938	129.7	+
	7	0.939	130.5	++
	8	0.940	135.0	+++
	9	0.940	135.5	+++
	11	0.941	136.5	+++
	14	0.944	136.7	+++

a; Well crystallized. *b;* Quenched from the melt by 15 min.
c; Transparency: + = good, ++ = very good, +++ = excellent.

parency as a function of compression ratio $1/\alpha_z$ together with the density measured at 30°C. Here, the melting temperature was obtained by differential scanning calorimetry with a heating rate of 10°/min and defined as the point at which the fusion curve in the calorimetry returned to the base line after completion of fusion.

Figure 1 shows the DSC fusion curves for the transparent films made from the tree crosslinked samples listed in Table 1. Extraordinarily high melting temperatures such as 155°C are observed for samples from the two higher molecular weight polymers (fractionated and unfractionated samples), although such high melting temperatures are not recognized for samples from Marlex 50 of ordinary molecular weight. It is to be noted here that excellent transparency appears for all samples when compressed

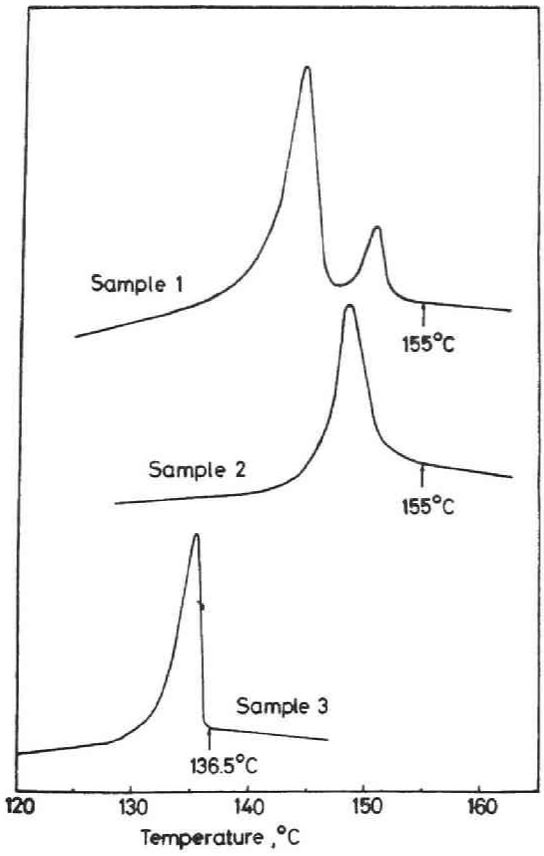

Fig. 1. DSC fusion scan for the transparent films made from crosslinked polyethylene listed in Table 1. Compression ratio;10. Rate of scan;10°C/min.

highly(higher compression ratios). The highly crystalline polyethylene samples are generally not transparent if well crystallized. Nevertheless, the coexistence of high melting temperatures and transparency has been sometimes reported for samples crystallized or processed under certain conditions such as high shear and high pressure, involving molecular orientation(1-11). Such high transparency for the crystalline polyethylene is thought to be couased by the special phase structure of the samples. We will discuss the phase structure of the crosslinked samples with different compression ratios in the following sections.

6.4. The Crystallite Size by Small Angle X-ray Scattering Techniques

To study the crystallite size for samples with different degrees of compression, low-angle X-ray patterns were first obtained by the technique described in the Experimental Part. When the X-ray beam was introduced into the samples perpendicular to the film surface, always very diffuse patterns were obtained, the intensity of which was distributed circularly around the beam direction in the range of very small angles. Those patterns implied a random uniaxial distribution of crystallites around the beam direction, namely around the normal to the film surface of samples in good accord with the information from the wide angle X-ray patterns, but maxima in intensity were hardly recognized in the radial direction of the patterns if any. However, when samples were illuminated by the X-ray beam parallel to the film surface, patterns

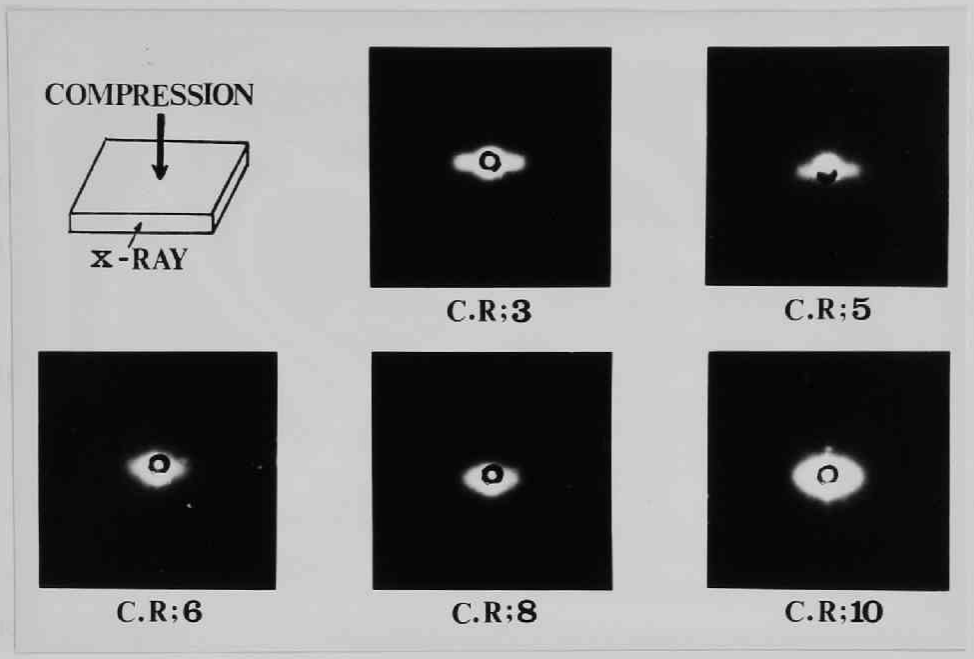

Fig.2. Small angle X-ray diffraction patterns from a cross-linked polyethylene crystallized under compression. (Sample; Marlex 50)

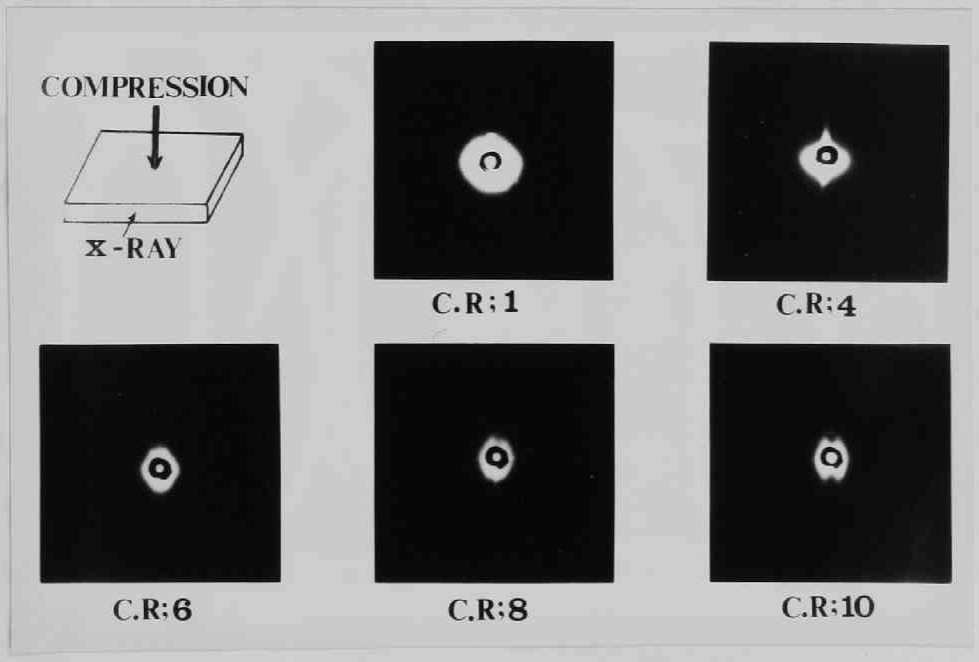

Fig.3. Small angle X-ray diffraction patterns from a cross-linked polyethylene crystallized under compression. (Sample; Hostalen)

were obtained that indicated periodical fluctuation in density in a direction perpendicular to the beam, namely in the molecular chain direction in the crystallites. Figure 2 and 3 show the low-angle X-ray patterns for samples with different degrees of compression which were made from Marlex 50 or Hostalen (see Table 1), respectively.

The patterns in Figure 2 generally indicate a discrete two-point diffraction along the edge direction of the sample film. As the compression ratio increases, this two-point diffraction shifts into the lower angular range but no fluctuation in density is recognized in the direction perpendicular to the film edge, namely in the direction of the normal to the film surface. On the other hand the patterns shown in Figure 3 are different from those in Figure 2; discrete lamella type of maxima are discernible in the direction along the film edge for samples with compression ratios higher than 5.

This lamella type of maxima appears in a range of very small angles and further shifts into the lower angular range with increasing compression ratio.

In any case these patterns indicate a periodicity of density fluctuation in samples that corresponds to the size of crystallites in the structure in a direction of molecular chains. This periodicity was determined as d-spacing by measuring the distance between the points or lamella type maxima in the patterns and using Bragg's law. The results are plotted against the compression ratio of the samples in Figure 7.

It is seen that the d-spacing for the samples made from the higher molecular weght polymer with smaller crosslink densities is generally

larger than that for the samples made from a lower molecular weight polymer with larger crosslink density and for both series of samples the d-spacing increases systematically as the degree of compression increases.

In addition to the small-angle X-ray photograph work, the small angle X-ray diffraction scan was made for samples with different degrees of compression by the two techniques described in the Experimental Part. First, for two series of samples made from Marlex 50 and Hostalen (see Table 1) with different compression ratios an X-ray scan was made by the "X-ray Scan 2". The X-ray beam was introduced parallel to the film surface and the scanning was made parallel to the film edge of the samples according to a suggestion from the above-mentioned X-ray patterns. The data are shown in Figure 4 and 5 as plots of the scattering intensity vs. angle 2θ in minutes. For the samples made from the lowest molecular weight polymer as shown in Figure 4, very clear peaks are discernible in an angular range between 10' and 20'. These peaks should clearly indicate a periodical fluctuation in density in the molecular chain direction of crystallites in the samples.

On the other hand, no intensity peak can be recognized for the samples made from the larger molecular weight polymer as shown in Figure 5. But also in this case the existence of the density fluctuation is indicated by weak shoulders appearing in an angular range smaller than 12'. The d-spacings evaluated from these peaks or shoulders in the diffraction intensity according to Bragg's law are also plotted against the compression ratio in Figure 7.

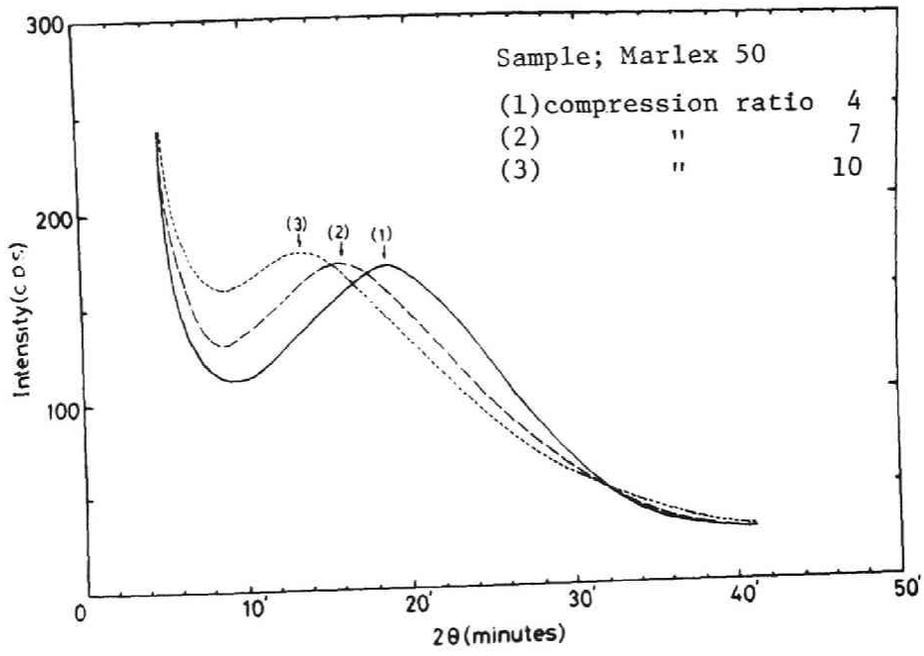

Fig.4. Angular dependence of small angle X-ray scattering of crosslinked polyethylene compressed at molten state.

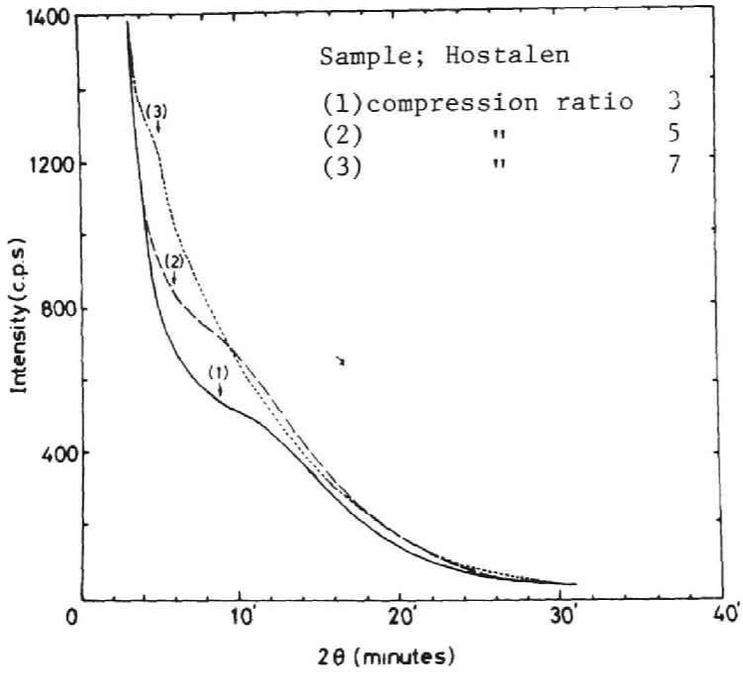

Fig.5. Angular dependence of small angle X-ray scattering of crosslinked polyethylene compressed at molten state.

Since d-spacings longer than 500 Å or 1000 Å could not be determined by the above-mentioned photograph work or "X-ray Scan 2" with sufficient precision, further X-ray studies were made by the "X-ray Scan 3" for samples with a compression ratio of 10. The scanning was accomplished along the film edge of the samples according to a suggestion from

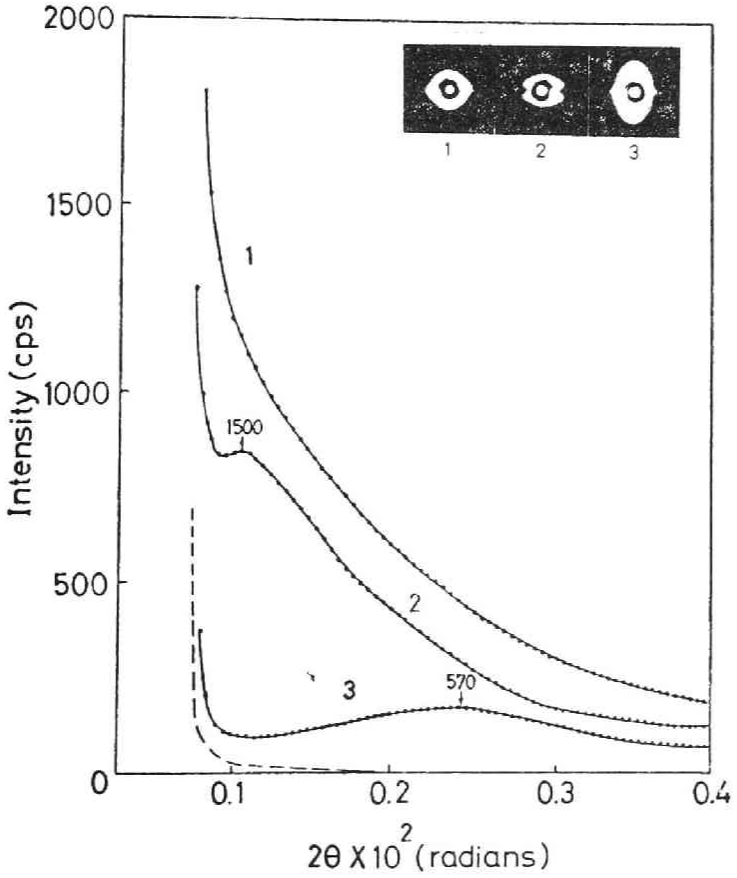

Fig.6. X-ray diffraction profiles in the low angular range for crosslinked polymer samples with a compression ratio of 10, by the "X-ray Scan 3". Sample 1: Molecular weight fraction from Hostalen. Sample 2: Commercial whole polymer Hostalen. Sample 3: Commercial whole polymer Marlex 50. The photographs of the diffraction patterns for samples 1, 2, and 3 are also shown. Maxima correspond to d-spacings of 1500 Å and 570 Å. Dashed curve: Base line.

the low-angle X-ray patterns. The data are shown in Figure 6. For the sample made from the lowest molecular weight polymer (Marlex 50) an intensity peak is clearly recognized at an angle of $0.24 \cdot 10^{-2}$ radians, that corresponds to a d-spacing of 570 Å. Also for the sample made

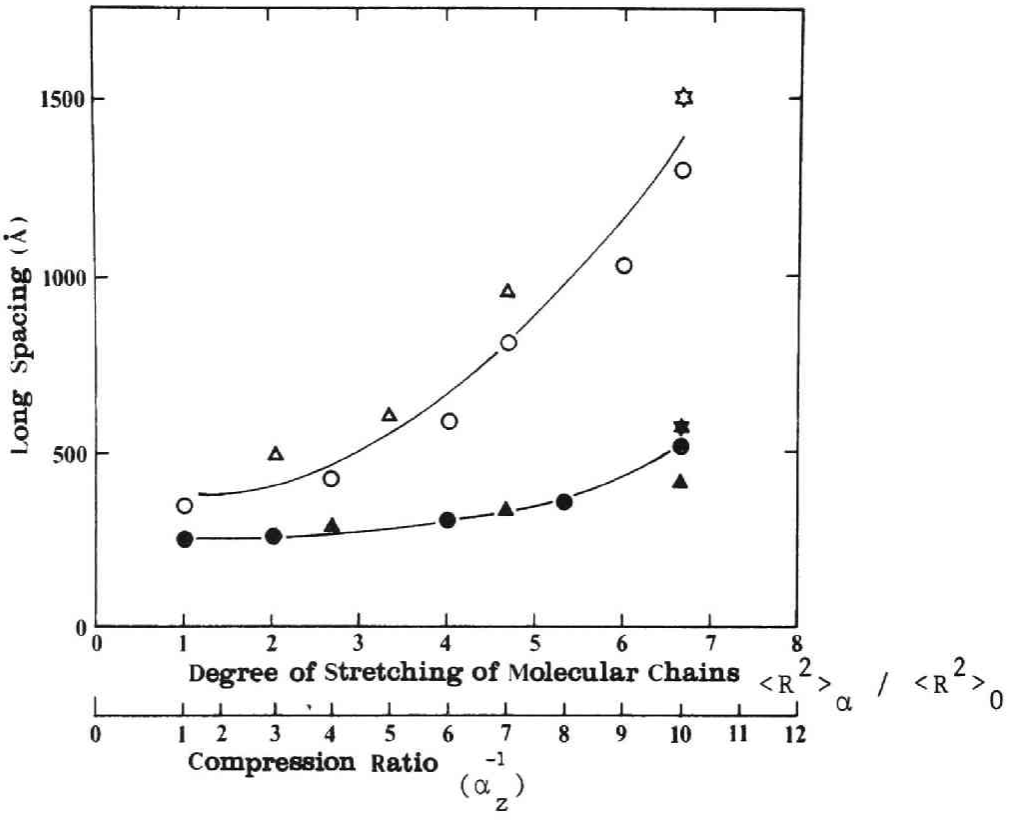

Fig. 7. Long spacing *vs.* compression ratio or degree of stretching of molecular chains. Data are from the X-ray low angle diffraction patterns (o,●) the "X-ray Scan 2" (△,▲), and the "X-ray Scan 3" (✡,✱), where open and closed marks are the data for the crosslinked samples made from Hostalen and Marlex 50, respectivery. See Chapter 5 for the horizontal scale.

from the higher molecular weight polymer (Hostalen), a clear peak is discernible in an angle of $0.11 \cdot 10^{-2}$ radians that corresponds to the very large d-spacing of 1500 Å. For the sample made from the largest molecular weight polymer (a molecular weight fraction, sample 1 in Table 1) no peak or shoulder could be recognized. The d-spacing for this sample is thought to be larger than 2000 Å at least.

All d-spacings evaluated by different procedures are summarized in Figure 7 as a plot against the degree of compression or the degree of stretching of the molecular chains under the compression. Although Figure 7 includes data obtained by different procedures, a systematic dependency of the d-spacing on the compression ratio is clearly recognized, depending on the source of the samples.

We consider first the data for the samples made from the higher molecular weight polymer (Hostalen). When this crosslinked polymer is crystallized from the isotropic melt by cooling to room temperature for 15 min, the d-spacing of the sample is about 350 Å as seen in the Figure 7. But if it is crystallized from the melt under compression, the d-spacing is greatly increased. E.g., the d-spacing exceeds 1000 Å and reaches 1500 Å for compression ratios of 7 or 8 and 10, respectively. Since such a large d-spacing cannot be expected by crystallization from the melt in the isotropic state unless it is crystallized very slowly at high temperatures near the melting temperature, formation of a structure with such large d-spacing will have been brought about by the special mode of crystallization under high degrees of compression. The authors previously assumed(18) a structure for lightly crosslinked polyethylene crystallized

under high degrees of compression which is composed of aggregations of plate-like crystallites, the planes of which are oriented parallel to the macroscopic film surface and coincide with either the (110) or the (200) crystal plane. Since the d-spacings obtained here should coincide with the linear dimension of the crystallite size in a direction parallel to the film surface, the very large value of the d-spacings at high compression ratios should support the assumption made above. Thus it is concluded that the formation of the plate-like crystallite structure by this mode of crystallization is completed as the degree of compression increases, the parallel orientation of crystallites becoming completed and the size of the crystallites in a direction parallel to the film surface being increased limitlessly.

On the other hand it is seen in Figure 7 that the d-spacing for the crosslinked sample made from the lowest molecular weight polymer (Marlex 50) does not increase so enhancely by increasing the degree of compression. For this crosslinked sample it is pointed out in the foregoing chapter and in the recent paper(18) that the orientation of the crystal planes and the increase of the melting temperature accompanying the increase of the compression ratio are not so enhanced. This sample contains a great number of crosslinked units and free end groups owing to the limited molecular weight of its starting polymer and high irradiation dosage. Therefore, molecular chains in the sample will not be able to correspond to the macroscopic compression in the molten state and the special mode of crystallization under compression will not take place so appreciably for this sample. As the result, the appearance of

the crystal plane orientations and an increase of the d-spacing accompanying the increase of the compression ratio, both characteristic for this mode of crystallization, would not be so enhanced.

Up to the present in this section, we have been concerned only with d-spacings of diffraction angles where intensity maxima are observed. However, an estimation of the diffraction intensities from Figure 4, 5 and 6 seems to point to an increase of the scattering intensities with an increase of the compression ratio, in addition to the increase of the d-spacing. This can be brought about by an increase of the density difference between the crystalline and amorphous phases, assuming that no change in crystallinity occurs(18). As shown in the recent paper(19) the unit-cell density of the samples crystallized under uniaxial compressions increases to unity as the degree of compression increases. On the other hand, there is no information about the density in the amorphous phase at the present, but it is pointed out (18, 20) from birefringence studies of a cross-linked polyethylene crystallized from the melt under uniaxially stretched state(21) that molecular chains in the amorphous phase of the sample are in an unoriented and probably relaxed state. Accordingly, the density of the amorphous phase is thought to stay constant or at least not to increase appreciably in accord with increasing of the degree of compression. As the result, the density difference between the crystalline and amorphous phases will increase as the degree of compression increases which may result in the increase of the scattering intensity in the low-angular range.

The above-mentioned increase in the scattering intensity in the

low-angular range as well as in the d-spacings was recognized for the crosslinked samples also when they were crystallized from the melt under uniaxially stretched states as discussed in Chapter 1. Since, when those samples are either uniaxially compressed or stretched at the melt, molecular chains in the structure are to be stretched as explained in the last section, the mode of crystallization is likely to be similar for the both cases and the crystalline structures of the samples obtained are also similar.

6.5. The Crystallite Size Perpendicular to the crystal planes (200) and (110)

The crystallite size perpendicular to the crystal planes (200) and (110) was evaluated from the X-ray reflection profiles obtained by the "X-ray Scan 1" according to the method developed by Scherrer(22).

The crystallite size is related to the broadening of the X-ray reflection profile of the samples, β by the equation(22),

$$L_{hkl} = \frac{K' \lambda}{\beta \cos\Theta_{hkl}} \qquad (1)$$

if the broadening takes place only due to the finiteness and distibution of the crystallite size. Here, L_{hkl} is the crystallite size in a direction perpendicular to the corresponding crystal plane. K is a constant close to unity and related to both the crystallite shape and the way in

which β and L are defined. β is to be obtained from the pure X-ray reflection profile, $I(\chi)$ by the relation,

$$\beta = \int I(\chi)d\chi \; / \; I_{max} \qquad (2)$$

Here χ is the scattering angle to the incident beam and the integration is to cover the whole angular range in which the diffraction from the crystal plane concerned takes place due to the distribution of crystallite size.

In this work the value of β was evaluated from the line broadening of the experimentally obtained X-ray reflection profile by correcting the instrumental and K_α-doublet broadening with use of the X-ray reflection profile for quartz that was obtained under the same condition as for the samples and with the use of a value of 0.90 for K according to the Jones' procedure(23) where the distribution of crystallite size was assumed to be Gaussian.

Thus for samples with different compression ratios the crystallite size L was evaluated with the use of Eq.1 and β determined for the (200) and (110) reflection profiles for the samples by the above-mentioned procedure with use of the reflection profiles for the crysta planes (10·1) and (10·0) of quartz, respectively. The results are summalized in Table 3. It is seen in the table that the dimensions of the crystallites in directions perpendicular to the (200) or the (110) crystal plane are generally in a range of 170 to 350 Å, decreasing of the compression ratio.

Table 3. The size of crystallites of the lightly crosslinked polyethylenes crystallized under different degrees of uniaxial compression obtained by Scherrer's procedure(22).

Samples	Compression ratio	L_{110} Å	L_{200} Å
1. Molecular weight fraction of Hostalen, $\bar{M}\eta=3.4\times10^6$	4	236	281
	5	270	243
	6	236	228
	10	254	216
2. Commercial whole polymer, Hostalen, $\bar{M}\eta=2.5\times10^6$	6	315	289
	8	217	211
	10	208	172
3. Commercial whole polymer, Marlex 50, $\bar{M}\eta=0.14\times10^6$	4	348	299
	7	298	237
	8	261	256
	10	246	231

6.6. Unit-Cell Density and Crystallinity

The radiograph was taken with a 114.6 mm powder camera, with manganese-filtered Fe K_α radiation, and with the film fixed asymmetrically. A number of d-spacings of the crystal planes of the orthorhombic crystalline form of the samples were determined. The errors due to film shrinkage and to radius deviation of the camera were corrected using forward and backward diffractions of samples containing NaF(24). Other systematic errors caused by factors, such as miscentering of samples in the camera, were corrected by the use of a plot of the lattice parameter of NaF against $\cos^2\theta$ according to the method of Bradby and Jay(25), where θ is the Bragg angle for different crystal planes of NaF. Thus, the a-axis dimension was determined from d-spacings

for crystal plane (400) and the d-spacing pairs for (210) and (020), (310) and (020), and (310) and (110), respectively. The b-axis dimension was determined from the d-spacing for (020) and a pair of d-spacings for (310) and (110). The different calculation procedures yielded values that were in close agreement for both a and b lattice parameters. The average values of the cell dimensions were used for further studies. Furthermore the c-axis in sample 2 was determined from the cell-dimensions a and b together with any one of the d-spacings determined for (111), (201), or (211). The average value of the c-axis was 2.547 ± 0.0005 Å. However, the c dimension of samples 1 and 2 could not be obtained experimentally, because the diffractions from crystal planes (111), (201), and (211) were too faint to read, probably due to a highly crystalline orientation for the former and to imperfections in the crystalline phase of the latter sample.

The unit-cell density was obtained from the cell prameters a, b, and c, using the relation $d_u = 4 M_0 / abcN$. Here, M_0 is the molecular weight of the methylene unit and N is Avogadro's number. With atomic weight c = 12.011, H = 1.0080, and $N = 6.023 \times 10^{23}$, the equation reduces to $d_u = 93.153/abc$, where the unit-cell dimensions are in Angstrom units. All a-, b-, and c-axis dimensions were experimentally obtained for sample 2 as described above. The c axis for samples 1 and 3 was assumed to be 2.547 Å, the value obtained for sample 2. The results are summarized in Table 4 together with the macroscopic density and the degree of crystallinity at 30°. The degree of crystallinity was calculated either from the macroscopic density assuming

Table 4. Macroscopic, Unit-Cell Densities, and Other Thermodynamic Properties of Films Made from the Crosslinked Polyethylene Listed in Table 1 with Compression Ratio of 10.

Properties	Sample 1	Sample 2	Sample 3
Macroscopic density	0.942	0.938	0.942
Degree of crystallinity[a]			
$(1-\lambda)_d$	0.65	0.62	0.64
$(1-\lambda)_{\Delta H}$	0.560	0.566	0.570
Lattice parameters			
a	7.392	7.398	7.427
b	4.939	4.943	4.952
Unit-cell density[b]	1.002	1.000	0.994

a; $(1-\lambda)_d$, calculated from densities at 30°C, $(1-\lambda)_{\Delta H}$, calculated from the enthalpy of fusion. *b;* Assumed c = 2.547.

additivity in densities of the crystalline and amorphous phase or from the enthalpy of fusion divided by 70 cal/g (the enthalpy of fusion for a perfect crystal of polyethylene).

First, it is noted that the lattice parameters a and b observed in this study are very small values, and the unit-cell densities are either equal to or larger than unity for samples 1 and 2. Particularly, the unit-cell density of sample 1 (1.002) is the largest value reported for linear polyethylene to data(24, 26-31). Such a highly stable crystalline phase also should be expected from the extraordinarily high melting temperature of 155.0° observed for the samples. A slightly smaller unit-cell density is observed for sample 3. However, the macroscopic densities and, therefore, the calculated degrees of crystallinity of all samples are rather low contrary to expectations based

on the high melting temperatures and high unit-cell densities. A higher melting temperature and a larger unit-cell density for an isotropically well-crystallized polyethylene are generally associated with a larger macroscopic density and, therefore a higher degree of crystallinity. The converse is observed for samples in this study and is attributed to a stable crystalline phase. It must be concluded that the samples contain a very stable but smaller crystalline fraction coexisting with a rather large amorphous fraction.

At this moment, no information about the amorphous phase in these samples is available, but some is available for the uniaxially stretched and crystallized crosslinked sample. Birefringence studies by Chu, Kitamaru, and Tsuji(21) showed that in a lightly crosslinked polyethylene, prepared by high stretching in the molten state and subsequent cooling, a very highly uniaxially oriented crystalline phase coexisted with a large amorphous fraction having a low orientation. A low degree of orientation of molecules in the amorphous phase of a transparent strand prepared by the capillary-flowing procedure was also proposed by Jackson, Miller, and Porter(32) from ir dichroism measurements and by Desper, Southern, and Ulrich(3) from a birefringence study. Thus, it is supposed that the molecular chains in the amorphous phase of the transparent films in this study are also unoriented. Furthermore, it is confirmed by broad-line NMR studies as will be described in Chapter 7 that the molecular chains in the amorphous phase are associated with a larger molecular mobility. As can be seen in Table 4, the degree of crystallinity obtained from the enthalpy of fusion is slightly lower than that

derived from the macroscopic density. The lower degree of crystallinity calculated from the enthalpy of fusion indicates that the interfacial region in the structure makes a larger contribution to the enthalpy of fusion than to the macroscopic density as discussed by Mandelkern, Allou, and Gopalan (33). However, the difference between the degrees of crystallinity calculated from the density and from the enthalpy of fusion is smaller for all samples studied here than for that reported for normally crystallized polyethylene (30). This may imply that the structure of the interfacial region in these samples is rather simple, consisting with the conclusion reached from broad-line NMR studies that molecular chains in the amorphous phase are in a relaxed state.

6.7. Origin of Transparency

In section 3, it is pointed out that the crosslinked samples compressed highly in the melt are associated with a very high melting temperature and excellent transparency. For this polymer higher melting temperature is generally associated with nontransparency. Therefore, the excellent transparency with higher melting temperature recognized for the compressed samples should be considered in terms of their particular phase structure reviewed in the preceding sections. The appearance of excellent transparency for this polymer, holding its high melting temperature, has been sometimes reported for samples crystallized or processed under high degrees of molecular orientation as already

pointed out(1-11). The origin of the transparency for those samples is thought to be similar if the preparative processes for those are quite different.

In general the nontransparency or opaqueness of crystalline polymers is thought to be due to the existence of light-scattering entities such as voids or aggregates of crystallites, whose refractive index is different from that of the amorphous phase. Therefore if the sizes of those entities are smaller than the wavelength of visible light, the samples should become transparent. Wang, Chen, and Kwei supposed that smaller sizes of crystallites accounted for the transparency of the quenched-rolled film made by them(4). On the other hand, it is pointed out by Stein and Wilson(34) and by Keijsers, Van Aartsen, and Prins(35) that between the two terms of fluctuation -density and orientation- within crystalline polymers, the latter term usually is primarily responsible for the light scattering in crystalline polyethylene. Based on this fact Desper et al.(3) have accounted for the transparency of their samples, made by the capillary-flowing procedure, by assuming a very high orientation of c-axis and a high degree of crystallinity that could minimize intensity of light scattering. Moreover, based on observations of the light-scattering patterns of samples made by the quenched-rolled technique, Stein and Prud'homme(36) assert that the transparency of such polyethylene films is not primarily related to crystallite size but rather to the type of morphology and to the size of superstructures much bigger than the crystallites themselves.

Thus, the origin of transparency might be different in samples

produced by different techniques. However, the excellent transparency of our samples cannot be attributed to either a high degree of crystallinity or to smaller crystallites, since the degree of crystallinity of the samples was unexpectedly low in spite of the high melting temperatures (18). Also, the low-angle X-ray d-spacings were either not observed or were larger than 1500 Å (19). Therefore, we must suppose that the transparency is related to the very special spatial orientation of crystallites in the samples as proposed by Stein and others cited above, and also to the absence of spherulitic structure as concluded by Kawai and Hashimoto (37) from light-scattering data.

Note that the c-axis of the crystallites in our samples not only orients almost perfectly parallel to the film plane but also that crystal planes (200) or (110) orient predominantly in that direction, and that the low-angle d-spacings in the direction of the film plane are as large as 1500 Å. Based on these results, we assume that the structure of the samples is composed of aggregations of plate-like crystallites, the planes of which are coincident with either the (110) or (200) crystal planes. It is proposed that major molecular chains cannot exist in the amorphous state between the plane surfaces of the plate-like crystallites but only on their end surfaces, because molecular chains will be mostly parallel to the surface of the crystallites and, hence, will crystallize further. Such a structure accounts for the excellent transparency of our films. Alternatively, light-scattering entities in the samples may be regarded as amorphous phases located in the continuous ordered crystalline phase. Since the amorphous phases are

thought to be limited in size, the samples should be transparent.

6.8. Mechanism for Crystallization under High Degree of Compression

The experimental results cited in the foregoing sections suggest the formation of plate-like crystallites coexisting with rather large amount of amorphous material with a larger molecular mobility when a crosslinked sample is uniaxially compressed in the melt. The plane of the plate-like crystallites coincides with either (200) or (110) crystal plane, they are limited in the thickness 170-350 Å but they are as wide as 1000 or 1500 Å in the direction parallel to the film plane.

Figure 8 shows the torn edge surface of a lightly crosslinked sample (made from Hostalen) crystallized under a compression ratio of 10, taken by a scanning electron microscope. A lamellar structure with a thickness of about 200-300 Å can be recognized. This dimension approximately coincides with the linear dimension of the above-mentioned plate-like crystallites perpendicular to the plane surfaces. Thus the photograph visibly supports the crystalline structure concluded above. The formation of such crystalline structure is to be considered in terms of the nucleation mechanism of the crystallization. If a crosslinked sample is uniaxially compressed in the melt, molecular chains in the structure are to be stretched as mentioned in Section 1 of Chapter 5. Accordingly the equilibrium melting temperature of the system will be elevated owing to the decrease of the entropy of the molten state by

stretching and the degree of undercooling in the crystallization will be increased as discussed in Chapter 1. If the degree of undercooling is increased even to a less extent, the rate of crystallization is greatly amplified. Since the sample is uniaxially compressed and the molecular chains are deformed according to the macroscopic deformation, it is very likely that the crystal nuclei are born from the stretched molecular chains in the shape of very thin lamellae, which are oriented parallel to the macroscopic film surface. Furthermore, to minimize the interfacial free energy contribution for forming such nuclei, a nucleus to be born is likely to be composed of a very thin layer of a certain crystal plane with higher planar densities parallel to the molecular chains, becuase the interfacial free energy contribution is to be

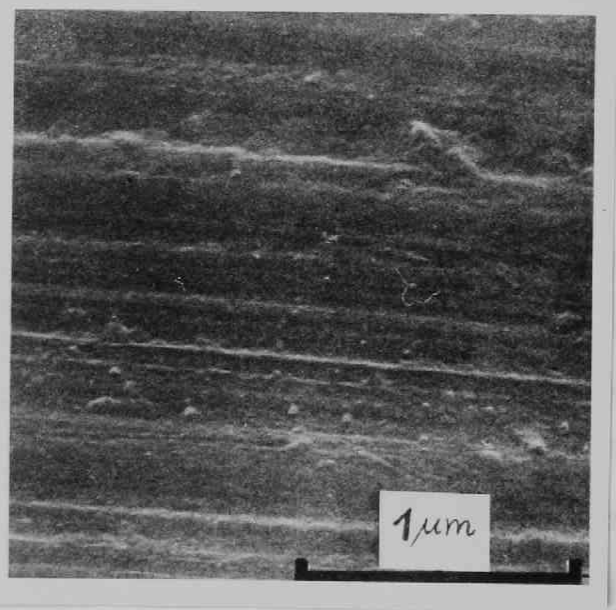

Fig.8. Torn edge surface of a lightly crosslinked sample (made from Hostalen), crystallized under a compression ratio of 10, taken with a scanning electron microscope.

minimum in a surface parallel to the molecular chains and maximum in a surface perpendicular to them. The nucleus may be a mono- or multimolecular layer of the crystal plane, which probably is the (200) crystal plane since the (200) planar orientation preferentially appears at a relatively low degree of compression.

So far as stretched molecular chains exist in the structure, this type of nucleation and the growth of the nuclei following the nucleation will proceed with an accelerated rate but accompanying these procedures stretched molecular chains will be rapidly dissipated and a part of the molecular chains will remain in an unstretched state unless the repeated folding back of the molecular chains into the same crystallite occurs. Since such repeated folding back of molecular chains is inhibited for the stretched samples with extremely high rate of crystallization so that the major crystallization takes place within a second, a part of the molecular chains eventually will remain in an unstretched and noncrystallizable state.

The argument mentioned above will plausibly explain the origin of the (200) crystal plane orientation and the very perfect crystalline phase coexisting with a rather great amount of unoriented amorphous material with larger molecular mobility. However, since two different types of nucleation are unlikely to occur simultaneously in the incipient stage of the crystallization, the origin of the (110) crystal plane orientation should be sought in other ways. Probably this orientation is produced by a partial destruction of crystallites gliding along the (110) crystal planes in the later stage of the crystallization.

References

1. J.H.Southern and R.S.Porter, J.Macromol.Sci., Phys., 4, 541 (1970).
2. J.H.Southern and R.S.Porter, J.Appl.Polym.Sci., 41, 2305 (1970).
3. C.R.Desper, J.H.Southern, R.D.Ulrich, and R.S.Porter, J.Appl.Polym. Sci., 41, 4284 (1970).
4. T.T.Wang, H.S.Chen, and T.K.Kwei, J.Polym.Sci., Part B, 8, 505 (1970).
5. T.K.Kwei, T.T.Wang, and H.E.Bair, J.Polym.Sci., Part C, 31, 87 (1970).
6. R.G.Crystal and J.H.Southern, J.Polym.Sci., Part A-2, 9, 1641 (1971).
7. K.Imada, T.Yamamoto, K.Shigematsu, and M.Takayanagi, J.Materials Sci., 6, 537 (1970).
8. A.Buckley, H.A.Aong, Polym.Eng.Sci., 9, 115 (1969).
9. D.Krueger and G.S.Y.Yeh, J.Appl.Phys., 43, 4339 (1972).
10. V.Tan and C.G.Gogoes, Polym.Eng.Sci., 16, 512 (1976).
11. J.R.Collier, T.Y.T.Tam, J.Newcome, and N.Dinos, Polym.Eng.Sci., 16, 204 (1976).
12. R.Kitamaru and H.-D.Chu, Bull.Inst.Chem.REs., Kyoto Univ., 46, 97 (1968).
13. W.H.Stockmayer, J.Chem.Phys., 12, 125 (1944).
14. P.J.Flory, J.Am.Chem.Soc., 69, 30 (1947).
15. R.Kitamaru, L.Mandelkern, and J.Fatou, J.Polym.Sci., Letter Ed., 2, 511 (1964).
16. O.Kratky, G.Porod, and Z.Skala, Acta Phys.Austriaca, 13, 76 (1960).
17. O.Kratky, Adaptation of the Technique of Diffuse Small-Angle X-ray Scattering to Extreme Demands, in Small Angle X-Ray Scattering, edited by H.Brumberger, Gordon and Breach, New York 1965, P.63.
18. R.Kitamaru, H.-D.Chu, and S.-H.Hyon, Macromolecules, 6, 337 (1973).
19. R.Kitamaru and S.-H.Hyon, Makromol.Chem., 175, 255 (1974).

20. S.-H.Hyon, H.Taniuch, and R.Kitamaru, Bull.Inst.Chem.Res., Kyoto Univ. 51, 19 (1973).

21. H.-D.Chu, R.Kitamaru, and W.Tsuji, J.Appl.Polym.Sci., 10, 1377 (1966).

22. P.Scherrer, Gottinger Nachrichten, 2, 98 (1918).

23. F.W.Jones, Proc.Roy.Soc, [London] A166, 16 (1938).

24. R.Kitamaru and L.Mandelkern, J.Polym.Sci., Part A-2, 8, 2079 (1970).

25. H.P.Klug and L.E.Alexander, "X-ray Diffraction Procedures," John Wiley and Sons, Inc., New York, N.Y., 1954, p.461.

26. C.Bunn, Trans.Faraday Soc., 35, 482 (1939).

27. E.R.Walter, F.P.Reding, J.Polym.Sci., 21, 561 (1956).

28. P.R.Swan, J.Polym.Sci., 42, 525 (1960); ibid., 56, 403 (1962).

29. M.I.Bank and S.Krimm, J.Appl.Phys., 39, 4951 (1968).

30. G.T.Davis, R.K.Eby, and G.M.Martin, J.Appl.Phys., 39, 4973 (1968).

31. S.Kavesh and J.M.Schultz, J.Polym.Sci., Part A-2, 8, 243 (1970).

32. J.F.Jackson, P.J.Miller, and R.S.Porter, Polym.Prepr., Amer.Chem.Soc., Div.Polym.Chem., 13 335 (1972).

33. L.Mandelkern, A.L.Allou, Jr., and M.Gopalan, J.Phys.Chem., 72, 309 (1968).

34. R.S.Stein and P.R.Wilson, J.Appl.Phys., 33, 1914 (1962).

35. A.E.M.Keijsers, J.J.Van Artsen, and W.Prens, J.Appl.Phys., 36, 2874 (1965).

36. R.S.Stein and R.Prud'homme, J.Polym.Sci., Part B, 9, 595 (1971).

37. H.Kawai and T.Hashimoto, Private Communication.

Chapter 7.

PHASE STRUCTURE AND MOLECULAR MOBILITY IN LIGHTLY CROSSLINKED POLYETHYLENE, CRYSTALLIZED FROM THE MELT UNDER UNIAXIAL COMPRESSION BY BROAD-LINE NMR SPECTROSCOPY

7.1. Introduction

The preceding chapter have been concerned with the crystallographical structure of the crosslinked samples compressed in the melt. However, Significantly smaller macroscopic density of the samples than the unit-cell density obtained from an X-ray diffraction exclusively suggests the existence of an amorphous material in the structure. They have a phase structure composed of the crystalline and amorphous materials at room temperature.

Several studies have recently been reported on the molecular motion of elongated polyethylene using broad-line NMR(1-4). However, there has been no report on sample crystallized from the melt under molecular orientation.

This chapter deals with a more detailed analysis of the phase structure and molecular mobility in a lightly crosslinked polyethylene prepared under various conditions involving molecular orientation by a refined NMR analysis.

7.2. Experimental Part

Material

Starting material was commercial Marlex-50 with a viscosity average molecular weight of 136,000. It was used without any molecular weight fractionation. A lightly crosslinked sample was made by irradiation of this material with γ-ray from ^{60}Co. Films about 2.0 mm thick of the polymer was irradiated to a dose of 20 Mrad in vacuum at room temperature. The gel fraction of this irradiated sample was 0.76 and the densities of crosslinked units and the free end groups were evaluated (5, 6) approximately to be 1.1×10^{-3} and 2.0×10^{-4}, respectively.

Compression and Crystallization

a. Crystallization from the melt under uniaxial compression (melt-compressed samples); The crosslinked sample was compressed to different extents between two metal plates in the completely molten state at 180°C and crystallized at 120°C for 60 minutes.

b. Plastic deformation at a temperature below its melting point under uniaxial compression (plastically compressed samples); The crosslinked sample was compressed to different extents between two metal plates after pre-heating for 5 minutes at 120°C and annealed at 120°C for 60 minutes.

In these procedures, the film thickness was reduced in accord with the increase of the degree of compression. The compression ratio was expressed by the ratio between the film thicknesses before and after compression.

Density and Degree of Crystallinity

The density measurement was made at 30°C by a density gradient column of toluene and dioxane. The density was converted to the degree of crystallinity $(1-\lambda)_d$, assuming the additivity densities of the crystalline and amorphous phases, using the relation $(1-\lambda)_d = (1/\rho_a - 1/\rho) / (1/\rho_a - 1/\rho_c)$. Here ρ, ρ_a, and ρ_c are the measured density of samples, densities of amorphous and crystalline states of the polymer, respectively. $\rho_a = 0.851$, $\rho_c = 1.000$ were adopted here.

Spectrometry and Analysis

The first derivative NMR spectrum was obtained over a wide range of temperature -80 ∿ +40°C for the two series of samples with a JNM-PW-60 NMR Spectrometer (JEOL Ltd.). The sample films were packed in a pyrex tube 18 mm diameter for the NMR measurement, after cutting finely to avoid complication arising from the anisotropical orientation of molecular chains in the structure. The NMR spectrum obtained indicated no dependency on setting angle of samples to the main magnetic field. The detailed procedure for analysis of spectrum was described in Chapter 2.

7.3. Phase Structure at Room Temperature

In Chapter 5, it is described that, if a lightly crosslinked polyethylene film is compressed between two metal plates in the molten state and crystallized by cooling to room temperature, the (200)-planar orientation parallel to the film surface first appears at relatively low

compression ratio and the (110)-orientation follows at higher compression ratios. This planar orientation of the crystal planes was also recognized for a lightly crosslinked polyethylene compressed at a high temperature below its melting point. However, the morphological aspects of amorphous region of samples prepared under the two conditions showed a marked difference(7).

Figure 1 demonstrates the three-component analysis of the spectra at room temperature for crosslinked samples compressed to different degrees. For comparison, the results are shown also for samples compressed in the partially crystallized state at 120°C.

As can be seen, the samples compressed in the melt comprise abundant narrow component with lesser medium component whereas the samples compressed at 120°C comprise large amounts of medium component with larger line-widths. These results suggest that the former samples have a mobile amorphous content whereas the latters have a greater amount of immobile amorphous content.

The numerical results of the three-component analysis are summarized in Table 1. It is evidently recognized that, when the crosslinked sample is compressed in the partially crystallized state at 120°C, the mass fraction w_m as well as the second moment $\langle \Delta H_2^2 \rangle_m$ of the medium component increase with diminishing narrow component as the degree of compression increases. It is thought that, when the sample is compressed in the partially crystallized state, the molecular chains in the amorphous region are first stretched and realignment of crystallites accompanying those partial destruction follows. In such a case,

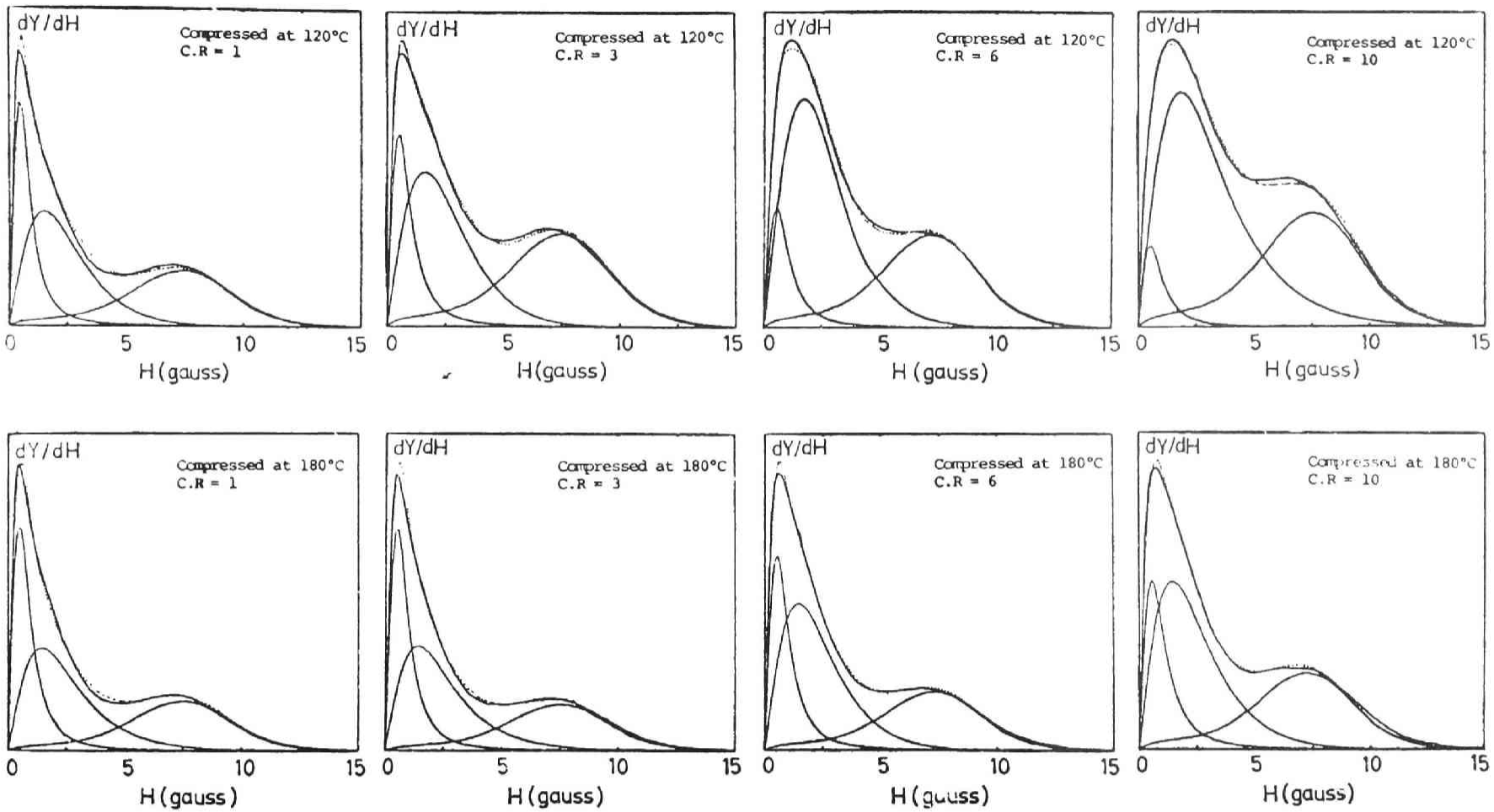

Fig. 1. Broad-line NMR spectra at room temperature for the crosslinked sample compressed to different degrees. The compression ratio is indicated in each spectrum. Upper and lower series show the data for samples compressed at 120°C and at 180°C, resp. Thin solid lines indicate the narrow, medium, and broad components, resp., from the left side.

Table 1. Three-Component Analysis of Spectra at Room Temperature for Crosslinked Samples Compressed to Different Degrees in the Melt at 180°C or in the Partially Crystallized State at 120°C

Sample	CR*	Density g/cm^3	$(1-\lambda)_d$	Mass fraction			Line width or Second moment (G or G^2)		
				w_b	w_m	w_n	ΔH_b	$\langle \Delta H_2^2 \rangle_m$	ΔH_n
Compressed at 180°C	1[a]	0.9396	0.633	0.617	0.284	0.099	14.6	6.3	0.80
	3	0.9410	0.642	0.608	0.288	0.104	14.7	6.0	0.80
	6	0.9418	0.647	0.612	0.293	0.095	14.7	4.8	0.85
	8	0.9432	0.656	0.608	0.300	0.092	14.6	4.7	0.85
	10	0.9454	0.670	0.623	0.303	0.074	14.6	5.4	0.98
Compressed at 120°C	1	0.9489	0.689	0.661	0.237	0.102	14.6	4.7	0.80
	3	0.9489	0.692	0.648	0.290	0.062	14.6	5.2	0.85
	6	0.9492	0.694	0.609	0.352	0.039	14.5	6.3	0.90
	8	0.9495	0.696	0.582	0.386	0.032	14.7	7.6	0.95
	10	0.9498	0.699	0.578	0.405	0.017	14.6	9.0	1.04

* CR : Compression ratio.

a. Uncompressed, but after melted 180°C it was quenched to room temperature for 15 min.

amorphous molecular chains with restricted mobility will be produced to high extents, and the amorphous content with liquidlike molecular mobility will hardly be produced. The above-observed increase of the w_m and $\langle \Delta H_2^2 \rangle_m$ and decrease of w_n are thought to reflect this situation.

On the other hand, it is recognized for the sample compressed in the melt that both w_m and $\langle \Delta H_2^2 \rangle_m$ are not increased appreciably until the highest degree of compression ($1/\alpha_z = 10$). Furthermore, the broad and narrow components are also not changed appreciably with increasing degree of compression. Even in the structure of the highly compressed sample, rather large amount of narrow component such as $w_n \geq 0.074$ still exists. These results evidently show the coexistence of amorphous material with larger molecular mobility with the stable crystalline phase. It is to be noted here that the amorphous material in the samples produced by this mode of crystallization is associated with larger molecular mobility although the crystallites in the structure are highly oriented in space as mentioned in Chapter 5.

7.4. Temperature Dependence of the Phase Structure

I have discussed the phase structure of the film samples as a function of the compression ratio in terms of molecular mobility by analyzing the spectrum at room temperature. I next consider the phase structure as a function of temperature by the three-component analysis

of spectrum in a wide range of temperature.

Figure 2 demonstrates the three-component analysis of spectra for the two kinds of samples with compression ratio of 10. Despite of the large difference in the overall line shape, the composite curve of the three components analyzed is in good accord with the spectrum observed in the wide range of temperature.

In Figure 3,the mass fractions of the three components and second moments of medium component for the two samples with compression ratio of 10 are plotted against temperature. It is evident that the temperature dependence of the three components can be essentially understood in connection with the β- and γ-relaxation phenomena recognized in mechanical and dielectric measurements as discussed for the bulk-and solution-crystallized samples(8,9). However, the detailed temperature dependence varies greatly with the preparation condition of samples. For the both samples, at a temperature below -100°C the medium component w_m appears and increases with the decrease of the broad component w_b as temperature increases. This suggests that a local molecular motion, which corresponds to the so-called γ-relaxation temperature, originates in a non-crystalline region and spreads over the whole noncrystalline region.

At about -50°C the narrow component appears with decreasing w_m for the sample compressed in the melt. This suggests that a molecular motion with larger mobility such as a micro-Brownian motion of molecular chains, corresponding to the so-called β-relaxation, originates and spreads in a some region of the noncrystalline region. On the other hand, for the sample compressed at 120°C, the narrow component

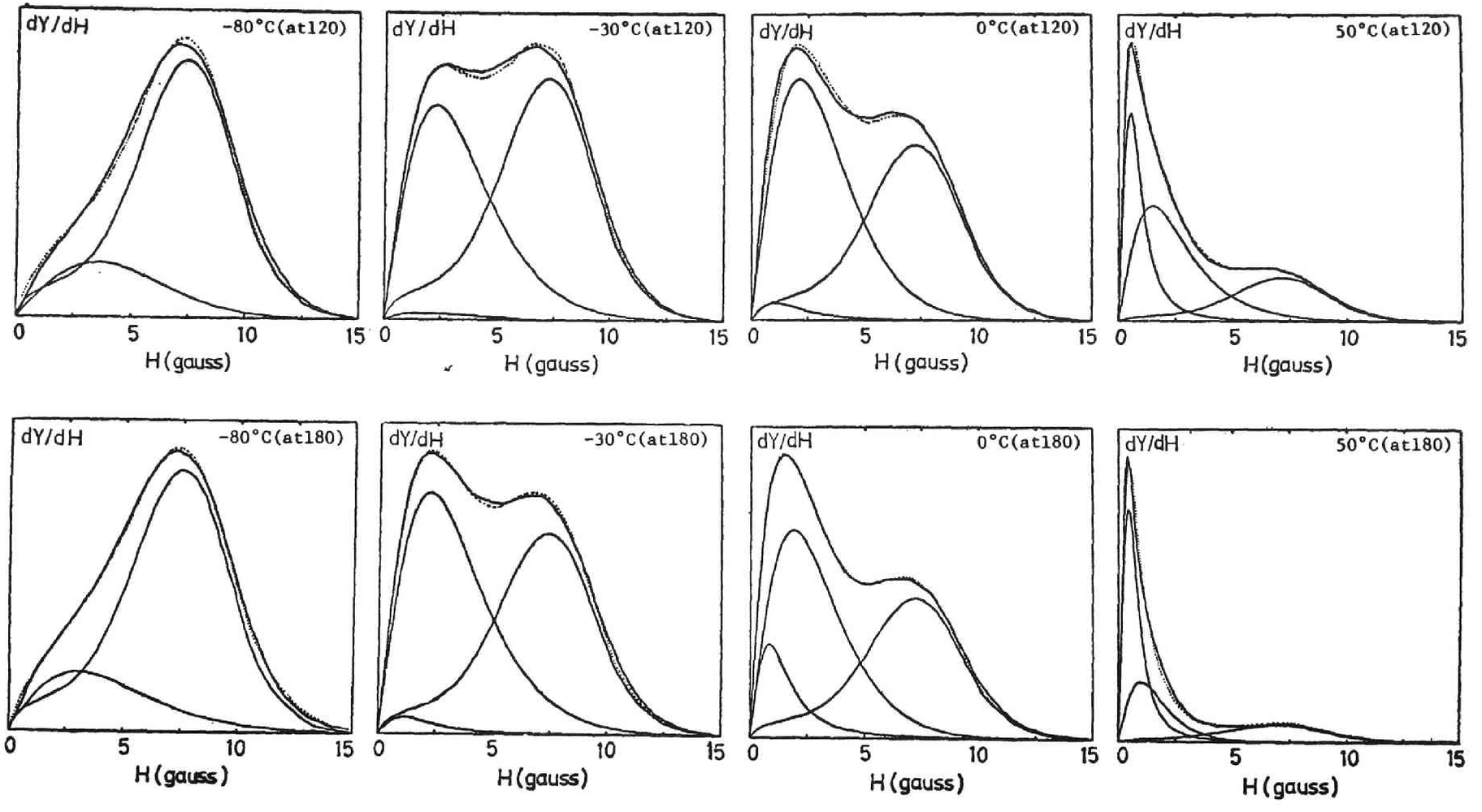

Fig. 2. Three-component analysis for samples compressed at 120°C and at 180°C(compression ratio = 10) in a wide range of temperature. See the legend in Figure 1 about the distinction of lines.

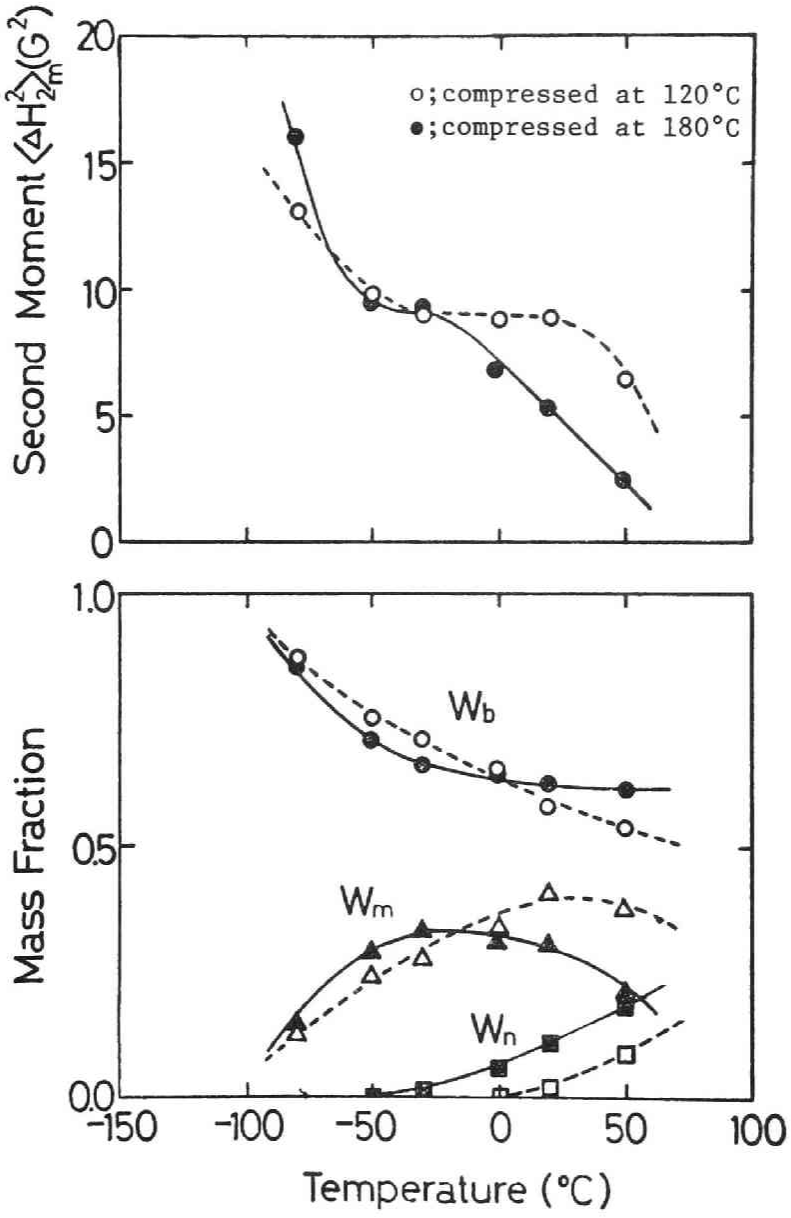

Fig. 3. Mass fraction and second moment of three-components as a function of temperature for samples compressed at 120°C and at 180°C.

does not appear until 0°C and even if the temperature further rises it does not increase appreciably. This suggests that the noncrystalline material of this sample has a rather restricted conformation of molecular chains and such molecular motion as the micro-Brownian motion with larger mobility could not appear appreciably but to only a limited extent.

The difference in the phase structure between the two samples is evidently recognized also in the second moment and the line-width of the medium and narrow component, respectively. Smaller values for both of $\langle \Delta H_2^2 \rangle_m$ and ΔH_n are associated with the sample compressed in the melt over a wide range of temperature. This evidently shows larger molecular mobility in the noncrystalline regions for this sample. On the other hand, the $\langle \Delta H_2^2 \rangle_m$ of the sample compressed at 120°C decreases until -50°C with increasing temperature with the increase of the w_m but it holds a very high level larger than 8 G^2 in a temperature range of about -50°C to +50°C and again decreases above 50°C.

This characteristic S-type behavior and the high values of $\langle \Delta H_2^2 \rangle_m$ are approximately equivalent with those for the bulk-crystal with a low molecular weight (10) and for the filaments with high draw ratio(11). In these bulk crystal and highly drawn filaments, molecular chains that contribute to the medium component must be composed of short molecular chains that are excluded from the basal plane of lamella crystallites. Such molecular chains must be in a rather extended chain conformation and comprise a parallel intermolecular alignment perpendicular to the basal plane of a crystallite. The large values

and characteristic temperature dependence of $\langle \Delta H_2^2 \rangle_m$ recognized for the both kinds of samples may be associated with the highly extended molecular chain conformation in the amorphous region.

7.5. Conclusion

The broad-line NMR spectroscopy for a lightly crosslinked polyethylene prepared under various conditions involving molecular orientation, has led to the following conclusions.

The NMR spectrum analysis shows that the phase structure of the samples compressed in the melt is quite different from that of the sample compressed below the melting point. For the samples crystallized from the melt under uniaxial compression, the crystalline region is as stable as comparable to that in the isothermally well crystallized samples. This kind of sample comprises amorphous material associated with a liquidlike molecular mobility. On the other hand, for the samples compressed at a temperature below its melting point, the crystalline region is not so stable and molecular chains in the noncrystalline region are rather strongly constrained, not associated with liquidlike molecular mobility.

Reference

1. D.Hyndman and G.G.Origlio, J.Polym.Sci., 39, 556 (1959).
2. H.G.Olf and A.Peterlin, J.Appl.Phys., 35, 3108 (1964).
3. E.W.Fischer, H.Goddar, and W.Piesczek, J.Polym.Sci., C-32, 149 (1971).
4. J.B.Smith, A.J.Manel, and I.M.Ward, Polymer, 16, 57 (1975).
5. W.H.Stockmayer, J.Chem, Phys., 12, 125 (1944).
6. P.J.Flory, J.Am.Chem.Soc., 69, 30 (1947).
7. S.-H.Hyon, R.Kitamaru, H.Taniuch, N.Tamura, and N.Hayakawa, Kobunshi Ronbunshu, 32, 240 (1975).
8. R.Kitamaru, F.Horii, and S.-H.Hyon, J.Polym.Sci.Polym.Phys.Ed., 15, 821 (1977).
9. F.Horii and R.Kitamaru, J.Polym.Sci.Polym.Lett.Ed., in press.
10. R.Kitamaru, F.Horii, and S.-H.Hyon, ACS.Polym.Prepr., 17, 549 (1976).
11. S.-H.Hyon, F.Horii, and R.Kitamaru, Bull.Inst.Chem.Res.Kyoto Univ., 55, 248 (1977).

Chapter 8.

PREPARATION OF TRANSPARENT POLYETHYLENE PRODUCT THROUGH CONTINUOUS ROLLING BY IRRADIATION CROSSLINKING

8.1. Introduction

The so-called high density polyethylene, associated with a high crystallinity and high melting temperature, generally possesses many useful practical properties such as excellent mechanical properties, chemical and thermal stabilities, electric insulation and etc. Accordingly it is widely used commercially when such properties are demanded. But because it is usually not transparent, the practical use is sometimes restricted. On the other hand, the so-called low density polyehtylene is very transparent, but its practical use is restricted because it is devoid of many properties as crystalline polymers. In this case the transparency is thought to have been brought about by the sacrifice of the crystallinity.

It has been generally believed that high crystallinity and transparency could not coexist for this polymer. However, it is found in the preceding chapters that if a lightly crosslinked polyethylene is uniaxially compressed in the melt, a very transparent film with a high melting temperature could be produced. This suggests a possibility of the production of transparent film by a conventional rolling process in a commercial scale.

8.2. Samples and Irradiation

Two commercial high density polyethylenes were used as starting materials, Sholex S5008 and Hizex 7000F with average molecular weights of 52,000 and 200,000, respectively. Films about 250 μ thick and 15 cm wide were continuously irradiated with a rate of 2 m/min. to electron beam from 2 MEV Van de Graaff in nitrogen atmosphere. The procedure is shown schematically in Figure 1.

The irradiation was carried out at room temperature.

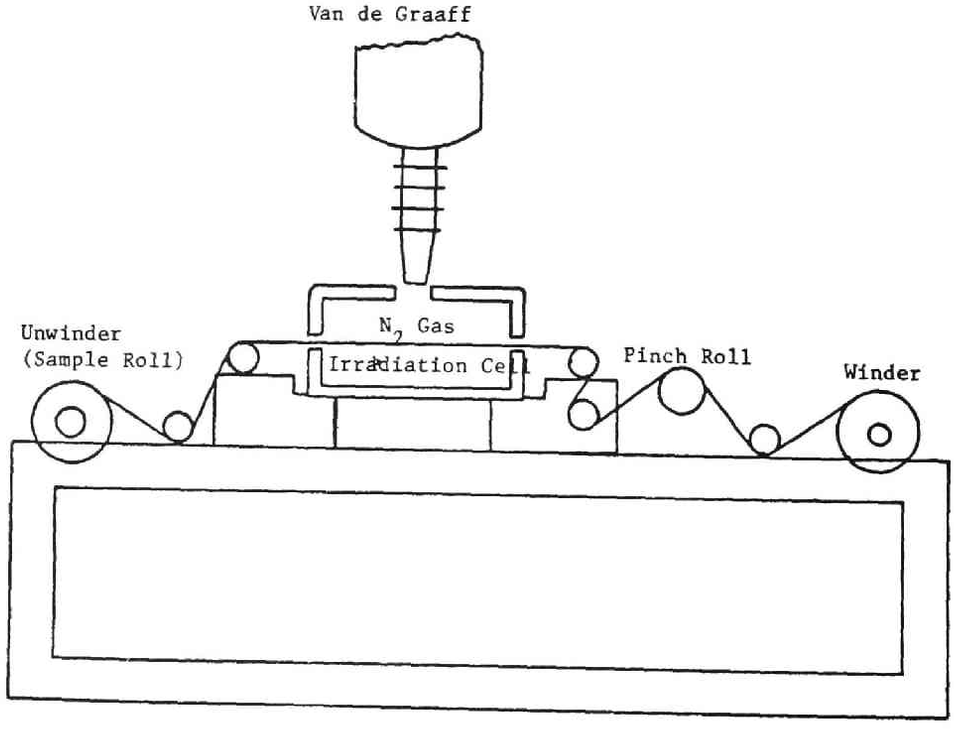

Fig. 1 Schematic diagram for continuous irradiation procedure.

8.3. Rolling Procedure

The irradiated films were continuously rolled at different temperatures with modified calender roll as shown schematically in Figure 2. The irradiated films (A) were preheated to a predetermined temperature under controlled tension in the Sections B and C and rolled in the Section D and wound under controlled tension. In this procedure the tensions were controlled so that the thickness of the films was reduced while the width was held unchanged. Namely, the deformation was performed in the directions parallel to the rolling and perpendicular to the film plane.

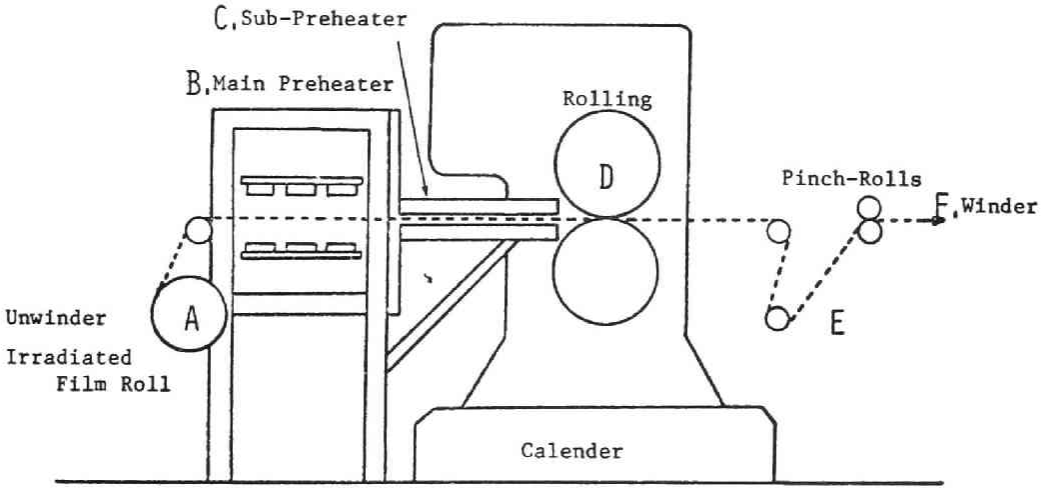

Fig. 2 Schematic diagram for continuous rolling procedure.

8.4. Results and Discussion

The results are summarized in Table 1. It is seen that transparent films could be produced by the continuous rolling procedure. It is noted first that the transparency is obtained by a relatively low compression ratio by this procedure. When a crosslinked sample is uniaxially compressed in the melt, the transparency is not obtained unless highly compressed to such extaents that the compression ratio exceeds 4 or 5. Contrary, in the case of the rolling process the transparency is obtained for samples with compression ratios smaller than 2.4.

In this case, if a coordinate system (x, y, z) is fixed so that x, y, and z axes correspond to the direction parallel to the rolling direction, and to the directions in the width and thickness of the film, respectively, the deformation of molecular chains can be expressed by the following equation in terms of the average squares of the end-to-end distance of molecular chains.

$$\langle R^2 \rangle_\alpha \; / \; \langle R^2 \rangle_0 = (1 + \alpha_z^{-2} + \alpha_z^{\;2}) \; / \; 3 \qquad (1)$$

with

$$\alpha_x \, \alpha_y \, \alpha_z = 1, \qquad \alpha_y = 1, \qquad \alpha_z = 1 \; / \; \alpha_x$$

Here $\langle R^2 \rangle_\alpha$ and $\langle R^2 \rangle_0$ designate the mean squares of the end-to-end distance of the molecular chains in the deformed and isotropic states, respectively. α_z is the degree of macroscopic deformation of the sample in z-direction and coincides with the reciprocal of the compression ratio in the rolling

Table 1. Preparation of Transparent Film by a Continuous Rolling

No	Sample[a]	Irradiation, Mrad	Gel Content, %	Rolling Condition: Temperature, °C: Preheat	Rolling Condition: Temperature, °C: Roll	Rolling Condition: Compression: Pressure kg/cm²	Rolling Condition: Compression: Ratio[d] $1/\alpha_z$	Heat Shrink in MD Direction, %: at 100°C	at 110°C	at 120°C	Tensile Properties at Break: Strength kg/cm²	Tensile Properties at Break: Elongation %	Tear Strength in MD Direction, kg/cm	Transparency[c]
1	S	0	0	no	115	453	4.6	2	6	19	1430	39	4	-
2	S	5	21	no	122	434	4.2	1	2	11	1226	22	4	++
3	S	7	32	no	114	——	4.2	–	11	75	1192	75	3	++
4	S	10	47	140	100	50	4.6	–	17	66	1261	55	6	++
5	S	20	69	145	115	50	2.4	0	0.8	2.5	1200	71	Ext.[b]	++
6	H	20	70	145	115	50	2.8	0	1.0	9.4	1800	41	Ext.[b]	++

a) S: Sholex S5008, H: Hizex 7000F, see the text.

b) Impossible to tear in the machine direction (MD).

c) Transparency, -: no, ++: excellent.

d) Ratio of the thicknesses between the original and the compressed film.

process.

Since the value of the right hand side in eq.(1) is a little larger than that of eq.(1) in Chapter 5 for $\alpha_z < 1$ which describes the deformation of molecular chains for the uniaxial compression, the molecular chains will be stretched to a slightly larger extent in the rolling process than when compressed uniaxially at the equivalent compression ratio. Furthermore, in the case of rolling such stretching of molecular chains should be conducted predominantly in one direction, namely in rolling direction (x-direction). Therefore, it is very likely that the plate-like crystallites produced by the rolling process are further ordered in the direction so that the transparency appears at a relatively low degree of compression.

The X-ray diffraction photographs taken in the three directions (Sample 5) are shown in Figure 3. The patterns taken in the 1- and 2-directions show a c^*-axis orientation parallel to the machine direction. These two patterns may not give information of the orientation of crystal planes owing to those strong uniaxial orientation in the machine direction. However, the pattern taken in the 3-direction clearly shows firm existence of both (200)- and (110)-plane orientations parallel to the film surface of the sample in addition to the c^*-axis orientation. For the (110)-diffractions, intensity peaks are recognized in the meridional and intermediate directions. The intensity in these directions will respectively correspond to Ω=0 arising from the (110)-orientation and to Ω=67.0 and 55.6°(superposed) arising from the (110)- and (200)-orientations. Also for the (200)-diffraction enhanced intensity

is recognized in the meridional and intermediate directions, that will correspond to Ω = 0 and 55.4° arising from the (200)- and (110)-orientations, respectively. Thus it is concluded that both (200)- and (110)-orientations exist in this sample.

In this way, the (200) and (110) planar orientations were confirmed by X-ray diffraction studies also for the crosslinked sample rolled by this mode of rolling. The former orientation appeared at relatively low degree of compression and the latter followed at a higher degree of compression. Therefore, the phase structure of the samples is similar to that of the samples uniaxially compressed in the molten state.

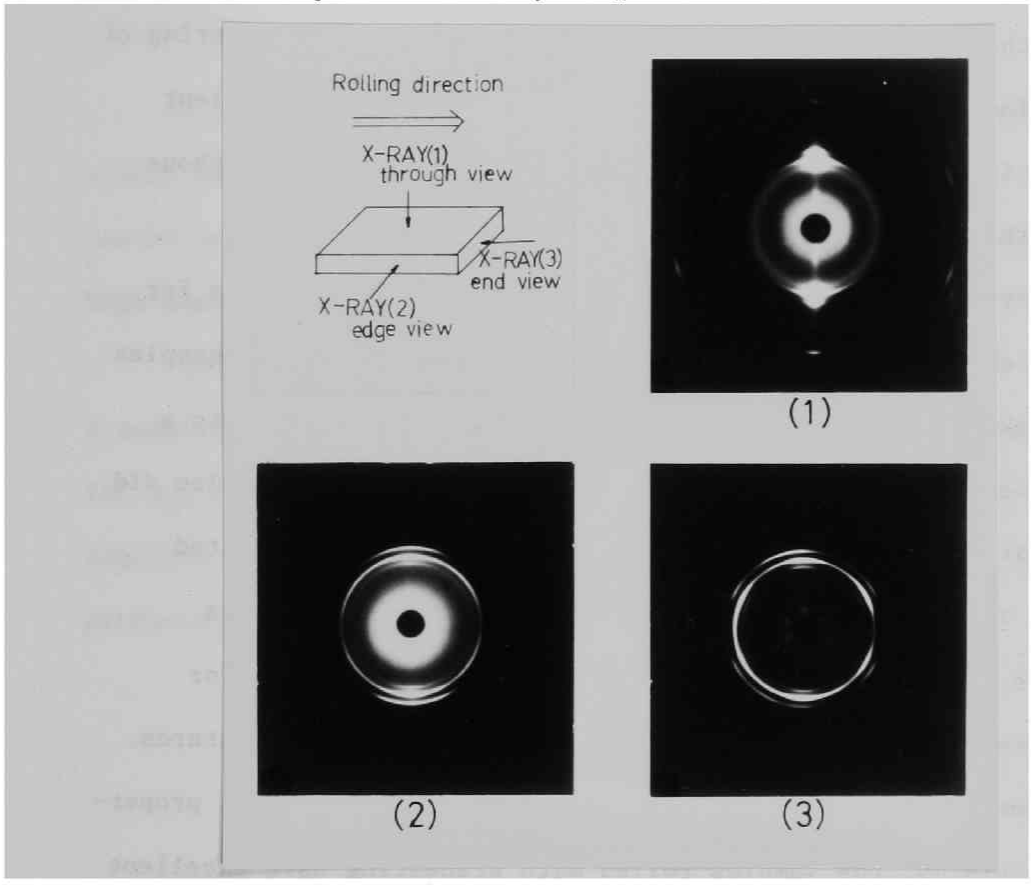

Fig. 3. The flat camera X-ray patterns with X-ray incident beam in different directions for the crosslinked sample rolled at temperature of 115°C after premelting.

Table 1 includes the results for the crosslinked samples which were rolled in the partially crystallized state without preheating. It is seen that excellent transparency was obtained in these cases. Contrary, when the samples were compressed only uniaxially at the corresponding temperatures without melting, such excellent transparency was hardly recognized. It is thought that the molecular chains in the amorphous region for the samples rolled without preheating are rather strongly stretched and their molecular mobility is restricted in a similar manner for the samples compressed uniaxially without melting. But the rolled samples will have more ordered crystalline contents as pointed out even if the rolling is conducted without melting. Such ordering of the crystalline contents is thought to have brought about excellent transparency irrespective of the detailed structure of the amorphous material in the structure.

It is noted secondly that excellent demensional stabilities for heating were obtained for samples rolled after melting. Those samples did not shrink appreciably at 110°C (Samples 5 and 6) and only to a small extent even at 120°C (Sample 5). Furthermore, those samples did not lose their excellent transparency by the heating unless melted completely. This excellent demensional stability for heating is thought to be very advantageous for the practical use such as for wrapping films of foods for the sterilization at higher temperatures.

The films rolled in this mode exhibit excellent mechanical properties. Particularly, the samples rolled with preheating have excellent strength for tearing in the rolling direction so that those are

impossible to tear in the direction. It is known that, if crystalline polymers are rolled in an usual manner at high temperatures but below the melting temperatures, the tensile strength in the rolling direction is increased but the tear strength becomes poor so that those could be easily torn with fingers. It is seen Table 1 that when the cross-linked samples are rolled without premelting the tear strength in the rolling direction becomes poor as expected but when those are rolled in the melt the products could not be torn in the machine direction. This is thought to correlate with the relaxed state of molecular chains in the amorphous content.

In conclusion, it is shown that excellent transparent films with a high demensional heat-stability and excellent mechanical properties can be produced continuously by a rolling process from a commercial high density polyethylene.

Furthermore, the transparent products obtained showed a high transmittance for ultraviolet light(1) and excellent gas permeabilities for N_2, CO_2, Ar, etc.(2). Therefore, when such properties are demanded together with higher melting temperature and transparency, those products will be used in a commercial scale.

References

1. S.-H.Hyon and R.Kitamaru, unpublished data.

2. H.Yasuda, S.-H.Hyon, and R.Kitamaru, unpublished data.

Chapter 9.

ORIENTATION OF CRYSTAL PLANES IN LIGHTLY CROSSLINKED ISOTACTIC POLYPROPYLENE CRYSTALLIZED FROM THE MELT UNDER UNIAXIAL COMPRESSION

9.1. Introduction

In recent papers(1-12) it was reported that if crystalline polymers are crystallized from the melt or processed under conditions of high molecular orientation, a particular spatial orientation of crystal planes appears on a macroscopic scale. It was confirmed by authors (1, 3) that, if a lightly crosslinked polyethylene is uniaxially compressed in the melt and then crystallized by cooling, there appears a unique alignment of polymer chains in the crystalline phase. Crystallites with (200) planes parallel to the film surface form at a relatively low degree of compression; at higher compression, crystallites with the (110) planes are parallel to the film surface.

An analogous alignment of crystal planes has also been noted for lightly crosslinked isotactic polypropylene treated similarly (8-12). This chapter deals with a more detailed analysis of this phenomenon and discusses the mechanism of the alignment.

9.2. Experimental Part

Material

A fraction with a viscosity-average molecular weight of 4.0×10^5

was obtained from a commercial isotactic polypropylene by liquid-liquid separation technique using xylene and a polyethylene glycol with a molecular weight of 380-420. Intrinsic viscosity measurements were made in decalin with 0.1% 2,6-di-t-butyl-p-cresol at 135 °C, and molecular weights were calculated using the relation $[\eta] = 1.38 \times 10^{-4} M_{\eta}^{0.8}$ of Kinsinger et al.(14) The isotacticity was estimated to be 96% from infrared absorptions at 998 and 974 cm^{-1} (18). Films about 2.0 mm thick were obtained by molding at 200°C and quenching in ice water.

Crosslinking

The crosslinking efficiency of high-energy radiation for isotactic polypropylene is rather low. Hence, γ-ray irradiation in an acetylene atmosphere was examined, following a procedure developed by Todoki et al. for nylon-6(15). The films were irradiated with ^{60}Co γ-rays with a dose rate of 7.7×10^{4} rad/hr at room temperature. After irradiation, the gel fraction W_g (mass fraction of the insoluble part in the total mass) was evaluated by extracting with boiling xylene and drying. As shown in Table 1, the crosslinking efficiency of the irradiation in vacuo is very low, but irradiation in acetylene produces high gel content with relatively small doses. The gel sample obtained from experiment no. 3 was used after extracting the soluble part (20%) with boiling xylene. It was 94% isotactic.

Uniaxial Compression

The gel samples in film form were next uniaxially compressed in

Table 1. Irradiation of Isotactic Polypropylene

Expt. No.	Acetylene pressure[a], (atm)	Dose, Mrad	Gel fraction
1	1.5	5.0	0.39
2	1.5	10.0	0.55
3	2.0	10.0	0.80
-	*in vacuo*	20.0	0
-	*in vacuo*	30.0	0.42
-	*in vacuo*	100.0	0.59

a; The pressure was not measured precisely; values are indicative only within $\pm$ 1 atm.

the melt at 180°C between two metal plates and cooled to room temperature over a period of 15 min. The compression ratio of the samples was characterized by the ratio of film thicknesses before and after compression. This compression factor ranged from 1 to 15.

X-Ray Diffraction

The X-ray diffraction measurements were carried out with a flat camera and two kinds of diffraction scan with a Ni-filtered Cu K_α beam. These experimental techniques are the same as were previously used in Chapter 5 for studying the orientation of crystallites in crosslinked polyethylene(1-3).

9.3. The Orientation of Crystal Planes

X-ray diffraction photographs were obtained for samples prepared with different compression ratio. With the X-ray beam perpendicular to the film surface, the diffraction pattern consisted of uniformly intense Debye-Scherrer rings for all compressions. This indicates a random distribution of crystallites in the samples about the normal to the film surface.

However, with the X-ray beam parallel to the film surface, the X-ray patterns in Figure 1 were obtained with significant changes in the intensity in each ring. These patterns suggest that, as compression increases, not only do the molecular chain axes in the crystallites orient parallel to the film surface but particular crystal planes also orient parallel to the film surface.

In order to understand this orientation of crystal planes in more detail, X-ray diffraction scans were performed.

The data for the (040), (110), and (130) scans are shown in Figure 2 and the reciprocal lattice diagram of the monoclinic form of the polymer is shown in Figure 3. In the (040) scan, I sinϕ has a maximum at $\phi = 0$ for all compressions; but in (110) or (130) scans the maximum is found only for samples with compressions of 10 or 15. This implies that the (040) planes orient parallel to the macroscopic film surface in all cases, and that (110) or (130) planes also orient parallell to the surface of samples with the highest compressions.

This "parallel" orientation of various crystal planes is conformed by the maxima or an increased value of I sin ϕ for $\phi = 0$ if it is

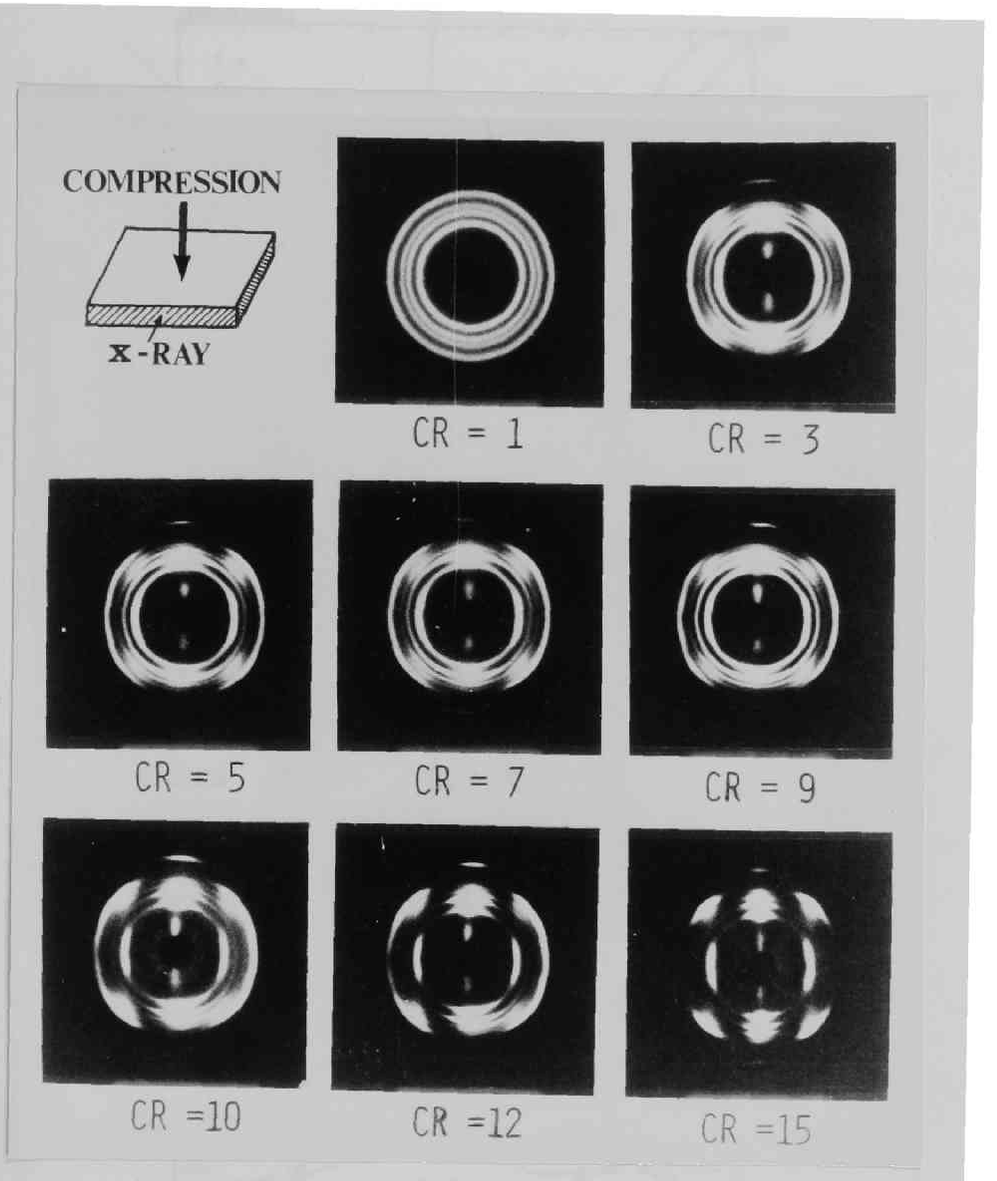

Fig.1. Wide-angle X-ray photographs for the crosslinked isotactic polypropylene with different compression ratios. The X-ray beam was parallel to the film surface. The compression ratio (CR) is indicated in each pattern.

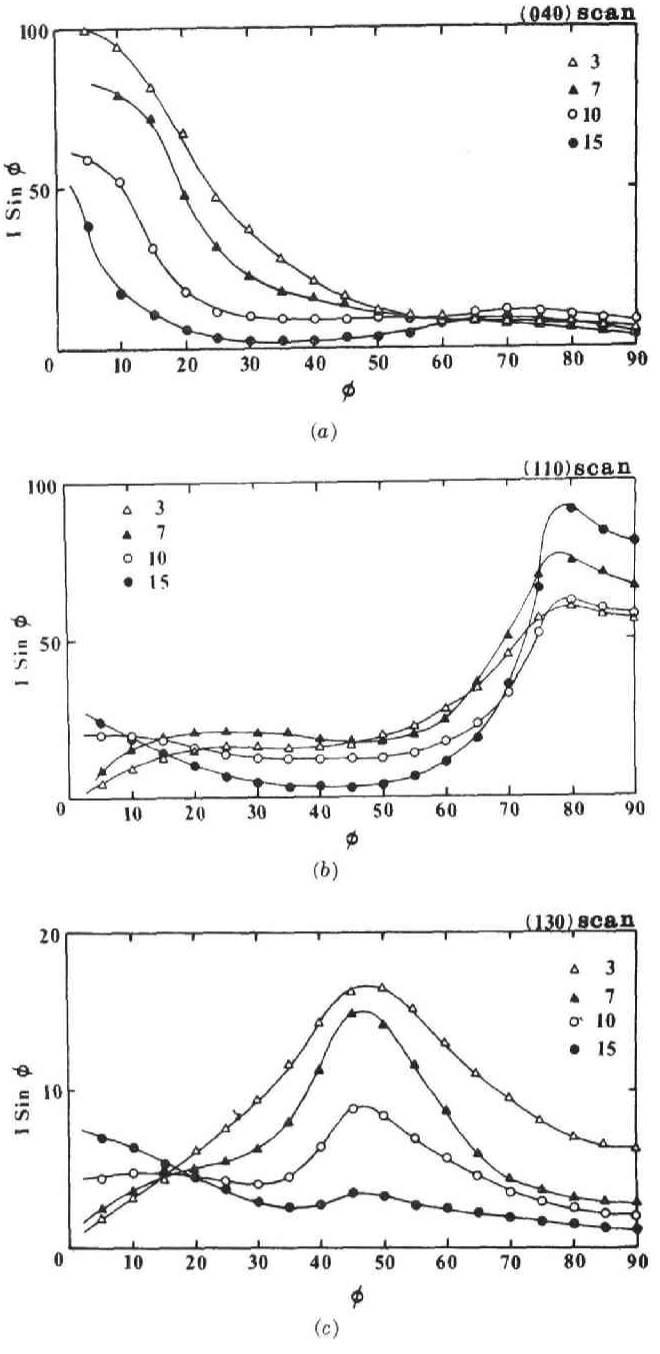

Fig.2. The dependence of $I(\phi)\cdot\sin\phi$ on ϕ for the (040), (110), and (130) scans. ϕ is the angle between the normal to the film surface of samples and a chosen direction, the crystallites in the sample contribute the (hkl) diffraction, if those crystal plane vector P^*_{hkl} points in this direction.

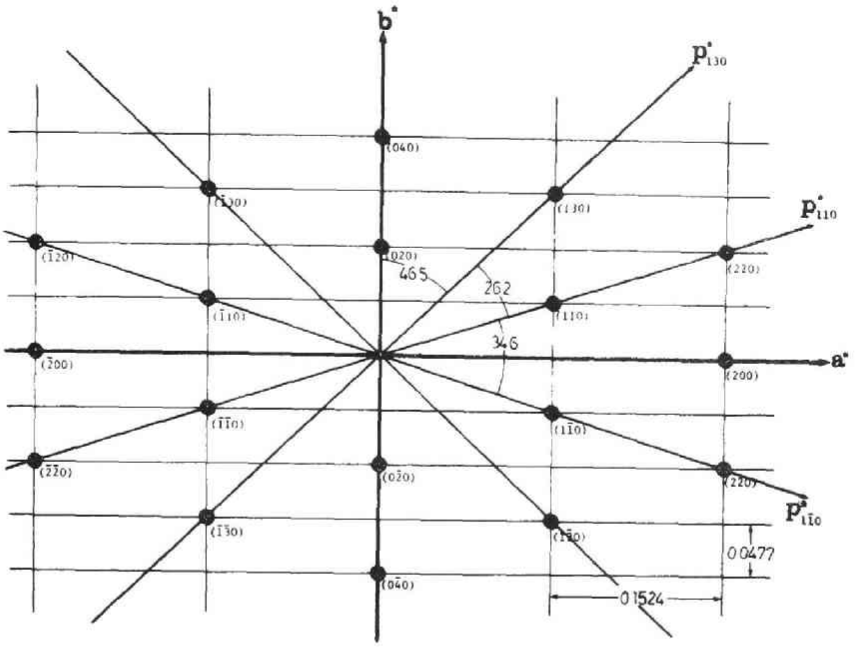

Fig.3. a*-b* plot of the reciprocal lattice for the monoclinic crystal form of isotactic polypropylene. Here, the crystallographic parameters established by Natta and others(16) are employed. a = 6.65, b = 20.96, and c = 6.50 A°, β = 99.33°. The c-axis (molecular chain axis) is perpendicular to the a*-b* plane.

assumed that the chain axis (c-axis) is parallel to the film surface. Since the vector P^*_{040} makes angles of 46.5 and 72.7° with vectors P^*_{130} and P^*_{110}, respectively, increased values of I sin ϕ at ϕ = 46.5 in the (130) scan and at 75° < ϕ < 80° in the (110) scan are to be understood as additional evidence of the appearance of the (040) orientation. Similarly the (110) orientation for highly compressed samples will also be clearly certified by an increases of I sin ϕ at $\phi \approx 70°$ in the (040) scan because P^*_{110} makes an angle of 72.7° with

P^*_{040}.

The (130) orientation can be detected only by the aforementioned increase of I sin ϕ at ϕ = 0 for the sample with a compression ratio 10 or 15 in the (130) scan. It is to be noted that I sin ϕ increases rapidly as ϕ increases from 50° and 60° in the (040) and (110) scans. This reflects the appearance of the (130) parallel orientation at high compression since P^*_{130} makes angles of 46.5° and 60.8° with P^*_{040} and P^*_{110}, respectively.

9.4. Relative Mass Distribution in the (040), (110), and (130) Orientations

In order to confirm the progressive appearance of the (040), (110), and (130) orientations parallel to the surface with increasing compression and to study the distribution among these orientations, an X-ray diffraction scan was made according to a procedure described in Chapter 5. The data are shown in Figure 4. In this scanning mode, the diffraction intensity recorded at angles of $2\theta_{hkl}$, where θ_{hkl} is the Bragg angle for the crystal planes (hkl), is due only to crystal planes parallel to the film surface. Thus the relative mass fractions of material with the parallel orientations of the crystal can be determined from the data.

The ratios of intensities at each $2\theta_{hkl}$ angle of (040), (110) and (130) for the uncompressed isotropic sample after baseline substraction is found to be*

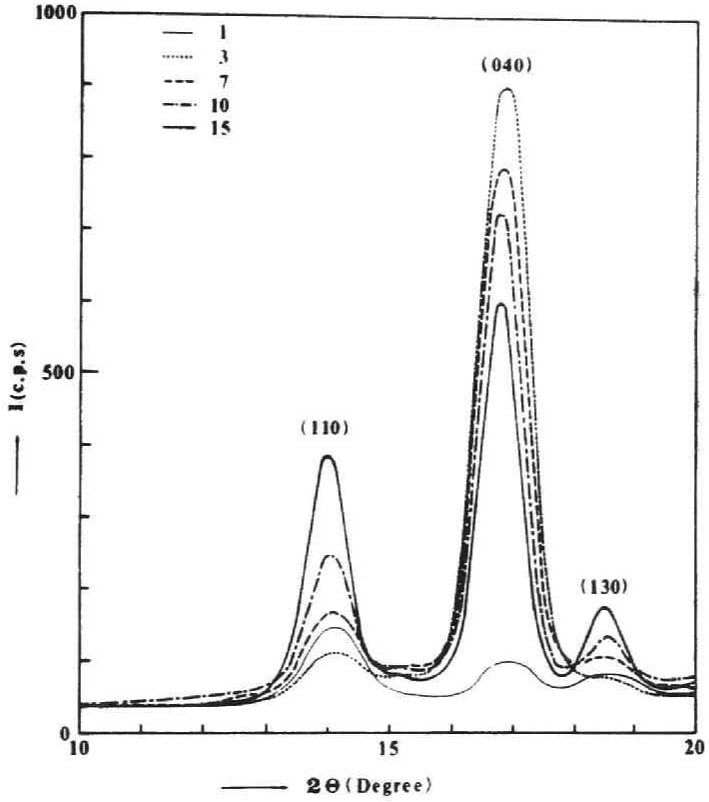

Fig.4. X-ray scan for samples with various compression ratios. The scan intensity is caused by crystal planes parallel to the film surface of the samples. The compression ratio is indicated for each symbol.

$$I^{\circ}_{040} : I^{\circ}_{110} : I^{\circ}_{130} = 100 : 214 : 89$$

---

* This relative ratio for the isotropic sample was not read off from the data in the figure but obtained from other data on an amplified intensity scale for accurate estimation.

If we designate I_{040}, I_{110}, and I_{130} as intensities of the (040), (110), and (130) diffractions at each $2\theta_{hkl}$, the relative mass fraction in the three orientations of the crystal planes, may be evaluated from

$$M_{040} : M_{110} : M_{130} = I_{040} / I^{\circ}_{040} : 2I_{110} / I^{\circ}_{110} : 2I_{130} / I^{\circ}_{130}$$

A factor of 2 for intensities for the (110) and (130) planes is introduced because all crystal planes designated as {040} can contribute to the diffraction but only half of the {110} and {130} planes contribute to the diffraction if the planar orientations of those crystal planes exist. This is true because, for example, if the crystal plane (110) is parallel to the film surface the planes $(1\bar{1}0)$ or $(\bar{1}10)$ in the same crystallite cannot be parallel to it. Here, braces { } are used to designate a family of planes related by the symmetry of the crystal lattice. This relative mass fraction of the different orientations was determined from the data in Figure 4 by use of proper base lines for each curve and is listed in Table 2.

It is concluded from Table 2 that the (040) orientation appears at a compression factor of 3 without appreciable occurrence of other orientations. The (110) and (130) orientations begin to appear at a compression factor of 7. As the compression factor is increased further from 10 to 15, the latter mass fractions relative to the (040) orientation increase from 25% and 19% to 58% and 47%, respectively.

Table 2. Relative Mass Fraction between the (040), (110), and (130) Orientations Parallel to the Film Surface.

Compression ratio	M_{040} : M_{110} : M_{130}		
1	--	--	--
3	1.00	0.06	0.05
7	1.00	0.13	0.11
10	1.00	0.25	0.19
15	1.00	0.58	0.47

9.5. Discussion

Parallel orientation of crystal planes has been sometimes noted in uncrosslinked isotactic polypropylene stretched biaxially at high temperatures but below the melting point. Adams(9) reported the appearance of (040) and (110) orientations for biaxially stretched polymer, and Takahara and others(8) examined the possibility of occurrence of planar orientations of various crystal planes. Uejo and Hoshino(11) pointed out the occurrence of another type of plane orientation and Matsumoto and others(10) observed a (130) orientation. In these papers, however, evidence for the three types of plane orientation is not sufficient and, particularly, the order of appearance and quantitative relations among the orientations remain obscure.

The previous discussions(8-11) were based on the pole figures for the crystal planes or diffraction patterns taken by a flat camera with X-rays parallel to the film surface. The pole figure for a crystal

plane generally indicates clearly the spatial distribution of the crystal plane in the samples. However, when chain axes are preferentially aligned parallel to the film surface, as in the present case, the reciprocal vectors for crystal planes parallel to the chain axes point preferentially in the direction perpendicular to the film surface, even if crystallite orientations in the structure are randomly distributed around the molecular chain axes. Thus, interpretation of the pole figures for the (040), (110), and other (hk0) planes is somewhat difficult and is sometimes confused by the orientation of the molecular chain axes that necessarily takes place.

Interpretation of the patterns obtained with a flat camera is based on the assumption that lattice points such as (040)* in the a*-b* plane (shown in Figure 3) directly reflect diffraction spots on the patterns, if the a*-b* plane is appropriately rotated around the center of the reciprocal lattice, because of the planar orientation of the crystal planes concerned. However, unless a very clear pattern is obtained so that each diffraction is distinguishable from the others, interpretation involves some arbitrariness. Since clear patterns cannot generally be obtained, this technique is only a qualitative method of studying planar orientations. To reach a firm conclusion as to the planar orientations more detailed investigations must be done with a technique such as that we have used.

We have confirmed quantitatively the occurrence of the three kinds of crystal plane orientation for the crosslinked polymer crystallized under compression. What is to be noted first is that the (040) orienta-

tion appears, without other orientations, at relatively low compression. The origin of this orientation is presumably analogous to that of the (200) parallel orientation observed for lightly crosslinked polyethylene in advance of other kinds of orientation when it is treated similarly (1, 3).

These phenomena may be understood in different ways, but one possible explanation is as follows: If molecular chains are stretched, the equilibrium melting temperature of the system is elevated owing to an entropy decrease in the molten state, and accordingly, the degree of undercooling on crystallization is increased. If the degree of undercooling is increased even to a small extent, the rate of crystallization is greatly accelerated. Therefore, since the sample is uniaxially compressed and chains are stretched during the macroscopic deformation, it is very likely that crystal nuclei are formed from the stretched chains at a very high rate. Since parallel alignment of the chains in face occurs with high probability under uniaxial compression, crystal nuclei will be produced in the form of thin layers of the crystal planes with a higher density parallel to the molecular chains. One cannot decide unambiguously which crystal planes comprise this form of nucleus, but if the symmetry of the monoclinic crystal form of the polymer is presumed, the nucleus will be a multimolecular layer of the (040) crystal planes. Since a nucleus of this form should orient mechanically parallel to the macroscopic film surface under compression and the nucleus likely grows while maintaining its form and orientation, the (040) orientation will appear.

This nucleation machanism should not be assumed correct without evidence. However, regardless of its form if the nucleus grows in either the a*-axis or c-axis direction more rapidly than in the b*-axis (b-axis) direction, the result is formation of a planar crystallite composed of the (040) planes, just as expected from the above argument.

To the extent that stretched polymer chains exist in the structure, this type of nucleation and the succeeding growth of the nucleus will proceed at an accelerated rate. During these processes, the stretched chains will disappear but some chains will remain in an unstretched, and noncrystallizable state unless multiple folding of a chain into a single crystallite occurs. However, multiple folding is inhibited in stretched samples by the crystallization of stretched chains which is generally thought to be very rapid, in view of data for stretched crosslinked polyethylene(17). As a matter of fact in the structure formed by this mode of crystallization, it was confirmed from NMR studies that chains remaining in amorphous regions are in a relaxed state(19).

The above argument plausibly explains the origin of the (040) orientation. However, since different types of nucleation are unlikely to occur simultaneously in the incipient stage of crystallization, the (110) and (130) orientations should have different origins. There is established explanation for these other orientations but it will probably be analogous to that for the (110) orientation of uniaxially compressed polyethylene(3). i.e., the (110) and (130) orientations may arise from less stretched molecular chains after the (040) orientation has proceeded to an appresiable extent. The orientations may also be

produced by a partial destruction of crystallites gliding along the (110) or (130) planes in the later stage of crystallization.

On the other hand, the mode of formation of the different kinds of crystal plane orientations reported for biaxially stretched uncrosslinked polymers(8-11) is not necessarily the same as that discussed above, because the uncrosslinked polymer was stretched below the melting temperature. Since biaxial deformation below the melting temperature involves recrystallization of stretched chains produced by partial melting of crystallites, the mechanism of crystal-plane orientation may plausibly be regarded as similar to that for stretching crosslinked polymer above the melting temperature. However, it must be remembered that the mode of crystallization of crosslinked polymer described in this chapter eventually leaves unstretched chains in the amorphous phase after completion of the crystallization while biaxial stretching of uncrosslinked polymer below the melting point results in stretched chains in the amorphous phase. This difference in structure should be reflected in the properties of the samples.

In addition to the planar orientation of crystallites, it is found that the crosslinked sample crystallized from the melt under uniaxial compression exhibit characteristic properties such as a high melting temperature and high unit-cell density. These results will be discussed in Chapter 10.

References

1. R.Kitamaru, H.-D.Chu, and S.-H.Hyon, Macromolecules, 6, 337 (1973).
2. S.-H.Hyon, H.Taniuchi, and R.Kitamaru, Bull.Inst.Chem.Res., Kyoto Univ., 51, 19 (1973).
3. R.Kitamaru and S.-H.Hyon, Makromol.Chem., 175, 225 (1974).
4. I.Sakurada, K.Kaji, and K.Nakamae, Bull.Inst.Chem.Res., Kyoto Univ., 44, 168 (1966).
5. G.C.Adams, J.Polym.Sci., Pt. A-2, 9, 1235 (1971).
6. K.Imada, T.Yamamoto, K.Shigematsu, and M.Takayanagi, J.Mater.Sci., 6, 537 (1971).
7. G.Meinel and A.Peterlin, Kolloid-Z.Z.Polym., 242, 1151 (1970).
8. H.Takahara, H.Kawai, Y.Yamaguchi, and A.Fukushima, Sen-i Gakkaishi, 25, 8 (1969).
9. G.C.Adams, Structure and Properties of Polymer Films, R.W.Lenz and R.S.Stein, Eds., Plenum Press, New York, p.169 (1973).
10. K.Matsumoto, K.Satō, K.Ishii, and Imamura, Sen-i Gakkaishi, 26, 537 (1970).
11. H.Uejo and S.Hoshino, J.Appl.Polym.Sci., 14, 317 (1970).
12. H.Tanaka, T.Masuko, and S.Okajima, J.Appl.Polym.Sci., 16, 441 (1972).
13. R.Kitamaru and S.-H.Hyon, 22nd Ann.Disc.Meet., Soc.Polym.Chem., Tokyo, 1973, preprint I-501.
14. J.B.Kinsinger and R.E.Hughes, J.Phys.Chem., 63, 2002 (1959).
15. M.Todoki and T.Kawaguchi, Kobunshi Ronbunshu, 31, 106 (1974).
16. G.Natta, P.Corradini, and M.Ceasri, Atti.accad.Lincei.Rend., Classe Sci.fis. mat e nat., 21, 365 (1956).

17. R.Kitamaru, T.Ando, and L.Mandelkern, 22nd Ann.Meet., Soc.Polym.Chem. Japan, 1973, preprint, p.I-56.

18. J.P.Luongo, J.Appl.Polym.Sci., 3, 302 (1960).

19. S.-H.Hyon and R.Kitamaru, to be published.

Chapter 10.

STRUCTURE AND PROPERTIES OF LIGHTLY CROSSLINKED ISOTACTIC POLYPROPYLENE FILMS, CRYSTALLIZED FROM THE MELT UNDER UNIAXIAL COMPRESSION

10.1. Introduction

In Chapter 9, it is described that unique planar orientations of various crystal planes appear when a crosslinked isotactic polypropylene is crystallized from the melt under uniaxial compression. In addition to the planar orientations, samples made in such a mode will be associated with unique macroscopic properties. This chapter deals with the macroscopic properties such as mechanical, thermal properties in relation to the phase- and supermolecular structures.

10.2. Experimental Part

Preparation of Samples

The gel sample in film form filed in Table 1 in Chapter 9 as No.3 was used for the studies of this chapter. It was crystallized from the melt under uniaxial compression according to the procedure described in Chapter 9. For comparison, studies were made also for samples compressed at 150°C without melting in a partially crystallized state. For these two series of samples the degree of compression ranged from 1 to 15.

Density and Crystallinity

Densities of samples were measured at 30°C by a density gradient column composed of ethylene glycol and n-propylalcohol. The crystallinity was obtained from the measured density according to the relation;

$$\text{Crystallinity} = \frac{0.983 + 9(t + 180) \times 10^{-4} - 1/d}{4.8(t + 180) \times 10^{-4}}$$

established by Natta(6) with the assumption of the additivities of the specific volumes of the crystalline and amorphous phases. Here, d and t designate the measured density and the ambient temperature in centigrade.

Small Angle X-ray Scattering

The procedure was described in Chapter 1.

Fusion and Enthalpy Change in Fusion

The fusion curve was obtained by a differential scanning calorimetry with use of the Perkin Elmer DSC 1-B. The amount of the sample used was about 3-4 mg and the correction of temperature was made with use of pure Indium. The melting point was defined to be a temperature where the fusion finally terminated. The enthalpy change in the fusion was estimated by planimetry of the fusion curve with a reference datum for purified benzoic acid.

Dimensional Change with Temperature

The dimensional change was measured with increasing temperature in air at a constant load. The applied load was 1 g/mm^2 and dimensional change was followed by a cathetometer. The temperature was increased at the rate of 1 °C/min.

Dynamic Mechanical Properties

The temperature dependency of the loss tangent tan δ, the dynamic modulus E' and the dynamic loss E'' were measured with the Vibron DDV-2 from the Toyo Baldwin Co., a type of forced vibrational method. The selected frequency for the measurements was 110 cps throughout this work and the values tan δ, E' and E'' were obtained in a range of temperature -30° to + 140 °C with a heating of 0.5 °C/min. The dimensions of the test piece were 30 mm in length, 0.1-0.2 mm^2 in cross section.

10.3. Results and Discussion

Small Angle X-ray Scattering(SAXS)

Small angle X-ray scattering has proved to be a powerful method for the investigation of structure of oriented crystalline polymers. Therefore, this section deals with the morphological aspects for samples crystallized either from the melt under uniaxial compression or prepared by usual compression at 150°C below the melting point.

SAXS patterns for the two series of samples, compressed at 150°C

in the partially crystalline state and compressed at 180°C in the melt were first obtained. When the X-ray beam was introduced perpendicular to the film surface of samples, diffuse patterns were obtained for all samples and the diffractive intensity was distributed circulary around the beam direction in the range of small angles. Those patterns implied a random uniaxial distribution of crystallites around the beam direction, namely around the normal to the film surface of samples in good accord with the information from the wide angle X-ray patterns, but maxima in intensity were hardly recognized in the radial direction of the patterns. However, when samples were illuminated by the X-ray beam parallel to the film surface, patterns were obtained that indicated a periodical fluctuation in density in a direction perpendicular to the beam, namely in the molecular chain direction in the crystallites.

Figure 1 illustrates the dependence of the SAXS patterns on compression ratio. Figure 1(A) shows the SAXS photographs of non-crosslinked samples compressed at 150°C for compression ratio between 6 and 12. The patterns in sample I are arc-like shape characteristic of irregular lamella crystallites structure. With increasing compression ratio the lateral width of the meridional maxima increases. This is similar to the behavior of polyethylene(7-9) and polypropylene(10-12) which had been uniaxially stretched at different temperatures. Figure 1(B) shows the SAXS photographs of crosslinked samples compressed at 180°C for compression ratio between 5 and 15. The patterns for sample II are quite different from these for sample I, i.e., there are discrete two-point diffraction of regularities lamella type. As the

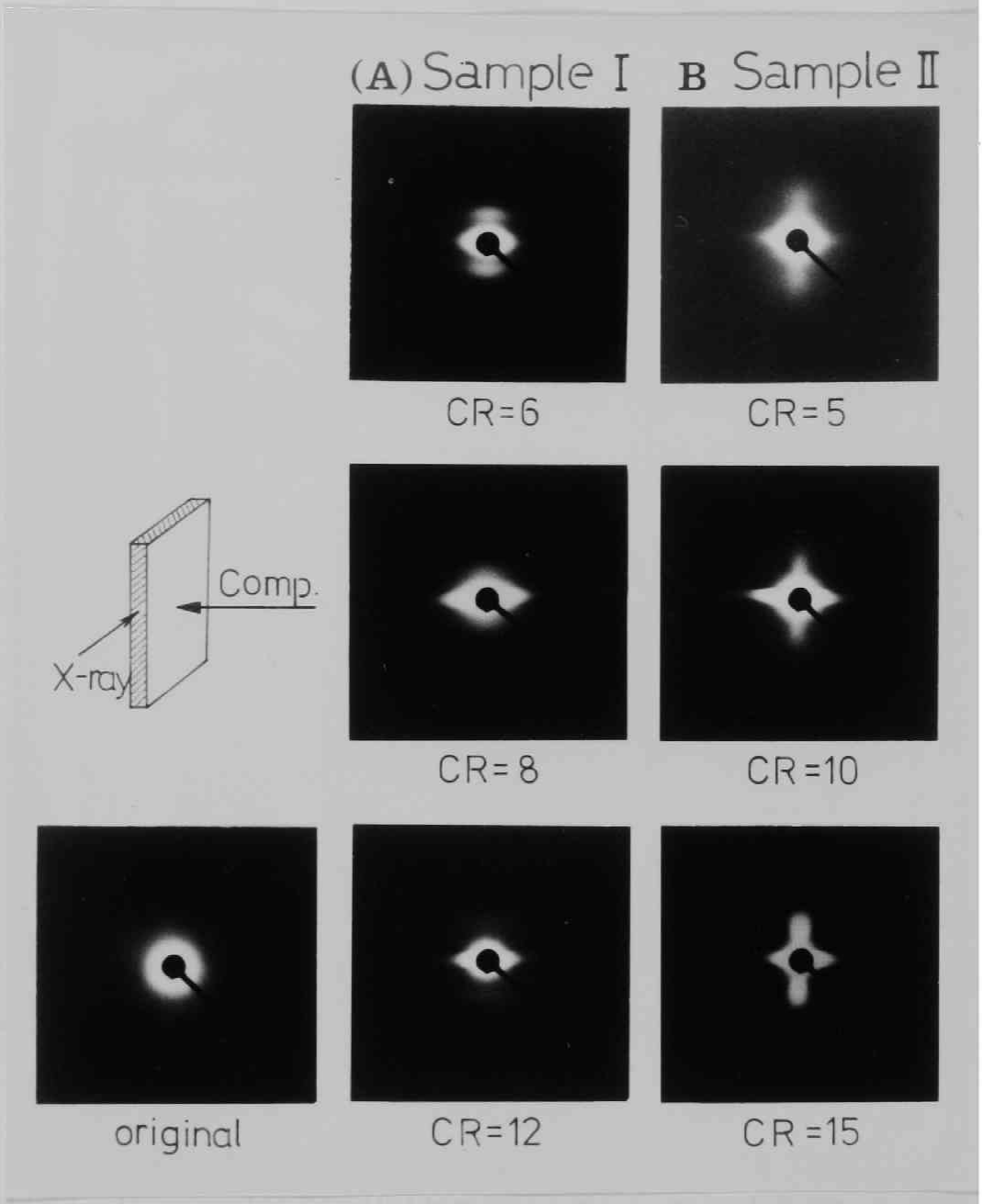

Fig. 1. Small angle X-ray diffraction patterns for polypropylene sample compressed to different degrees at 150°C(Sample I) and at 180°C(Sample II). Compression ratio is indicated in each pattern.

compression ratio increases, this two-point diffraction shifts to the lower angular range.

A very enhanced diffraction is recognized at angles much smaller than angles for the meridional maxima, with a rather small extension perpendicular to the equator. This indicates the existence of a discrete distribution of electron density also in the direction of the film thikness. It is usually assumed that such a center streak scattering arises mostly from rod-like voids(13) or microfibrils(14) in the structure of samples. This center streak scattering may be existence of microfibrils, because this sample is highly transparent.

Figures 2 and 3 show the SAXS profile for the two series of samples with different compression ratios; the ones compressed at 150°C in the partially crystalline state (hereafter designated "plastically compressed samples") and the seconds compressed at 180°C in the melt (hereafter designated "melt-compressed samples"). It is evident that for the plastically compressed samples the 2θ angle at the maxima shifts to higher angles and the scattering intensity decreases as the compression ratio increases. Contrary, for the melt-compressed samples the 2θ angle at the maxima shifts to lower angles and the scattering intensity increases as the compression ratio increases.

Consider first the change of the scattering intensity with changing compression ratio. As can be seen in Table 1, the degree of crystallinity slightly increases with increasing degree of compression for the both series of sample. If the crystallinity increases, the scattering intensity must increase. However, as the crystallinity increases

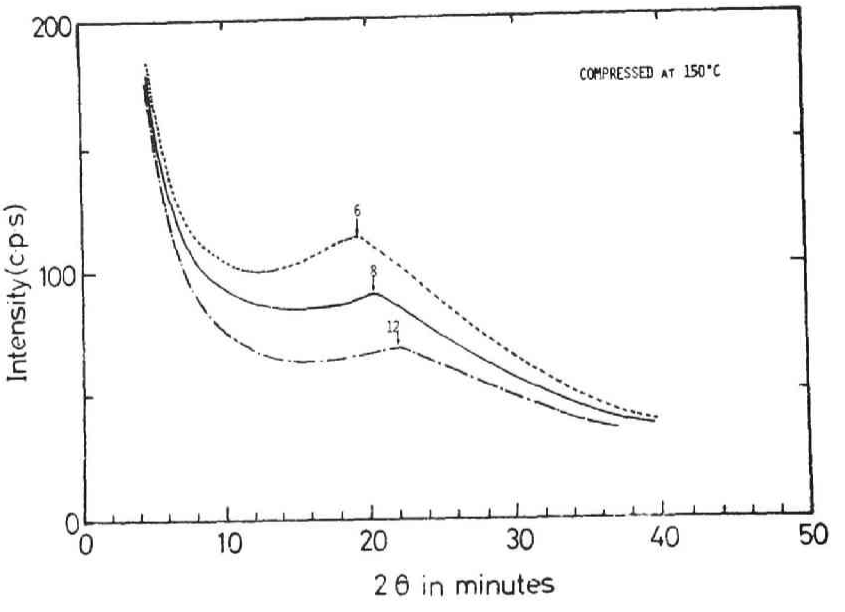

Fig.2. Angular dependence of SAXS of polypropylene films compressed at 150°C. The compression ratio is indicated in each curve.

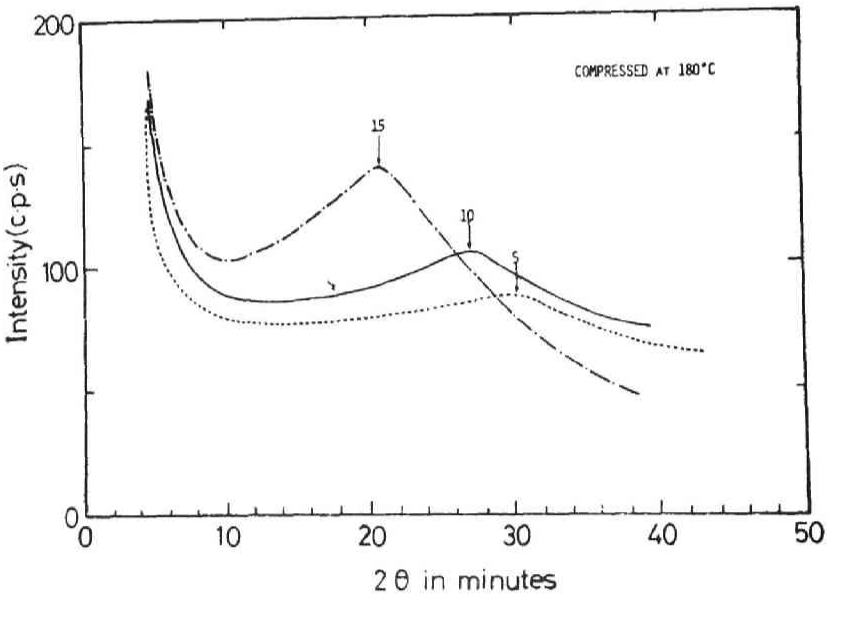

Fig.3. Angular dependence of SAXS of polypropylene films crystallyzed from the melt under compression. The compression ratio is indicated in each curve.

Table 1. Density, Melting Point and Heat of Fusion of the Crosslinked Polypropylene Samples of Different Compression Ratios.

Sample	Comp. Ratio	Density g/cm^3	Crystallinity $(1-\lambda)_d$	T_m (°C)	ΔH cal/g
Original		0.9045	0.657	163.0	18.6
Gel		0.9042	0.652	160.8	16.6
Non-cross Comp. at 150°C	1	0.905	0.664	163.3	19.2
	6	0.9055	0.672	163.7	19.7
	8	0.906	0.676	164.6	18.5
	12	0.906	0.676	164.0	17.8
Gel sample Comp. at 180°C	1	0.9035	0.645	160.0	13.6
	2	0.904	0.651	162.2	16.2
	3	0.9042	0.652	162.8	15.7
	5	0.9055	0.672	163.0	18.3
	7	0.9050	0.664	162.8	17.4
	9	0.9055	0.672	169.3	19.7
	10	0.906	0.676	170.0	20.7
	15	0.906	0.676	173.0	21.5

the scattering intensity appreciably decreases for the plastically compressed samples although if increases for the melt-compressed samples. Therefore, the major origin for the different behaviors in the scattering intensity between these two series of sample must be sought in other ways. Peterline et al.(7-9) observed a decrease in the scattering intensity when a polyethylene sample was uniaxially stretched in the partially crystalline state as pointed out in Chapter 1. They have attributed this origin to an decrease in the density difference between the crystal-

line and amorphous phases accompanying the plastic stretching. They considered that the density of the crystalline phase decreased due to a production of defects and that of the amorphous phase increased due to parallel alignment of amorphous molecules accompanying the stretching. The decrease of the scattering intensity observed have for the plastically compressed polypropylene samples may be similar to that as discussed by them. However, the crosslinked polypropylene is compressed in the melt, it is supposed that the density of the crystalline phase does not decrease or slightly increase while that of the amorphous phase is held unchanged in a similar manner to the case that a crosslinked polyethylene is compressed in the melt. Therefore, the increase of the scattering intensity for the melt compressed polypropylene will be well explained by an increase of density difference between the crystalline and amorphous phases together with the increase of the crystallinity, refrecting their unique phase structure.

In Figure 4 the long periods calculated from the SAXS profile are plotted against the compression ratios for the two series of samples. It is evident that with increasing compression ratio, the long period of the melt compressed samples increases conspicuously in the direction perpendicular to the compression direction. Contrary, the long period of the plastically compressed samples is decreased with increasing compression ratio. This difference will reflect the difference of the phase structure between these series of sample in a similar way to the case that crosslinked polyethylene is compressed either in the melt or in the partially crystalline state as discussed in Chapter 5.

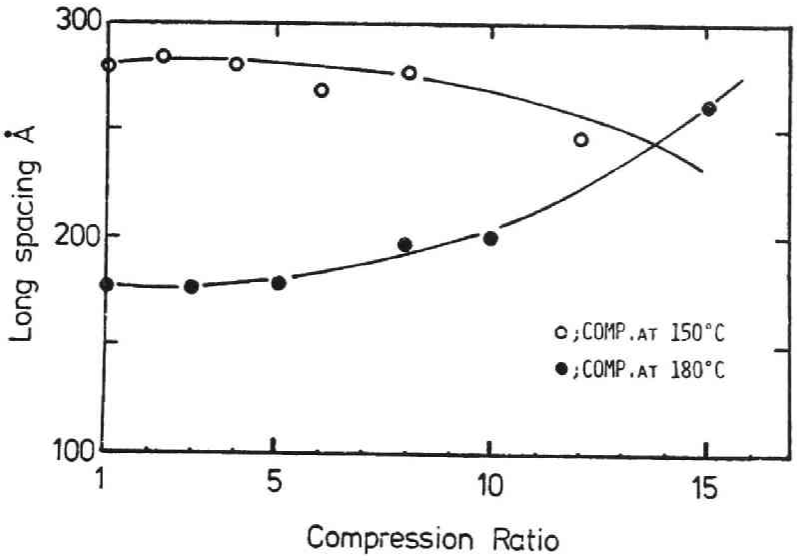

Fig. 4. Variation of the long period as a function of compression ratio for polypropylene films prepared under different conditions.

Fusion Behavior

The fusion curves obtained by the DSC with a heating rate of 10 °/min for un-crosslinked and crosslinked gel samples made by compressing at 150°C are shown in Figure 5. By compressing, the melting point arises. Note here that a small shoulder associated with the fusion peak for the compressed samples is detectable in a low temperature range in the thermograms. Appearance of similar small shoulder has been recognized by Adams(15) and Okajima et al.(16) with a DSC measurement for biaxially stretched polypropylene samples. It should indicate a heterogeneity or dual crystalline structure in samples. But the shoulders in the figure are too week so that no further consideration is allowable. However, for the samples made by compressing in the

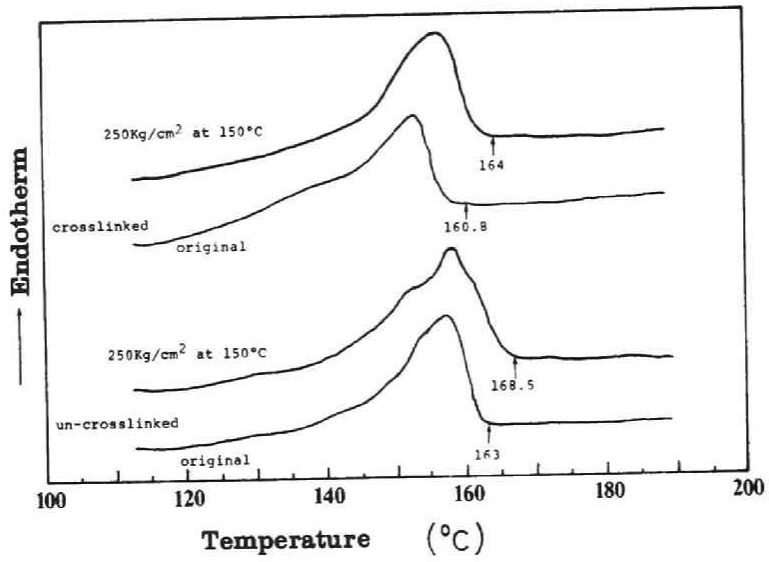

Fig. 5. DSC thermograms for polypropylene films compressed below the melting temperature.

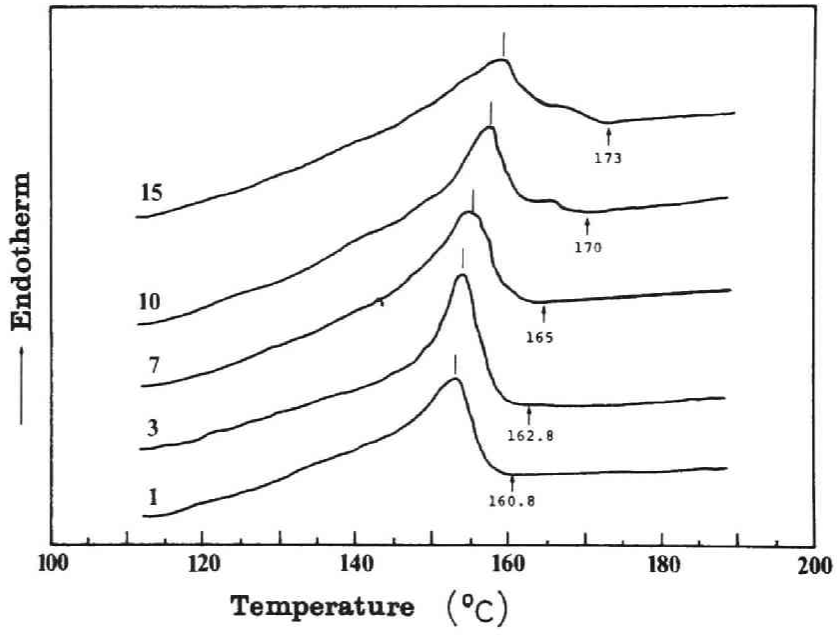

Fig. 6. DSC thermograms for crosslinked polypropylene films made from the melt under compression.

molten state the dual crystalline structure is distinctly recognized. Figure 6 represents thermograms for the gel films compressed at the molten state. The shape of the fusion curves varies greatly according to the preparative condition for samples. As can be seen, the melt-compressed samples show an endothermic peak with a long "tail", persisting to 173°C. Similar dual or multiple fusion curve is sometimes reported for other polymers such as polyethylene(17-19), polyethylene terephthalate(20), nylon 66(21), and polyvinyl alcohol(23) with an abnormally high melting temperature, when such polymers are crystallized under very high pressure or under conditions involving molecular orientation. Also for polypropylene such high melting temperaure is reported by Monobe et al.(23), and Ishikawa et al.(24), when the polymer is crystallized either from the solution under high degree of stirring or from the melt under uniaxial stretching, but such dual peak never has been recognized up to data. Thus we should note that the mode of compressing and subsequent crystallization for polypropylene examined in this chapter bring very characteristic unique feature in the structure of the polymer. The dual fusion curve as well as abnormally high melting point are generally characteristic for samples, regardless of polymer sort, which were crystallized under condition involving molecular orientation and those should indicate dual structure or the presence of very highly ordered crystalline phase with large dimensions in the samples.

In Table 1, the density and the degree of crystallinity derived from the density, the melting temperature, and the enthalpy of

fusion for the compressed samples. It is shown that the melting temperature and heat of fusion rise in accordance with increasing compression ratio.

Effect of Heating Rate

In measuring the melting temperature for a polymer by DSC, one most consider the simultaneous and competitive kinetics of superheating and reorganization followed by recrystallization during the scanning. Figure 7 shows the melting point for the two series of samples as a function of heating rate. For the samples compressed at 150°C the curve shows a minimum at moderate heating rate. At very low heating rates, higher values are obtained. This is probably due to an annealing effect, which involves some recrystallization, disappearance of

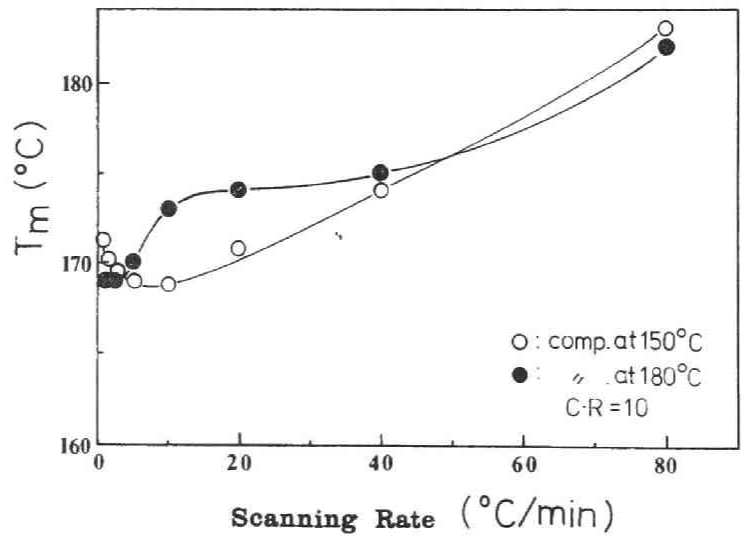

Fig. 7. Melting temperature vs. scanning rate for crosslinked polypropylene crystallized from the melt under compression and polypropylene films compressed below the melting temperature.

small crystallites and growth to larger ones. As a result, the melting points may rise. On the other hand, for the sample crystallized from the melt under compression, the melting point drastically increases with increasing heating rate, superheating recognized. It is thought that superheating occurs if the oriented state and therfore reduced entropy of the amorphous material is maintained during the scan due to the high rate of heating. Fibrillar or extended chain crystals have been shown to be particularly susceptible to this phenomenon(25). In general, the larger size of the crystallites and the more ordered crystal phase are associated with the greater tendency for this phenomenon. Consequently, this difference may be due to the presence of very stable crystallites in the melt compression samples.

Shrinkage with Heating

The characteristic phase structure and the thermal properties of the oriented polymer mentioned above will be closely related to the macroscopic thermal shrinkage or thermal expansion behavior.

In Figure 8 the shrinkage of the films compressed at temperature below or above the melting point by heating in air is plotted against temperature. Here, we see again a great difference in the thermal shrinkage between the two series of sample, the ones compressed in the partially crystalline states and the others compressed in the melt. The former series of samples begin to shrink at about 50-70°C and the shrinkage increases until the melting point. But the melt compressed sample does not shrink up to 145°C, at which the partial fusion is

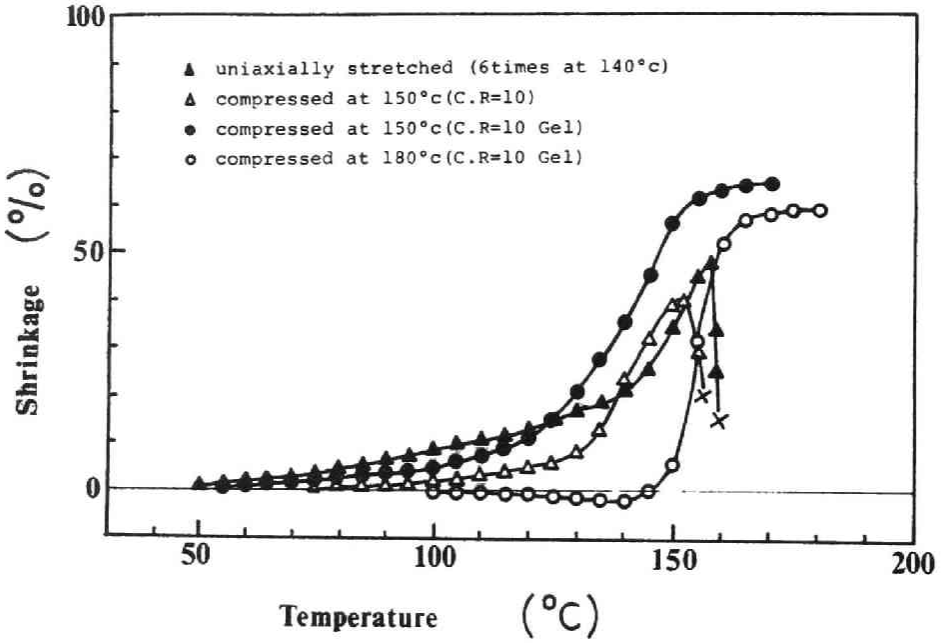

Fig. 8. Thermal shrinkage curves of polypropylene films.

indicated by the DSC scanning described in the last section and above 150°C the sample shrinks very rapidly. These shrinkage behavior is quite similar to the plastically compressed and melt-compressed cross-linked polyethylene as shown in Chapter 4.

The excellent dimensional stability observed here for the melt compression sample must be caused by the relaxed state in the amorphous chains and the perfection of the crystallites.

Dynamic Mechanical Properties

In Figure 9 and 10 tan δ and E', E'' are plotted against temperature for samples compressed at 150°C or 180°C. It is seen that, for samples at 150°C compressed irrespective of the presence of crosslinked units, the absorption peak temperature in a vicinity of room temperature T_a shifts to a higher temperature according to the compression. Concomitantly the absorption peak becomes wider and somewhat vague. On the other hand, for the absorption peak of the melt-compressed sample, such enhanced elevation of the peak temperature is not recognized and the peak width does not wider appreciably, although the value of tan δ becomes small.

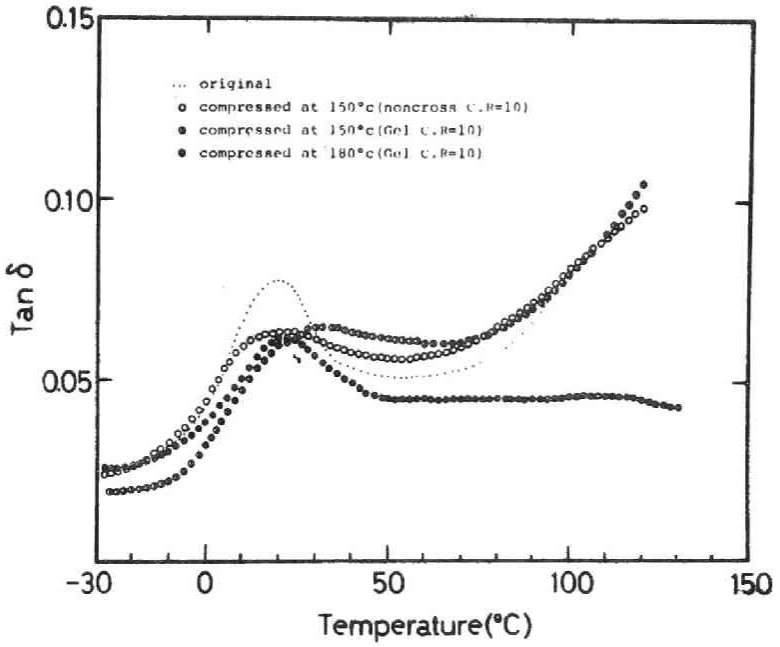

Fig.9. Loss tangent vs. temperature of the uncrosslinked and crosslinked samples compressed at 150°C and 180°C.

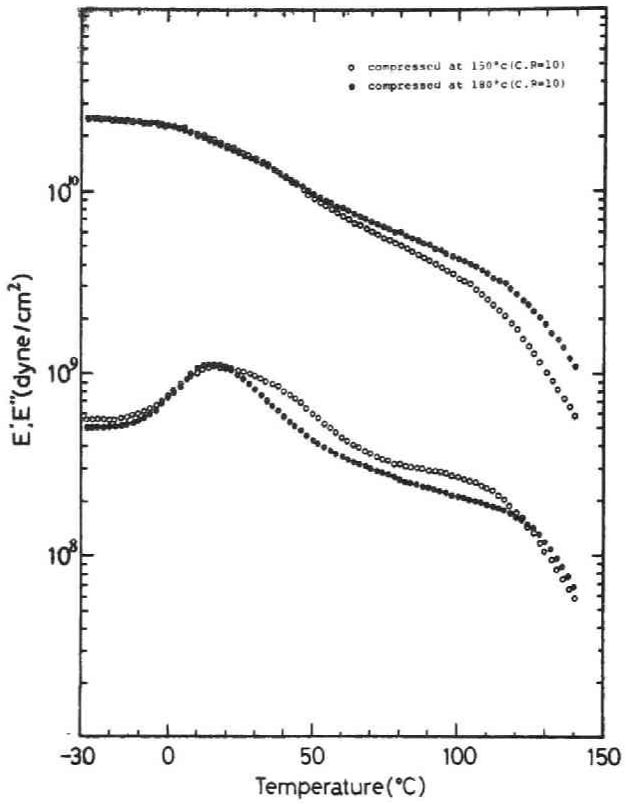

Fig.10. Temperature dependency of dynamic modulus E' and dynamic loss E'' for the crosslinked gel samples compressed at 150°C and 180°C.

The distinct difference in the dynamic viscoelastic behavior recognized here for the two series of sample should reflect the difference in the phase structure of samples. For a cold-drawn polypropylene film, Owen and Wyckoff reported a similar behavior to that for the samples compressed here in the partially crystalline state and they attributed the origin to a paracrystalline state of their sample(26). The T_a transition is generally assigned to a micro-Brownian movement of amorphous molecular chains. Therefore, the higher temperature of T_a

of the plastically compressed samples will indicate the stretched state of molecular chains. On the other hand, the lower temperature of T_a for samples compressed in the melt indicates un-stretched and relaxed state of molecular chains in the amorphous phase.

As discussed above, the molecular state of the noncrystalline phase of the compressed samples differ greatly, depending on the mode of compression; compressed in the melt or in the partially crystallized state. I next consider the effect of the degree of compression, when

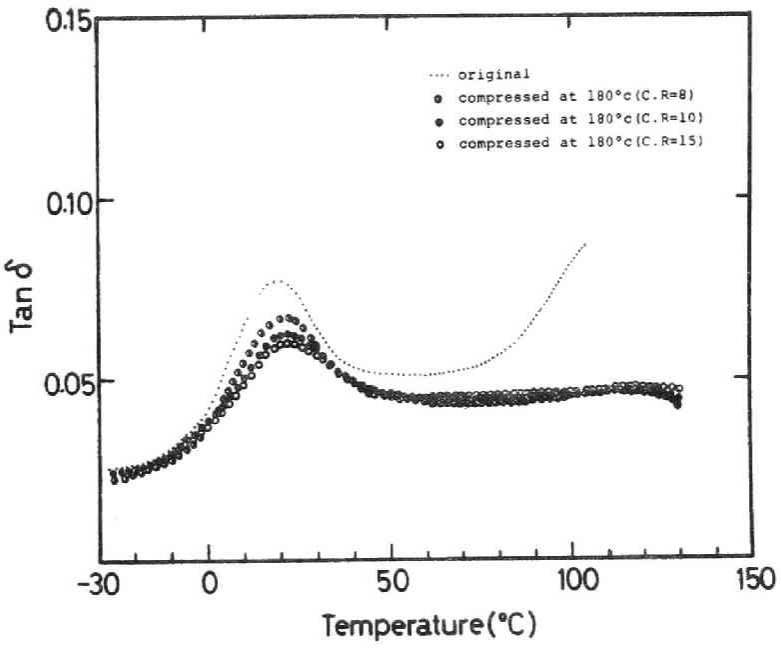

Fig.11. Loss tangent vs. temperature for the crosslinked gel samples compressed in the melt to different degrees.

the crosslinked samples is compressed in the melt. In Figure 11 the value of tan δ for the melt-compressed samples with different compression ratio is plotted against temperature. There is observed clear peaks in the vicinity of room temperature for all samples, corresponding to the α_a transition. The peak area of the tan δ curve decreases appreciably with increasing degree of compression, probably corresponding to minor increase of the degree of crystallinity as expected from the density increase (see Table 1). But it is to be noted here that the peak temperature T_a is not increased appreciably even if the sample is compressed as highly as 1/15. This indicates that the noncrystalline molecular chains are in a rather non-restricted state to be able to exhibit a segmental motion in the temperature range, almost equivalent to the uncompressed sample, although slight increase of restriction for molecular motion can be suggested by slightly of T_a to a high temperature for samples with larger degrees of compression. This is quite contrary to the case of the plastically compressed samples, in which enhanced elevation of T_a was observed on a lesser degree of compression, showing that the conformation of noncrystalline molecular chains was strongly restricted by such a compression as expected.

In Figure 12, the values of E' and E'' are plotted against temperature. There is again observed clear peaks of E'' in the vicinity of room temperature corresponding to the α_a-transition. This behavior well supports the above-mentioned structural characteristics concerning the noncrystalline molecular chains of the sample. Furthermore, the data

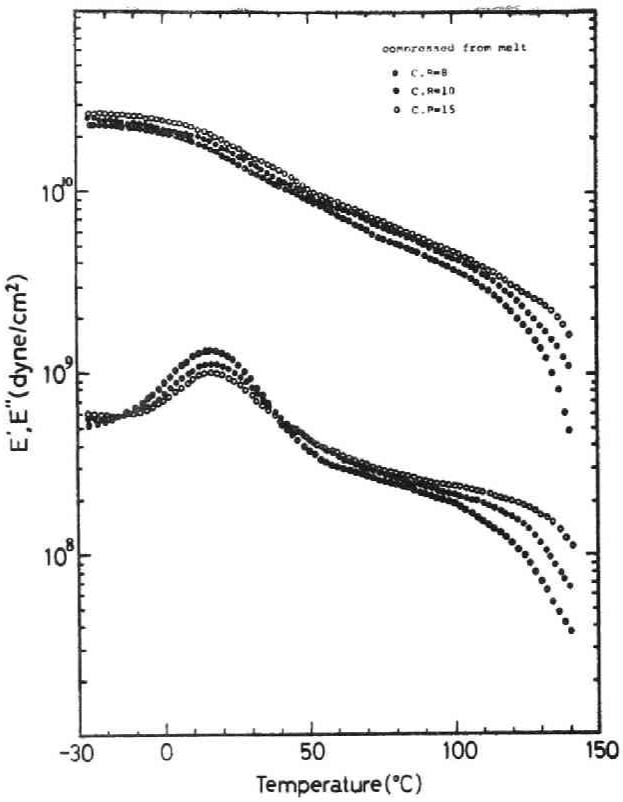

Fig.12. Temperature dependency of dynamic modulus E' and dynamic loss E'' for the crosslinked gel samples compressed in the melt to different degrees.

in the figure give some information of the crystalline phase of the samples. There are observed shoulderlike peaks in the E" plot in the temperature range of 100-140°C. The position of the peak shifts to high temperature and the intensity thereof increases as the degree of compression increases. It is also seen that higher value of E' is associated with samples of higher degrees of compression and pronounced

decrease of the value of E' in the temperature range above 100°C occurs at higher temperatures for samples with larger degrees of compression. Since the absorption of this polymer in this temperature range can be assigned as an energy loss in the crystalline phase(27), these results will lead a conclusion that the degree of crystallinity not only increases but also the crystalline phase in the structure becomes stable as the degree of compression increases.

10. 4. Conclusion

The study for the phase structure and properties in a lightly crosslinked isotactic polypropylene films, crystallized or processed under uniaxial compressions involving molecular orientation, has led to the following conclusions.

It has been evidently shown that if the crosslinked gel sample is compressed to a high extent in the molten state, the resultant product is generally associated with various characteristic properties such as regular lamella crystalline structure and extraordinarily high melting point with excellent dimensional stability for heating.
The results of small-angle X-ray scattering and thermal properties shows that the phase structure of the sample compressed in the melt is quite different from that of the sample compressed below the melting point. This characteristic crystalline structure of the product resembles that of lightly crosslinked polyethylene which show rubbery elasticity in the molten state, when these are crystallized from the molten and compressed state involving molecular orientation.

References

1. R.Kitamaru and S.-H.Hyon, J.Polym.Sci.Polym.Phys., 13, 1085 (1975).
2. S.-H.Hyon, H.Taniuchi, and R.Kitamaru, Bull.Inst.Chem.Res., Kyoto University, 51, 91 (1973).
3. R.Kitamaru, H.-D.Chu, and S.-H.Hyon, Macromolecules, 6, 337 (1973).
4. R.Kitamaru and S.-H.Hyon, Makromol.Chem., 175, 255 (1974).
5. S.-H.Hyon, R.Kitamaru, H.Taniuchi, N.Hayakawa, and N.Tamura, Kobunshi Ronbunshu, 32, 240 (1975).
6. F.Danusso, G.Moraglio, and G.Natta, Ind.Plast.Mod., 40, Jan., (1958).
7. R.Corneliussen, A.Peterlin, Makromol.Chem., 105, 193 (1967).
8. A.Peterlin, R.Cornelliussen, J.Polym.Sci., A-2, 6, 1273 (1968).
9. A.Peterlin, G.Meinel, Makromol.Chem., 142, 227 (1971).
10. Yu.D.Andrichenko, T.V.Druzhinina, Ya.A.Zubov, A.A.Konkin, and D.Yu.Tsvankin, Vysokomol.Soedin., 7, 2126 (1965).
11. F.J.Balta-Calleja, A.Peterlin, J.Materials Sci., 4, 722 (1969).
12. B.M.Ginzburg, K.B.Kurbanov, M.A.Martynov, S.Ya.Mezhirova, Sh.Tuichiev, and A.A.Khusainov, Vysokomol.Soyedin, A15, 1407 (1973).
13. W.O.Statton, J.Polym.Sci., 58, 205 (1962).
14. R.Hoseman, J.Appl.Phys., 34, 25 (1963).
15. G.C.Adams, "Structure and Properties of Polymer Films" edited by R.W.Lenz and R.S.Stein, Plenum press, New York, p.169 (1973).
16. H.Tanaka, T.Masuko, and S.Okajima, J.Appl.Polym.Sci., 16, 441 (1972) ibid, 17, 1715 (1973).
17. A.J.Pennings and A.M.Kiel, Kolloid-z., 205, 160 (1965).
18. A.M.Rijke and L.Mandelkern, J.Polym.Sci., A-2, 8, 225 (1967).

19. A.Keller and M.J.Machin, J.Macromol.Sci., Phy., B1, 41 (1967).

20. R.Kamoto, K.Ehara, T.Matsumoto, T.Kawai, and H.Maeda, Seni-Gakkaishi, 26, 28 (1970).

21. J.P.Bell, P.E.Slade, and J.H.Bumbleton, J.Polymer Sci., A-2, 6, 1773 (1968).

22. S.-H.Hyon, H.-D.Chu, and R.Kitamaru, Bull.Inst.Chem.Res., Kyoto University, 53, 367 (1975).

23. K.Monobe, H.Fujiwara, and H.Yamashita, Kogyo Kagaku Zasshi, 73, 7 (1970).

24. H.Shii and K.Ishikawa, Reports on Progress in Polymer Physics in Japan, 13, 131 (1970).

25. E.Hellmuth, B.Wunderlich, and J.M.Rankin, Appl.Polym.Symposia, 2, 101 (1966).

26. A.J.Owen and I.M.Wyckoff, J.Polym.Sci., 62, 83 (1962).

27. M.Takayanagi, J.Japan Soc. for Testing Materials, 11, 320 (1962).

Chapter 11.

STRUCTURE AND PROPERTIES OF A LIGHTLY CROSSLINKED POLYVINYLIDENE FLUORIDE CRYSTALLIZED FROM THE DEFORMED MOLTEN STATE

11.1. Introduction

The polyvinylidene fluoride (hereafter, abbreviated as PVDF) is known as having a characteristic electric property and widely used as piezoelectric films. It has good physico-mechanical properties as well as excellent resistance to chemical agents and radiation. Depending on the conditions of polymerization(1), crystallization(2) and thermo-mechanical treatment(3), this polymer indicates different crystalline forms such as the α- and β-forms with different molecular conformations (4).

Lando et al.(3) and Galpelin et al.(5) reported the increase of α-form when it was stretched at higher temperatures, although the β-form could not be removed perfectly.

In this manner, PVDF is one of few crystalline polymers which may be obtained comparatively easily in the two different crystalline forms according to the oriented conditions.

As described in previous chapters, very characteristic structure and properties appear for linear polyethylene(Chapter 1-8) and isotactic polypropylene(Chapter 9, 10), if these polymers are crystallized from the molten state under high degrees of molecular orientation, using irradiation crosslinking. This chapter deals with a similar attempt

for polyvinylidene fluoride.

11.2. Experimental Part

Sample Preparation

The starting material used in this work was a commercial grade Kynar 400 polymer of Pennsalt Chemical Corporation. Viscosity measurements were made in N-N- dimethylacetamide at 25°C, and the viscosity average molecular weight was calculated using the relation(7) $[\eta]=1.93\times10^{-4} M^{0.677}$. The density measurement was made at 30°C with

Table 1. Characterization of Material

Intrinsic Viscosity	$[\eta] = 2.0$
Molecular Weight	$\bar{M}_\eta = 8.5 \times 10^5$
Density at 30°C	1.785 g/cm^3
Melting Point (DSC)	165°C
Amount of head-to tail structure (NMR)	*89.8 %

* A reference value cited in (6)

a mixture of bromoform and chloroform. Table 1 designates the characteristics of the starting material.

The intermolecular crosslinking of this polymer is easily achieved with the irradiation of high energy radiations in vacuo(8). A γ-ray from ^{60}Co was used in this work to prepare crosslinked samples. Films about 1 mm thick of the polymer was irradiated to a dose of 10 and 20 megarads (Mrad) at room temperature in vacuum. The gel fraction(w_g) was evaluated by extracting with N-N- dimethylacetamide at 80°C, for 50 hrs and dried in vacuum at about 50°C. The w_g was evaluated to be 0.58 and 0.66, respectively. But the irradiated samples were used for this study without extracting their soluble fraction.

Deformation

The unirradiated and irradiated (uncrosslinked and crosslinked) samples were uniaxially stretched or compressed in two modes described below.

a. Elastic deformation; A piece of crosslinked samples (10 Mrad) was uniaxially stretched at a rate of 500 %/sec after melted perfectly in a silicon oil at 180°C to different extents and cooled to room temperature while holding the stretched length. For uniaxial compression, the 20 Mrad irradiated sample was compressed in the melt at 180°C between two metal plates and cooled to room temperature over a period of 15 min.

b. Plastic deformation; A piece of uncrosslinked samples was uniaxially stretched at a rate of 200 %/min at 100°C to different extents and

after kept for 5 min it was cooled to room temperature. For uniaxial compression, the sample was compressed at a temperature of 150°C below the melting point between two metal plates. Biaxially stretching was also made for this sample. It was simultaneously stretched in two directions at a rate of 200 %/min at 150°C to different extents and after kept for 5 min it was cooled to room temperature.

In the procedures a and b, the uniaxial or biaxial stretching and compression were achieved in either the molten state or partially crystallized state. The stretched samples will be designated by the temperature when stretched and the draw ratio which is defined to be the ratio of the stretched length to the original length. The degree of compression was expressed by the ratio between the film thicknesses before and after compression.

Measurements of Crystal Transformation (from the α-form to the β-form) by Wide Angle X-ray Diffraction

The transformation of the crystal forms from α to β accompanying the various modes of deformation or deformed-crystallization described above was examined with an X-ray analysis using the (002)-diffraction of the α-form and (001)-diffraction of the β-form. The degree of the transformation is defined to be

$$\Phi_w = \frac{I_{\beta(001)}}{I_{\alpha(002)} + I_{\beta(001)}} \times 100\ (\%)$$

Here, $I_{\alpha(002)}$ and $I_{\beta(001)}$ are the integrated X-ray diffractions from

the (002) and (001) crystal planes of the α and β forms, respectively. These quantities were obtained by an X-ray analysis using the relation,

$$I_{hkl} = \int_{\theta} d\theta \int_{0}^{\pi/2} X(\phi, \theta) \sin\phi \, d\phi$$

Here, X is an X-ray diffraction to express the distribution function of P^{*}_{hkl} (the normal to the each crystal plane) to the stretching direction, when P^{*}_{hkl} makes an angle of ϕ to the stretching direction. The value of X was obtained as a X-ray diffraction intensity when the stretching direction of sample made the angle ϕ to the inner bisector of the X-ray incident and diffractive beams (the inner bisector of an angle, connecting the X-ray counter, sample, and X-ray incident beam). The angle θ designates the Bragg's angle of the each crystal plane and the integration concerning θ was done in the whole θ range where the diffraction from the crystal plane appeared. (Refer Fig.1 in Chapter 5, considering that the stretching direction coincides with Z-axis).

Small Angle X-ray Scattering (SAXS)

The procedure was described in Chapter 1 and 6.

Estimation of Planar Orientation by Wide Angle X-ray Diffraction

In order to examine the planar orientation of crystal planes for uniaxially compressed samples, X-ray diffraction analysis was carried out with a flat camera and a diffraction scan technique with a Ni-filtered Cu-K_{α} beam. These techniques are the same as were previously used for compressed crosslinked polyethylene (Chapter 5).

Thermal Properties

The fusion curve was obtained by a differential scanning calorimetry with use of the Perkin Elmer DSC1-B by a heating rate 10°C/min. The dimensional change was measured with increasing temperature in air at a constant load. The applied load was 1 g/mm^2, and dimensional change was followed by a cathetometer. The temperature was increased at the rate of 1 °C/min.

11.3. Crystal Transformation

X-ray photographs of PVDF samples drawn at temperatures of 50 to 180°C are shown in Figure 1. These patterns were obtained with X-ray beam, normal to sample film and virtical to the drawing direction. It can be seen that the diffraction pattern depends on the draw temperature. The sample drawn at 50°C is found in a single crystalline form, refered to as β-form. The samples drawn at 160°C are found in a mixture of β-form and another crystalline form, designated α-form. On the other hand, for samples crystallized from the melt under uniaxial stretch, the β-form is not recognized and they consit of highly oriented α-form crystal.

Figure 2 shows meridional X-ray diffraction for samples drawn at verious temperatures. At first sight it is evident that each sample is highly oriented. For a sample drawn at 100°C, the β-(001) diffraction peak in the vicinity of $2\theta=35°$ is strong but the α-(002) diffraction peak at $2\theta\simeq39°$ is extremely small. However, as the draw temperature

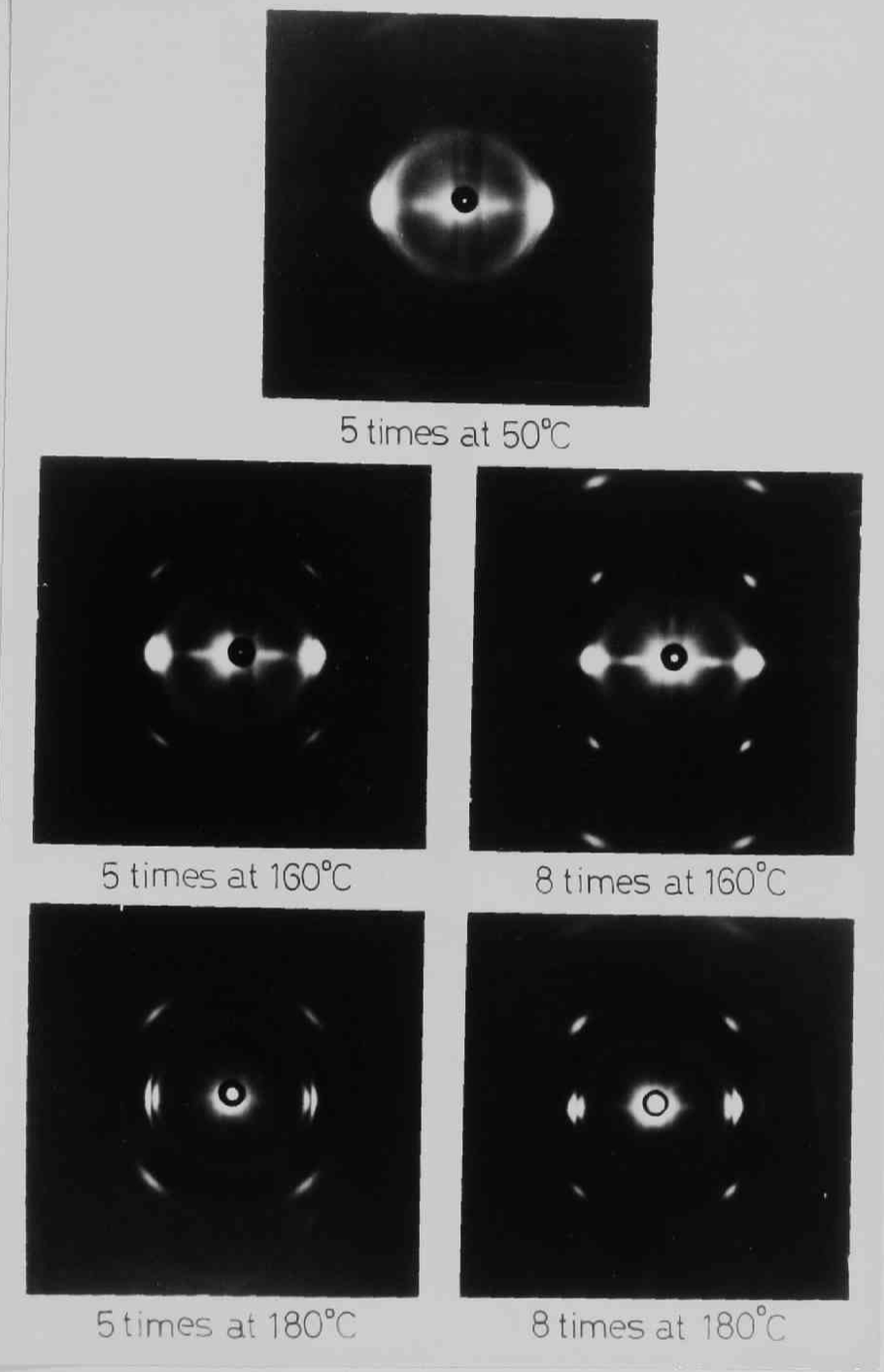

Fig. 1. Wide angle X-ray diffraction patterns of PVDF uniaxially stretched at various temperatures. X-ray beam was introduced perpendicular to the drawing direction (vertical in the figure).

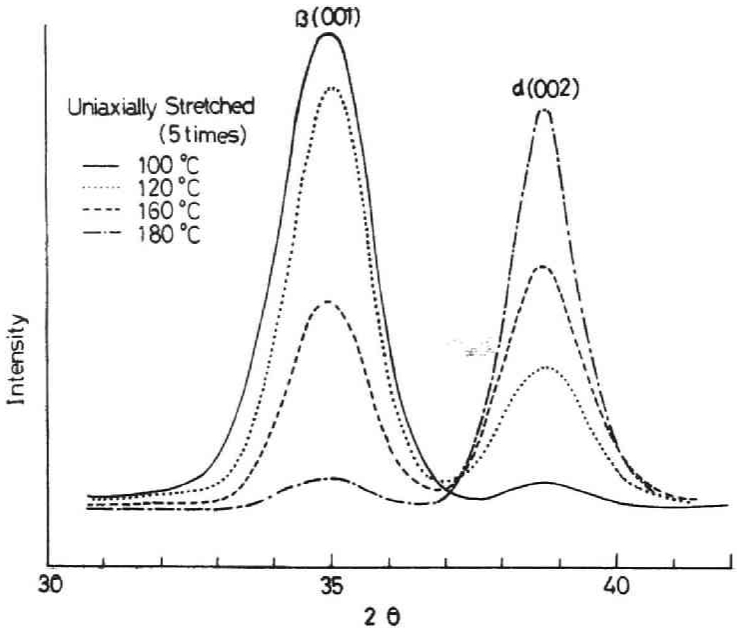

Fig.2. Meridian scanning of X-ray diffraction for PVDF uniaxially stretched at various temperatures.

is increased the intensity of the β-(001) diffraction decreases and that of the α-(002) diffraction increases. These facts indicate that the fraction of α-form increases with increasing of draw temperature; the crystalline form in drawn PVDF films is markedly influenced by draw temperature.

In Figure 3 and 4 the indices of degree of crystal transformation Φ_w for drawn sample are plotted against draw temperature and draw ratio, respectively. As can be seen from the figures, the value of Φ_w drastically decreases with increasing draw temperature. For samples

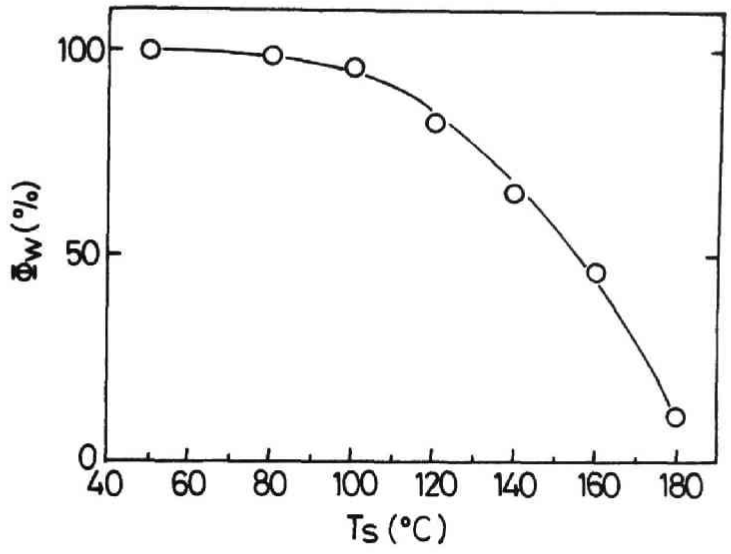

Fig. 3. Change in fraction of crystal transformation (α → β form) with stretching temperature for PVDF 5times uniaxially stretched at various temperatures.

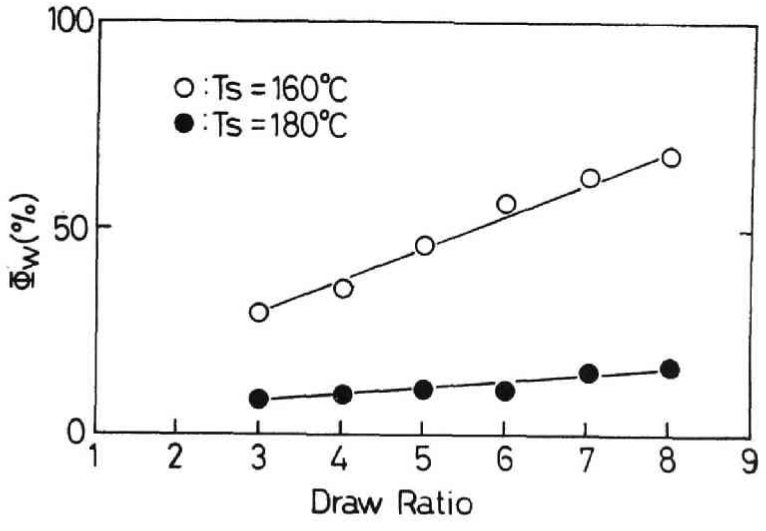

Fig. 4. Changes in fraction of crystal transformation (α → β form) with drawing for PVDF uniaxially stretched at 160°C and at 180°C.

drawn at 160°C, the value of Φ_w drastically increases with increasing draw ratio. On the contrary for samples drawn at the molten state, it does not increase appreciably with increasing draw ratio but to lesser extents. Thus, it is confirmed that the transformation of crystalline form, $\alpha \rightarrow \beta$, becomes pronounced as the drawing temperature decreases and the degree of drawing increases.

These results indicate that the transition at a low draw temperature from the unoriented to the oriented state occurs suddenly and is accompanied by the $\alpha \rightarrow \beta$ transition, namely, drawing at low temperature pulls out the polymer helix (α-form) into a planar zigzag conformation (β-form). At high draw temperature the α-crystals become orientated gradually and the $\alpha \rightarrow \beta$ transition occurs after considerable orientation of the α-crystallites has occured. It was found that the relative tatio in the concentration of crystallites of the two forms is dependent on the variation in draw temperature and draw ratio.

11.4. Small Angle X-ray Scattering

Next we consider the small angle X-ray scattering for samples drawn at 160°C and at molten state to different degrees. Figure 5 shows the SAXS patterns for the two series of samples, stretched at 160°C in the partially crystalline state and at 180°C in the molten state, respectively. It is seen that, when stretched at 160°C, a diffuse six-point diffraction appears at a draw ratio of 2 and

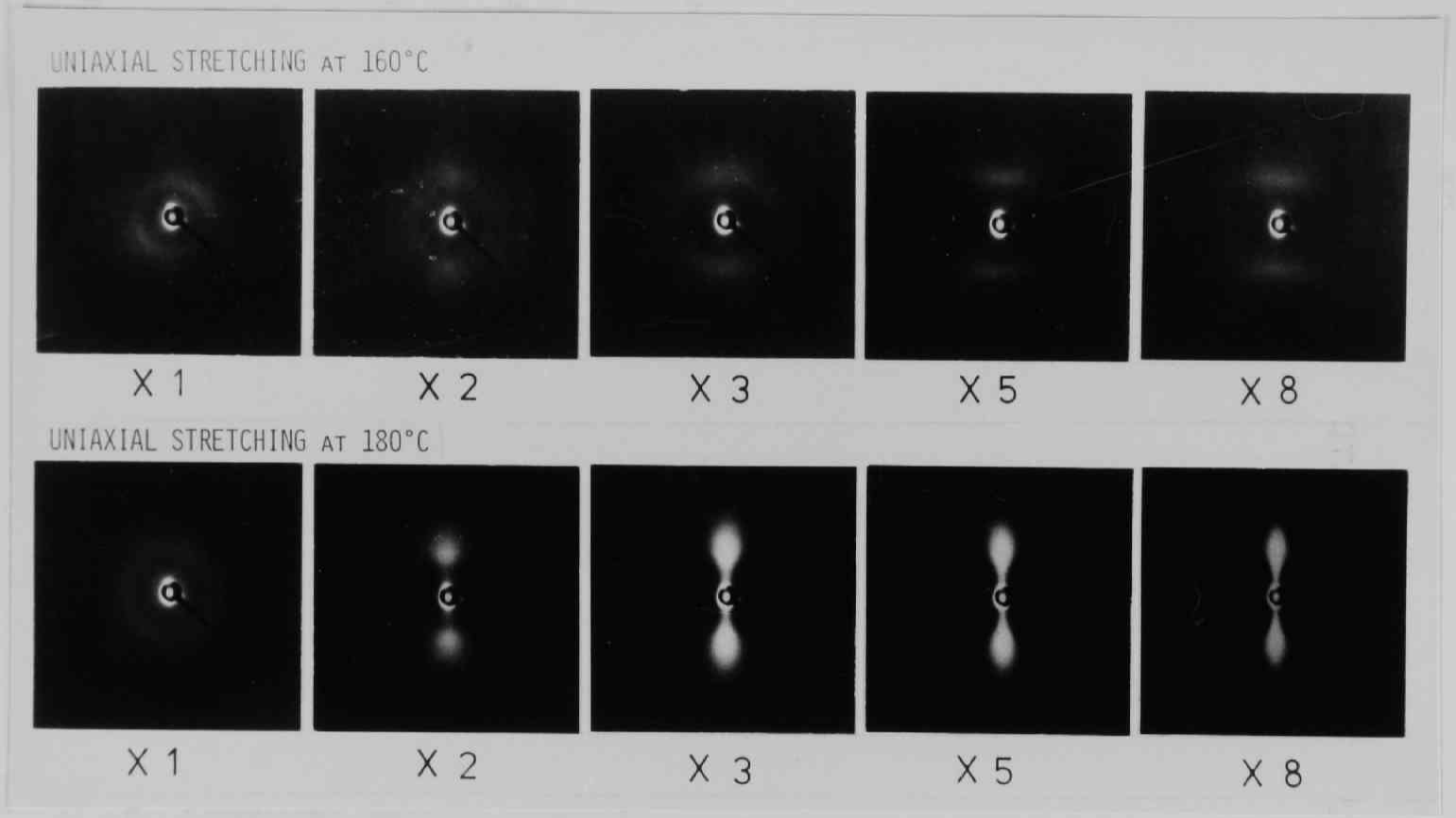

Fig. 5. Small angle X-ray diffraction patterns for PVDF uniaxially stretched to diffrent degrees at 160°C upper series) and at 180°C (lower series). X-ray beam was introduced perpendicular to the drawing direction (vertical in the figure).

an arc-like shaped diffraction appears at a draw ratio of 3 and upon further drawing a discreate line diffraction appears, which shows a irregular lamella structure. On the other hand, when stretched at molten state the patterns obtained are quite different as can be seen from the figure. The two-point pattern is always recognized from the drawn sample independent of the draw ratio from 2 to 8-fold. The diffraction points approach the center of the pattern with increasing draw ratio, showing qualitatively increasing of the long period. Such two-point pattern has been reported for a stretched sample when it was shrunk with annealing at a high temperature (close to melting point)(9). But we note here that the crosslinked sample drawn highly such as to 8-fold exhibits two-point shape without shrinkage.

The result implies that the drawing in the un-molten state produces enhanced disordering of the lamellar interfacial structure while the stretching in the melt does not produce such disordering.

In Figures 6 and 7 the long period evaluated from the 2θ angle at the maximum and the maximum intensity are plotted against draw ratio for the two series of samples. When the uncrosslinked sample is stretched in the partially crystallized state, the long period decreases and the maximum intensity either decreases or stays unaltered as the draw ratio increases. This is similar to the case of the polyethylene and polypropylene samples, reported by Peterlin et al.(10, 11). On the other hand, for the crosslinked sample drawn at molten state, the both of long period and maximum intensity evidently increase with increasing draw ratio. These phenomena were also recognized for the cross-

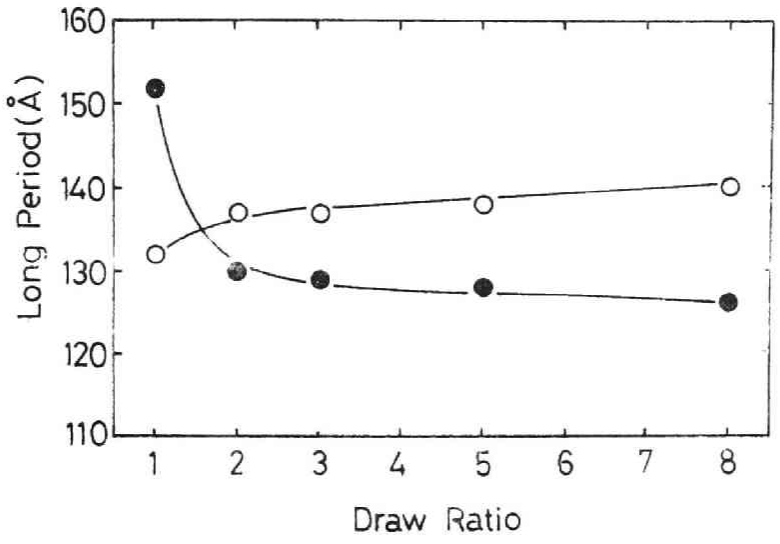

Fig. 6. Variation of the long period as a function of draw ratio for PVDF uniaxially stretched at 160°C (●) and at 180°C (○).

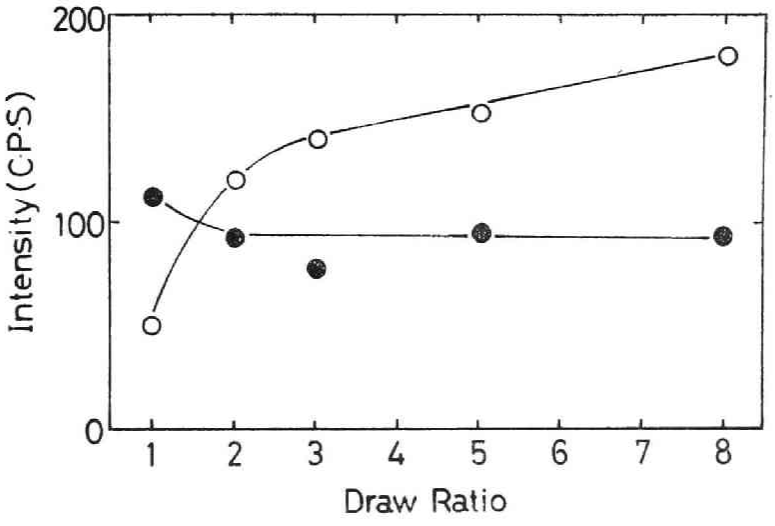

Fig. 7. Variation of the scattering intensity as a function of draw ratio for PVDF uniaxially stretched at 160°C (●) and at 180°C (○).

linked polyethylene and polypropylene samples when they were crystallized from the melt under uniaxially stretched or compressed states as described in Chapter 2, 6, and 11.

In any case the above-mentioned distinct difference in the small angle X-ray scattering phenomena between samples either crystallized from the melt under uniaxial stretching or stretched plastically in the partially crystalline state will be well reflected in the difference in the structures of both kinds of samples.

11.5. Orientation of Crystal Planes

X-ray diffraction photographs were obtained for samples prepared under different conditions. With an X-ray beam perpendicular to the film surface of sample, a Debye-Scherrer diffraction was obtained for all samples. This indicates random distribution of crystallites about the normal to the film surface. However, as can be seen in Figure 8 with an X-ray beam parallel to the film surface, different types of X-ray patterns were obtained depending on the deformation condition. These patterns suggest that the planar orientation of some crystal planes exists in the samples to different degrees. As described in Section 11.3 the transformation of the crystal forms $\alpha \rightarrow \beta$ takes place accompanying deformation. But here only planar orientation of the α-crystal form is considered since the melt-compressed samples are mostly in the α-form although the plastically deformed samples contain a β-crystal form.

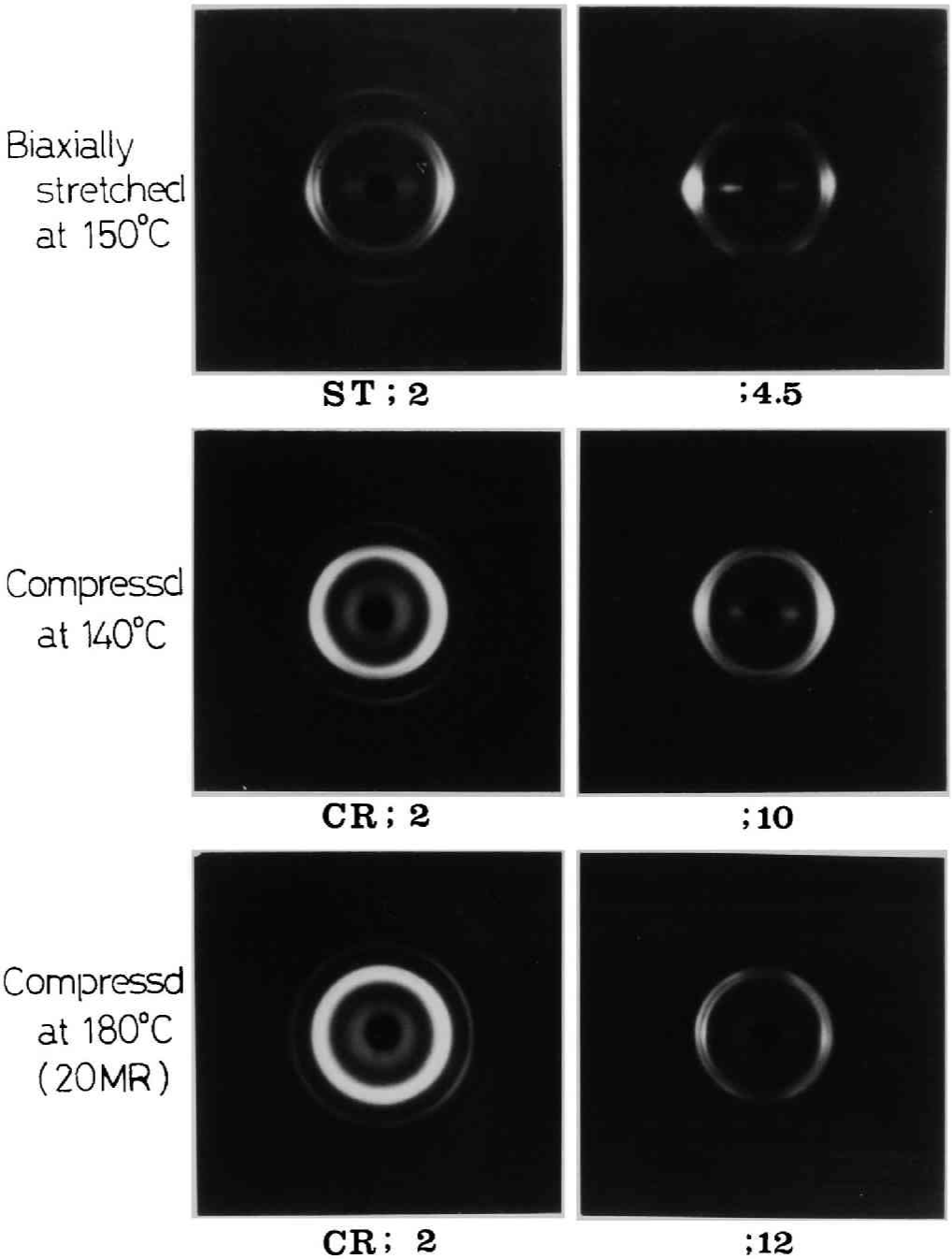

Fig. 8. Wide angle X-ray diffraction patterns for PVDF deformed under various conditions. X-ray beam was introduced parallel to the film surface. (See p.184)

The diffraction intensity $I(\phi)$ from each crystal plane (010), (200), (110) and (210) was recorded as function of the angle ϕ, by rotating the sample stepwisely. The detailed procedure and base line correction for the scan are described in Chapter 6. The products $I(\phi)\sin\phi$ for the (010)-, (200)-, (110)-, and (210)-diffractions for the each samples with different degree of deformation are plotted against ϕ in Figure 9. This product indicates the probability density that the vector P^* for each crystal plane points to the direction between ϕ and $\phi + d\phi$ in an arbitrarily chosen crystallite in samples as mentioned before. Hence, one can inquire the appearance of the crystal plane orientations with the increase of the degree of deformation by examining these figures. For samples biaxially stretched at 150°C [Figure 9(A)] the value of $I \cdot \sin\phi$ for the (010) crystal plane has maximum at $\phi=0°$ for a draw ratio of 2, but as the draw ratio increases a peak in the vicinity of $\phi=28°$ appears. In the (200)-scan, $I \sin\phi$ has a maximum at $\phi=90°$ for a draw ratio of 2, but as the draw ratio increases a peak at about $\phi=63°$ appears. Similarly, in the (110)-scan, $I \sin\phi$ has a maximum at about $\phi=28°$ for a draw ratio of 2, but as the draw ratio increases a peak at $\phi=0°$ and about $\phi=56°$ appears. For the sample compressed at 140°C [Figure 9(B)] the result is quite different; any planar orientation of crystal plane is not difinitely recognized at a relatively low degree of compression. In the (010), (200) and (110) scans for a sample with compression ratio of 12, $I \sin\phi$ has maxima at $\phi=0°$, $\phi=90°$, and $\phi=28°$, respectively. For samples compressed to a compression ratio

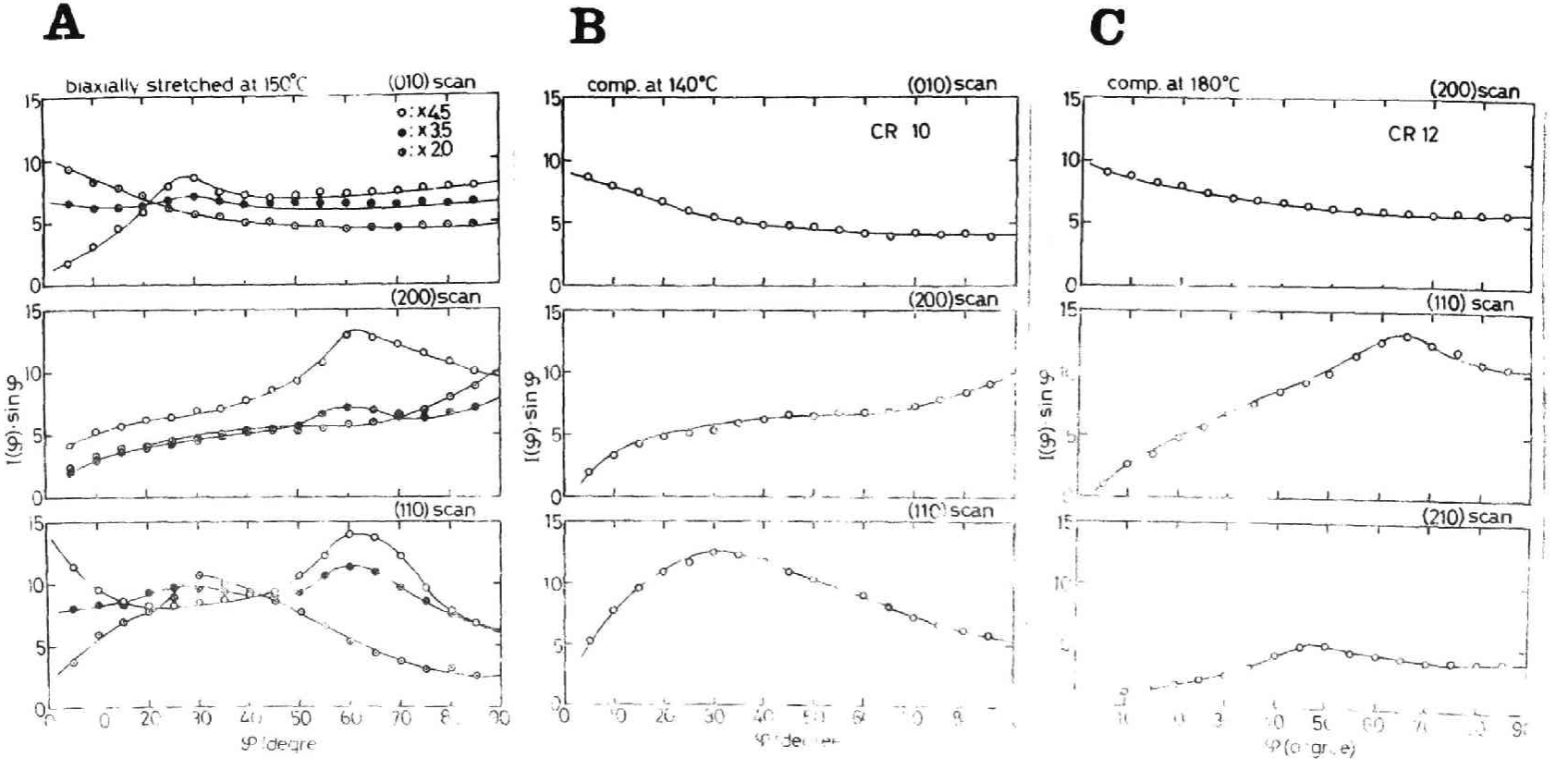

Fig.9. I (ϕ) sinϕ vs ϕ of the crystal planes (010), (200), (110), and (210) for PVDF deformed at various conditions.

of 12 at molten state of 180°C [Figure 9(C)] I sinϕ has maxima at ϕ=0°, ϕ=62°, and ϕ=44° in the (200), (110) and (210) scans, respectively.

The results mentioned above should indicate the appearance of planar orientations of some crystal planes. We next consider these results refering to the reciprocal lattice diagram of the orthorhombic crystal form (α) shown in Figure 10. The planar orientation of a crystal plane should be confirmed by the maxima or an increased value of I sinϕ at ϕ=0° in the respective scanning if it is assumed that the chain axes (c-axes) are parallel to the film surface. Hence, maximum or enhanced values of I sinϕ at 0° for the (010) and (110) of the biaxially stretched sample (4.5x4.5) should indicate the planar orientation of these crystal planes. Since the vector P^*_{010} makes angles of 28 and 46° to vectors P^*_{110} and P^*_{210}, respectively, the maximum values of I sinϕ at ϕ=28° in the (110) scan and at 90° in the (200) scan are to be understood as additional evidence of the appearance of the (010) orientation. Similarly the (110) orientation will also be further certified by an increased value of I sinϕ at ϕ=28° in the (010) scan because P^*_{110} makes an angle of 28° with P^*_{010}. A minor (200) planar orientation can be detected by the increased value of I sinϕ at ϕ=0 for the sample compressed at 180°C in the (200) scan(Figure 9(C)).

In Table 2 summarized the results of the planar orientation. When the crosslinked sample was crystallized from the melt under uniaxial compression, the (200) crystal plane is selectively oriented parallel to the film surface. On the other hand, for the sample deformed at a high temperature but below its melting point, it is

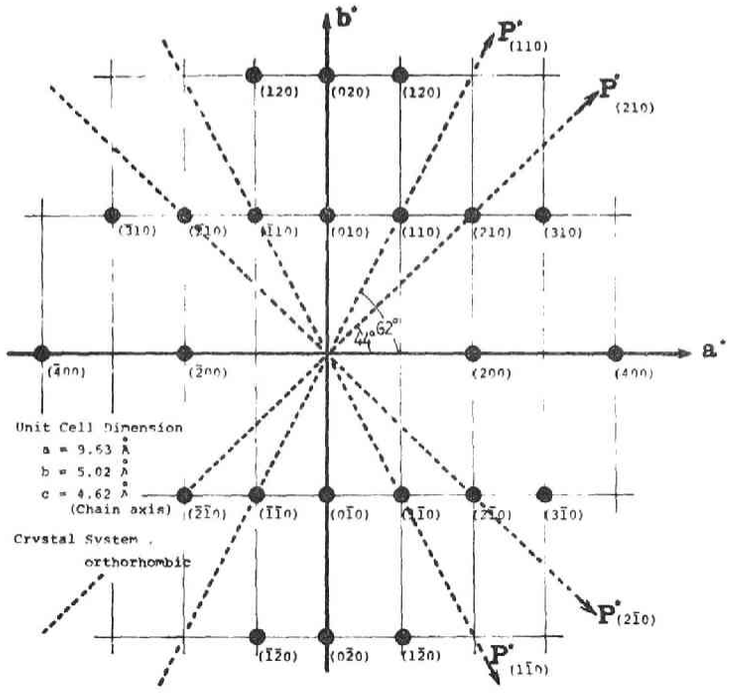

Fig. 10. a*- b* plot of the reciprocal lattice of the orthorhombic crystal form of PVDF. Here, c-axis (=c*-axis,molecular axis) is perpendicular to the a*- b* plane.

confirmed that the (010) crystal plane is preferentially oriented parallel to the film surface at relatively low degrees of deformation, and the (110) crystal plane is oriented parallel to the film surface at higher degrees of deformation.

11.6. Thermal Properties

The DSC thermograms for samples drawn 4-fold at verious temperatures are shown in Figure 11. As the draw temperature is increased,

Table 2. Planar Orientation of PVDF Films Obtained by Various Methods of Deformation.

Simultaneously biaxial stretched at 150°C		Compressed at 140°C		Compressed at 180°C	
S.R*	Planar orientation	C.R*	Planar orientation	C.R*	Planar orientation
2	010 $_{s}$**	4	010 $_{w}$**	8	200 $_{w}$**
3.5	010 $_{w}$ + 110 $_{w}$	6	010 $_{w}$	10	200 $_{s}$
4.5	110 $_{s}$	10	010 $_{s}$	12	200 $_{s}$

* S.R = Stretch ratio
C.R = Compression ratio

** S = Strong
W = Weak

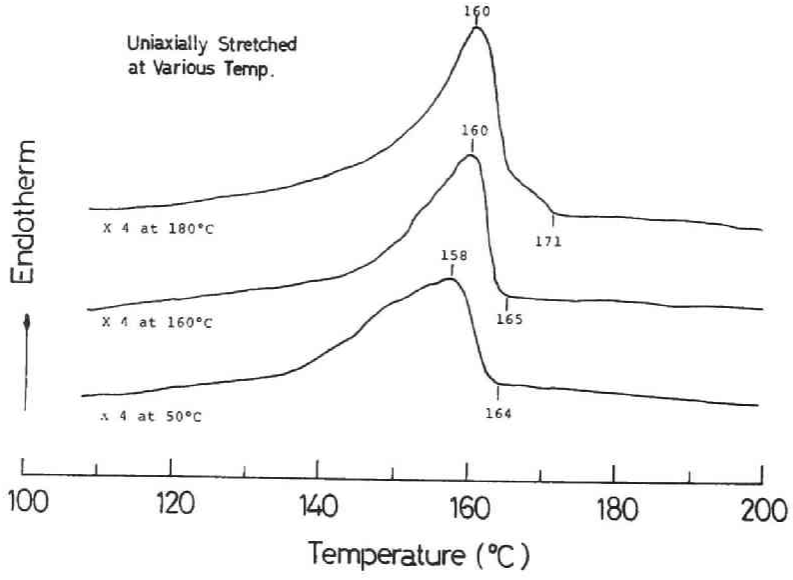

Fig. 11. DSC fusion curve for PVDF 4-fold uniaxially stretched at various temperatures.

the melting temperature increases. The fusion curve depends greatly on the prepararion condition of samples. For the samples drawn at a temrerature below melting point a small shoulder is observed in the low temperature range. However, for the sample drawn in the molten state an endothermic peak with a long "tail" persisting to 171°C is recognized. Similar persisting tail is sometimes reported for other polymers such as polyethylene (Chapter 1, 6), polypropylene (Chapter 10) and polyvinyl alcohol (Chapter 12) with an abnormally high melting temperature, when the polymers are crystallized under conditions involving molecular orientation.

Figure 12 shows thermal shrinkage curves for the films deformed at temperatures below or above the melting point. The most remarkable feature is the difference between the samples compressed at temperature below the melting point and the sample compressed at the molten state. The former samples begin to shrink at about 50°C and the shrinkage increases continuously up to about the melting point, but the latter sample does not shrink up to 140°C at which a partial fusion of oriented crystallites may begin, and after going through this temperature it shrinks very rapidly. These shrinkage curves are quite similar to the curves for polyethylene (Chapter 3) and polypropylene (Chapter 10) made in a similar manner. The good dimensional stability of the melt-compression sample must be caused by its relaxed amorphous chains and the perfection of the crystalline phase in the structure.

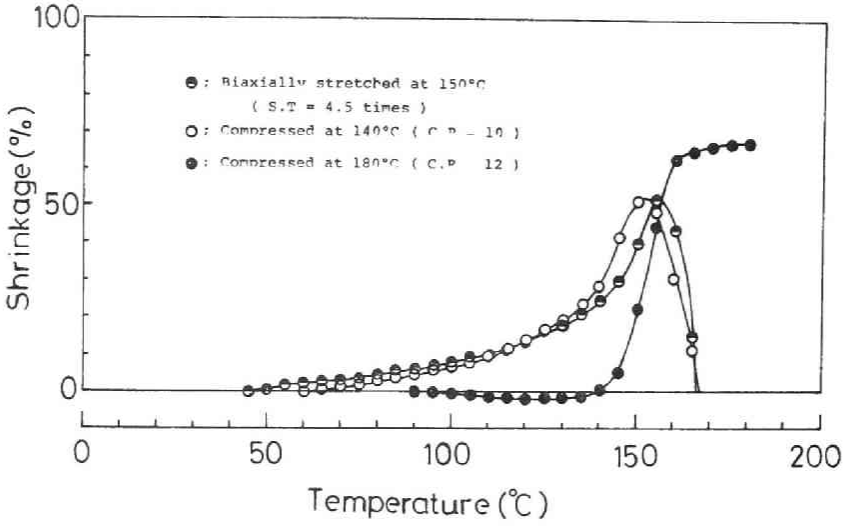

Fig. 12. Thermal shrinkage of PVDF films.

11.7. Conclusion

The crosslinked polyvinylidene fluoride, when highly stretched or compressed in the molten state, exhibits a unique phase structure with characteristic thermodynamic and physical properties similar to other polymers such as crosslinked polyethylene and polypropylene. The sample stretched uniaxially in the molten state is characterized by a very ordered crystalline phase and rather unoriented and relaxed amorphous material. The orientation factor to the stretching direction for the chain axes in the crystalline phase is very close to unity but that in the amorphous phase stays in a low level.

When compressed uniaxially in the molten state, a special planar

orientation of the crystal planes of the orthorhombic form of this polymer appears in which the (200) crystal plane is preferentially oriented parallel to the film surface while no appreciably amount of the β-form appears. On the contrary, when compressed or biaxially stretched in the partially crystallized state, other planar orientations such as the (010) and (110) planar orientations are produced without the (200) orientation. This result indicates that this mode of crystallization involves less restriction to the molecular mobility during the crystallization despite of the high degrees of compression.

References

1. Ye.L.Gal'perin, B.P.Kosmynin, L.A.Aslanyan, N.P.Mlenik, and V.K.Smirnov, Vysokomol.Soyed.A12, 7 (1970).
2. W.W.Doll and J.B.Lando, J.Macromol.Sci.Phys., B4, 889 (1970).
3. J.B.Lando, H.G.Olf, and A.Peterlin, J.Polymer Sci., A-1, 4, 941 (1966).
4. Ye.L.Gal'perin, Yu.V.Strogalin, and M.P.Mlenik, Vysokomol.Soyed., 7, 933 (1965).
5. B.P.Kosmynin, Ye.L.Gal'perin, and D.Ya.Tsvankin, Vysokomol.Soyed., A12, 1254 (1970).
6. C.W.Wilson, E.R.Santee, J.Polym.Sci., C3, 97 (1965).
7. G.J.Melch, Polymer, 15, 429 (1974).
8. R.Timmerman, J.Appl.Polym.Sci., 22, 456 (1962).
9. B.P.Kosmynin, Ye.L.Galperin, and D.Ya Tsvankin, Vysokomol.Soyed., A14, 1365 (1972).
10. A.Peterlin and R.Cornelliussen, J.Polymer Sci., A-2, 6, 1273 (1968).
11. F.J.Balta-Calleja, and A.Peterlin, J.Materials Sci., 4, 722 (1969).

Chapter 12.

STRUCTURE AND PHYSICO-CHEMICAL PROPERTIES OF POLYVINYL ALCOHOL, STRETCHED AT THE AMORPHOUS STATE AND ANNEALED

12.1. Introduction

The stretching or drawing to produce molecular orientation along the fiber axis, which is one of important processes in manufacturing of synthetic or man-made fibers,can be achieved in a temperature range between the glass transition and melting temperatures of the material polymers. It is evident as exemplified in the fiber forming processes of various fibers that this process should be performed in the absence of the crystallinity or at least in a reduced crystalline state of the polymers to promote the molecular orientation and obtain excellent fiber properties. However, in the industrial manufacturing of Vinylon from polyvinyl alcohol (hereafter, abbreviated as PVA), the stretching is necessarily conducted at high temperatures in the presence of the crystallinity after spinning, during which the crystallization of the polymer takes place to some extents due to the high crystallizable ability.

Whether the crystallinity exists or not in stretching process will give extremely enhanced effects not only on the process to molecular orientation but also to form of the crystalline structure. For example, it was found (Chapter 1-8) that, if a lightly crosslinked polyethylene is crystallized after stretching or compressing at the melt; namely

in the absence of crystallinity, a very unique crystalline structure is produced with extra ordinarily high melting temperature and excellent transparency. The polymer molecules in the crystalline region of this structure are highly ordered in the three-dimensional space in accordance with the macroscopic deformation at the melt but those in the amorphous region are rather disordered and exhibit high degree of mobility (Chapter 1, 2, and 7). This is thought to be caused by the fact that the state of the molecules stretched in the amorphous state is elastically maintained until the crystallization occurs and the crystallization is performed from the stretched molecules. The similar phenomena are observed for various polymers such as isotactic polypropylene (Chapter 9, 10) and polyvinyliden fluoride (Chapter 11). (1-10).

The above result is not expected generally unless chemically crosslinked points exist in the structure since the molecular orientation cannot be held in the molten state. However, in the case of PVA without crosslinking points a similar result may be expected if the polymer is stretched in the swollen or amorphous state, because the molecules of the polymer have rather strong intermolecular attractive forces due to the hydrogen bond formation and entanglement effects of molecules.

In this chapter a mode of stretching of PVA in a swollen state without crystallinity and following crystallization is studied under the expectation mentioned above.

12.2. Experimental Part

Material

A fraction with a viscosity-average molecular weight of 1.45×10^5 was obtained from a commercial PVA from the Kuraray Co. with a listed viscosity-average molecular weight of 77,000 and degree of saponification of 99.94%. Intrinsic viscosity measurements were made in water at 80°C, and molecular weights were calculated using the relation $[\eta] = 9.4 \times 10^{-4} M^{0.56}$ of Matsuo and Inagaki(11). Film ca. 0.3 mm thick was obtained from the 10% aqueous solution according to a routine casting technique. The degree of crystallinity of this film was evaluated to be 0.38 by the density measurement.

Stretching and Annealing

a. Stretching in Swollen State (Swell-Drawing).

The sample film was immersed in water at 60°C for 5 minutes and stretched to various predetermined extents with a rate of stretching of 500 %/sec and then it was transferred into methanol at 60°C or acetone at 50°C with the length held constant and dried in vacuo and finally annealed at a temperature of 220°C for 2 minutes.
In the water-swollen sample to about 1.6 times the original volume no crystallinity was detected by an X-ray diffraction analysis but it exhibited rubbery elasticity for high degrees of stretching.
It is supposed that in the above-described processes molecular chains in the sample were stretched without crystallization and the crystallization was carried out from the stretched molecular

chains. The degree of stretching was characterized by the ratio of film lengths after and before stretching. This draw ratio ranged from 1 to 7.

b. Stretching in Non-Swollen State at High Temperatures (Heat-Drawing).

The sample film was stretched in air at a temperature of 120°C or 180°C and annealed at 220°C for 2 minutes at constant length.

Density and Degree of Crystallinity

The density measurement was made at 30°C by a density gradient column of benzene and tetrachlorocarbon. To avoid the effect of air bubbles the sample was dipped in benzene in vacuo and transferred into the gradient column. The degree of crystallinity was caluculated from the density using the relation $1/\rho=(X/\rho_c)+(1-X)/\rho_a$. Here, ρ, ρ_c, and ρ_a designate the experimentally observed density and the crystalline and amorphous densities of the polymer, respectively. ρ_c and ρ_a were taken as 1.345 and 1.296(12). X designates the degree of crystallinity.

Birefringence

The birefringence was obtained by measuring the retardation of sample at room temperature in white light with polarized light microscope using the Bereck compensator.

X-ray Diffraction

The radiograph was taken with a 114.6-mm powder camera, using

Ni-filtered Cu-K_α radiation; the photograph film was fixed asymmetrically. A number of d-spacings of the crystal planes of the nomoclinic crystalline form of the polymer were determined. The errors due to the shrinkage of photographic film and the deviation of the camera radius were corrected using forward and backward diffractions of NaF compounded in the sample(13).

Fusion and Enthalpy Change in Fusion

The fusion curve was obtained by a differential scanning calorimetry with use of the Perkin Elmer DSC 1-B at a heating rate of 10°C/min. The amount of the used sample was about 3-4 mg and the correction of was defined to be a temperature where the fusion finally terminated. The enthalpy change in the fusion was estimated by planimetry of the fusion curve with a reference datum for purified benzoic acid.

Dynamic Modulus

The dynamic modulus was measured at room temperature by a dynamic viscoelastometer Vibron DDV-2 from the Toyo Baldwin Co. at a frequency of 110 cps.

Shrinkage with Heating

The dimensional change with increasing temperature in the direction of stretching was measured in air and water at a constant load of 1 g/mm^2. The change in the length with heating of 0.5 °C/min was

read off by a cathetometer, and expressed in percents by dividing with the original length.

12.3. Results and Discussion

According to the procedure described in the experimental section the molecular fraction of PVA used in this work could be stretched to high extents in the swollen state in water without breaking. Figure 1 shows the X-ray diffraction photograph for the sample stretched sixfold and annealed. It indicates very high degree of molecular orientation as well as high degree of crystallinity. It is concluded, therefore, that although the sample without crosslinked points was stretched in the

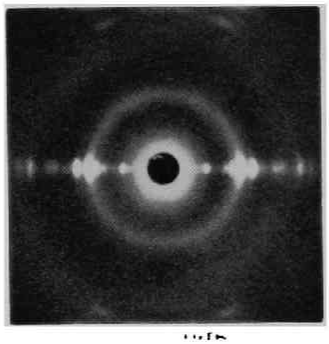

Fig.1. Wide angle X-ray photograph of the PVA film stretched sixfold in the swollen state and annealed. The photograph was taken with X-ray perpendicular to the stretching direction (meridian of the pattern).

swollen amorphous state molecular chains in the structure were stretched in accordance with the macroscopic deformation and that stretched state of molecular chains was maintained until major crystallization took place by annealing. Note here that, if the starting commercial unfractionated PVA with the lower average-molecular weight was dipped in water at 60°C in the same manner, partial dissolution of the sample took place and no stretching could be achieved. The stretching in the swollen state could be performed only for a sample with high molecular weights, where intermolecular attractive forces due to hydrogen bond formation and entanglement effects of polymer chains prohibit plastic flow of molecular chains and reserve the rubbery elasticity just like as chemical crosslinkings for other polymers such as polyethylenes(1-3).

In any case in this preparing mode of sample the crystallization is thought to have been brought about from stretched amorphous chains. On the other hand since the sample film has a degree of crystallinity of about 38% in the non-swollen state, the usual stretching in air at high temperatures should involve many complicated phenomena such as stretching of molecular chains in the amorphous region and crystallization of those, orientation of the crystalline region or crystallites, partial melting of the crystallites and recrystallization of those, and etc. Thus, the crystalline structures and hence various properties of the samples that are prepared by these two kinds of stretching; the swell-drawing and heat-drawing, are thought to be quite different with each other. In fact we have confirmed various characteristic properties for the former sample. In the following sections we will

show and discuss the data, considering the detailed crystalline structure of samples.

Density and Crystallinity

Figure 2 shows the density and degree of crystallinity for samples stretched under various conditions and those further annealed. Here, closed and open triangles indicate data for the samples swell-drawn

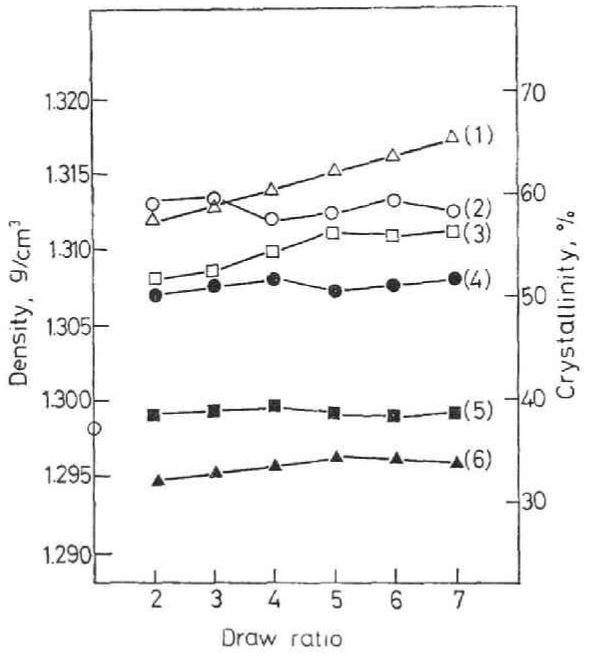

Fig.2. Density and crystallinity vs. draw ratio for drawn PVA films. Curves; (1) stretched in the swollen state and annealed, (2) stretched at 180°C in air and annealed, (3) stretched at 120 °C in air and annealed, (4) stretched at 180°C in air and not annealed, (5) stretched at 120°C in air and not annealed, (6) stretched in the swollen state and not annealed.

before and after annealing. The squares and circles indicate data for heat-drawn samples before and after annealing as detailed explanations are given in the caption of the figure. As can be seen by the triangle data, when the sample is stretched in the swollen state and dried the crystallinity does not appear so much. It remains almost constant at less than 34 % with increasing of stretching. But by annealing at 220°C it conspicuously increases proportionally with increasing of the draw ratio, reaching 66 % at sevenfold stretching (data indicated by open triangles). Contrary, when the sample is stretched in air at high temperatures the crystallization proceeds appreciably during stretching but it does not reach so high level by annealing. The degree of crystallinity of the annealed samples stays almost constant or slightly increases with increasing draw ratio so that it cannot go over 59 %. We note here that the degree of crystallinity of 66 % for sevenfold stretched and annealed sample is the highest among data reported for atactic PVA up to date(12).

Birefringence

The birefringence of samples stretched under different conditions with subsequent annealing is plotted in Figure 3 against draw ratio. Increase of the birefringence with increasing of draw ratio is most pronounced for the sample stretched in the swollen state. The sevenfold swell-drawn sample is associated with the largest birefringence of about 4.5×10^{-2} that indicates the highest degree of molecular orientation along stretching direction. As will be discussed

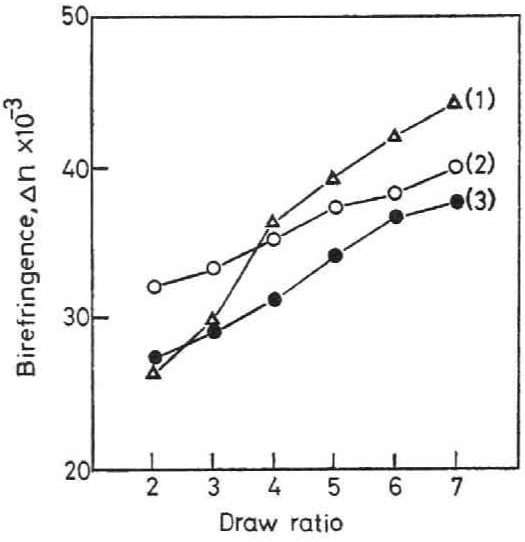

Fig.3. Birefringence vs. draw ratio for drawn PVA films. Curves; (1) stretched in the swollen state and annealed, (2) stretched at 180°C in air and annealed, (3) stretched at 120°C in air and annealed.

later the molecular orientation in the amorphous region in this sample is not so enhanced, so that highest molecular orientation should be contributed by the molecular alignment in the crystalline region, which is in good agreement with the result of its X-ray photograph in Figure 1.

Crystallographic Parameters

The d-spacings for various crystal planes for samples made in the different manners are listed in table 1. It is seen that either the sample is stretched in the swollen state or in the non-swollen state

Table 1. d-Spacings in A° of Drawn PVA Films Obtained by X-ray Powder Camera

(hkl)	unstretched, annealed	5-fold stretched in air at 120°C and annealed	7-fold stretched in air at 120°C and annealed	5-fold stretched in swollen state and annealed	7-fold stretched in swollen state and annealed
100	8.192	7.900	7.830	7.830	7.762
001	5.609	5.680	5.505	5.471	5.471
$10\bar{1}$	4.671	4.671	4.599	4.575	4.599
101	4.552	4.484	4.396	4.396	4.352
200	3.969	3.986	3.917	3.900	3.900
$20\bar{1}$	-----	3.290	3.243	3.231	3.231
201	-----	3.143	3.110	3.110	3.110
002	2.788	2.788	2.739	2.730	2.730

at 120°C, the d-spacings of various crystal planes (h0l) which are aligned parallel to the stretching direction become smaller. But it is noted that the degree of shrinkage of the d-spacings with stretching is pronounced when stretched in the sowllen state. The dimensional change of the unit-cell has been sometimes reported (14-16), but such enhanced shrinkage has never been recognized.

Based on the d-spacings for (200), (002), and $(20\bar{1})$ or (201) of the sevenfold heat-drawn and swell-drawn samples, the unit-cell parameters are calculated as a = 7.842, c = 5.484 Å and β = 92.55° for the former sample and a = 7.808, c = 5.466 Å and β = 92.55° for the latter sample. These parameters are the average values estimated with use of the d-spacing of (201) or $(20\bar{1})$. The unit-cell densities were estimated to be 1.341 and 1.352 for the heat-drawn and the swell-drawn samples, respectively, using the fiber identity period of 2.52 Å which was experimentally determined by Sakurada and others(14).

The data shown here should indicate excellent perfection of the crystalline phase in the structure for the swell-drawn sample which has been stretched in the swollen state and annealed, comparing with the data for the heat-drawn sample and referring to the crystallographic data reported up to date(14-18).

Fusion Behavior

The fusion curves obtained with the Perkin Elmer DSC 1-B for samples made by stretching in air at 120°C and subsequent annealing are shown in Figure 4. As draw ratio is increased, the melting point where major fusion occurs arises. Note here that a small shoulder associated with the fusion peak for the most highly stretched samples is detectable in the low temperature side of the peak. Appearance of similar small shoulder has been recognized by Mochizuki and others(19) with a DTA measurement for stretched PVA samples. It should indicate a heterogeneity or dual crystalline structure in samples, but the shoulders in the figure are too weak to make further consideration. However, for the PVA samples stretched in the swollen state the dual crystalline structure is distinctly

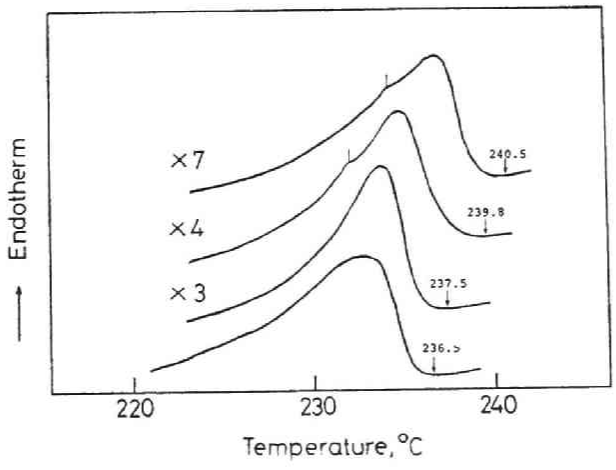

Fig.4. DSC thermograms for PVA films stretched at 120°C and annealed. The draw ratio is indicated to each curve.

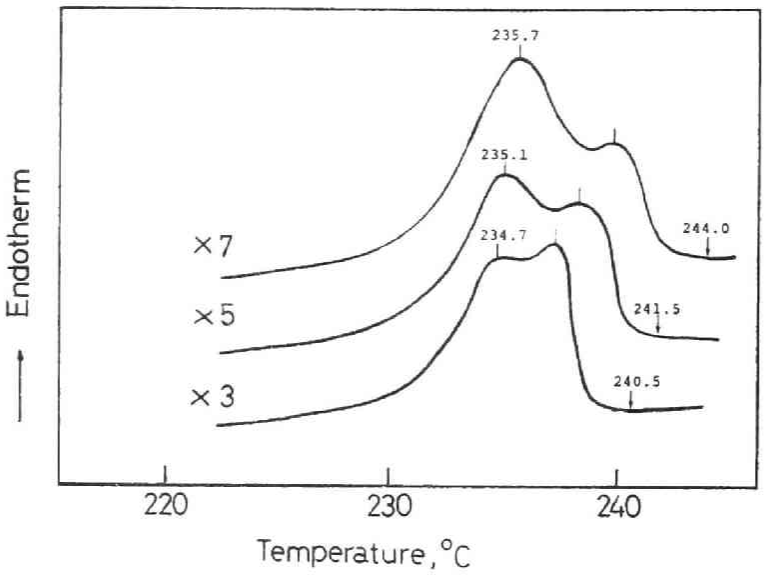

Fig.5. DSC thermograms for PVA films stretched in the swollen state and annealed. The draw ratio is indicated to each curve.

recognized. As is shown in Figure 5, each of the curves for these samples consists of well-isolated two peaks. The lower peak appears at temperatures of 234.7, 235.1, and 235.7°C for the three-, five-, and seven-fold stretched samples, respectively, which are a little higher than the fusion peak of 232.8°C for an unstretched well-crystallized PVA (see Figure 4). The peak is much higher than the normal melting point of PVA. The melting points where the fusion finally terminates are determined to be 240.5, 241.5, and 244.0°C for the three-, five-, and seven-fold stretched samples, respectively (see Figure 5 with the melting points listed in Table 2).

Similar dual or multiple fusion curve is someties reported for

other polymers such as polyethylene(20-22), polyethylene terephthalate (23), and nylon-66(24) together with an abnormally high melting temperature, when the polymers are crystallized under very high pressure or under conditions involving molecular orientation. Also for PVA such an abnormally high melting temperature is reported by Mochizuki et al.(19), Yamaura et al.(25), and Monobe et al.(26), when the polymer is crystallized from the aqueous solution under high degree of stirring but such dual peak never has been recognized up to date. Thus we should note that the mode of stretching and subsequent crystallization for PVA examined in this paper brings very characteristic unique feature in the structure of the polymer. The dual fusion curve as well as abnormally high melting point are generally characteristic for samples, regardless of polymer sort, which were crystallized under condition involving molecular orientation and those should indicate dual structure or the presence of very highly ordered crystalline phase with large dimensions in the samples.

However, we point out here a very intimate similarity in the fusion behavior between the swell-drawn PVA samples and the lightly crosslinked polyethylene gel(4) which was crystallized from the molten and stretched or compressed state. Very distinct dual fusion curve is reported for the sample that was obtained from a molecular weight fraction with a very large molecular weight with minimum amount of crosslinkings. Since this sample indicates a very good rubbery elasticity in the molten state, the crystallization from the molten and compressed state is considered to comprise two kinds of crystallization, the mechanism of

which is quite different with each other. The first one is the crystallization from stretched molecular chains. It proceeds with a very enhanced rate because of the elevation of the equilibrium melting temperature (and hence increase of supercooling) due to the decrease of entropy change in the transformation by stretching. It produces highly ordered crystallites with larger dimensions associated with the higher melting temperatures, remaining a part of the molecular chains in an unstretched state. After this crystallization terminates with dissipation of stretched molecular chains, the other kind of crystallization takes place from less- or non-streched molecular chains in the structure. It produces less ordered crystallites with smaller dimensions associated with lower melting temperatures in a normal range of melting of the polymer. Thus it is concluded together with data of molecular mobility or molecular orientation obtained by NMR (7) or birefringence (2) studies that the highly ordered crystalline region or crystallites with larger dimension coexist with less-oriented amorphous molecular chains in a relaxed state with smaller size of crystallites. The dual fusion behavior for this crosslinked polyethylene is well understood by the dual crystalline structure produced by the above-mentioned mode of crystallization.

For the swell-drawn PVA samples, there is no chemical crosslinkings in the molecular structure. However, as was pointed out in the introductory section, the structure will have been brought about from thus stretched molecular chains in the course of deswelling, drying, and annealing, since the polymer molecules are thought to be stretched in

accordance with the macroscopic stretching in the swollen state due to rather strong intermolecular attractive forces. Thus a crystalline structure that corresponds to the dual fusion behavior will be brought about in a similar mechanism of crystallization to cross-linked polymers cited above. It is concluded for the swell-drawn PVA samples that highly ordered crystallites with larger dimension coexist with smaller size of crystallites. As can be seen in Figure 3, however, the total birefringence at room temperature for these highly drawn samples is larger than that for samples drawn in air. If amorphous chains in the structure are not oriented, the total birefringence can not be so large as observed values since the higher orientation of the crystallites is not thought to compensate all of lowering in the birefringence by the amorphous chains. Therefore, it cannot be concluded that the highly ordered crystallites coexist with less-oriented amorphous chains at room temperature. Nevertheless, the extraordinarily high melting points of these samples still suggest such coexistence. Thus we reach a conclusion that the highly ordered crystallites coexist with crystallites with smaller size in the absence of relaxed amorphous chains at room temperature but melting of the latter crystallites at high temperatures produces less-oriented amorphous molecular chains in the course of fusion. The amorphous chain thus produced will be in equilibrium with the highly ordered crystallites in the time-scale of the DSC measurement.

Table 2 lists the enthalpy of fusion for the drawn samples estimated from the fusion curves with planimetry. There is no notice-

Table 2. Melting Point and Heat of Fusion of Drawn and Annealed PVA Films

Sample	Draw ratio	Melting point T_m (°C)	Heat of fusion ΔH (cal/g)
Stretched in air at 120°C and annealed	-	236.5	15.3
	2	236.2	17.5
	3	237.5	18.1
	4	239.8	18.6
	5	239.5	19.3
	6	240.5	19.8
	7	240.5	19.9
Stretched in the swollen state and annealed (MeOH)*	2	239.2	19.7
	3	240.5	20.6
	4	241.0	21.3
	5	241.5	22.4
	6	243.0	22.8
	7	244.0	23.1
Stretched in the swollen state and annealed (acetone)**	4	240.6	20.6
	5	241.3	22.4
	6	241.0	22.6
	7	243.0	23.0

*; Dipped in methanol before annealing
**; Dipped in acetone before annaeling

able difference between two series of swell-drawn samples which were stretched in the swollen state and then dipped in either methanol or acetone and annealed after drying. But as is expected from the density data cited in the former section the quantities for the swell-drawn samples are appreciably greater than those for the heat-drawn samples

of a same draw ratio. From the enthalpy of fusion a quantity corresponding to the degree of crystallinity can be also obtained; it is calculated as the ratio of the enthalpy of fusion for the sample to that for the perfectly crystalline phase of the polymer, which was obtained by Tubbs(27) to be 37.3 cal/g from the melting point measurement of the polymer-diluent system.

In Figure 6 the quantity thus obtained is plotted as the degree of crystallinity $(1-\lambda)_{\Delta H}$ against the value $(1-\lambda)_d$ derived from the density measurement. In such a plot for crystalline polymers it is generally observed that the data progressively departs from the straight line of $(1-\lambda)_{\Delta H}=(1-\lambda)_d$ as the value of $(1-\lambda)_d$ decreases due

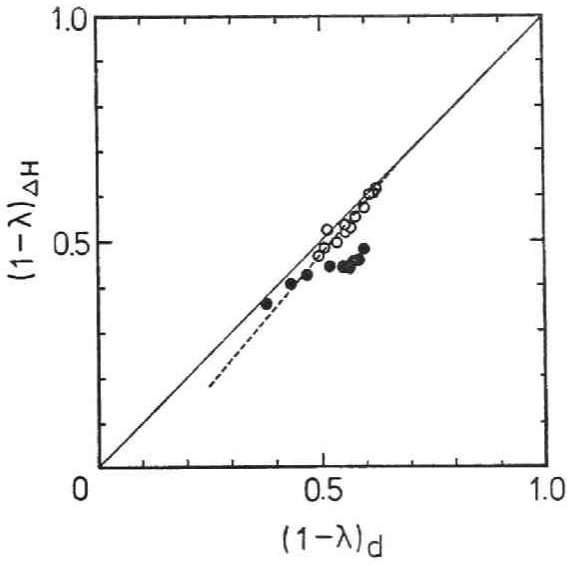

Fig.6. Crystallinities for drawn PVA films, estimated from enthalpy of fusion and density. Open and closed circles show the data for annealed samples stretched to various degrees in the swollen state and those stretched in air at 180°C, respectively. The dotted line is drawn for the open circles.

to the contribution from the interfacial domain between the crystalline and amorphous phases in the structure(28). Open circles in the figure, which are the data for the swell-drawn samples, indicate such tendency. It implies the coexistence of the well-defined pure crystalline and amorphous phases with the interfacial domain as is predicted from the afore-mentioned consideration of the fusion behavior. On the other hand, the $(1-\lambda)_{\Delta H}$ for the heat-drawn samples is appreciably smaller than that for the swell-drawn samples and does not show such tendency. This implies either greater contribution from the interfacial domain due to the complexities of its structure as is predicted from the mechanism in forming of the crystalline structure or less-defined crystalline and amorphous phases. However, further consideration of these data should be awaited until more reliable definite quantities about the density and enthalpy change of fusion for the perfectly crystalline phase of the polymer become available since it evidently depends on these quantities.

Dynamic Modulus

The dynamic moduli for the swell- and heat-drawn samples measured at room temperature by a frequency of 110 cps are plotted against draw ratio in Figure 7. The moduli for the swell-drawn samples not only increase with increasing of draw ratio but also are about 30% greater than that for the heat-drawn samples. This is in good agreement with a prediction from the high degree of molecular orientation as well as the existence of the pure highly ordered crystallites with a larger dimension.

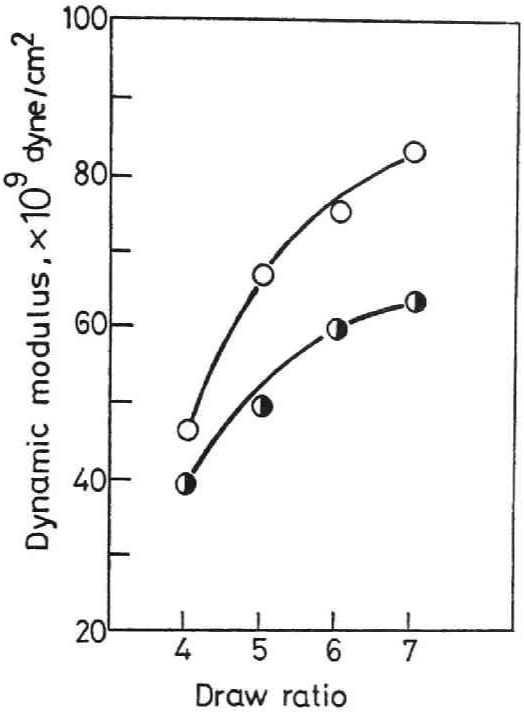

Fig.7. Dynamic modulus vs. draw ratio for annealed PVA films stretched either in the swollen state or in air at 180°C. Open and half closed circles show the data for the former and latter samples, respectively.

Shrinkage with Heating

In Figures 8 and 9 the shrinkage with heating in air or water for the samples drawn sixfold under different conditions is plotted against temperature. As can be seen in the figures, the temperature for the swell-drawn sample where appreciable shrinkage initiates is about 40° higher than that for the heat-drawn samples. It shrinks appreci-

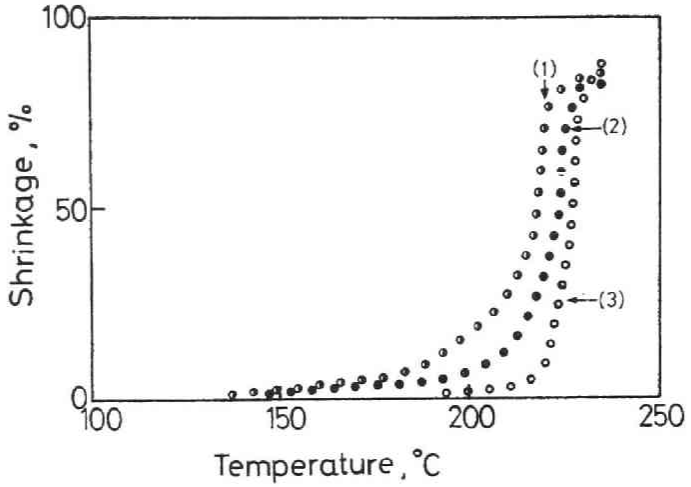

Fig.8. Thermal shrinkage in air vs. temperature for sixfold stretched and annealed PVA samples. Curves; (1) stretched in air at 120°C (half closed circles), (2) stretched in air at 180°C (closed circles), (3) stretched in the swollen state (open circles).

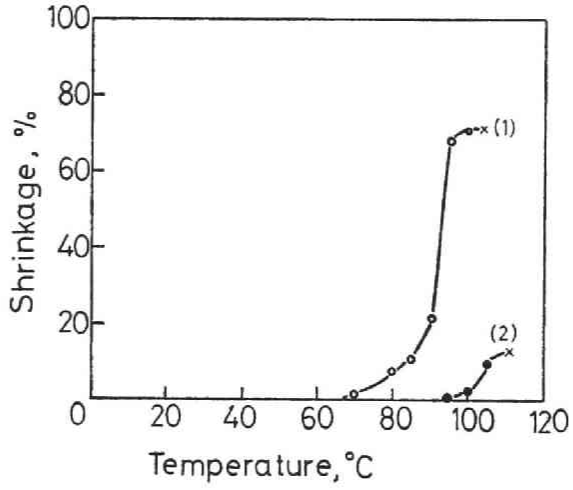

Fig.9. Thermal shrinkage in water vs. temperature for sixfold stretched and annealed samples. Curves; (1) stretched in air at 180°C (open circles), (2) stretched in the swollen state (closed circles). The cross markes show the point where the test piece broke.

ably only above 190°C and 95°C in air and water, respectively. This excellent dimensional stability to heating is not surprising if one consider the hydrophilic molecular character of the polymer, and it is very useful in the practical application. Since, as is discussed repeatedly, in this sample the highly ordered crystallites coexist with less-oriented amorphous chains after major melting of crystallites of smaller size completes, the shrinking will not complete until the melting or dissolution finally terminates.

12.4. Conclusion

It has been evidently shown that if the molecular fraction of PVA is stretched to a high extent in the water-swollen state and annealed after replacing of the water with acetone or methanol and drying, the resultant product generally shows various characteristic properties such as high degree of molecular orientation and extraordinarily high melting point with excellent dimensional stability to heating. The detailed structure of the product is supposed as follows. As is discussed in the experimental section particularly concerning the fusion behavior, a highly ordered crystallites with larger dimension coexist with less-ordered crystallites with smaller size and at higher temperatures with less-oriented amorphous molecular chains. This characteristic structure of the product resembles that of lightly crosslinked polymers such as polyethylene, isotactic polypropylene,

and polyvinylidene fluoride which show rubbery elasticity in the molten state, when these are crystallized from the molten and stretched or compressed state involving molecular orientation.

The crystallization mechanism of these crosslinked polymers has been extensively studied and general feature of the crystallization under molecular orientation is elucidated in detail(Chapter 1-11). Thus the very characteristic properties of the PVA sample well elucidate a general feature when crosslinked polymers are crystallized from the molten and stretched state. In addition PVA sample without chemical crosslinkings also crystallized by the strong intermolecular forces in the similar manner as in the case of the crosslinked polymers.

References

1. R.Kitamaru, H.-D.Chu, and W.Tsuji, J.Polym.Sci., B-5, 257 (1967).
2. H.-D.Chu, R.Kitamaru, and W.Tsuji, J.Appl.Polym.Sci., 10, 1377 (1966).
3. R.Kitamaru, C.Tsuchiya, and S.-H.Hyon, Bull.Inst.Chem.Res., Kyoto Univ., 52, 558 (1974).
4. R.Kitamaru, H.-D.Chu and S.-H.Hyon, Macromolecules, 6, 337 (1973).
5. S.-H.Hyon, H.Taniuchi, and R.Kitamaru, Bull.Inst.Chem.Res., Kyoto Univ., 51, 91 (1973).
6. R.Kitamaru and S.-H.Hyon, Makromol.Chem., 175, 255 (1974).
7. S.-H.Hyon, R.Kitamaru, H.Taniuchi, N.Tamura, and N.Hayakawa, Kobunshi Ronbunshu, 32, 240 (1975).
8. R.Kitamaru and S.-H.Hyon, J.Polym.Sci., Polym.Phys.Ed., 13, 1085 (1975).
9. S.-H.Hyon and R.Kitamaru, Presented on the 20th Ann.Meeting at Kobe, Soc.Polym.Sci.Japan (Sept.1974), Abstr.A1-8.
10. S.-H.Hyon and R.Kitamaru, Report of The Poval Committee, No.65, p.65 (1974).
11. T.Matsuo and H.Inagaki, Makromol.Chem., 55, 150 (1962).
12. I.Sakurada, Y.Nukushina, and Y.Sone, Kobunshi Kagaku, 12, 506 (1955).
13. R.Kitamaru and L.Mandelkern, J.Polym.Sci., A-2, 8, 2079 (1970).
14. I.Sakurada, K.Fuchino, and N.Okada, Bull.Inst.Chem.Res., Kyoto Univ., 23, 78 (1950).
15. I.Nitta, I.Taguchi, S.Nishimaki, and T.Sekiya, Ann.Rept.Inst.Textile Sci.Japan, 8, 48 (1954).
16. T.Mochizuki, Nippon Kagaku Zasshi, 81, 15 (1960).

17. R.C.L.Mooney, J.Amer.Chem.Soc., 63, 2828 (1941).

18. C.W.Bunn, Nature, 161, 929 (1948).

19. T.Mochizuki, U.Kawase, S.Fujii, and J.Uda, Presented on the 15th Ann. Meeting, Soc.Polym.Sci.Japan (May.1966), Abstr.166.

20. A.J.Pennings and A.M.Kiel, Kolloid-Z., 205, 160 (1965).

21. A.M.Rijke and L.Mandelkern, J.Polym.Sci., A-2, 8, 225 (1970).

22. A.Keller and M.J.Machin, J.Macromol.Sci., Phys., B1, 41 (1967).

23. R.Kamoto, K.Ehara, T.Matsumoto, T.Kawai, and H.Maeda, Seni-Gakkaishi, 26, 28 (1970).

24. J.P.Bell, P.E.Slade, and J.H.Dumbleton, J.Polym.Sci., A-2, 6, 1773 (1968).

25. K.Yamaura, Y.Hoe, S.Matsuzawa, and Y.Go, Kolloid-Z, Polym., 243, 7 (1971).

26. K.Monobe, Y.Fujiwara, and U.Yamashita, Kogyo Kagaku Zasshi, 73, 1420 (1970).

27. R.K.Tubbs, J.PolymSci., 3, 4181 (1965).

28. L.Mandelkern, A.L.Allou, and M.Gopalan, J.Phys.Chem., 72, 309 (1968).

SUMMARY

Chapter 1. Structure and Properties of Lightly Crosslinked Polyethylene Crystallized from the Melt under Uniaxially Stretching.

The phase structure and thermodynamic or physical properties of a lightly crosslinked polyethylene crystallized from the molten state under uniaxially stretching are studied by X-ray, birefringence and DSC techniques, in comparison with those of the sample stretched in the partially crystalline state. It is confirmed that, if a lightly crosslinked polyethylene is highly stretched in the perfectly molten state, upon cooling to room temperature a unique fibrous structure appears, which comprises highly oriented crystallites and almost unoriented relaxed amorphous chains with larger molecular mobility. A mechanism for appearing of such a unique fibrous structure is presented.

Chapter 2. Phase Structure and Molecular Mobility of Lightly Crosslinked Polyethylene Crystallized from the Melt under Uniaxially Stretching by Broad-Line NMR Spectroscopy.

The phase structure and molecular mobility of lightly crosslinked polyethylene films crystallized from the melt under uniaxially stretching are studied by broad-line NMR spectrometry. The broad-line spectrum is analyzed in terms of contributions from three components; 1) a crystalline region with crystals of orthorhombic form, 2) a noncrystalline region with liquid-like character which produces a Lorentzian contribusion to the spectrum, and 3) an intermediate region in which the rotation of methylene groups about C-C bonds is partly hindered.

It is found that the sample crystallized from the melt under uniaxially stretching is associated with an increased amount of narrow component with liquid-like character. It is concluded that the amorphous molecular chains are in a relaxed and unrestricted state in comparison with the sample stretched in the partially crystalline state below the melting point of the polymer.

Chapter 3. The Preparation of New Type of Synthetic Fiber from Linear Polyethylene by Irradiation Crosslinking.

A lightly crosslinked polyethylene filament was obtained by a conventional melt-spinning and an irradiation with an electron beam from Van de Graaff. This crosslinked filament was stretched to a high extent in the perfectly molten state at high temperatures above its melting point and quenched. Through these procedures a new type of synthetic fiber having a high melting temperature as well as excellent mechanical and fiber properties was prepared. The fiber obtained did not shrink appreciably if boiled in water for more than two hours and held its fiber properties.

Chapter 4. Phase Structure and Molecular Mobility of Polyethylene Fibers by Broad-Line NMR Spectroscopy.

It is found that the mass fraction and molecular mobility of each region depend greatly on the degree of drawing. (1) The broad and medium components increase with decreasing narrow component as the degree of drawing increases. (2) The molecular mobility of the medium component decreases greatly with increasing degree of drawing.

Such a change in the three components of spectra upon drawing is enhancely reflected in the NMR spectrum for the samples swollen in a non-protonated solvent CCl_4. The results for such three components are discussed in relation to the morphological phase structure of samples.

Chapter 5. Orientation of Crystal Planes in Lightly Crosslinked Polyethylene Crystallized from the Melt under Uniaxial Compression.

If lightly crosslinked polyethylene films are crystallized from the melt under uniaxial compression, a very unique alignment of the crystal planes of the orthorhombic form of the polymer appears.

It is confirmed that, when the sample is compressed between two metal plates in the molten state, the (200)-orientation parallel to the film surface of the sample first appears at a relatively low degree of compression and the (110)-orientation follows at higher degrees of compression.

Chapter 6. Structure and Properties of Lightly Crosslinked Polyethylene Crystallized from the melt under Uniaxial Compression.

If a crosslinked polyethylene of adequate crosslink density is uniaxially compressed in the molten state, a very unique orientation of the crystal planes appears upon cooling to room temperature as shown in Chapter 5. This unique orientation of the crystal planes is though to have been brought about from a crystal habit due to the intrinsic crystallographical structure of this polymer.

The appearance of such planar orientations is of particular importance in relation to the mechanism of the crystallization of this polymer under conditions involving molecular orientation independent of the presence of the crosslinked units.

Furthermore, the samples made in this mode of crystallization comprise generally a large amount of amorphous material of larger molecular mobilities with the very ordered crystalline contents and are associated with characteristic properties. Of particular importance here in a practical point of view is that the samples exhibit excellent transparency while holding the properties as a crystalline polymer such as the high melting temperature.

Chapter 7. Phase Structure and Molecular Mobility in Lightly Crosslinked Polyethylene Crystallized from the Melt under Uniaxial Compression by Broad-Line NMR Spectroscopy.

The phase structure and molecular mobility in a lightly crosslinked polyethylene crystallized under various conditions involving molecular orientation are investigated by broad-line NMR. It is confirmed that the crystalline region of samples crystallized from the melt under uniaxial compression is as stable as comparable with the isothermally well crystallized sample in the isotropic state. Furthermore, these samples are associated with amorphous material with a higher molecular mobility of a liquidlike character. On the other hand, for the sample compressed at a temperature below its melting point, the crystalline region is unstable and the molecular chains in noncrystalline region is strongly constrained.

Chapter 8. Preparation of Transparent Polyethylene Product through Continuous Rolling by Irradiation Crosslinking.

Highly transparent films were made from crosslinked polyethylene by continuous rolling. The thermal and mechanical properties as well as the crystalline structure of the films were studied. It is confirmed that the excellent transparent films have a high demensional heat-stability and excellent mechanical properties, but a rather low degree of crystallinity. X-ray studies revealed that the samples had a very special spatial orientation of the crystal plane.

Chapter 9. Orientation of Crystal Planes in Lightly Crosslinked Isotactic Polypropylene, Crystallized from the Melt under Uniaxial Compression.

A lightly crosslinked polymer film was made from isotactic polypropylene by gamma-ray irradiation in an acetylene atmosphere. When the crosslinked polymer film was crystallized from the melt under uniaxial compression, a unique alignment of crystallites is found. The (040) crystal plane is preferentially oriented parallel to the film surface at relatively low degrees of compression, and the (110) and (130) crystal plane are oriented parallel to the film surface at higher degrees of compression. The origin of these orientations, analogous to that previously found in a lightly crosslinked polyethylene, is discussed.

Chapter 10. Structure and Properties of Lightly Crosslinked Isotactic Polypropylene Films, Crystallized from the Melt under Uniaxial Compression.

Structure and properties in lightly crosslinked isotactic polypropylene films prepared under various conditions involving molecular orientation is studied. It is confirmed by small angle X-ray scattering, DSC technique and dynamic mechanical measurements that the sample films crystallized from the melt under uniaxial compression have a highly ordered and stable crystalline phase associated with very high melting and shrinking temperature. The long period, scattering intensity and melting temperature increase in accordance with increasing compression ratio and a characteristic dual peak appears in the fusion curve.

Chapter 11. Structure and Properties of Lightly Crosslinked Polyvinylidene Fluoride Crystallized from the Deformed Molten State.

Effects of the deformation upon the supermolecular structure and thermal properties of lightly crosslinked polyvinylidene fluoride are investigated by X-ray diffraction and calorimetric technique. It is confirmed that the chain conformation in drawn sample film depends markedly on the draw temperature and draw ratio, and that the long period and scattering intensity increase with increasing draw ratio, when the sample is uniaxially stretched in the molten state. On the contrary, when the sample uniaxially stretched at a high temperature

below its melting point, the long period and scattering intensity decrease with increasing draw ratio. Furthermore, when compressed uniaxially in the molten state, a special planar orientation of the crystal planes of the orthorhombic form of this polymer appears, while no appreciably amount of the β-form appears. The (200) crystal plane is preferentially oriented parallel to the film surface for samples made in such a mode, but when compressed or biaxially stretched in the partially crystallized state, other planar orientations such as (010) and (110) are produced without the (200) orientation.

Chapter 12. Structure and Physico-Chemical Properties of Polyvinyl Alcohol, Stretched at the Amorphous State and Annealed.

A stretching mode of polyvinyl alcohol film in the swollen state without crystallinity is examined. Comparison is made of the physico-chemical properties as well as the crystalline structure between samples which were prepared either in this manner or in a usual manner of stretching in the dry state with a crystallinity. It is confirmed by X-ray diffraction and differential scanning calorimetric techniques that the former sample has a highly ordered and stable crystalline phase in the structure with very high melting and shrinking temperatures. The melting temperature rises in accordance with increasing of the stretching degree and a characteristic dual peak appears in the fusion curve for samples stretched more than 3 times. The temperature where detectable shrinkage appears with heating (shrinking temperature) is about 40°C higher than for the latter samples.

List of Publications

Major part of this dissertation is scheduled to be published in Macromolecular Review (John Wiley and Sons Inc, New York), Vol. 14 (1978) as a review paper entitled " Structure and Properties of Lightly Crosslinked Crystalline Polymers, Crystallized or Processed under Molecular Orientation ".

Chapter 1.

(1) "Structure and Properties of Lightly Crosslinked Polyethylene Crystallized from the Melt under Uniaxially Stretching"
Polymer Preprints, Japan, 25, No.2, 342 (1976)
Macromolecular Review, 14, in press (1978)

Chapter 2.

(2) "Phase Structure and Molecular Mobility of Lightly Crosslinked Polyethylene Crystallized from the Melt under Uniaxially Stretching by Broad-Line NMR Spectroscopy"
Polymer Preprints, Japan, 25, No.7, 1469 (1976)
Macromolecular Review, 14, in press (1978)

(3) "Proton Magnetic Resonance Studies of the Phase Structure of Bulk-Crystallized Linear Polyethylene"
J. Polym. Sci. Polym. Phys. Ed., 15, 821 (1977)

(4) "NMR Studies of the Phase Structure of Bulk- and Solution-Crystals of Polyethylene"
ACS. Polymer Preprints, 17, (2), 549 (1976)

Chapter 3.

(5) "The Preparation of a New Type of Synthetic Fiber from Linear Polyethylene by Irradiation Crosslinking"

Bull. Inst. Chem. Res. Kyoto Univ., 52, 436 (1974)

Macromolecular Review, 14, *in press* (1978)

Chapter 4.

(6) "Phase Structure and Molecular Mobility of Polyethylene Fibers by Broad-Line NMR Spectroscopy"

Bull. Inst. Chem. Res. Kyoto Univ., 55, 248 (1977)

Chapters 5, 6.

(7) "The Properties of Transparent Film Made from Linear Polyethylene by Irradiation Crosslinking"

Macromolecules, 6, 337 (1973)

(8) "The Orientation of Crystal Planes in Polyethylene Crystallized under Compression"

Bull. Inst. Chem. Res. Kyoto Univ., 51, 91 (1973)

(9) "Size and Orientation of Crystallites in Lightly Crosslinked Polyethylene, Crystallized from the Melt under Uniaxial Compression"

Makromolekulare Chem., 175, 255 (1974)

(7),(8) and (9) are also contained in *Macromolecular Review*, 14, *in press* (1978)

Chapter 7.

(10) "Broad-Line NMR Studies of Molecular Motion in Lightly Crosslinked Polyethylene Crystallized from the Melt under Uniaxial Compression"

Kobunshi Ronbunshu, 32, 240 (1975)

(11) "Phase Structure and Molecular Mobility in Lightly Crosslinked Polyethylene Crystallized from the Melt under Uniaxial Compression by Broad-Line NMR Spectroscopy"

Polymer Preprints, Japan, 25, No.2, 341 (1976)

Macromolecular Review, 14, in press (1978)

Chapter 8.

(12) "Preparation of Transparent Polyethylene Product through Continuous Rolling by Irradiation"

Macromolecular Review, 14, in press (1978)

Chapter 9.

(13) "Orientation of Crystallites in Lightly Crosslinked Isotactic Polypropylene Crystallized from the Melt under Uniaxial Compression"

J. Polym. Sci. Polym. Phys. Ed., 13, 1085 (1975)

Chapter 10.

(14) "Structure and Properties in Crosslinked Isotactic Polypropylene Films Crystallized from the Melt under Uniaxial Compression"

Presented on the 20th Ann. Meeting at Kobe, Soc. Polym. Sci., Japan, A.1, P.8 (Sept. 1974)

Chapter 11.

(15) "Structure and Properties of Lightly Crosslinked Polyvinylidene Fluoride Crystallized from the Deformed Molten State"

Polymer Preprints, Japan, 24, 340 (1975)

Chapter 12.

(16) "Structure and Physico-Chemical Properties of Polyvinyl Alcohol Stretched at the Amorphous State and Annealed"

Bull. Inst. Chem. Res. Kyoto Univ., 53, 367 (1975)

Acknowledgement

The present investigations have been carried out in the Institute for Chemical Reserch, Kyoto University from 1969 to 1977.

The author wishes to express his gratitude to Professor Ryozo Kitamaru for his guidances and valuable discussion with constant encouragement.

The author also wishes to express his thanks to Emeritus Professor Waichiro Tsuji, Professor Yoshito Ikada, Dr. Masao Hosono, Dr. Hyon-Don Chu, Dr. Keisuke Kaji and Dr. Fumitaka Horii for their valuable suggestions and criticisms throughout this work .

November, 1977 Suong-Hyu Hyon